R11

Certificate of Research

This is to certify that, except where specific reference is made, the work described in this thesis is the result of the candidate's research. Neither this thesis, nor any part of it, has been presented, or is currently submitted, in candidature for any degree at any other University.

Signed .....C.J.....Wells.....
Candidate

Date .....2/12/2008.....

Signed .....
Director of Studies

Date .....02/12/2008.....

Investigation and Modelling of the Yarn Splicing Process

Carwyn James Webb

Ph.D. Thesis

December 2008

Investigation and Modelling of the Yarn Splicing Process

By Carwyn James Webb

Prifysgol Morgannwg
The University of Glamorgan

A thesis submitted in partial fulfilment of the
requirement for the degree of Doctor of Philosophy

December 2008

Abstract

The pneumatic splicing technique was developed in the 1960's to overcome the deficiencies of knotting of textile yarns, but there has been little research into splicing because it is a complicated process, very difficult to observe. A splice is formed very quickly, using highly turbulent air within a closed environment. Direct observation is almost impossible. The poor understanding of the mechanism has led to ad-hoc solutions, and can yield unpredictable splice characteristics. A better understanding of the splicing process is long overdue.

The objective of the research is the evolution of a theoretical model which would offer a better understanding of the splicing process than existing models, and which would be capable of being used as a predictive design tool for future splicers.

The research programme presented in this thesis demonstrated the feasibility and efficiency of the Taguchi design of experiment method, as applied to the splicing process. The Taguchi method simplified the research, and facilitated the identification of the design parameters most relevant to splice quality.

Mechanical aspects of experimental splicers were altered to establish how design features affect splicing performance. The effects of commonplace process parameters such as air pressure and blast duration were examined in detail. These experiments demonstrated the importance of air mass flow rate as a fundamental parameter in splicing; they also revealed the existence of a phenomenon which was called "scaling". Scaling describes the change in performance of a splicer, when it is confronted with yarns of a size which are outside its normal envelope of performance.

Other techniques were used in conjunction with Taguchi; these included flow visualisation, computational fluid dynamics simulations, and the use of scanning

electron microscopes. These approaches have been used together, to optimise splicer parameters and to investigate the airflow within the splicing chamber – the component which ultimately determines the splice structure. These techniques were also used to model the airflow within a wide range of commercially available splicing chambers.

The validity of the visualisation and simulation methods are discussed, and a degree of confidence in the accuracy of the outcomes is established.

By combining simulation images with the conventional experimental results, it was possible to develop an improved theoretical model for the splicing process. The model proved sufficiently robust to explain a number of phenomena in splicing previously poorly understood. The new model has been used as a prediction tool for splicer design characteristics. It is likely that the model will permit the creation of a new generation of high-performance splicing tools.

Table of Contents

Symbols and Abbreviations

I. Symbols

a : Speed of sound

β : Coefficient of thermal expansion

E : Total energy

ε : Dissipation rate

k : Kinetic energy per unit mass

k_{eff} : Effective thermal conductivity

M_t : Turbulent Mach number

n : Number of values at each test condition

Pr : Prandtl numbers

SRS : Spliced retained strength

S/N : Signal to noise ratio

$(\tau_{ij})_{eff}$: Deviatoric stress tensor

y_i : Each observed value

Y_M : Dilatation dissipation

II. Abbreviations

3D : Three dimensional

ANOVA : Analysis of variance

CFD : Computational fluid dynamics

CAD : Computer aided design

DOE : Design of experiment

OA : Orthogonal array

POY : Partially oriented yarn

RYA : Retained yarn appearance

SRS : Spliced retained strength

SNR : Signal to noise ratio

SEM : Scanning electron microscope

Acknowledgments

Firstly I would like to thank my industrial supervisor Graham Waters for his invaluable help and guidance throughout this research project. He identified the research area of the splicing process and provided me with the support and access to all equipment needed, which enabled me to contribute to this research area.

My deepest and foremost gratitude is expressed to my lovely wife Carol Webb, for her constant support and understanding, which was truly vital. I am also very grateful to my family (Jacqueline, Robert and Gavin Webb) for their emotional support and helpful assistant. Without all their support this work could not have been finished.

It has been a difficult and emotional task to complete this research because during my 2nd year, Dorothy Jones, my close and very dear grandmother, passed away and I would just like to say that I owe her a great deal in getting where I am today and for her loving support through my 1st year of research.

My sincere thanks are also due to the University of Glamorgan, Advanced Control and Network Technology Research Unit group for providing the facilities and equipment to carry out the research.

Last but not least, I would like to thank my supervisors and research group at the University of Glamorgan who guided me through this research process and provided the necessary support to accomplish my goals.

Chapter I

Introduction

Abstract – *This chapter gives a brief introduction into the state of the textile industry and familiarises the reader with the splicing process. The aims of the research throughout the thesis along with the proposed methodologies and chapter-by-chapter descriptions are discussed.*

1.1 Splicing history

Since all bobbins of yarn and balls of wool have a finite length, it has always been necessary to join lengths of yarn together, so that a fabric being knitted or woven would maintain structural integrity and good appearance. For centuries, such yarn joining was accomplished by the use of simple knots (Gebald, 1982).

Until the Industrial Revolution, and the advent of textile machinery, most fabrication processes proceeded slowly, at the pace of the hand-weaver or hand-knitter. In such circumstances, when it became necessary to join yarn ends, the knot could be hidden on the back face of the fabric, such as is done to this day in domestic hand-knitting. Then the appearance and construction of the knot was of no particular significance, as long as it could survive the everyday rigours of handling of the finished fabric. Even when there was a need for a better finish to the fabric, relatively crude methods could be used, such as spit splicing (Morrison, 2005), provided that speed was not of great importance.

The theory and practice of knot construction is extremely complex, and the mathematical principles of knot structure are addressed in many abstract academic texts. Even at the strictly practical level, the sheer number of knot constructions, used in everyday applications, will surprise the lay observer (Suber, 2004).

As textile machinery became more refined, and the fabrication processes ran faster, it became necessary to improve the structure of knots. Specific forms were evolved to meet the particular needs of textile processes. Thus, there were knots for absolute strength, knots with slim profiles for passing through needle eyes, etc (Ropers Knots Page, 1997).

The quality of these more refined knot structures, and the efficiency of the corresponding fabrication processes, was clearly dependent on the skill of the operator who did the knotting. Later, this process was made more consistent, with the

development of mechanical knotters, which could produce good quality knots with great consistency. Though largely supplanted by yarn splicers, knotters remain in use in parts of the industry.

Around the late 1960s and early 1970s, the form and function of the traditional textile knot was not deemed to be of great significance. One of the most important handbooks in the textile industry is the publication "Textile Terms and Definitions" (The Textile Institute, 1963), a comprehensive dictionary of terms used in the industry. As late as the 6th edition, published in 1970, knots were not mentioned, let alone specific knots for specific purposes.

However, a revolution in the industry was about to begin:

- Textile fabrication machines were being designed to run faster
- The new machines were being designed to be computer-controlled
- Factory manning levels were being reduced

These changes made great demands on the quality and "runnability" of all textile yarns, and the result was a sharp change in the quality demands made by end-users such as knitters and weavers.

A private communication from Waters, G.T. of ICI Fibre Ltd (Waters, 2007), who was responsible for the technical textile development from 1969 - 1974, demonstrates the profound effect, which these new demands had on the producers of synthetic yarn. At the time, the company was a massive producer of nylon and polyester, selling worldwide. Historically, ICI Fibres sold yarn to processors, who would then ship the processed yarn on to the users. The company was therefore largely insulated from the demands of the end-users. For technical and commercial reasons, ICI conducted a big programme of work, which led to the now well-established disciplines of draw-texturing. With new, very efficient yarn-processing capability of its own, ICI now bought out many of the processors, closed them and started dealing directly with the end-users.

Only then did it become apparent that the processors had been producing yarn to meet old, out-dated quality standards. They had been satisfying British knitters, who were using relatively primitive knitting machines, but by 1970 there was new investment in much more advanced machines, by the better UK companies, and by the then emerging producers in Hong Kong and elsewhere. These new machines ran faster, and they were using finer, more fragile, yarns. The old yarns were completely inadequate for the future environment, and ICI found itself facing a whole new raft of technical demands.

The most pressing problem turned out to be that of knots in the yarn, which ICI was producing. The older, slower knitting machines were tolerant of knots, but the new, faster machines were finer-structured with smaller needles. The number of knots per bobbin became a quality issue of huge significance, as they became caught in the needle eyes and caused considerable disruption in modern knitting plants worldwide (Cheng and Fung, 2004; Oinuma *et al.*, 1995). It will come as no surprise, therefore, that the Experimental Engineering Department of ICI Fibres Ltd. produced the first working pneumatic splicer (Iwnicki, 1964).

Along with pneumatic splicing, other various methods were introduced to produce knot free yarn joints:

- Wrapping – The two yarn ends are overlapped and wrapped around by an auxiliary thread to produce a high strength joint. Disadvantages of this method include complicated mechanism, long splice time, increased rigidity, and appearance due to both the increase in diameter and the colour after wet processing.
- Welding – The two yarn ends are welded together. Disadvantages are that the joint will have different structure from the rest of the yarn and can only be used for certain thermoplastics.
- Latex-Jointing – The two yarn ends are joined by latex. Disadvantages include continuous monitoring, proper storage of latex, skilled operators, reduction in strength after wet processing and discolouration of the final fabric when in use.

This is particularly relevant to carpets, in the past a common environment for latex splicing, residual adhesive in the carpet structure picks up soiling from footwear, and after short service life causes a dark blemish in the carpet.

- Bonding – Yarn ends are overlapped and glued together. This method produces increased rigidity and increased splice time because of the need to dry the adhesive. It also suffers from similar problems in service to those experienced by later joints.
- Mechanical splicing – In this system the yarn ends are untwisted and the fibres pulled apart. These ends are then twisted together again resulting in a similar process to wrapping but far superior, due to the slight increase in diameter and weight. Disadvantages of this method are the complexity of the process and the cost of maintenance.
- Electrostatic splicing – This process is similar to mechanical splicing but instead of spreading the fibres mechanically they are spread apart (in an umbrella formation) by an electrostatic field. The fibres are intermingled and closed by a pole change. Disadvantages include long splice time and the provision of high voltage.
- Pneumatic splicing – Yarn ends are inserted and overlapped in a chamber to which an air blast is connected. The joining operation combines the transverse application of air to the fibres with a simultaneous rotating movement of air. Pneumatic splicing can be carried out in a relatively short splicing time and on a wide range of yarn types. The only disadvantage is the additional power requirement for the supply of compressed air.

The features of each method were compared with the characteristics of the pneumatic splicing technique (Cheng and Fung, 2004; Cheng and Lam, 1997). Pneumatic splicing was found to be the optimum method for further development, and since its introduction has come to occupy a dominant position in the textile industry.

Apparently simple, splicing is actually a fairly complicated process. The splice is formed very quickly, within a closed environment, in which the highly turbulent air radically disrupts the arrangement of the fibres. Though there are various forms of splicer, made by different manufacturers, most of the mechanical processes for the splicers remain similar. The principal differences lie in the designs of the splicing chamber, which may take various forms, It is the existence of this vast range of splicing chambers which reveals that no great body of research has been undertaken into splicing; therefore the poor understanding of the mechanism has led to ad-hoc solutions, which can yield unpredictable splice characteristics. Ignorance has limited the ability of a user to produce consistently high splice strengths with acceptable aesthetics when yarn characteristics change. Direct observation is almost impossible, which is the reason why splicing is poorly understood. This observation may seem a lame excuse, but the reality is that most splicer development has taken place in relatively small companies, with limited budgets. So there has been very little published work on splicing, and there is little evidence of any understanding of the fundamental principles of the technology. A better understanding of the splicing process is long overdue.

A recent publication by Lewandowski & Drobina (2004, pp.31) confirms this by stating that before the year 2000

"No publication has been found about the optimisation
of the splicing device"

After the year 2000 many researchers have attempted to optimise the splicing process for specific processes using only indirect testing, for example (Gosh *et al.*, 2005; Witkowska and Frydrych, 2004).

The increasing rate of adoption of new fibres, such as carbon, requires an effective, novel technical splicing solution (Satapathy and Bijwe, 2004). This need serves to emphasize the urgency of a new understanding of splicing.

1.2 Forms of splice joint

It is possible to make two different kinds of splice, which have different geometries, and which are made by two completely different procedures. These two forms of splices are called respectively "ends-together" and "ends-opposed".

Ends opposed splicing: This form of splice was first used when splicing technology was being developed. The two yarn ends to be joined are overlapped in opposite directions and placed into a splicing chamber. Following the air blast, the result is a neat strong bond between the yarns is produced as shown in Figure 1-1, which significantly improves the joint quality and factory productivity (Paliwal and Patel, 1989; Mingjie *et al.*, 1999).

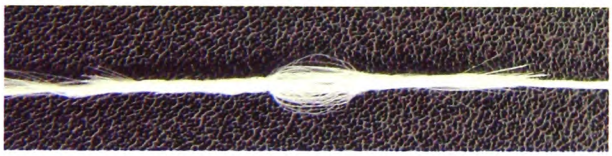

Figure 1-1. Ends opposed splice joint.

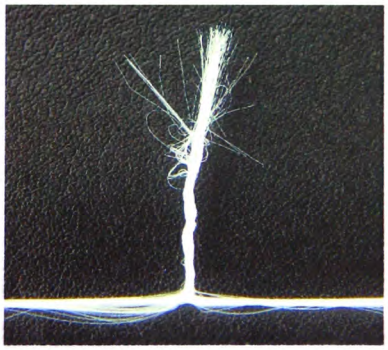

Figure 1-2. Ends together splice joint.

Ends together splicing: This form of splicing is simpler than the ends opposed method. Two yarns are placed in the splicing chamber, overlapping in the same direction.

Though the yarns are entangled very effectively, it is necessary to open up the yarns into a single line after the operation is completed. The result is that a tail of entangled fibres project from the jointed yarn at an angle of approximately 90^{o} as shown in Figure 1-2.

The ends together form of splicing was eliminated from the research since it is only applicable to a minority of industrial processes.

1.3 Splicer design

The design of a splicer is complex (Figure 1-3) in that there are many factors which affect the performance of the splice. The designer of a splicer is serving the textile industry, which has something less than a cutting-edge image and where the layperson might imagine that the design problems are trivial. However, the designer is confronted by problems which in the real world are startlingly complex.

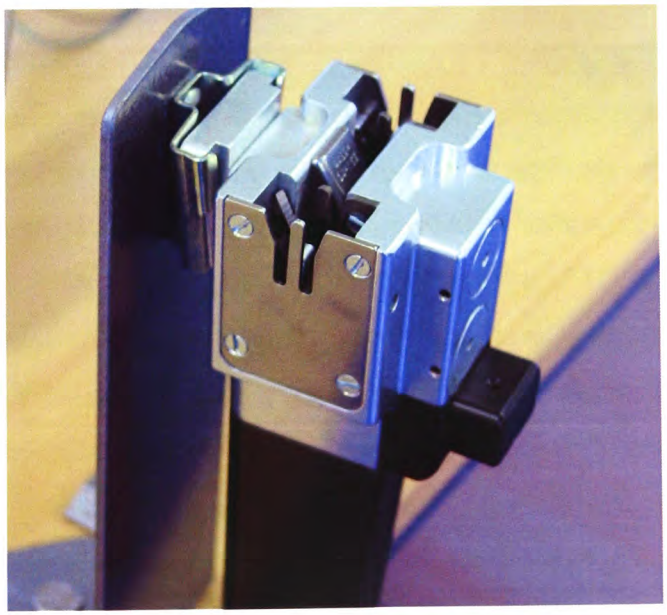

Figure 1-3. Commercial splicer.

A typical yarn splicer, as shown in Figure 1-3, is about twice the size of a mobile telephone. The splicer will be expected to join yarns made from continuous-filament or staple yarn. The yarns can be made from all manner of materials from nylon, through wool, to glass, or to material such as rabbit hair blended with cotton. Yarn counts (mass per unit length) typically cover a range of three full orders of magnitude. In one common textile measure of linear density, the figure varies from about 50dtex (which converts to 200 kilometres per kilogram) to 50000dtex.

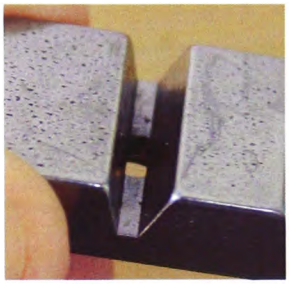

Figure 1-4. 4483 straight chamber.

The splicer has a primary active element, here called a splicing chamber, in which the splicing action actually takes place (Figure 1-4). The chamber usually takes the form of a channel with an open top, which is closed during the splicing operation. Chambers are small, they are usually less than 25mm in length and commonly have a cross-section in the form of a trapezium, with its two parallel sides at top and bottom, with the smaller dimension at the base. The non-parallel sides of the splicing chamber usually diverge uniformly and symmetrically, typically at a total included angle of around 30°. The splicing chamber may be of any depth, but in most practical splicers, the chamber depth is between 2.5 and 7mm depending on yarn count being spliced. It will have one or more blast holes, through which air can enter. The blast hole(s) may be in any position. Various forms of splicing chamber designs exist, ranging from circular chambers (Logan, 2001) to 'V' shaped chambers (Waters, 1998) as shown in Figure 1-5. All splicing chambers have a very similar effect on the yarns which are presented to them.

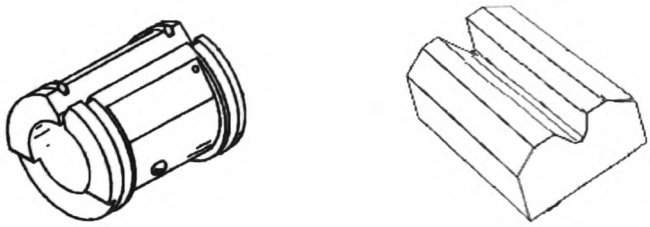

(A) (B)

Figure 1-5. (A) Circular chamber (B) 'V' shaped chamber.

Once the yarn ends are placed in the chamber, they are secured in place by closing the chamber lid. The chamber lid prevents the yarns from escaping and creates the confined space needed for the splicing process to take place. The yarns are then subjected to a high pressure turbulent flow of compressed air that has a very high Reynolds number. Symmetrically positioned either side of the splicing chamber are two knife assemblies. The knives cut the yarn ends not being bound into the splice and are discarded as waste.

The interior of the splicing chamber, and the yarns within, are obscured during the splicing operation by other mechanical parts, and the airflow within the chamber is violently turbulent, completing a cycle of the cross-section of the chamber in about 50 microseconds. It is an environment in which it is difficult to observe or conduct experiments.

The highly turbulent air might be expected to destroy the yarns, especially delicate materials such as fine wool. However, the design of the splicing chamber is such that, after approximately half a second, the chamber can be opened to reveal a smooth, elegant joint, almost as strong as the parent yarn, which passes smoothly through subsequent textile processing (Cheng and Fung, 2004).

There is general consensus that the airflow within the splicing chamber is the most important single component in deciding the resulting splice formation (Oxenham and Basu, 1993). Previous research undertaken has revealed that splice consistency and

strength are closely associated with the design of the splicing chamber and with the pressure of the air supply (Mingjie *et al.*, 1999). Optimising of splicing parameters was made more difficult by the fact that there is a certain amount of variation between splices made under the same conditions.

The small scale of the splicing chamber and the very high levels of turbulence, make direct observation of the splicing process almost impossible. Most research into splicing has therefore avoided direct observation, relying instead on a more indirect approach, and concentrating on external parameters, which are simple to measure. For example, work done by Cheng and Lam (2003), addressed the effect of variables such as air pressure upon splice strength and appearance to optimise the splicing process. However, they do not offer any hypothesis behind how a splice is formed or offer any comment about how splicing parameters interact to produce splice characteristics.

Such indirect observations are valuable up to a point, in that it does at least allow operators to establish optimum splicing conditions for a very specific application. However, indirect observation offers no insight into the mechanism of how a splice is formed, and of the detailed processes which produce splice characteristics such as strength. Understanding of the process of splicing has failed to move beyond the qualitative. As Zhou and Qin (2005) said "Understanding of the splicing process is based only on interpretation rather than theoretical analysis."

The general ignorance about the process is clear. Moreover, the diversity of commercial splicing chamber designs suggests that splicer development has in most cases been conducted on an empirical basis. There is little evidence for the existence of a strong theoretical basis. A number of descriptive models of splicing exists in the published literature, but even the most superficial analysis shows that these models were profoundly deficient (Oxenham and Basu, 1993; Cheng and Lam, 2000a).

For example an article written by Mingjie *et al.* (1999) stated that

> "a splice with intermingles in the middle, many small wrappings on both sides and near overlapping loopy wrappings at both ends should be ideal".

This description is at best vague; it certainly falls far short of being rigorous. Early in the history of splicing, the splicing process and splice structure was presumed to be as shown in Figure 1-6 (Shea, 1981; Kaushik and Sharma, 1988), a visual representation which broadly corresponds to the quote by Mingjie *et al.* (1999). This splice model is now believed to be completely inaccurate.

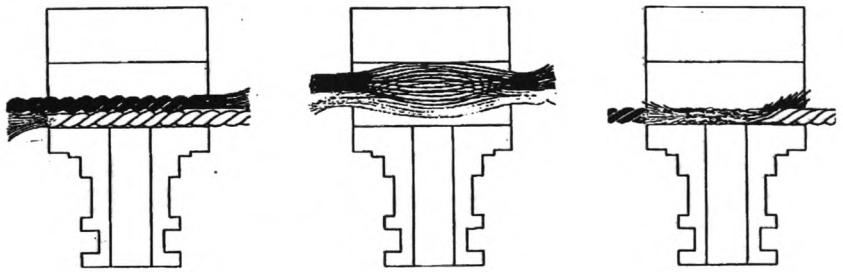

Figure 1-6. Basic splicing chamber with an (A) ends opposed layout; (B) separation of fibres; (C) intermingling of fibres.

One model, however, has proved fairly resilient (Waters, 1996). First proposed in an internal research document about a decade ago, the model has been very useful to one splicer manufacturer. This theoretical model of the splicing process was founded on an investigation involving close examination of splice structures as shown in Figure 1-7. Work conducted in the mid-1990s led to a conclusion that filament migration should be considered as relevant to the splicing process. The elements of the filament migration model of splicing are described in detail in section 1.4. Application of this model has enabled the company to produce splicers, which accomplish high levels of performance with one third of the complexity of earlier designs. However, the model was clearly not perfect, and its validity could only be tested by a suitably rigorous experiment as described in detail in subsequent chapters.

Figure 1-7. Characteristic form of a splice.

1.4 The existing (1996) migration model of splicing

There is general agreement that the first function of a splicing chamber is to mix the filaments as uniformly and as completely as possible. The process of mixing is thought to occur as shown schematically in Figure 1-8 below.

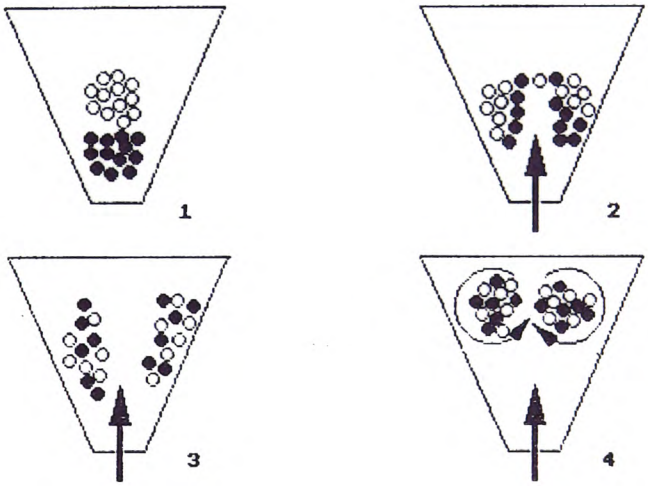

Figure 1-8. The intermingling of yarn ends (Waters, 1996).

When the blast enters the chamber, its first function is to split the yarn bundles apart, as equally as possible. Half of each yarn is then hurled to left and right. This splitting is a necessary condition for filament mixing, and hence splicing. If the splitting does not take place reliably (approximately 50% each), then satisfactory mixing of yarn ends and splicing cannot follow.

It will be clear that, in this model, the dimensions of the yarns and the dimensions of the blast hole must be of the same order of size. If, for example, the yarns are very small, and the chamber floor (thus orifice size) very large, the yarns can rest side by side on the chamber floor and not in an overlapping relationship, and therefore will merely be blown apart when the air enters, thus very little or no mixing will occur.

Assuming that mixing is accomplished properly, the two mixed halves will be thrown upward and outward, exposed to two contra-rotating swirls of air. The air separates the mixed bundles, and twists them in opposite senses. As seen from above, the resulting effect is as shown in Figure 1-9.

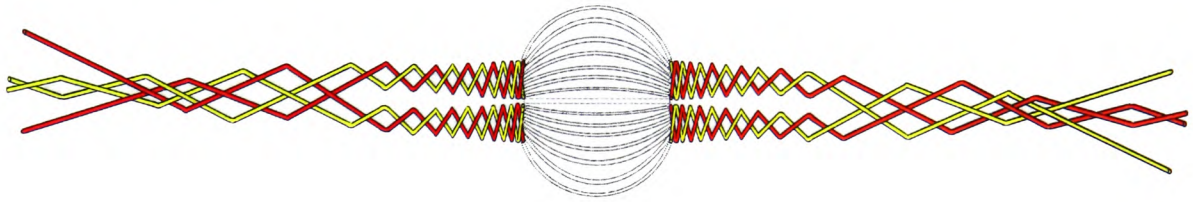

Figure 1-9. The formation of a splice.

As the process develops, twist runs outward from the centre in four regions. It tends to tear the bundle apart into a kind of diamond-shape. The dynamic picture begins to look very similar to the static structure of the fully formed splice. But all we have is four sets of helices; there is no evidence of intermingling. Once the blast is stopped, and if the four sections have been merely twisted together, it would seem that the splice will simply slip apart. For a splice to be fully formed, there should be some kind of intermingling in the structure.

Filament migration arising from twisting of the yarn bundles was proposed as a mechanism for intermingling. Migration is a phenomenon which has been extensively studied, in staple yarn spinning and particularly in the process known as false-twist crimping (Basel, 2003; Primentas and Iype, 2001).

In false-twist crimping, as soon as yarn enters the twist zone of the false-twist process, the bundle is violently distorted. The bundle immediately adopts a spiral form, with a steep helix angle. The filaments that find themselves on the outside of the bundle are stretched to a much greater length (typically about 40% longer) than those, which run down the centre line. The outside fibres are therefore highly stressed. This configuration is not stable; the outer filaments cut in towards the centre, while the inner ones are pushed outward. The result is that all filaments spiral into and out of the bundle; stresses overall are more-or-less equalised. The movement of the filaments in and out is called migration. It occurs fairly regularly along the length of the twisted yarn. The intervals are sufficiently regular that it is possible to identify a roughly constant distance between troughs and crests for each filament; this is known as the migration period. An example of migration is shown in Figure 1-10.

Figure 1-10. Migration of filament through the yarn bundle (Primentas & Iype, 2001).

It is suggested that splicing was a special case of false-twisting, and it proposed that migration would produce intermingling, as filaments moved from outside to inside and back. It predicted that there would be an optimum yarn geometry for mixing, where yarn diameter is roughly equal to the base width of the chamber.

There were some appealing aspects of the migration model. It looked right in that there was clearly rotation of the yarn bundles, and there seemed to be ample evidence of filament migration. There was plenty of literature, offering good explanations of migration and mixing (Pan, 1993; Merati *et al.*, 1998; Kothari *et al.*, 1980; Dogu,

1972). The model was consistent with the "trapping" of filaments at the location of tail ends (from here on named the critical point), and it could explain how filament breakage due to excessive pressure or excessive blast time could cause filament breakage at the blast hole.

However, from the outset, there were some problems with the model, in that it failed to explain some aspects of the splicing process, such as stray filaments and varying performance with chamber length.

The 1996 model was clearly imperfect, and its validity could only be tested by a suitably thorough experiment, which would analyse the performance of splicers against an extremely wide range of variables. The design of such an experiment was likely to be complex. Our research programme used various techniques to circumvent these problems of complexity. Taguchi Design of Experiment techniques proved useful (Thomas and Antony, 2003; Fox and Lee, 1990; Logothetis *et al.*, 1990), as did scaled flow visualisation, computational fluid dynamics simulations (Zeng *et al.*, 2005), and the use of a scanning electron microscope (Sreprateep and Bohez, 2006; Hassen *et al.*, 2008). These approaches have been used to optimise splicer parameters and to investigate the airflow within the splicing chamber, which is the component that ultimately determines the splice structure.

The work falls into a series of distinct categories:

- The influence of process parameters such as pressure and blast duration on splice strength.
- The influence of process parameters on splice appearance and filament rupturing.
- The influence of yarn count on the design of splicers.
- The use of visualisation and simulation techniques to observe features of the splicing process.

The outcome was the evolution of a new theoretical model which offers a better understanding of the splicing process than existing models, and which is capable of being used as a predictive design tool for future splicers.

1.5 Aims and objectives

As mentioned throughout the previous sections, the splicing process is partially understood on an empirical basis with no accurate theoretical knowledge supporting it. Many researchers have tried to create a theoretical model of the splicing process but have since been proved inaccurate. One model has proved rigorous until now as described in section 1.3. This lack of firm theoretical splicing process model has led to ad hoc solutions, which yield variable and unpredictable splicing performance. A solution to this problem is long overdue, especially with new advanced materials, such as carbon fibre, needing to be spliced.

The availability of new analytical methods and technology is exploited in the thesis to aid a better understanding of the splicing process. Therefore the primary aim of this research was to acquire a better understanding of the pneumatic splicing process, and use this to develop new splicing procedures. This was important to the company to maintain its commercial advantage.

The aims of the research project were:

- To understand the theoretical principles underlying the splicing process.
- To use that new understanding to develop new splicing methods.
- To apply the new systems to facilitate the development of a new generation of high-performance splicing tools.

1.6 Thesis layout

The thesis structure is shown in Figure 1-11, which reveals how each chapter is a narrative to reach the ultimate goal of a new theoretical splicing process model.

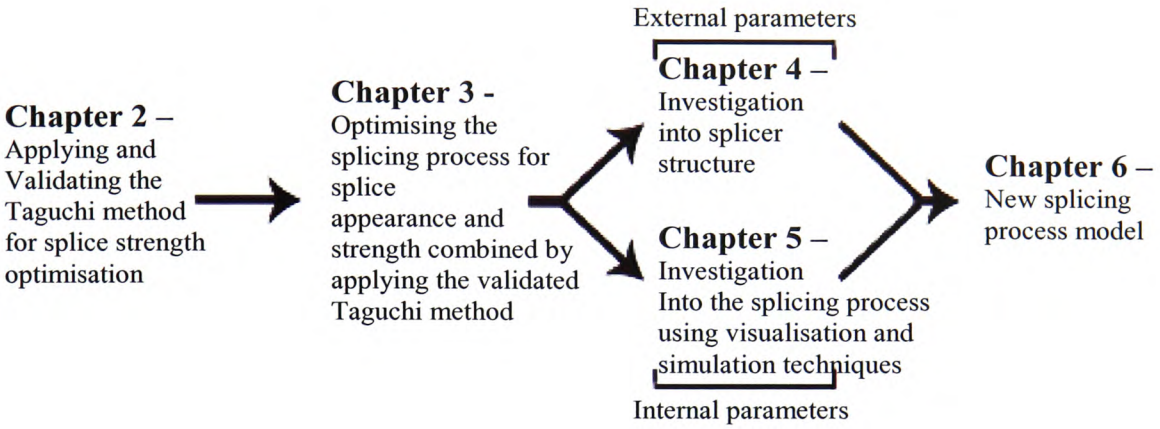

Figure 1-11. Thesis structure.

Chapter 1: This current chapter gives a brief introduction into the state of the textile industry and familiarises the reader with the splicing process. It outlines the obstacles which had to be confronted during the research, and the nature of the experimental design adopted to overcome those obstacles.

Chapter 2: This chapter describes the application of the Taguchi design of experiment method for splice strength parameter optimisation, with the aim of validating the method for applying to the splicing process. The Taguchi technique is a partial factorial analysis that improves process and product design. It identifies easily controllable factors and settings that minimise the variation in the product response, while keeping the mean response on target. Many papers have reported on the industrial application of the Taguchi DOE method, but none have ever been applied specifically to splicing.

Chapter 3: In this chapter, the validated Taguchi technique is first used to optimise splice appearance, as a single outcome. The process conditions which produced the best appearance, were not necessarily the same as those which produced the maximum strength. The analysis was therefore extended to reveal whether the two outcomes (strength and appearance) could be brought together to produce an overall optimised splice. Filamentation was characterised using a scanning electron microscope to distinguish between rupture modes which is an aspect of splice appearance. Together, Chapters 2 and 3 optimised a commercial splicer to obtain a splice that closely resembles the strength and appearance of the parent yarn.

Chapter 4: This chapter considers the way in which the structure and geometry of a splicer may affect the resulting splice. It had been observed that, though the performance of a splicer could be optimised for a particular yarn count, poorer results ensued when the splicer was confronted with yarns of substantially different characteristics. In particular, if yarn count increased markedly, splicer performance (from all manufacturers) deteriorated. The aim of this chapter was to investigate this effect, arbitrarily called "scaling", to determine whether there was some clear relationship between yarn geometry, splicer geometry, and performance. This work was conducted using an experimental splicer, which permitted the adjustment of structural splicer parameters over a wide range.

Chapter 5: This chapter addresses the problem that the splicing process cannot be observed directly. New methods were needed to represent the splicing process in a convincing manner. Visualisation techniques and flow simulations were considered, as a means of solving this problem. Two methods were selected:

- A transparent scaled (ten-times) model of a splicing chamber, which allowed direct observation of fluid flow
- A commercial software package, which could be used to simulate the airflow within a given chamber.

In this section, there is an account of how the visualisation and simulation processes was tested and validated. From the visualisation and simulation work, new insights were gained into the fundamentals, underlying the splicing process. The most significant outcome was the discovery that the use of air pressure as the most important splicing control parameter was based on flawed logic (Bar-Kohany *et al.*, 2007). A far better and properly direct parameter was that of mass flow rate of air within a splicing chamber.

Chapter 6: The analyses conducted in preceding chapters led to the development of a completely new theoretical model of the splicing process. In this final theoretical chapter, all the research from the whole project has been brought together. The results were first used to test the validity of the old model of splicing, which had been in use for ten years. The old model was found to be severely deficient.

Finally, a completely new theoretical model of the splicing process is described; the formulation of this theoretical model is the contribution of the research to the sum of knowledge in textile technology. The model is tested against a wide range of practical situations, which can be found in real textile environments. It was concluded that the new model represents a valid working hypothesis, which is substantially superior to its predecessor.

Work reported in the above chapters have been published in various journals as shown below:

- Chapter 2 – Webb et al. (2007a)
- Chapter 3 – Webb et al. (2007b)
- Chapter 4 – Webb et al. (2009)
- Chapter 5 – Webb et al. (2008).

Chapter II

The use of the Taguchi design of experiment method in optimising splicing conditions for a polyester yarn

Abstract – *This chapter discusses the design and practical implementation of the Taguchi design of experiment (DOE) method applied to splicing. The proposed DOE method can simplify the research for parameter optimisation, by reducing the amount of testing. This chapter also presents a record of controlled testing to establish the validity and effectiveness of the Taguchi method in this context. In order to validate the performances of the proposed Taguchi method, confirmatory runs were conducted to reveal if indeed an optimised splice was formed. The experimental results and post analysis illustrate the feasibility and efficiency of the proposed Taguchi method. All tests were performed using an industry standard synthetic yarn as a base line for the research.*

2.1 Introduction

In today's industry, companies need to improve the quality and productivity of their products while reducing production costs to remain competitive. There are many tools available today which satisfy these criteria through different methods. Dr. Genichi Taguchi developed one of these tools by applying a set of techniques based on statistical principles and utilising engineering knowledge (Peace, 1993)

Taguchi DOE method is an improvement of process and product design. It identifies easily controllable factors and settings that minimise the variation in the product response while keeping the mean response on target. A quote by Logothetis *et al.* (1990) confirms this Taguchi philosophy by stating the Taguchi DOE method "removes the bad effect of the cause rather than the cause of the bad effect". In mathematical terms Dr. Taguchi developed a model in which "loss" is a quadratic function of the deviation of the "quality" of interest from its target value.

"Quality" as defined by Taguchi is 'the loss imparted to the society from the time the product is shipped'. Taguchi's "loss function" is defined as 'a product causes a loss not only when it is outside specification, but whenever it deviates from its target value; this loss is proportional to the square of the deviation from the target' (Lochner, 1991).

Taguchi's method was developed in the 1950s in Japan but was not introduced outside of Japan until the 1980s (Bendell *et al.*, 1989, 39-56). Over recent decades, the Taguchi method has become a more widely and accepted method, in quality and productivity improvement.

Taguchi's first application of this method was in Morinaga Pharmaceuticals and it was reported that the productivity was increased tenfold annually (Peace, 1993, 13-22). A more recent industrial case study that adopted the Taguchi DOE method involved a company which required a reliable and optimised adhesive bonding performance under

a range of operating conditions (Thomas and Antony, 2003). The outcomes of the Taguchi DOE were an increase in direct, longitudinal and transverse strength of 36, 20 and 6% with a reduction in variance of 56, 22 and 3% respectively.

Taguchi DOE has many advantages and disadvantages over other DOE techniques. Taguchi's main advantage over other methods (in certain processes) is that it optimises specific processing parameters using a significantly reduced number of test runs, which is critical in various industrial processes or specific research areas. The reduction in test runs contributes to its main disadvantage, of the slight reduction in overall accuracy. This is discussed in greater detail about the relevant merits of this method compared to other methods in the subsequent sections.

As mentioned previously, many papers have reported on using Taguchi DOE method in industry, but none have ever been applied specifically to splicing. The proposal for this chapter is to implement the Taguchi DOE method to the splicing process with the outcome of achieving an optimised set of parameters to maximise the efficiency of the splicing process.

A step-by-step design approach in implementing the Taguchi DOE method to the splicing process was discussed in detail. Confirmatory runs were used to illustrate the performance of the proposed method and to validate its use in this context.

2.2 Design of experiment techniques

Two key DOE techniques are full factorial such as Shainin, and partial factorial such as Taguchi statistical quality improvement. These methods are being increasingly adopted in industry to improve product performance or production. There is a vast difference between these two methods with both having different merits. The main difference is the effective implementation of the Taguchi method and its complexity; for example,

companies cite the complexity of implementing the Taguchi method as being the major limiting factor for its use, while a full factorial is a simpler method to implement but very time consuming. However, if time is taken and Taguchi is implemented correctly, big rewards are given (Peace, 1993).

2.2.1 Taguchi design of experiment technique

The technique used by Taguchi begins with a brainstorming session attended by representatives of all levels. The first four steps need to be addressed within the brainstorming session for the Taguchi design to be a success:

Step1: Formulation of the problem. The success of any experiment is dependent on a full understanding of the nature of the problem.

Step 2: Identification of the output performance characteristics considered to be most relevant to the problem.

Step 3: Identification of control factors, noise factors, signal factors and interactions (if any). Control factors are those which can be controlled under normal production conditions. Noise factors are those which are either too difficult or too expensive to control under normal production conditions. Signal factors are those which affect the mean performance of the process. Interaction is a situation where a level change in one factor has a significant effect on the output response of a different factor.

Step 4: Selection of factor levels and the degrees of freedom associated with each factor and the interaction effects.

Step 5: Design of an appropriate orthogonal array. Orthogonal arrays (OA) are experimental designs which allow the factors to have different numbers of test levels and also have the pair wise balancing property so that every level of a factor occurs with

every level of all other factors the same number of times. In a sense OA are partial factorial designs that minimise the number of trial runs whilst keeping the pair wise balancing property as shown in Table 2-1.

Table 2-1 – Common Orthogonal arrays.

Orthogonal array	**Number of factors**	**Number of levels per factor**	**Number of trials required by orthogonal array**	**Number of trials in a traditional full factorial experiment**
$L_4 (2^3)$	3	2	4	8
$L_8 (2^7)$	7	2	8	128
$L_9 (3^4)$	4	3	9	81
$L_{12} (2^{11})$	11	2	12	2048
$L_{16} (2^{15})$	15	2	16	32768
$L_{16} (4^5)$	5	4	16	1024
$L_{18} (2^1 \times 3^7)$	1 & 7	2 & 3	18	4374

In selecting which OA best fits the process, linear graphs must be taken into consideration. Figure 2-1 below is an example of an L_{27} linear graph, which indicates the factors and interaction which correspond to the columns of the Taguchi array.

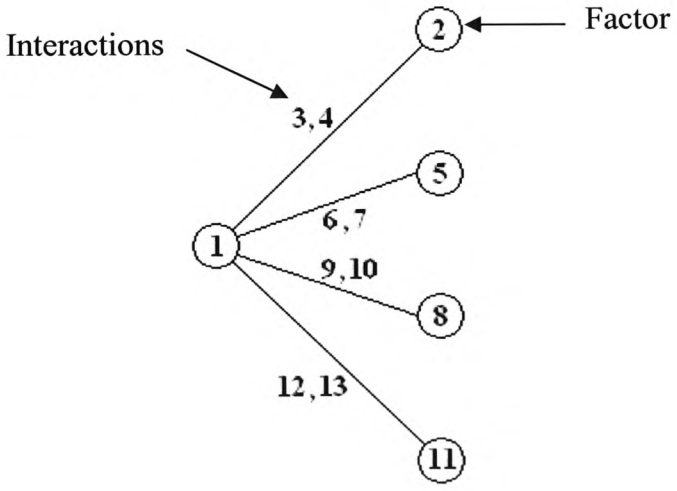

Figure 2-1. L_{27} linear graph.

Step 6: Preparation of the experiment.

- Calibration of measurement equipment and procedures.
- Maintenance of equipment, pre-test and during test.
- Set up recording procedures i.e. standardise the recording so that there is no variations between results due to measuring equipment.
- Carry out preliminary exploration of data and test conditions to reveal if the extreme combinations are viable and also gain insight into how the factors should affect the output response.
- Set up the test conditions

Step 7: Running of the experiment with appropriate data collection.

- Run the experiments whilst repeating the same method.
- Vary the sequence of test runs - e.g. do not conduct the tests 1 to 8 in chronological order because there could be a bias on the results due to noise factors – for example, machine warm-up.
- Collect all the appropriate information from the measuring equipment
- Repeat each test run 20 times to eliminate variation and increase reliability in the collected data and use the average value to conduct the statistical analysis.

Step 8: Statistical analysis and interpretation of experimental results. Prepare tables and plot means, both for direct response and signal to noise ratios (SNR). Graphical analysis is performed to determine the optimum controllable factor level in terms of their main response and SNR ratio. Analysis of Variance (ANOVA) is used to determine the statistical significance of the factors and their interactions (Wagner *et al.* 1993).

Step 9: undertaking a confirmatory run of the experiment (Wei and Wang, 2004). From the optimal factor levels derived, an estimate of the expected output response is obtained. Therefore a confirmatory experiment is needed to validate the results.

Planning of the next stage of the investigation must be derived, bearing in mind that all work of this nature should be a continuing iterative process, indicating where further work may most effectively be directed.

2.2.2 Evaluation of methods

The Taguchi partial factorial and full factorial methods have advantages and disadvantages each suiting specific industrial needs. Implementing the full factorial technique is simpler and has greater accuracy for the output response with the optimum setting but is very time consuming and expensive due to the vast amount of testing that is needed to complete the full factorial design. The greatest weakness of the Taguchi method is that it depends significantly upon the engineers' judgment in the brainstorming session. They need to identify variables and their rankings correctly, to reduce the size of the experiment and thereby speed up experimental process. The benefit of implementing the Taguchi method into the splicing process is the reduction in the number of test runs needed to undertake parameter optimisation.

In greater detail, the Taguchi method provides robust process enhancement through partial factorial testing to identify dominant variables that affect the output response. This approach is difficult to implement due to its mathematical complexity but will find relevance when there is a large number of dominant factors being considered. Its strength in partial factorial testing is also its weakness.

An estimated comparison of tests required between full factorial DOE technique and Taguchi's partial factorial DOE technique is shown below in Table 2-2.

Table 2-2. Comparison of partial factorial vs. full factorial DOE.

	Replications	Number of levels	Orthogonal array	Dominant factors within a group	Tests
Taguchi partial factorial DOE	20	3	L27	12	540
Full factorial DOE	20	3	-	12	10628820

The merits of the two methods are summarised in Table 2-3 (Thomas and Antony, 2005):

Table 2-3. Comparison between DOE techniques.

Characteristic	Taguchi partial factorial DOE	Full factorial DOE
Validity (on main effects)	Poor	High
Validity (on interaction)	High	Poor
Complexity	High	Low
Implementation	Difficult	Easy
Cost of experimentation	Low	High
Flexibility	Low	High

Since the project required the analysis of a large number of dominant factors, a full factorial analysis would have proved impossible. The Taguchi method offered the opportunity to reduce experimental time consumption; its potential loss of accuracy was offset by the skills and experience of the interdisciplinary team selected.

2.3 Experimental testing

An interdisciplinary team undertook a brainstorming session. This identified the factors that were expected to have an effect on the tensile strength of the splice. Figure 2-2 revealed the cause and effect graph resulting from the brainstorming session. There was a minimum of 18 possible factors found which were prioritised in terms of their likely effect on splice strength.

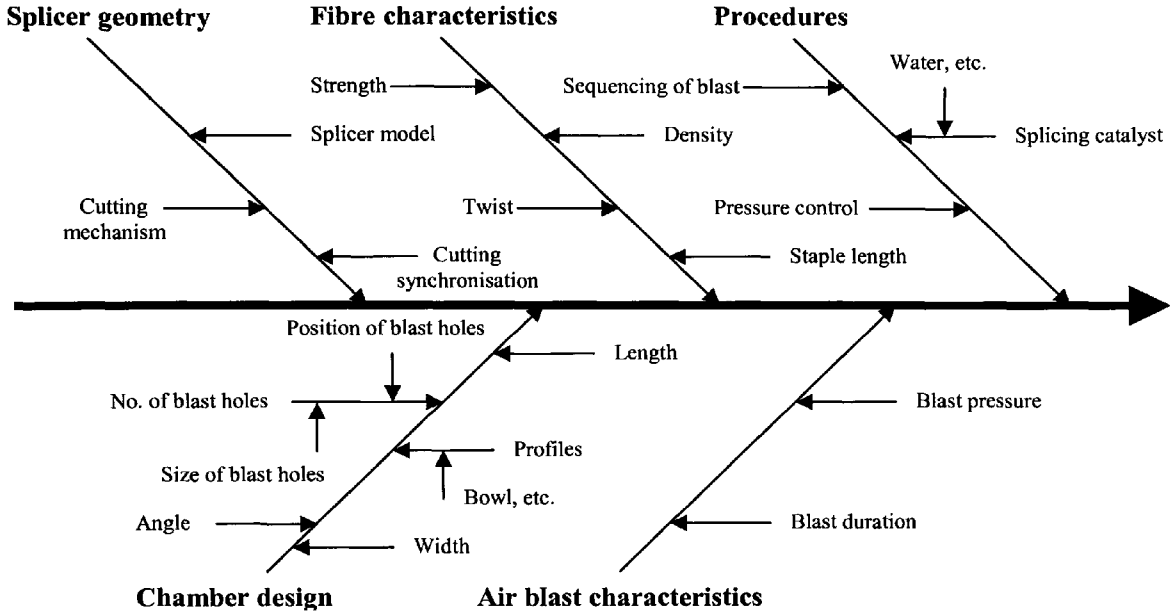

Figure 2-2. Cause and effect graph.

Due to the difficulty and cost of controlling certain parameters in practical production scenarios some have been discarded as noise factors (Coleman and Montgomery, 1993). The control and noise factors identified were:

Control factors:

Chamber width, Chamber depth, Chamber angle, Chamber blast hole diameter, Odd profiles, Blast duration, Blast pressure, Splice length, Number of blast holes, Sequencing of blasts, Cutting synchronisation.

Noise factors:

Temperature, Humidity, Fibre density (the structure of the filaments), Procedures, Blast hole (or holes) position, Testing and recording equipment tolerances.

A Pareto analysis was conducted on the possible control factors to identify major causes that affect the splice strength, resulting in the factor selection for Taguchi experimentation as displayed in Table 2-4.

Table 2-4. Selected splicing parameters.

Parameter	Factor
Blast pressure	A
Blast duration	B
Chamber design	C
Cutting synchronisation	D

Preliminary testing confirmed that each of the chamber design parameters (width, profile, angle, etc.) had an individual effect on the SRS. However all of the factors when pooled together in a particular chamber design had a significant overall effect on the splice strength. Chamber design was therefore included as a main factor for the experiment.

Before factor selection of the levels for the Taguchi experiment, the analysis of each control factor individually was needed to establish the boundary condition and the optimum setting that is understood to date to reveal how they each contributed to the strength of the splice.

Blast pressure was varied from 0 to 90psig on all chamber designs whilst maintaining all other parameters constant. Each recording was taken at intervals of 2.5psig to 5psig. Blast duration tests were conducted at four key pressures, namely 20, 40, 60 and 80psig. At each pressure, tests were conducted with blast durations of 0.5, 1, 2 and 3 seconds.

Three representative chamber designs were used. Two of these had the same basic V shaped geometry with only the width at the bottom of the splicing chamber differing as shown in Figure 2-3. The widths were 0.8mm (identified as 4483 straight) and 1.25mm (identified as 4485 straight) respectively. The third chamber design considered (identified as 4483 bowl) is of the same general profile as the 4483 straight chamber, but with a hemispherical bowl machined out at the centre of the chamber as shown in Figure 2-4. These three chamber designs represent the most common chambers developed by GTW Developments (Waters, 1998).

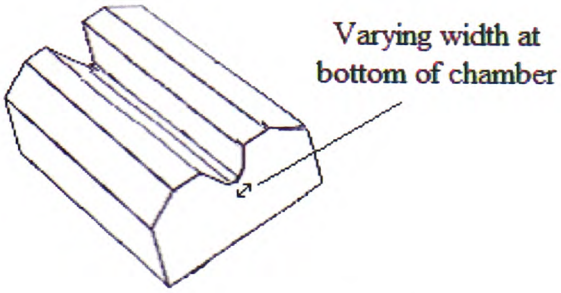

Figure 2-3. Straight chamber design.

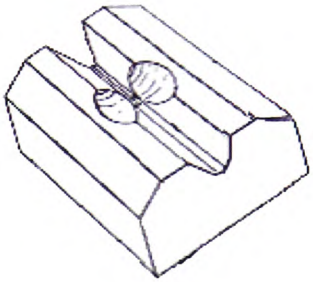

Figure 2-4. Bowl chamber design.

Another parameter, known as cutting synchronisation, was factored into the experiment. Splicers can be designed so that the air blast and cutting action may be separately controlled; this technique expands the range of performance of a splicer. On the experimental splicer, the range of cutting synchronisation was defined by an arbitrary scale ranging from 0 – 6. With the scale set at 0, the knives cut the yarns before the initial air blast, releasing the yarn ends filaments to move freely around the chamber from the outset. With the scale set at 3, the air blast and yarn cutting are simultaneous. With the scale set at 6 the yarns are cut during the air blast.

Splice strength is measured by its spliced retained strength (SRS). SRS is the strength of the spliced yarn expressed as the percentage of the parent yarn in which the splice was inserted (Sengupta, 2000). Equation 2-1 illustrates this relationship.

$$SRS = \frac{Spliced\ yarn\ strength}{Parent\ yarn(non-spliced)} \times 100 \qquad (2\text{-}1)$$

The chamber designs described previously were made on a milling machine with an accuracy of +/- 0.01mm and 0.1°. The parameters of the chamber that were not varied during this set of experiments were 4.8mm depth, 16mm length, 30° chamber angle and 4mm blast hole diameter at the centre of the chamber.

The splices were prepared on one type of polyester fibre, non-folded 1100dtex, 72 filament, with zero twist from Toray Fibers of Japan. Test samples were taken from a single bobbin to minimise variability.

The joints were made using a GTW Developments splicer, type 1-11. The compressed air was dried and filtered to create consistent air properties, using a Dominick Hunter dryer (type CRD refrigeration dryer), followed by an air filter (type AW30-F03D), and mist separator (type AFM30-F03D), with a 0.3μm 95% filtered particle size.

Pressure was controlled using an electro-pneumatic regulator (type ITV2050-312BS3-Q), which supplied a constant user specified pressure with an accuracy of +/- 0.03psig.

The tensile strength of the test samples were collected using a Lloyd Instruments tensile testing machine (type T5000), with a 100mm/min crosshead speed.

In order to maintain accurate results with the least amount of noise variation all the equipment was controlled with results collected electronically using an ARM7 control board and a PC. The experimental set-up used is shown schematically in Figure 2-5.

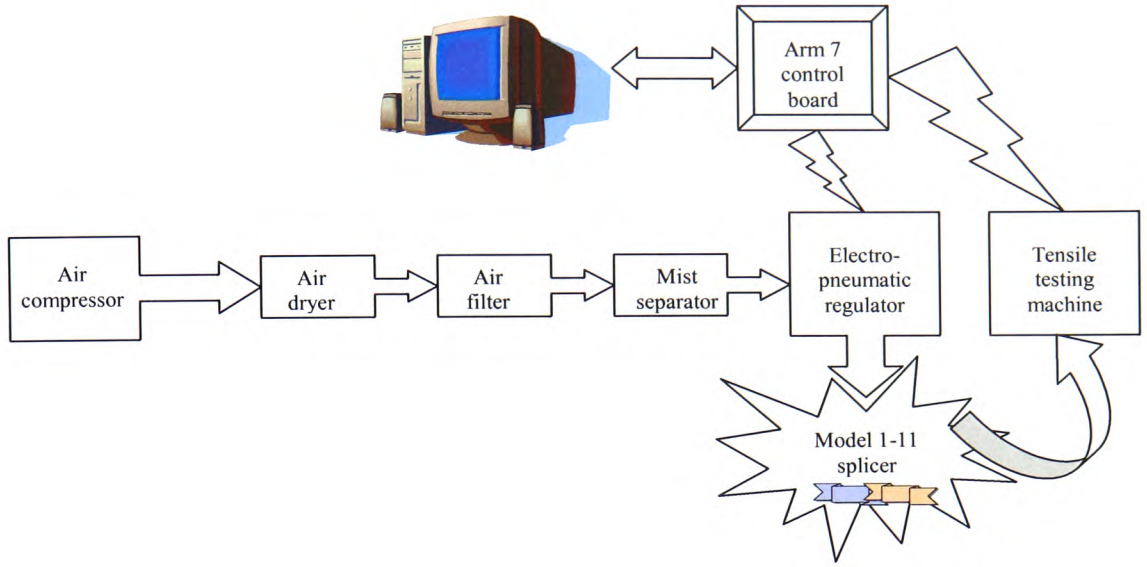

Figure 2-5. Experimental setup.

2.4 Data analysis

During the initial experimentation on the reference yarn, it was discovered that there was a substantial variation between *individual values* of SRS under the same experimental conditions as shown in Figure 2-6. It is possible that this variation is present because spliced bonds are unpredictable and consequently no two splices are the same due to the fact that the filaments are packed randomly throughout the yarn (Kaushik and Sharma, 1988; Kaushik *et al.*, 1987b; Rowlands *et al.*, 2000; Wei *et al.*, 2004).

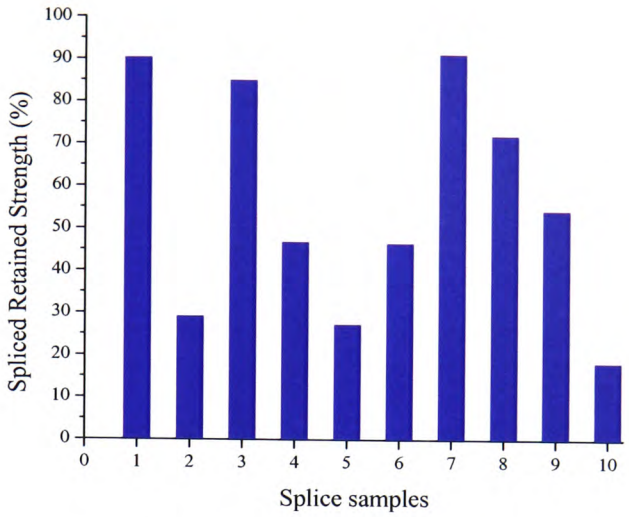

Figure 2-6. First 10 samples at 35psig on a 4485 straight chamber.

The variation previously described increases the complexity in discovering a correlation between the splicing parameters and strength. Therefore to minimise experimental error and assess variability of performance, 20 tests were executed for each experimental condition. Figure 2-7 shows the plot of SRS against pressure ranging from 0 to 90psig on a 4483 bowl chamber design. The SRS against pressure responses of the 4483 and 4485 straight chamber designs are shown in Figures 2-8 and 2-9 respectively.

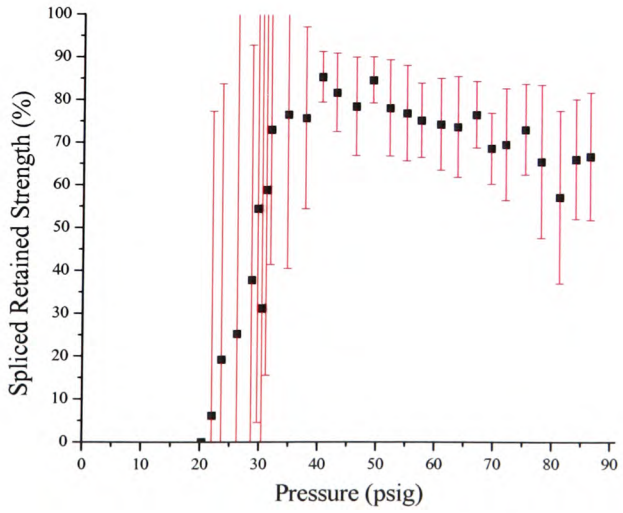

Figure 2-7. 4483 bowl chamber.

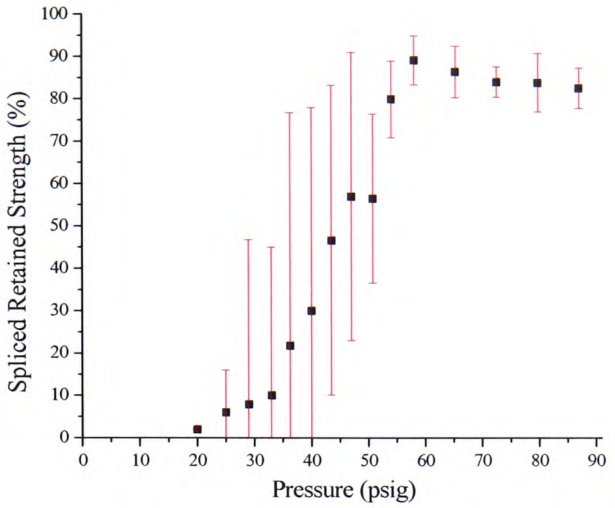

Figure 2-8. 4483 straight chamber.

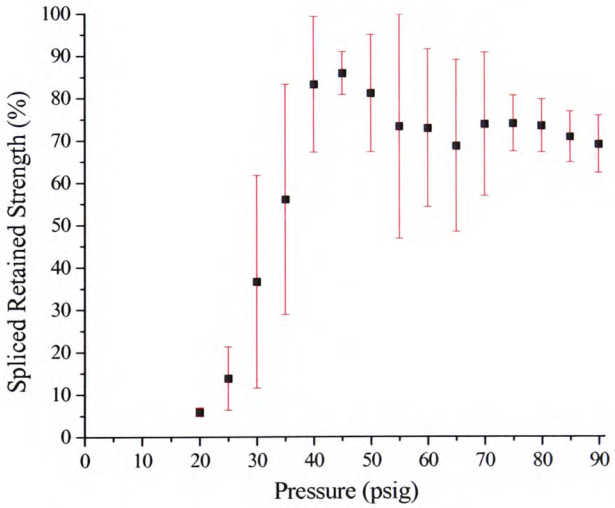

Figure 2-9. 4485 straight chamber.

Only specific test configurations were chosen for blast duration experimentation. Only selected pressures at key levels were selected for testing which covered the whole span of the experimental pressure range. Figures 2-10 to 2-12 revealed the blast duration responses across the four selected pressures on each of the three chamber designs. As

can be seen the SRS vs. pressure curves, Figures 2-7, 2-8 and 2-9, are all consistent with the blast duration test results shown in Figures 2-10, 2-11 and 2-12.

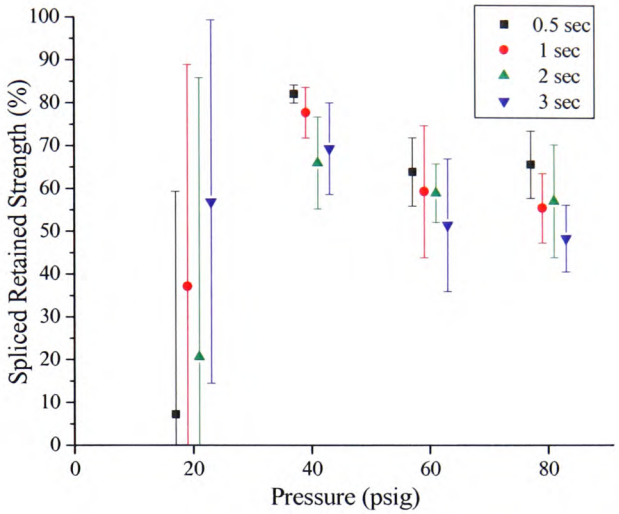

Figure 2-10. 4483 bowl chamber.

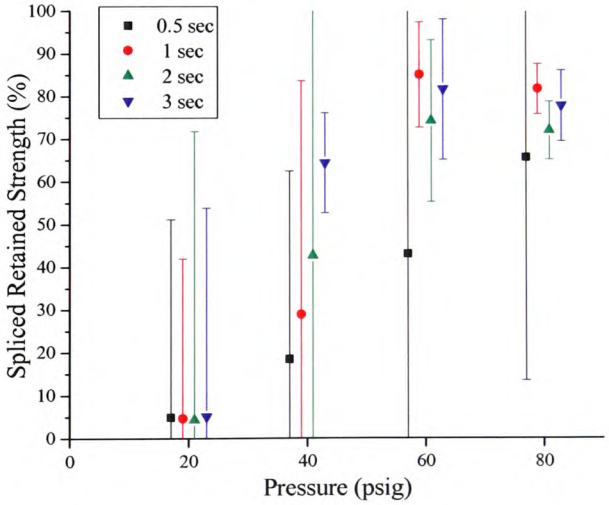

Figure 2-11. 4483 straight chamber.

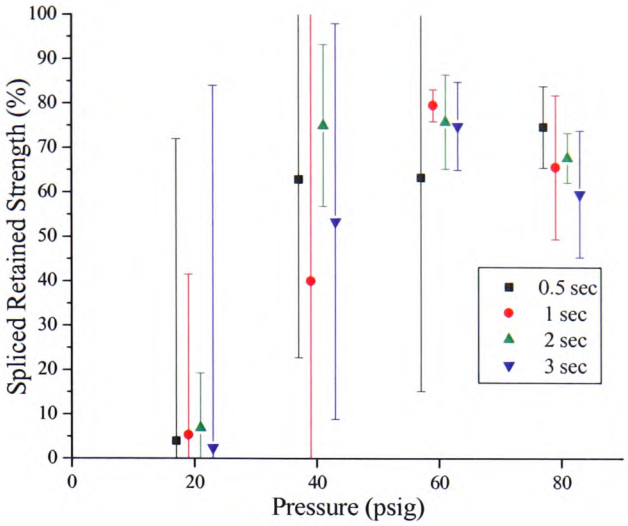

Figure 2-12. 4485 straight chamber.

Although the general form of the strength/pressure curves were similar for all splicing chambers, there were some significant differences that need to be addressed:

- The 4485 straight chamber produced splices of measurable strength only after about 35psig, at which pressure the 4483 bowl chamber was already producing strong splices.
- The 4483 straight chamber did not begin to produce strong splices until approximately 45psig.
- The 4483 straight chamber produced splices of maximum strength (89%) at approximately 60psig, whereas the 4483 bowl and 4485 straight chambers reached their maximum (85% and 86% respectively) at the much reduced figure of 45psig.
- After the relevant maximum SRS's were obtained, the rate of decrease was faster with the 4483 bowl than with the 4483 straight and 4485 straight chambers.

Below 0.5sec it was likely that there was insufficient intermingling for splices to form. Above 3sec had the opposite effect with filaments being ruptured, as a result of prolonged exposure to the blast. This would also result in weaker splices.

Following the preliminary investigation, approximate optimum settings for the Taguchi DOE were established. Three levels were considered due to the non-linearity of the splicing functions. Therefore an L_{27} OA was chosen for the experiment. These parameter settings are revealed in Table 2-5. Figure 2-13 displays the L_{27} OA and the factor identification results.

Table 2-5. Selected splicing parameters.

Factor	Level 1	Level 2	Level 3
A	40psig	50psig	60psig
B	1sec	1.5sec	2sec
C	4483 straight	4485 straight	4483 bowl
D	0	3	6

	Main Factors and Interactions									
Run	A	B	AB	AB	C	AC	AC	D	AD	AD	SRS (%)
1	1	1	1	1	1	1	1	1	1	1	51.63
2	1	1	1	1	2	2	2	2	2	2	73.24
3	1	1	1	1	3	3	3	3	3	3	81.42
4	1	2	2	2	1	1	1	2	2	2	79.18
5	1	2	2	2	2	2	2	3	3	3	78.94
6	1	2	2	2	3	3	3	1	1	1	77.77
7	1	3	3	3	1	1	1	3	3	3	70.82
8	1	3	3	3	2	2	2	1	1	1	76.39
9	1	3	3	3	3	3	3	2	2	2	76.08
10	2	1	2	3	1	2	3	1	2	3	82.33
11	2	1	2	3	2	3	1	2	3	1	88.10
12	2	1	2	3	3	1	2	3	1	2	74.51
13	2	2	3	1	1	2	3	2	3	1	76.70
14	2	2	3	1	2	3	1	3	1	2	86.27
15	2	2	3	1	3	1	2	1	2	3	73.65
16	2	3	1	2	1	2	3	3	1	2	77.85
17	2	3	1	2	2	3	1	1	2	3	77.94
18	2	3	1	2	3	1	2	2	3	1	68.46
19	3	1	3	2	1	3	2	1	3	2	78.20
20	3	1	3	2	2	1	3	2	1	3	60.56
21	3	1	3	2	3	2	1	3	2	1	65.52
22	3	2	1	3	1	3	2	2	1	3	71.98
23	3	2	1	3	2	1	3	3	2	1	80.52
24	3	2	1	3	3	2	1	1	3	2	67.86
25	3	3	2	1	1	3	2	3	2	1	54.27
26	3	3	2	1	2	1	3	1	3	2	71.72
27	3	3	2	1	3	2	1	2	1	3	65.57

Factor A		
L1	L2	L3
73.94	**78.42**	68.47

Factor C		
L1	L2	L3
71.44	**77.08**	72.32

Factor B		
L1	L2	L3
72.83	**76.99**	71.01

Factor D		
L1	L2	L3
73.06	73.32	**74.46**

Largest is best:	Factors	A2	B2	C2	D3

Interaction AB			
	B1	B2	B3
A1	68.76	78.63	74.43
A2	**81.65**	78.87	74.75
A3	68.09	73.45	63.86

Interaction AC			
	C1	C2	C3
A1	67.21	76.19	78.42
A2	78.96	**84.11**	72.21
A3	68.15	70.93	66.32

Interaction AD			
	D1	D2	D3
A1	68.60	76.16	77.06
A2	77.97	77.75	**79.54**
A3	72.59	66.04	66.77

Figure 2-13. L_{27} orthogonal array and optimum factor identification.

The results of the ANOVA for splice strength, as shown in Table 2-6, revealed that A was the only statistically significant factor with factors B and C marginally close to being 95% statistically significant. Factor D was found to be statistically insignificant.

Table 2-6. ANOVA of each splice characteristic.

Spliced Retained Strength				
Factors	**DOF**	**SS**	**MS**	***F* ratio**
A	2	8951	4475.5	7.71 **
B	2	3374.3	1687.2	2.91
C	2	3313.6	1656.8	2.85
D	2	199.8	99.9	0.17
AB1	2	523.6	261.8	0.45
AB2	2	3267.4	1633.7	2.81
AC1	2	4143.6	2071.8	3.57 *
AC2	2	1691.4	845.7	1.46
AD1	2	1749.4	874.7	1.51
AD2	2	2306.7	1153.3	1.99
Error	519	301389	580.7	N/A
Total	539	330909.8	N/A	N/A

Notes:
* Indicates factor/interaction is statistically significant at 5% level of significance - $F(0.05,2,519) = 3.01$
** Indicates factor/interaction is statistically significant at 1% level of significance - $F(0.01,2,519) = 4.65$

The main SNR that is of interest in the splicing process is the 'largest is best' as shown by Equation 2-2. Largest is best SNR was selected because the desired outcome of this experiment was to acquire the maximum splice strength (Wu *et al.*, 1991).

$$S/N_{\text{largest is best}} = -10\log\left(\frac{1}{n}\sum\left(\frac{1}{y_i}\right)^2\right) \tag{2-2}$$

Where n is the number of values at each test condition and y_i is each observed value.

Figures 2-14 and 2-15 illustrate the SNR and the mean response of the SRS at each level of the selected factors respectively. As can be seen, factors B & C resulted in the largest mean SRS at level 2, even though their corresponding largest values of SNR

were at level 3. Therefore, since neither factor was statistically significant, the levels were chosen in favour of their mean response (Bendell *et al.*, 1989, 99-112).

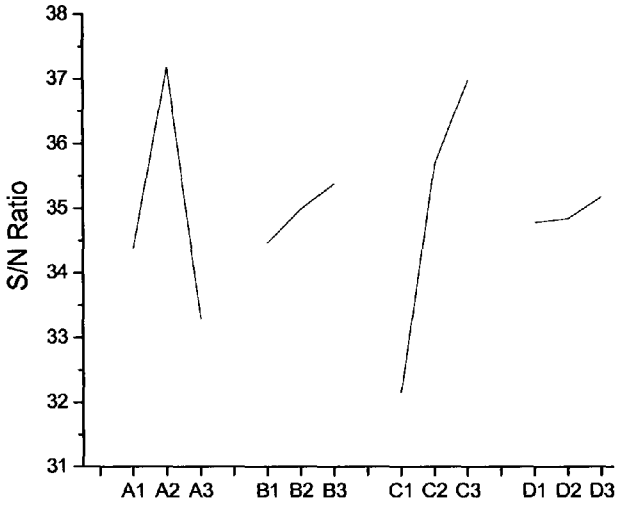

Figure 2-14. SNR response plot.

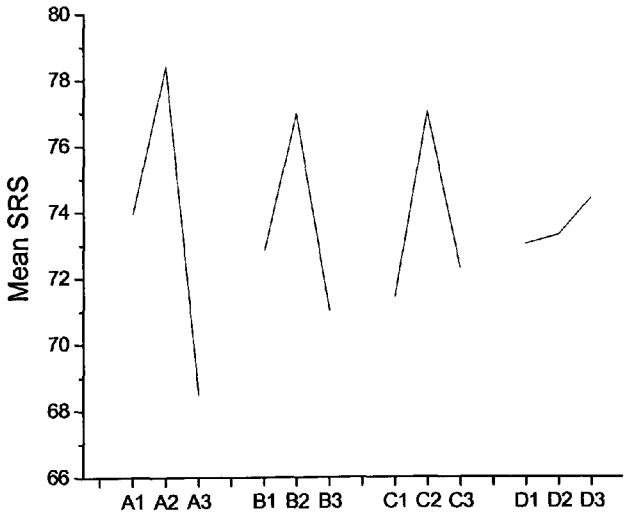

Figure 2-15. SRS response plot.

The strength of the interactions AC and AD required further investigation (Nair, 1992). The interaction plots as shown in Figures 2-16 and 2-17, revealed intersections, indicating strong interactions. As A is a dominant factor it was essential to select the corresponding factors at levels where the maximum SRS point resides. Therefore from the graphical analysis, ANOVA and the factor interactions, the optimum factor levels were selected as A2, B2, C2 and D3.

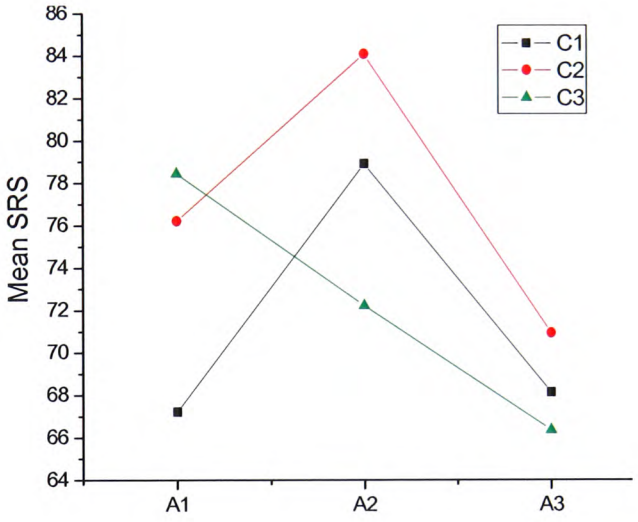

Figure 2-16. Interaction AC.

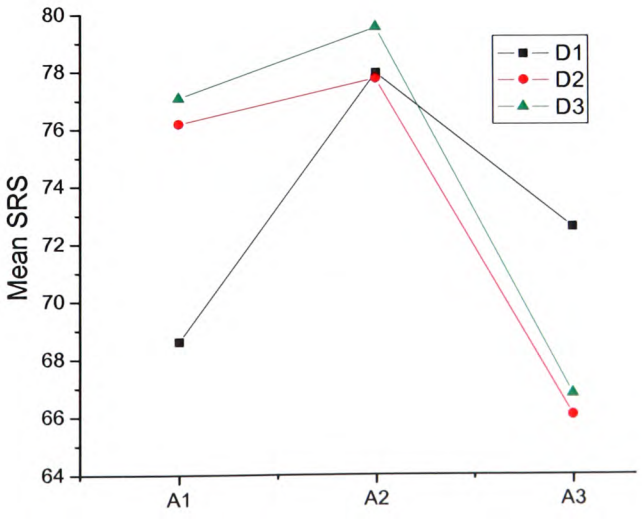

Figure 2-17. Interaction AD.

A confirmatory run was conducted to validate the deduced optimum factor levels. The results are shown in Table 2-7 (Antony and Antony, 2001; Bendell *et al.*, 1989, 99-112). The confirmatory run was undertaken using the same experimental setup as the Taguchi experimentation, and with the same number of replications. Table 2-7 compares the optimum set of parameters resulting from the Taguchi experiment, with the splice performance normally achieved using standard industry practice. The splice strength increased by 14% with a decrease in variance of 55.5%.

Table 2-7. Confirmatory run.

	Before	After	Increase/Decrease (percent)
Tensile Strength	77.21	88.04	+14.03%
Variance	0.2	0.089	-55.5%

2.5 Conclusion

In this chapter, the design and implementation of the Taguchi DOE method applied to the splicing process was undertaken. The method has been described in detail and compared to a full factorial analysis. The outcome of this experiment revealed that the Taguchi DOE method could be applied successfully to the splicing process. The optimum splicer parameter settings deduced from the Taguchi method were A2, B2, C2 and D3.

Factor A: Level 2 = 50psig
Factor B: Level 2 = 1.5sec
Factor C: Level 2 = 4485 straight chamber
Factor D: Level 3 = 6

The Taguchi analysis revealed that though relevant, blast duration (factor B) was the least significant of the four parameters, provided that extreme conditions were avoided. Of the remaining parameters, since the experiment had been designed to yield

maximum SRS as the desired outcome, blast pressure (factor A) emerged as the most important.

Strength was also affected by chamber design and cutting synchronisation (factors C and D) through their interaction with blast pressure. However, within the range of experimental parameters chosen, these were second order effects. Therefore the levels of factors C and D were selected to coincide with the maximum SRS of factor A at its optimum setting, level 2, due to factor A being statistically significant.

As mentioned above, chamber design has an influence on the splice strength of the reference yarn. This result has not been observed in published literature. However, this is no great surprise; the absence of such information is probably due to the fact that splicer manufacturers have been protective of their intellectual property. The wide variation in splicing chambers observed in real splicers serves to suggest that much work on chamber designs has been done, but remains unpublished in the interest of company confidentiality.

Improved strength and robustness of the splicing process on the reference yarn has therefore been demonstrated. Hence the Taguchi DOE method is a valid statistical tool in this context that can be used efficiently and effectively to achieve the optimum parameter settings of any specific target output with using only a truncated number of test samples.

Chapter III

Optimising splicing parameters for splice aesthetics for a continuous filament synthetic yarn

Abstract – *Earlier chapters have addressed the effect of variables such as air pressure and splicing chamber design upon the splice characteristic output of strength. This chapter continues the work on splice strength from the previous chapter, in this instance addressing the issue of splice appearance optimisation. The research uses the previously validated statistical methods of Taguchi DOE analysis. By combining the results from the splice strength experiments with this new work on splice appearance, it has been demonstrated that the strongest splice does not in general correspond with the best appearance. In general, therefore, it is necessary to establish an overall optimum splicer configuration, offering an acceptable compromise between splice strength and splice appearance.*

3.1 Introduction

For acceptable performance, manufacturers require a spliced joint to perform well and to resemble closely the strength and appearance of the original yarn (Lam and Cheng, 1997). It is generally agreed that the two most important splice characteristics are splice strength and appearance (Lewandowski and Drobina, 2004).

Though splice strength is an obvious requirement for a splice, appearance is not. Deterioration of splice appearance is generally associated with broken filaments, or filamentation. Filamentation has only a modest effect on splice strength, but its real importance is not related to strength, nor to aesthetics; however it was critically important to processing efficiency. Broken filaments may run back, getting caught in components of the machinery, making the splice unacceptably bulky and in extreme circumstances the entire yarn may break. An ugly splice with high levels of filamentation will be no better than a poor knot or weak splice and ultimately the machine efficiency and fabric quality will be unacceptable.

There already exists a general understanding of how splice parameters affects splice strength and splice appearance but there is little or no published literature on how the two parameters interact to produce a splice with good performance. In order to meet the combined requirements of achieving high joint strength and consistent quality of appearance, it was first necessary to assess the effect of the splicing parameters individually, and then assess how they might work in combination. The interaction needed to be understood, characterised and finely tuned (Peace, 1993, pp.23-54).

It was found from the previous chapter that splice strength was negligible until a critical lower value of pressure was reached. Splice strength then increases linearly with air pressure until a critical upper value of pressure was reached. Once that pressure was exceeded, strength begins to decrease.

The proposal for this chapter is to use the Taguchi DOE technique to perform two functions:

- Firstly to optimise the splicing process for splice appearance alone
- Secondly to optimise the splicing process for both strength and appearance combined.

The Taguchi DOE method, already validated in the earlier work, was equally relevant for splice appearance optimisation because the same large number of variables affect the splicing process.

This chapter discusses the design and implementation of the Taguchi DOE for achieving optimum splice appearance. It addresses the input parameters that affect the two output responses of splice strength and splice appearance alone and collective. The Taguchi DOE analysis for splice appearance was combined with the previous ANOVA for splice strength, giving preference to the statistically significant factors, to obtain an overall "compromise" optimum splice. Process parameters could then be identified to maximise the overall acceptability of the splices in a specific yarn. Finally, confirmatory runs were undertaken to illustrate the performance of the optimisation technique for both splice appearance and the optimum compromise.

3.2 Optimising splice appearance utilising the Taguchi DOE method

Applying the Taguchi DOE method to optimise splice strength, as discussed in the previous chapter, was very successful, yielding robust splices, which were stronger with a drastically reduced variability.

It seemed that the process of optimising splice appearance would be subjected to the same large range of control factors. The Taguchi method therefore seemed equally relevant, and could, if properly implemented, simplify significantly the experimental design. The same potential pitfalls needed to be addressed along with the potential loss

of accuracy arising from the partial factorial analysis. This would be accomplished by conducting confirmatory runs to prove the success or failure of the splicing process optimisation.

The experiments were designed to subject the standard yarn to a wide range of experimental conditions, measuring strength and appearance for each condition, using a sampling method defined by the Taguchi DOE. From the Taguchi factor identification and level optimisation analysis, an optimised set of processing conditions would emerge, giving a compromise between splice appearance and strength (Antony and Antony, 2001). The results emerging from the Taguchi method were to be confirmed through a set of individual confirmatory runs.

For the experiments to have any validity, acceptable and reproducible measures of splice strength and appearance were needed. SRS has already been established in Chapter 2 (Equation 2-1) and was expressed as a simple percentage of the parent yarn strength. This measure is well documented, and, within the normal limits of experimental error, is completely objective (Sengupta, 2000).

Splice appearance was more difficult to assess. Unlike SRS, appearance is a subjective measure. In principle, using a device such as an Uster could assess appearance, but the detailed structure of a splice is not completely analogous to that which is defined as yarn hairiness (Nikolic *et* al., 2003). The notion of using hairiness as a measure was soon rejected for the simple fact that a splice made in a continuous filament yarn, with just a few broken filaments, would score quite well on a hairiness test and yet such a splice could prove very disruptive to yarn processing. A method of assessment of appearance was therefore required, which would have some relevance to processing efficiency.

3.2.1 Splice appearance characterisation

Consider the general characteristics of a splice. In general, all splices have a characteristic and broadly reproducible form as indicated in Figure 3-1.

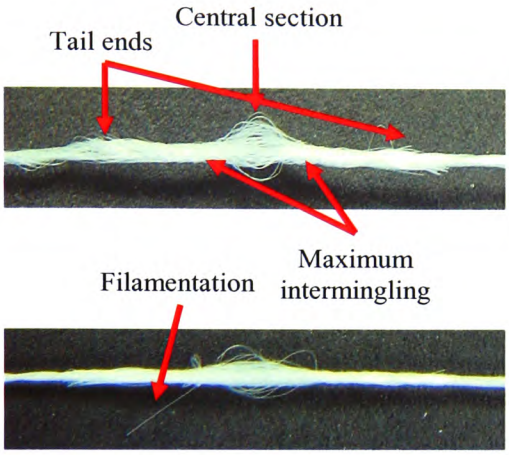

Figure 3-1. Characteristic form of a splice.

The central section of the structure remains untwisted and roughly parallel to the chamber axis. These pictures were taken on the 4483 "bowl" chamber, defined in the previous chapter, with the spreading of the filaments at the centre being very marked. Had a simple straight-section chamber been used, the filaments in the central section would have lain flatter, nearly parallel. The bowl form has been chosen to show the central section more distinctly.

Between the central section and the ends of the splice, the yarns are intertwined, with the maximum amount of intermingling occurring nearest to the central section. In the main section of the splice, the fibres lie in dense clusters; therefore there is an increase in yarn diameter in the splice, since two yarns occupy the space normally occupied by one. The increase in diameter is generally modest, because the fibres in the splice are generally more tightly packed than in the parent yarn. At each end, the splice usually

terminates in a small "tail" where the extreme tips of the spliced yarns have not been fully bound into the structure.

In certain circumstances, the splice may demonstrate filamentation. This will occur if some aspect of the splicing process, interacting with the mechanical properties of the yarn, has led to one or more filaments being broken or not being fully bound into the splice. As filamentation increases, appearance is degraded, and processing efficiency falls.

For this experiment to yield quantifiable results, it was necessary to use a scale which would describe the aesthetics of a splice. The approach is vulnerable to the criticism that it is inherently subjective. Therefore the scale of yarn appearance needed to incorporate as many objective elements as possible. The Retained Yarn Appearance (RYA) scale was devised and validated through the inspection and grading of hundreds of splices, Cheng and Lam (2000b).

It was necessary to analyse those elements of a splice which contributed to the quality of its appearance. At a subjective level, there was generally little dispute about what constitutes a "good" or a "bad" splice. Examples of these are:

- Splices that have no visible filamentation have a well-ordered structure in the main section of the splice, with all fibres bound into the structure thus have no tails, should have a high rating.
- Splices that have a moderate level of filamentation, though with a less ordered structure in the main section of the splice than that described above, are still just as acceptable in terms of appearance and processability. These splices should have a moderate rating.
- Splices that have extreme filamentation, causing severe disruption of the structure, are completely unacceptable in terms of appearance and processability. These splices should have a low rating.

Filamentation was assessed by counting the number of filaments which were protruding from the splice, either through stray filaments not being bound into the splice or through filaments being damaged during the splicing process. If 10% or less of the filaments within a splice were protruding, the filamentation level was defined as "slight".

If the yarn ends are not fully bound into the splice the result was an excessive tail length. Tail ends protrusion was assessed as "slight" if the tail length was less than or equal to the diameter of the splice, and as "large" if the tail length was greater than the splice diameter.

Levels of filamentation were not the only measure of splice appearance. Bulk or diameter of a splice was considered. Some increase in diameter is inevitable when yarns are spliced; theoretically a splice should have a diameter greater than its parent yarns by a factor of $\sqrt{2}$. In a good splice, the increase can be less than this, because the filaments become densely packed. In poorer splices, the filaments are less tightly bound into the structure and therefore can occupy a much greater volume.

Taking the value of $\sqrt{2}$ to be approximately 1.5, "slight" diameter increase was used to describe a diameter that was less than or equal to 1.5 times the diameter of a single yarn end while "large" diameter increase is anything above this.

The final grade of RYA was a combination of various attributes at different weights. Double weighting was given to tail ends and filamentation because these areas are most problematic in industry.

A scale from 1-10 was finally used, based upon the appearance of each spliced joint as summarised in Table 3-1.

Table 3-1. Splice appearance scale.

	Splice appearance scale									
Appearance features	1	2	3	4	5	6	7	8	9	10
Slight diameter increase			■	■	■	■	■	■	■	■
Large diameter increase	■	■	■	■	■	■				
Slight filamentation				■	■	■	■	■		
Large filamentation	■	■	■	■	■					
No tail ends								■	■	■
Slight tail ends		■	■	■	■	■	■	■	■	
Large tail ends	■	■								
Slight central section increase				■	■	■	■	■	■	■
Large central section increase	■	■	■	■						

Three examples should suffice to demonstrate the use of the system. Figures 3-2 to 3-4 show three examples A, B and C respectively. Each sample was placed under controlled tension while assessing the yarn diameter, tail ends, breakage and filamentation.

Sample A: This splice met virtually all of the criteria defined above relating to a splice of high quality. It was given a score of 9.

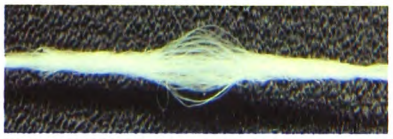

Figure 3-2. Splice sample A.

Sample B: This splice revealed a very high level of filamentation, and would almost certainly perform very badly in a textile process. It was given a score of 1.

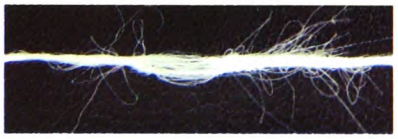

Figure 3-3. Splice sample B.

Sample C: This splice was the most relevant to the validation of the RYA scale, because it contains several elements, which are relevant to the scoring system. It was given an overall RYA score of 6 as shown below.

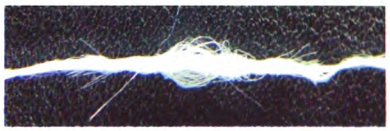

Figure 3-4. Splice sample C.

Tail length = 1.7mm

Score 3 (Weighted maximum 4).

Broken filaments = 4, loose filaments = 6, therefore filamentation = 7%
Score 2 (Weighted maximum 4)

Diameter = 2.5mm (4.2mm at centre), therefore diameter increase was slight
Score 1 (Weighted maximum 2).

The RYA scale was tested over a wide range, with good agreement between observers. With acceptable and reproducible measures of strength and appearance defined, the main experiment could be designed.

3.2.2 Factor level identification

The steps previously defined in section 2.2.1 are utilised here but with the outcome focused on the optimisation of splice appearance. The tests performed in this research were all done on the same simple continuous filament yarn that was chosen as a suitable baseline from the previous work on optimising splice strength. This yarn was an 1100dtex, continuous 72 filament polyester with zero twist.

The brainstorming session was undertaken with the same interdisciplinary team because of their experience of the previous Taguchi analysis relating to splice strength. Of course, splicing chamber design was by far the principal factor. In addition, it was concluded that, like splice strength, splice appearance was probably driven principally by blast pressure and blast duration. Cutting synchronisation was also factored into the experiment because it was known to have an effect on the appearance of a splice, specifically on the tail sections located at both ends of the splice.

Table 3-2 reveals the four parameters that were identified throughout the brainstorming session, which have an effect on splice appearance.

Table 3-2. Selected splicing parameters.

Parameter	Factor
Blast pressure	A
Blast duration	B
Chamber design	C
Cutting synchronisation	D

Initial experimentation was conducted on each test parameters individually to reveal the exact relationship they have with splice appearance. These relationships were used to select the factor identification levels to be used in the Taguchi DOE analysis. The test parameters were varied as follows:

- Blast pressure was tested over the range from 0 to 90psig, at intervals of 5psig.
- Four blast durations were used at four key blast pressures of 20, 40, 60 and 80psig, with 0.5, 1, 2 and 3 seconds, respectively.
- A system of cutting synchronisation was used, defined by an arbitrary scale ranging from 0 – 6:
    - 0 – With the control set at 0, the knives cut the yarns before the start of the air blast, releasing the yarn ends filaments to move freely around the chamber from the outset.
    - 3 – With the scale set at 3, the air blast and yarn cutting are simultaneous.
    - 6 – With the scale set at 6 the yarns are cut during the air blast.

Three representative chamber designs were used, the same designs used in the optimisation of splice strength.

For each experimental condition, 20 splice repetitions were undertaken, subjected and assessed under the same controlled tension to reduce variability. The average splice appearance was assessed using results from 5 independent engineers under each experimental condition, on the RYA scale from 1 to 10. The splices were prepared on a Model 1-11 splicer, from GTW Developments Ltd.

The experimental setup was identical to that used in the earlier experiments on splice strength, to which was added a large optical microscope, with an embedded digital camera. This experimental setup is shown schematically in Figure 3-5. Splice appearance of the test samples, measured under controlled tension, were assessed using two systems:

- Photographs of the entire splice, taken on the digital camera at 2016x1512 resolution embedded into a microscope
- Images of individual filaments, taken from a scanning electron microscope (SEM).

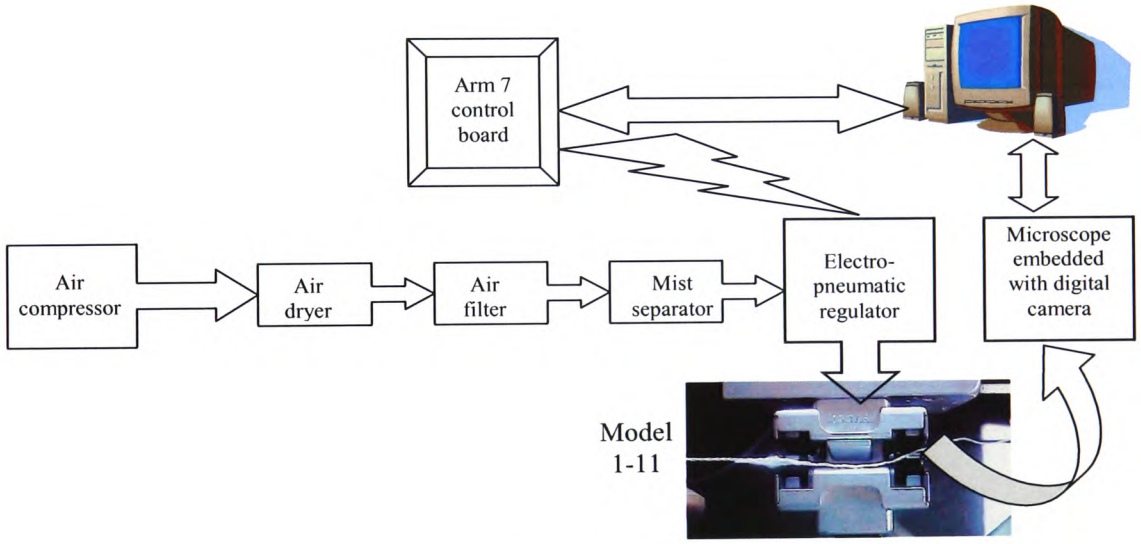

Figure 3-5. Experimental setup.

3.3 Initial experimentation results

The RYA rankings were on a scale of 1 to 10, but the intention was to compare the appearance results with the corresponding individual results for SRS. SRS had been recorded on a percentage scale, so the RYA rankings were simply multiplied by a factor of 10, to allow comparison graphs to be drawn on the same axes.

The first tests were conducted to reveal if splice appearance had the same output response to that of strength, when exposed to the same range of input parameters. The RYA responses over the key blast duration ranges, using the 4483 bowl, 4483 straight and 4485 straight chamber designs are shown in Figures 3-6 to 3-8 respectively.

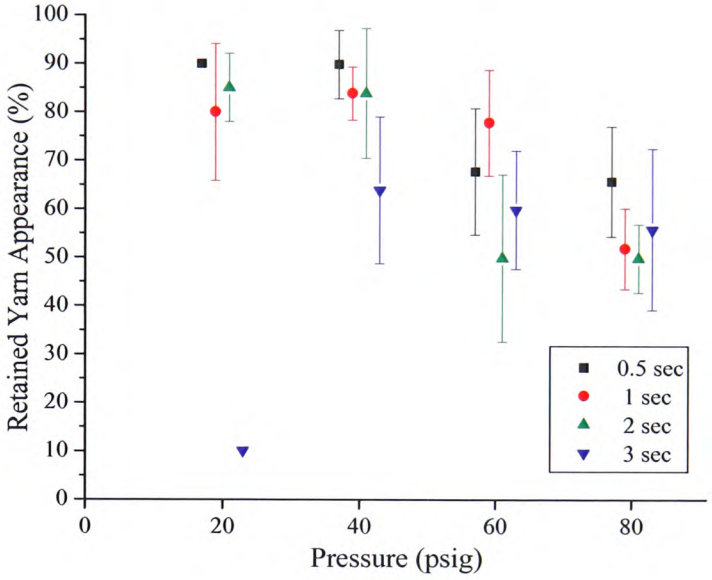

Figure 3-6. 4483 bowl chamber.

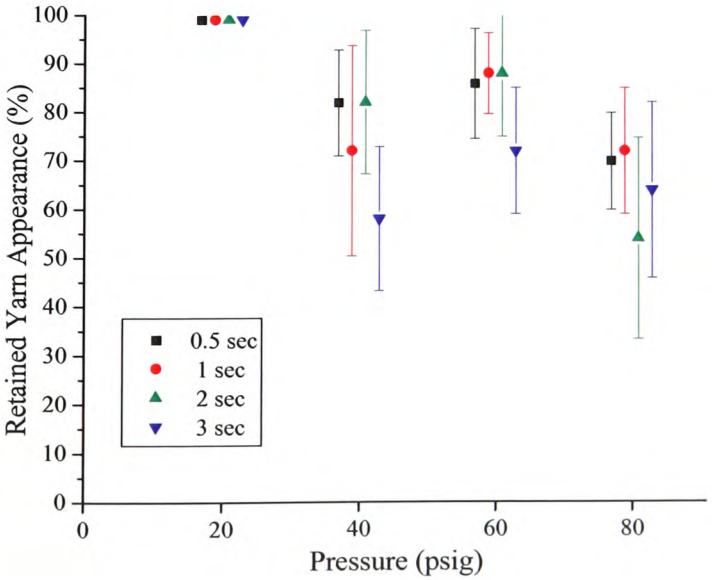

Figure 3-7. 4483 straight chamber.

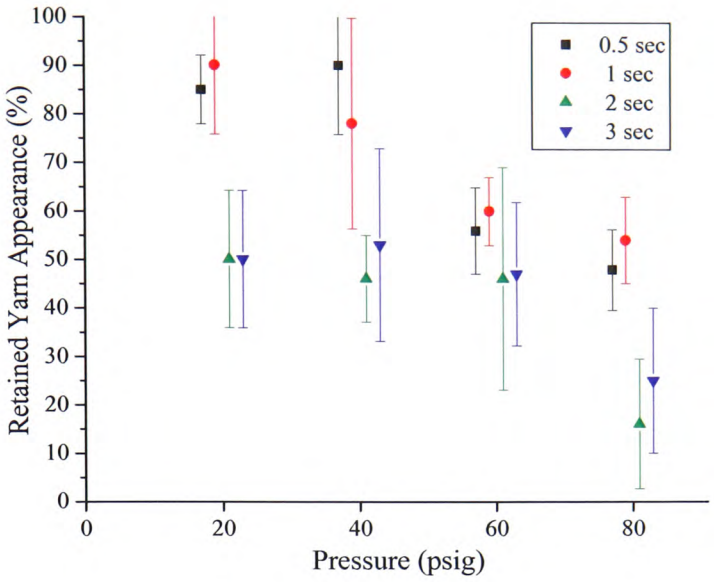

Figure 3-8. 4485 straight chamber.

Overall, as can be seen from Figures 3-6 to 3-8, all output responses are generally similar to their SRS equivalent from Chapter 2. There were a few detailed differences, for example, splice strength reached a maximum at a blast time of approximately 1.5 seconds, whereas splice appearance was acceptable at both 0.5 second and 1 second. However, the similarities were such that it was deemed appropriate to continue to the next stage, at greater detail, using a single blast time of 1 second. Figures 3-9 to 3-11 show the RYA and SRS responses over the experimental air pressure range, with the three chosen experimental splicing chambers, all at blast durations of 1 second.

Although the results for strength and appearance revealed a broad level of correspondence, on all three splicing chambers, the detail differences were such that a small amount of further analysis was necessary. This research work did, after all, have its origins in the application of real splicers in the real world of textiles, so a strong splice would be useless in a real environment, if it was too filamented to process well. Conversely, a very smooth splice would be useless if it failed under a reasonable load.

It was decided that it would be appropriate to identify some kind of compromise between the two spliced characteristics. In each case, a third response was generated, by multiplying the two mean percentages at each pressure level. This yielded a curve, which provided a means of identifying a compromise i.e. a set of conditions which produced a strong splice with acceptable appearance. The results are included in Figures 3-9 to 3-11.

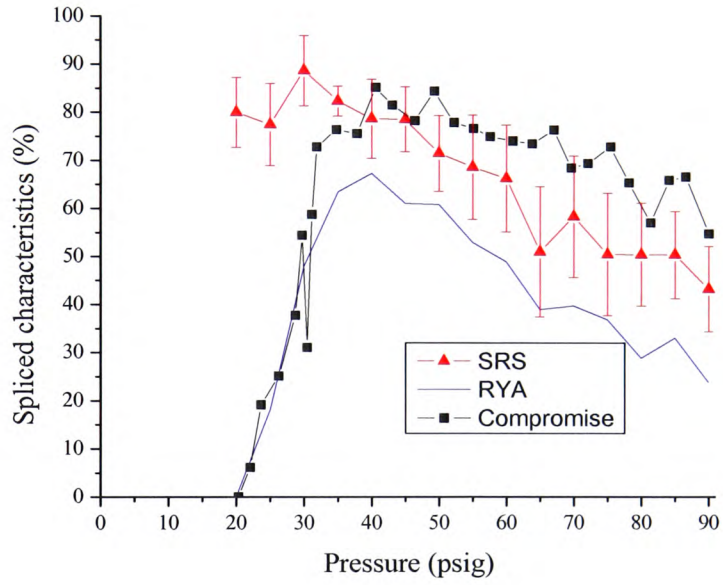

Figure 3-9. 4483 bowl chamber.

With the 4483 bowl chamber, the splice strength increased sharply after the air pressure exceeded 20psig, reaching a maximum at around 40-50psig. It then fell off fairly uniformly as air pressure was increased further.

The RYA shows that the splice made at the lowest pressure had good appearance, and remaining good until approximately 40psig. Splice appearance then decreased fairly uniformly as air pressure was increased further. It is likely that higher pressures create stronger vortices, which agitate the filaments enough to cause damage, affecting both

strength and appearance. The rate of decrease of RYA is broadly similar to the corresponding decline in SRS.

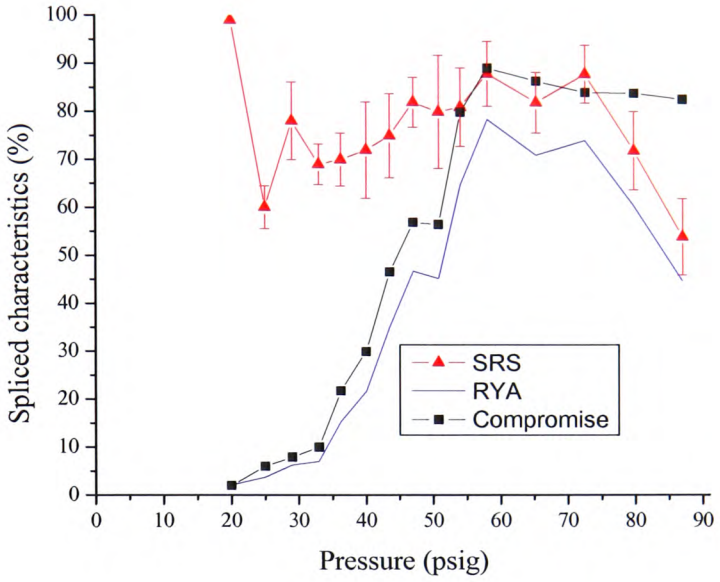

Figure 3-10. 4483 straight chamber.

With the 4483 straight chamber, splice strength increased after the air pressure reached 20psig. The rate of increase thereafter was much more gradual in comparison with the bowl chamber, reaching a maximum at around 55-60psig. It then fell off fairly uniformly as air pressure was increased further.

The splice appearance showed a local peak at 30psig, but the primary trend showed that it improves slightly with increasing pressure, but it did not reach a well defined maximum. In fact, it is probably likely (bearing in mind the subjective nature of the assessment) that RYA was constant across the range from 45-75psig. Over this range, the optimum amount of intermingling takes place with the least amount of filamentation.

As air pressure was increased further, appearance degraded fairly sharply, with increasing filamentation. At these levels, splice strength was far less sensitive than appearance to increasing air pressure.

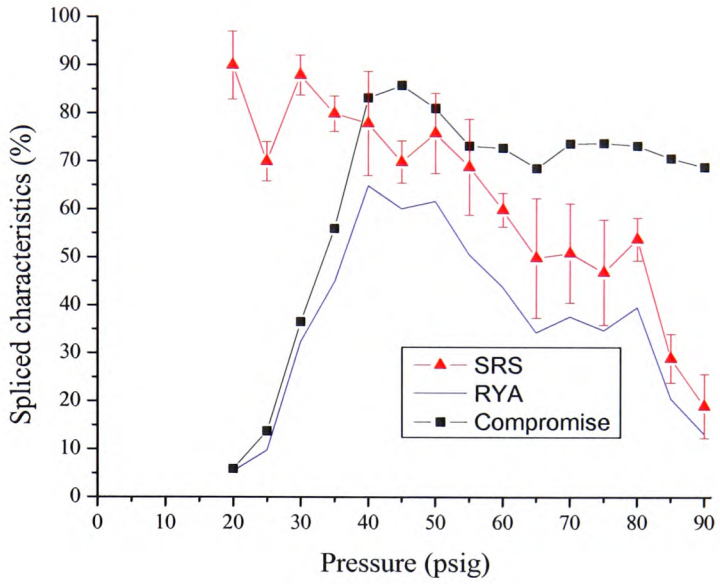

Figure 3-11. 4485 straight chamber.

With the 4485 straight chamber, SRS increased sharply after the air pressure reached 20psig, reaching a maximum at around 40-50psig. It then fell off fairly uniformly as air pressure was increased further. The splice appearance revealed a distinct peak at 30psig. It then fell off fairly uniformly as air pressure was increased further. The rate of decrease was somewhat faster than the corresponding drop of splice strength.

One clear conclusion can be drawn. Just as was the case in the splice strength experiments, the characteristics of the straight chambers and bowl chamber are very different. Perhaps the most significant observation was that the 4483 bowl chamber revealed that the strength and appearance curves are broadly in step, but with noticeable differences between the two curves in the straight chambers, startlingly so with the 4483 straight.

In terms of the quest for a compromise set of conditions, all three chambers seem to yield the same conclusion. The best compromise corresponds to that pressure when the splice strength first reaches its peak value.

At pressures exceeding 60psig, both the 4483 bowl and 4485 straight chambers consistently produced splices of poor appearance. Only at pressures exceeding 80psig do splices produced on the 4483 straight become constantly unacceptable. Below these pressures, most splices have very good appearance.

When all three curves representing compromise were examined, it revealed that the highest single value was obtained using the 4483 straight chamber, at approximately 60psig as shown in Figure 3-10. This observation suggested that the best appearance splices were created in the chamber with the smallest cross-section, where the splicer walls restrict the movement of the individual fibres thus reducing splice bulk and filamentation. However, there was a small price to pay for this benefit; the small cross-section requires a higher air pressure to produce a consistently strong splice.

3.4 The relationship between strength and appearance

The curves recorded thus far indicate a good level of consistency, with overall responses being quite consistent and with relatively little statistical scatter. However, it should be noted that each point on these curves was the result of the mean of 20 observations, so that individual variation had largely been smoothed out. At this level, it was quite clear that, although there were some differences, the strength and appearance curves had a fair degree of correspondence. Both parameters conform roughly to the simplified account of there being two limiting pressures, a minimum, below which nothing happens, and a maximum, beyond which damage occurs.

At first sight from these results, with strength and appearance marching very roughly in step, it might seem reasonable to expect splice strength and splice appearance to be

intimately linked. Further, it may seem obvious that a splice which has damaged filaments, is certain to be a splice that is weak. However, this assumption can be challenged. A splice may have a completely unacceptable appearance, and may be impossible to process, if it has, say, ten broken filaments. If, as was the case in these experiments, the parent yarn has 72 filaments, then the proportion of broken filaments is only 10:144. This will hardly be a major contributor to degradation of splice strength. Therefore there may be reason to argue that the two parameters may not be as closely linked as originally thought. It is valid to examine in a little more detail the link between strength and damage.

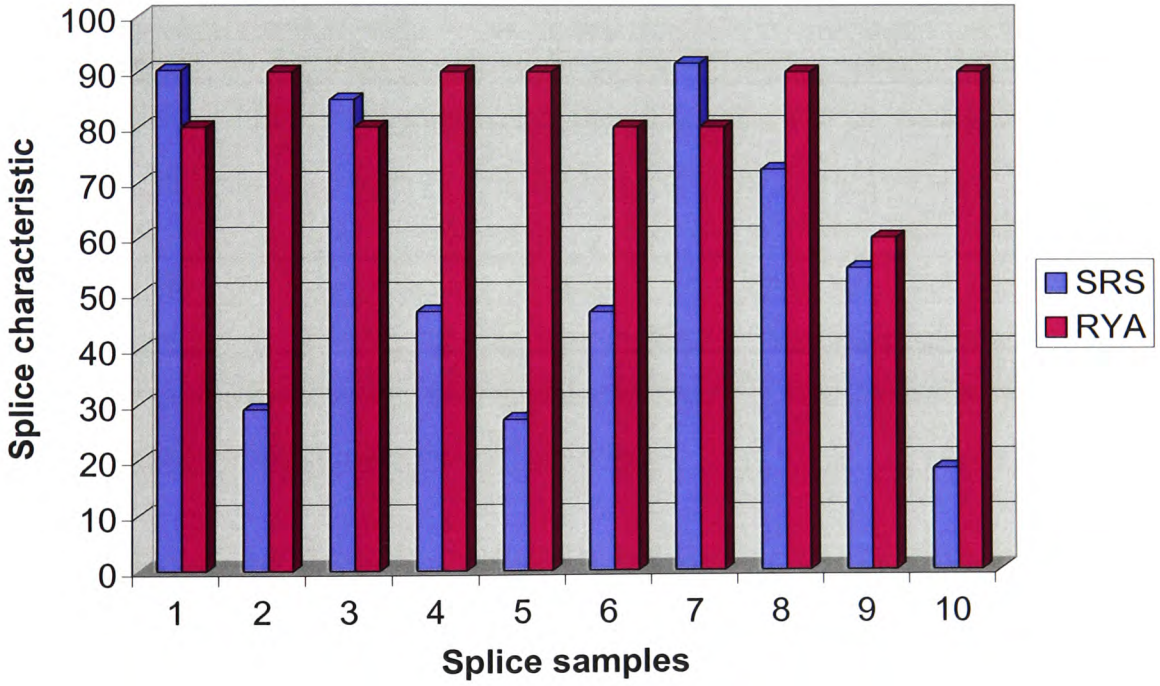

Figure 3-12. Variation between results under same experimental condition.

Examining the relationship between strength and appearance, at the level of the individual splice for the first 10 samples at 35psig on a 4485 straight chamber, is tabulated in Figure 3-12 (SRS is tabulated in Figure 2-6). It is obvious from these results that matters are far from clear-cut. For these ten splices, the individual results

for appearance and strength were very much out of step. The appearance results were noticeably more consistent than the strength results. This difference in consistency needs to be addressed.

Splice appearance is a function of filament damage; the greater the number of filaments which break on exposure to the air blast, the poorer the appearance. However, at least when the damage is moderate, most of the visible damage concerns only those filaments which lie on the outside, those that are at the core are largely protected from the blast. So the hypothesis is that, at moderate levels of filamentation, appearance is a feature of the outside of the bundle.

Splice strength on the other hand, seems to be different. Others have shown that spliced joints are inherently unpredictable (Kaushik *et al.*, 1987a), i.e. no two splices are the same, because the filaments are packed randomly throughout the yarn. This randomness may result in a wide range of filament geometry from splice to splice. Thus, the filaments may intertwine differently from splice to splice (Kaushik *et al.*, 1988; Kaushik *et al.*, 1987*b*; Rowlands *et al.*, 2000). The implication of this work is that, again at moderate levels of filamentation, strength is a feature of the manner in which filaments interact in the body of the splice.

The less-than-perfect fit between strength and appearance, and its eventual contribution to a model of the splicing process, is addressed in later chapters.

3.5 The nature of yarn damage

The characteristics of filament damage were assessed using a SEM. Two forms of filamentation had already been identified, by eye, and by using the optical microscope and digital camera combination:

1. By far the most common form of damage involves relatively short lengths of material, which project out of the ends of the splices. They were all of similar

length, and frequently appear badly twisted and distorted, as if they have been badly stressed.

2. Far less common was a long, relatively straight fibre. Typically, such a filament will be around twice as long as those in category 1, and it will not seem damaged or stressed in any way.

In practical terms, the distinction between a broken filament and a loose tail end filament is unimportant in the grand scheme of things, because any filamentation, whether from broken or loose ends, will cause problems in industrial practice (Hearle and Wilkins, 2006). However, in terms of understanding the mechanisms, and in the evolution of a new model for splicing, the difference did need to be examined. The SEM proved very enlightening. The SEM recordings for both filament ends are shown in Figure 3-13. These results provided some very useful information, and a new insight into the splicing process.

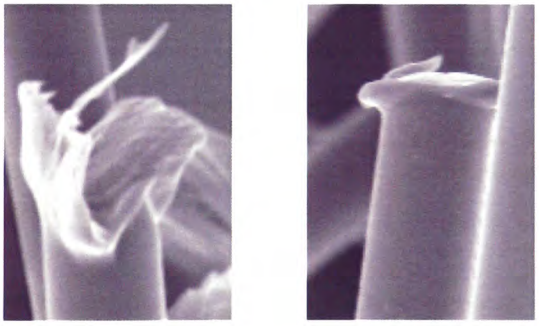

(A) (B)

Figure 3-13. A) Category 1 broken filament; B) Category 2 broken filament.

The first form is completely typical of a form of rupture described and photographed by Hearle *et al.* (1998, 13-114). This filament tip has been melted, despite that fact that it has been through a room-temperature process. It has been stretched and twisted violently and adiabatically, and ruptured by melting. Being over-stressed has broken category 1 filaments.

The second form is completely different. Its clean tip and small projections are characteristic of a plastic material, which has been simply cut. There is no evidence of melting. This evidence fits well with the secondary observation that "floating" filaments are always found to be relatively long and relatively straight. Together, the results provide powerful evidence to conclude that category 2 filaments have simply escaped from the yarn bundle after being cut, and have never been bound into the splice.

3.6 Taguchi implementation

Throughout the factor level identification experiments, the parameter levels for the Taguchi DOE were established and are shown in Table 3-3. Three levels were considered due to the nonlinearity of the splicing parameter relationships. An L27 OA was chosen for the experiment, Peace (1993, pp.114-166).

Table 3-3. Selected splicing parameters

Factor	Parameter	Level 1	Level 2	Level 3
A	Blast pressure	40psig	50psig	60psig
B	Blast duration	1sec	1.5sec	2sec
C	Chamber design	4483 straight	4485 straight	4483 bowl
D	Cutting synchronisation	0	3	6

With the factor level identification experiments completed, the resulting parameter levels were utilised and the Taguchi DOE testing array was executed. The L27 OA and the factor identification results for RYA are shown in Figure 3-14 along with the SRS results and optimum selected factors found from the previous splice strength optimisation in Chapter 2.

	Main Factors and Interactions											
Run	A	B	AB	AB	C	AC	AC	D	AD	AD	SRS (%)	RYA (%)
1	1	1	1	1	1	1	1	1	1	1	51.63	92
2	1	1	1	1	2	2	2	2	2	2	73.24	90
3	1	1	1	1	3	3	3	3	3	3	81.42	88
4	1	2	2	2	1	1	1	2	2	2	79.18	86
5	1	2	2	2	2	2	2	3	3	3	78.94	74
6	1	2	2	2	3	3	3	1	1	1	77.77	56
7	1	3	3	3	1	1	1	3	3	3	70.82	80
8	1	3	3	3	2	2	2	1	1	1	76.39	54
9	1	3	3	3	3	3	3	2	2	2	76.08	70
10	2	1	2	3	1	2	3	1	2	3	82.33	80
11	2	1	2	3	2	3	1	2	3	1	88.10	80
12	2	1	2	3	3	1	2	3	1	2	74.51	88
13	2	2	3	1	1	2	3	2	3	1	76.70	84
14	2	2	3	1	2	3	1	3	1	2	86.27	64
15	2	2	3	1	3	1	2	1	2	3	73.65	62
16	2	3	1	2	1	2	3	3	1	2	77.85	82
17	2	3	1	2	2	3	1	1	2	3	77.94	62
18	2	3	1	2	3	1	2	2	3	1	68.46	84
19	3	1	3	2	1	3	2	1	3	2	78.20	80
20	3	1	3	2	2	1	3	2	1	3	60.56	64
21	3	1	3	2	3	2	1	3	2	1	65.52	92
22	3	2	1	3	1	3	2	2	1	3	71.98	84
23	3	2	1	3	2	1	3	3	2	1	80.52	58
24	3	2	1	3	3	2	1	1	3	2	67.86	48
25	3	3	2	1	1	3	2	3	2	1	54.27	62
26	3	3	2	1	2	1	3	1	3	2	71.72	49
27	3	3	2	1	3	2	1	2	1	3	65.57	64

Factor A		
L1	L2	L3
76.67	76.22	66.78

Factor C		
L1	L2	L3
81.11	66.11	72.44

Factor B		
L1	L2	L3
83.78	68.44	67.44

Factor D		
L1	L2	L3
64.78	**78.44**	76.44

Selected Factors - SRS	A2	B2	C2	D3

Selected Factors - RYA	A1	B1	C1	D2

Interaction AB			
	B1	B2	B3
A1	**90**	72	68
A2	82.67	70	76
A3	78.67	63.33	58.33

Interaction AC			
	C1	C2	C3
A1	**86**	72.67	71..33
A2	82	68.67	78
A3	75.33	57	68

Interaction AD			
	D1	D2	D3
A1	67.33	82	80.67
A2	68	**82.67**	78
A3	59	70.67	70.67

Figure 3-14. L27 orthogonal array and optimum factor identification for RYA.

The SNR that will be of interest in the splicing process is again, the 'largest is best' as shown in Equation 2-2. This SNR was selected because the response to obtain from this experiment was to acquire the maximum RYA, Wu *et al.* (1991), Peace (1993, pp. 292-311).

Figures 3-15 and 3-16 illustrate the SNR and the mean response of the SRS and RYA at each level of the selected factors respectively. Figure 3-15 reveals that factors A, B and C have the largest mean RYA at level 1, while factor D had the largest mean RYA at level 2. Figure 3-16, the mean response plot, revealed that factors B and C were the most influential in attaining the optimum splice appearance. Closer inspection revealed that factor A could be selected at level 1 or 2 since the mean response plots were approximately equal. All the mean response plots coincide with their corresponding SNR plot.

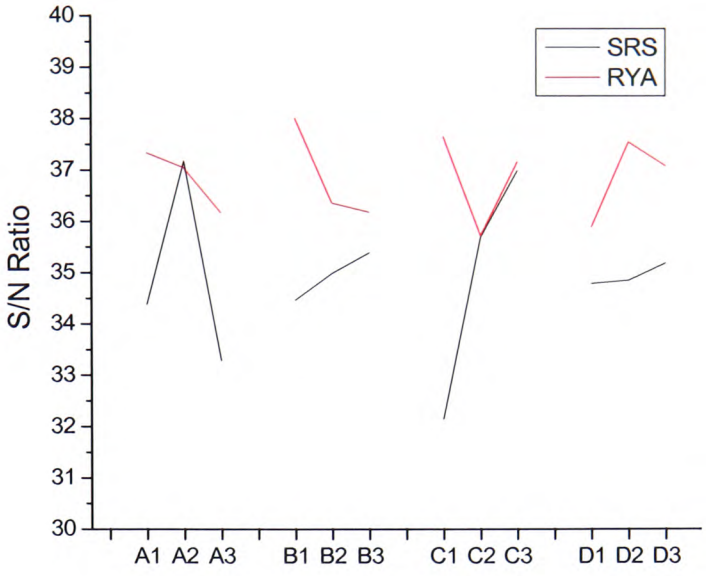

Figure 3-15. SNR response plot.

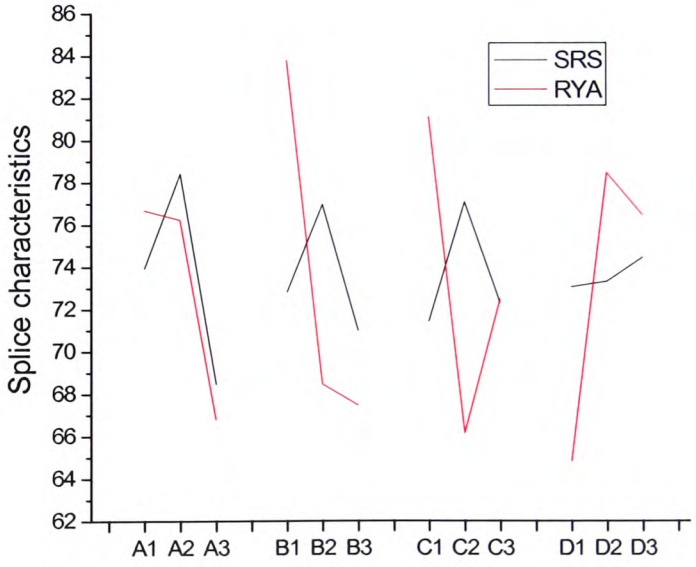

Figure 3-16. Mean response plot.

The strength of the interaction AB required further investigation (Nair, 1992). The outcome is shown in Figure 3-17. The interaction plot revealed intersections between B2 and B3 indicating a strong interaction. As B1 was the dominant factor with no intersections, it was considered that interaction AB could be omitted because it was not considered significant in the trials.

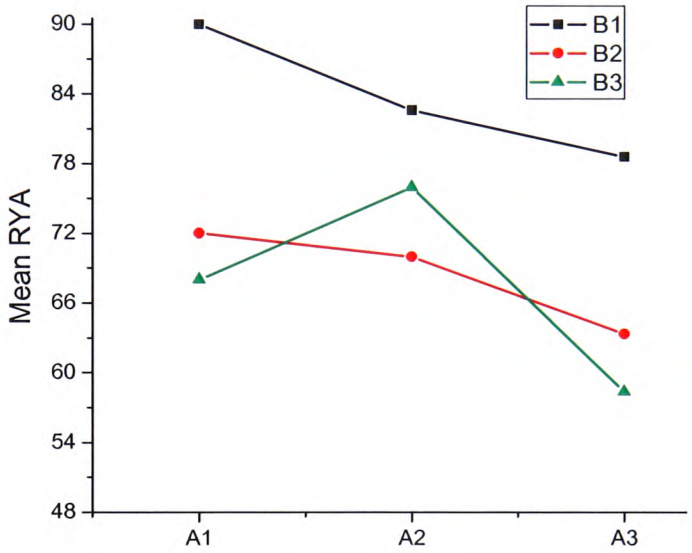

Figure 3-17. Interaction AB.

The ANOVA was conducted to reveal if any of the factors chosen were statistically significant. The results of the ANOVA for splice appearance, as shown in Table 3-4, revealed that factors B, C and D were statistically significant at 99% with factor A only marginally being 95% statistically significant.

Table 3-4.ANOVA of each splice characteristic.

Retained Yarn Appearance (RYA)				
Factors	**DOF**	**SS**	**MS**	***F* ratio**
A	2	15009.3	7504.6	4.42 *
B	2	44787	22393.4	13.18 **
C	2	30398.2	15199.1	8.95 **
D	2	28703.7	14351.9	8.45 **
AB1	2	4453.7	2226.9	1.31
AB2	2	2064.8	1032.4	0.61
AC1	2	1398.2	699.1	0.41
AC2	2	4592.6	2296.3	1.35
AD1	2	564.8	282.4	0.17
AD2	2	37	18.5	0.01
Error	519	881566.5	1698.6	N/A
Total	539	1014575.8	N/A	N/A

Notes:
* Indicates factor/interaction is statistically significant at 5% level of significance - $F(0.05,2,519) = 3\ 01$
** Indicates factor/interaction is statistically significant at 1% level of significance - $F(0.01,2,519) = 4.65$

It was necessary to validate the Taguchi conclusions, so a confirmatory run was undertaken. The run used the same experimental format as the main experiment, using the parameter settings, which had emerged from the Taguchi analysis. The objective was to verify that the optimised parameters found provided the maximum RYA, with the greatest robustness. The results of the confirmatory run are shown in Table 3-5, which compares the performance resulting from the Taguchi analysis with the results normally achieved using standard industry practice.

Table 3-5. Confirmatory run.

	Before	After	Increase / Decrease (percent)
Splice appearance	53.64	92	+71.51%
Variance	1.27	0.63	-50.39%

The RYA with the optimum parameter settings was 92% with a variance of 0.63. This represented a substantial improvement in splice appearance of 71.5% and a marked decrease in variance, when compared to normal industry practice. At the settings identified by the Taguchi analysis, 81.5% of the splices had acceptable splice

appearance, and 60% of the splices appeared almost identical to unspliced yarn (except for the inevitable slight enlarged central section).

The optimised parameters from both SRS and RYA Taguchi analyses were 2,2,2,3 and 1,1,1,2 respectively. In industry a compromise between the two is required. Therefore, statistically significant factors obtained from each ANOVA (Tables 3-4 and 2-6) were examined. These, taken together with the improved better understanding of the different effect individual parameters have on splice performance, to provide an optimum compromise.

The ANOVA from the previous research done on splice strength optimisation revealed that A was the only statistically significant factor. Factors B and C were close to being 95% statistically significant. Therefore, factors B, C and D can be altered without a great significant change in splice strength.

From splice appearance optimisation, the ANOVA revealed that all four factors were statistically significant with factor A, at 95%, being the least significant by a narrow margin. Therefore factor A can be changed without a significant change in splice appearance.

Combining the two Taguchi analyses revealed that, though all four factors were statistically significant, only factor A was dominant factor overall. The emergence of choice of the statistical significance of factor A (blast pressure) was completely consistent with experience of splicing performance and the importance of splice strength in the real world. Merging these factors together produced an optimised compromise set of splicer parameters at the setting of 2,1,1,2, yielding the values below:

Factor A: Level 2 = 50psig

Factor B: Level 1 = 1sec

Factor C: Level 1 = 4483 straight chamber

Factor D: Level 2 = 3

Having obtained the optimised factor settings for the combined splice characteristics of strength and appearance, confirmatory runs were conducted as shown in Table 3-6.

Table 3-6. Confirmatory run.

	Before	After	Increase / Decrease (percent)
Splice Strength	88	66.25	-24.72%
Variance	0.089	0.86	+866.29%
Splice appearance	92	85	-7.61%
Variance	0.63	0.85	+34.92%

These results were unsatisfactory, indicating that the results emerging from the Taguchi analysis leant too far towards optimising appearance, at the expense of splice strength. From practical splicing experience, and from earlier experiments on the 4483 straight chamber (Figure 3-11), it was concluded that a modest increase from the recommended 50psig could yield a splice strength which would meet industry requirements.

It was reasoned that an increase of pressure to 60psig could greatly improved the splice strength, with a negligible difference in appearance. A confirmatory run with the new suggested factor level setting for blast pressure was conducted, as shown in Table 3-7.

Table 3-7.Confirmatory run.

	Before	After	Increase / Decrease (percent)
Splice Strength	66.25	84.18	+27.06%
Variance	0.86	0.33	-61.63%
Splice appearance	85	89.67	+5.49%
Variance	0.85	0.48	-43.53%

As can be seen, with the Taguchi analyses and most importantly the engineers' knowledge of the splicing process, an acceptable combined parameter optimisation was obtained for splice strength and appearance. Compared with the preceding run at the lower pressure of 50psig, there was a marked increase in strength, with a decrease in variance. There was also a slight improvement in appearance, with a decrease in

variance. These revised combined splicing parameters represented a fully acceptable compromise.

3.7 Conclusion

In this chapter, the implementation of the Taguchi DOE method applied to the splicing process for splice appearance optimisation was undertaken. The optimum splicer settings for producing splices of good appearance were established, and verified by confirmatory experiments. The work yielded a significant improvement in appearance and variance compared to previously recommended optimum levels.

An earlier, similar, experiment had established the optimum splicer settings for producing strong splices. Now that both sets of optima, for strength and appearance had been found and validated, a compromise between the optimum settings for splice appearance and those for splice strength was sought, the target being to identify the best combination of settings for use in real textile environments. The ANOVA results for both sets of experiments were examined, together with mean response and the SNR, to yield a splice setting, which were predicted to produce a strong splice with a good appearance. A set of process parameters was established for this compromise.

The result was a splice which had a good appearance, but which was slightly lacking in strength. The recommended settings had been based purely on predictions from statistical analysis. Therefore, the experience of the splicer engineers was brought to bear, resulting in a slight increase of air pressure from 50psig to 60psig. This small change produced the desired result; a splice in which both strength and appearance were improved.

Therefore, for one yarn count and configuration, the Taguchi method proved extremely effective in yielding settings for splicing parameters which represent a significant improvement over those normally used. It provided a basis for assessing the

compromises, which was needed to produce the best combination of appearance and strength. The use of Taguchi principles promises to simplify splicer design and development time in the future.

This body of work described so far, relating to both strength and appearance, has been conducted on a single yarn count. The next stage of the research required that the analysis be extended to yarns of significantly different count. This problem is addressed in the next chapter.

Chapter IV

The influence of yarn count on the splicing of simple continuous filament synthetic yarns

Abstract – *This chapter continues the work on splicer parameter optimisation for splice strength and appearance. The research undertaken in this chapter deals with the variable of yarn count and its relationship with splicing performance. The tests were performed using multiples of an industry-standard synthetic yarn, which has been used throughout this research as the base line material. This chapter reports on the change in performance of industry standard and experimental splicers with various configurations as yarn count is varied. The chapter offers an explanation for the change of splicing performance with yarn count.*

4.1 Introduction

Textile manufacturers require certain characteristics from a spliced joint (Lam and Cheng, 1997; Lappage, 2005). The principal requirement is for splice strength; however, good splice appearance may also be required in specific cases where the resulting product needs to be snag-free to be accepted by the end user (Lewandowski and Drobina, 2004).

There are many input parameters that affect splice characteristics at different yarn counts. Until the yarn count becomes too big for the chamber, the splice characteristics are consistent. Therefore, in order to meet the requirement of achieving high and consistent splice characteristics, the yarn counts need to be optimised for various chambers. Earlier chapters have dealt with exclusively with the effects of splicing parameters upon a yarn of 1100dtex. In the real world yarn counts vary.

In real pneumatic splicers, increase of yarn count usually demands an increase of the cross-sectional area of the splicing chamber. The relevance of variation of splicing chamber cross-section can be understood very simply. Consider a splicing chamber, which is optimised for a particular yarn. If the yarn count increases, then the characteristic diameter of the yarn will increase. At some point, the cross-section of the chamber may be such that there is simply not enough room in the chamber for free fibre intermingling to take place. Indeed, if the yarn count increases sufficiently, fibres will become so closely packed in the chamber that there will be essentially no filament motion. In these circumstances, the logical option is to use a chamber of larger cross-section, to accommodate the increased yarn size.

This approach may yield a strong splice, but it frequently degrades the splice appearance, an effect that may be critical in some textile processes. It may increase the filamentation in the splice, and may yield more prominent tail ends (Mingjie *et al.*, 1999).

Merely increasing chamber cross-section therefore was not a complete solution to splicing of high-count yarns. There was a further and ultimately more important factor, which needs to be addressed when considering increasing yarn count. This factor was the fixed geometry of the splicer itself which limits the splicing performance regardless of changes in chamber design. The overall length of the splice is largely controlled by the separation of the splicer knives. In a simple continuous filament yarn, in which the individual filaments remain largely intact during the splicing operation, the length of the splice corresponds very closely to the knife separation. There is a slight reduction due to the intermingling process, but this is generally small. Thus, the absolute splice length is approximately constant, irrespective of yarn count as shown in Figure 4-1.

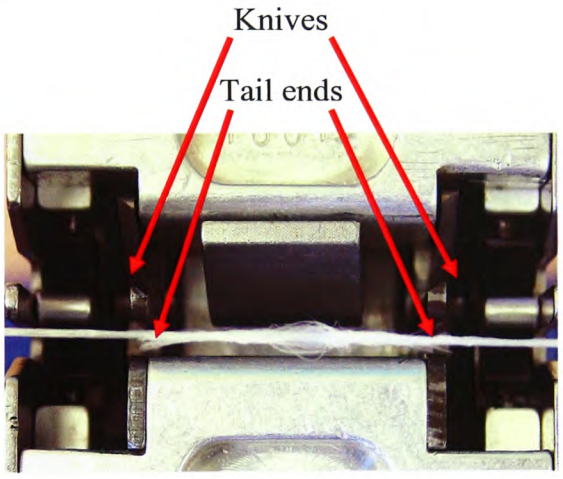

Figure 4-1. Comparison between total splicing length and splice length.

For simple engineering reasons, on a commercial splicer, knife separation is fixed. Once a splicer design is finalised, then the splice length for that particular splicer cannot be altered. As the yarn count increases, the cross-section of the yarn will increase, while the splice length remains constant; therefore the ratio between splice length and splice diameter decreases. Consequently as yarns get bigger, the absolute splice length remains constant, but the relative splice length is reduced as shown in Figure 4-2.

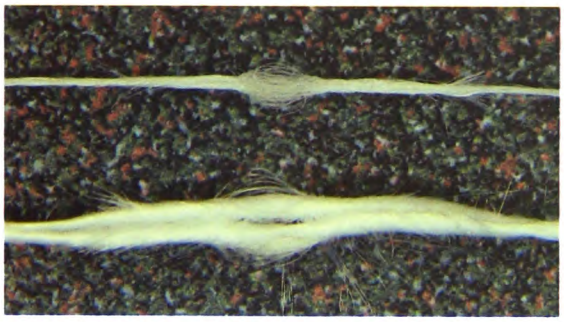

Figure 4-2. Comparison of relative splice lengths using 1100dtex (72 filament) and 11000dtex (720 filament) yarn counts.

At some point, this reduction of relative splice length might be expected to have an adverse effect on the splice quality. For the purposes of this report, the phenomenon will be described as "scaling". There has been little or no published work on the subject of scaling, therefore an analysis of the relevance of scaling the splicer geometry and chamber parameters may prove fruitful.

The principal aim of the research described in this chapter was to identify the relationship between splice quality and yarn count, with particular attention being paid to the following three major variables:

1. Splicing chamber cross-section.
2. Splicing chamber length.
3. Total splicing length (knife separation).

4.2 Scaling

In order to confirm the existence of scaling, the requirements of the experimentation demanded the variation of the three major variables declared above. Therefore a hybrid splicer was designed with various hybrid chamber lengths that accommodated all the above criteria.

There were two variations of knife separation distance. The standard splicer design had a knife separation distance of 32mm while the hybrid splicer design had an increased knife separation distance of double the standard splicer length, of 64mm. The hybrid splicer design is shown in Figure 4-3. The increased length was achieved by the use of large splicer body extensions, which can clearly be seen in the illustration.

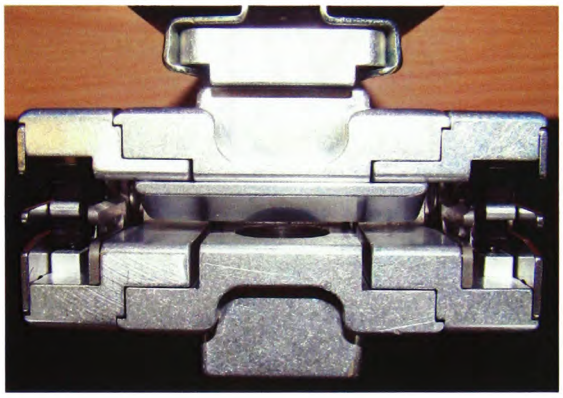

Figure 4-3. Hybrid splicer design.

An infinite number of splicing chamber cross-sections are possible. Earlier research from previous chapters has used some comparatively simple trapezium sections. Therefore the same chambers were used for this series of experiments to enable direct comparisons with the previous research (Webb *et al.*, 2007a; Webb *et al.*, 2007b). These chambers are shown in Figure 4-4 and had the following properties:

- Chamber 4483 straight: a chamber with a simple 30° profile, 4.8mm deep, 16mm long and with a width diverging from 0.8 mm at the base.
- Chamber 4485 straight: a chamber with a simple 30° profile, 4.8mm deep, 16mm long and with a width diverging from 1.25 mm at the base.

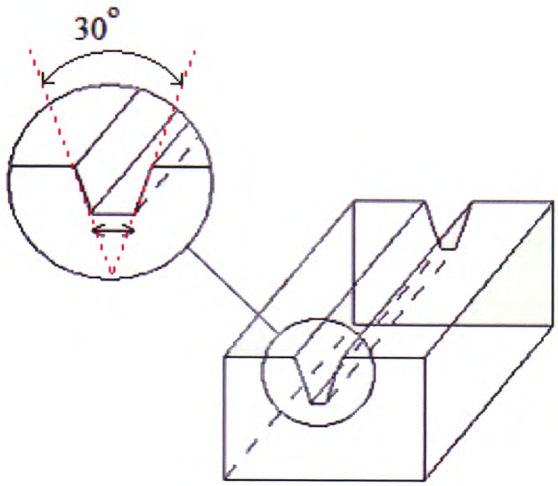

Figure 4-4. Chamber width design variations (increased width shown by inset).

Four key splicing chamber lengths were used as shown in Figure 4-5. The chamber lengths were based on the standard splicing chamber length of 16mm, in the 4483 and 4485 profiles as specified above. The normal 16mm production chambers, previously standardised as "4483 straight" and "4485 straight", were used throughout to represent existing splicing practice and allow direct comparison to previous research. From previous studies, both chamber profiles performed similarly. Therefore only the 4485 profile was used for experimentation.

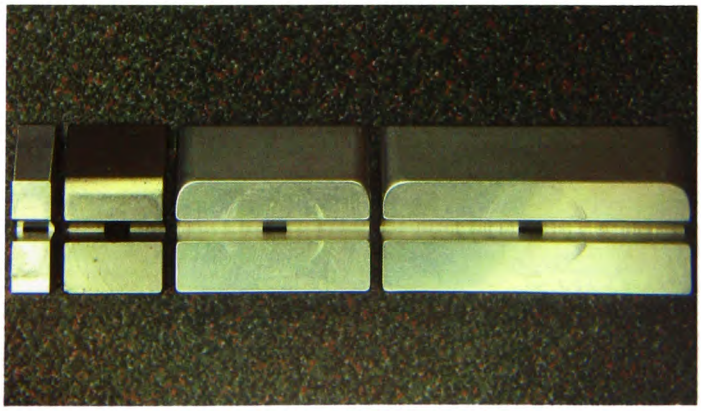

Figure 4-5. Variation on chamber lengths from left to right are 4485 small, straight, medium and long respectively.

The three variations on the straight chamber length were:

- A chamber of double the standard length, of 32mm. This chamber, described as "4483 medium", was selected so that, when it was fitted into the hybrid splicer, it maintained the same ratio between chamber length and overall splicing length as that which prevailed on the original splicer and chamber configuration.
- A chamber of three times the standard length, of 48mm. This chamber, described as "4483 long", was selected for use on the hybrid splicer, to maintain the same distance between the chamber ends and knife assemblies to that which prevailed on the standard splicer and chamber configuration.
- A very short chamber with overall length of 6mm. This chamber, described as "4483 small", was not designed to maintain any particular spatial relationship. It was the shortest possible chamber, which could be manufactured to fit the splicer. It was selected to illustrate an extreme case of the effect of splicing chamber length on splicing performance.

In previous research, only a specific yarn of a specific count was selected for experimentation using a specific splicer. No account was taken of the effect on splicing performance due to varying yarn count, although it was suggested at the time that yarn count could have an affect.

Therefore, in order to ensure consistency with earlier work stated above, the same experimental test setup was retained to allow direct comparisons. It was necessary to choose a means of achieving higher yarn counts. With a standard continuous-filament yarn, count can be changed by altering a number of parameters. For example:

- Keeping the filament dtex constant and doubling the number of filaments can double count
- Keeping the number of filaments constant and doubling the dtex of each filament can double count.

In this research, yarn count was increased by increasing the number of filaments. An industry standard polyester fibre was used (as stated in Chapter 2) starting from 1100dtex, 72 filaments increasing uniformly in steps of 1100dtex over the full experimental yarn count range (Webb *et al.*, 2009). The test samples for a given dtex were taken from a single bobbin to minimise variability.

Two experimental methods were used. The principal measure of splice quality was taken as the SRS. Splice appearance was only recorded as acceptable or not, since earlier work had identified it as a secondary variable (Cheng and Lam, 2000b; Lewandowski and Stanczyk, 2005).

The first experiment dealt with the relationship between splicing chamber cross-section and total splicing length. The experimental splicing chambers of different cross-sections were used to determine how splicing performance deteriorated as yarn count increased to a point where the scaling factor became too large for a particular section. Once the performance of splicing chambers in a standard splicer had been assessed, the changes of splicing performance in the hybrid splicer were measured.

The second experiment dealt with the relationship between splicing chamber length and total splicing length. The experimental splicing chambers of different lengths were used to determine whether chamber length had any significant effect on splice characteristics. Knife separation distance was altered, thereby examining the relationship between varying chamber length and knife separation.

4.2.1 Effects of chamber cross-section and total splicing length on splicing performance

The experiments relating splice strength to blast pressure were repeated, using both 4483 and 4485 straight chambers to splice yarns over a wide range of counts. The first set of experiments used the standard splicer, which had a knife spacing of 32mm. The

next set of experiments used the longer hybrid splicer, which had a knife spacing of 64mm.

Each yarn splice sample or parent yarn is clamped in the Lloyd Instruments tensile testing machine (type T5000) and extended at a rate of 100mm/min until it ruptured. The load/extension curve is recorded electronically. A 1100dtex parent yarn tensile test recording is shown in Figure 4-6.

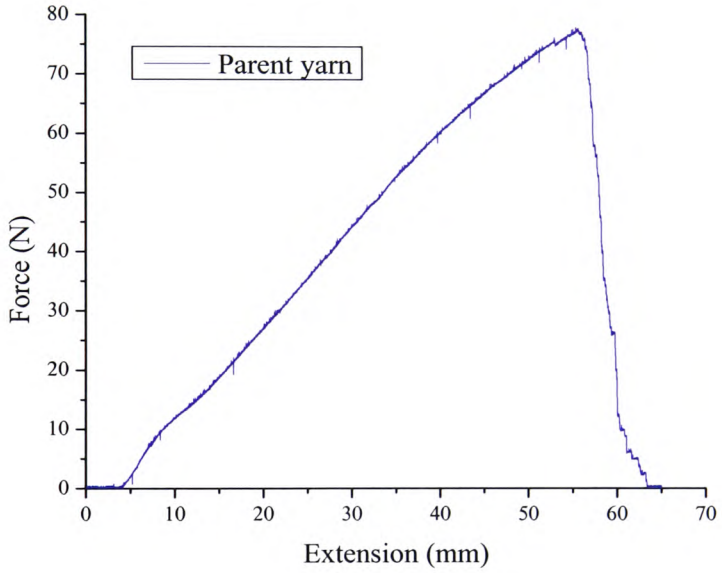

Figure 4-6. 1100dtex parent yarn tensile test sample.

The parent yarn tensile strength values over the full yarn count range tested are shown in Table 4-1.

Table 4-1. Parent tensile strength over tested yarn count range

Yarn count (dtex)	Force (N)
1100	81.44
2200	161.58
3300	242.90
4400	323.50
5500	396.57
6600	478.76
7700	556.83
8800	618.06
9900	692.93

For each splicer, chamber configuration and yarn count above 1100dtex (1100dtex was recorded earlier in Chapters 2 and 3), the pressure was varied between 20psig and 90psig with SRS and appearance recordings taken at intervals of 5psig. The maximum count used was 9900dtex, because at that level the 4483 straight splicing chamber, in the standard splicer body, failed completely. The results are as shown in Figures 4-7 to 4-10, revealing the change of splice strength with pressure, for each of several yarn counts.

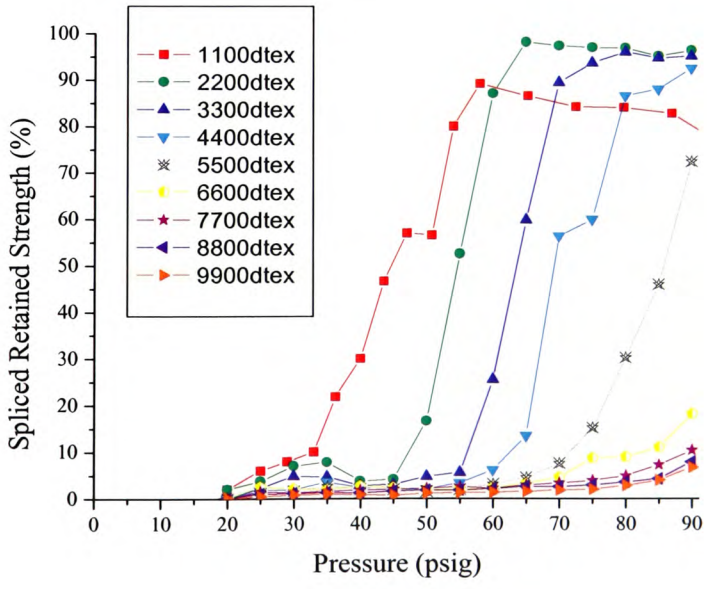

Figure 4-7. Yarn count range on 4483 straight chamber in standard splicer.

Figure 4-7 revealed fairly clearly that 4483 straight chamber can splice yarns quite satisfactorily up to a count of around 5500dtex. Additional air pressure was required to produce satisfactory splices, as count increased, presumably because a greater mass of yarn needs to be agitated by the blast. Above 5500dtex, the chamber fails; this was thought to be the result of the area ratio between chamber cross section and combined filament cross section becoming too small, so that it restricts the filaments.

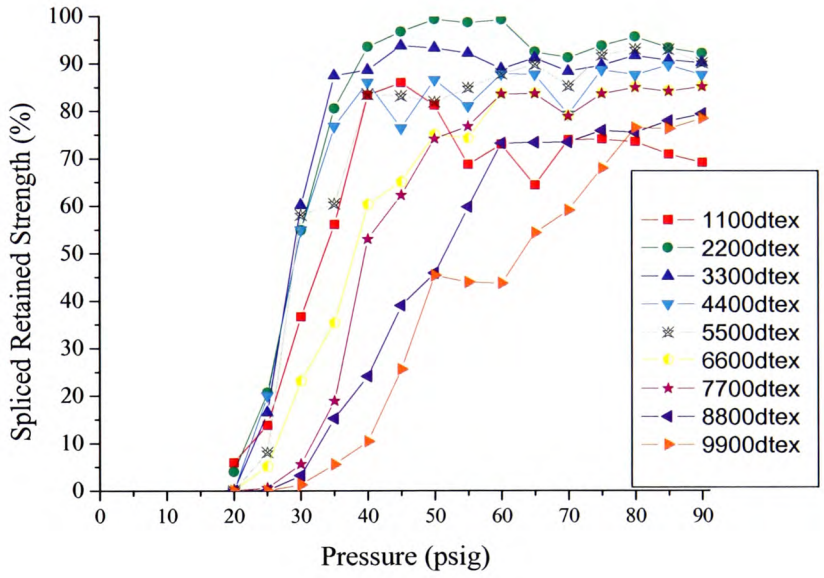

Figure 4-8. Yarn count range on 4485 straight chamber in standard splicer.

Figure 4-8 revealed that the wider 4485 straight chamber cross-section can splice yarns quite satisfactorily up to a count of at least 9900dtex. Adequate splices are created at lower pressures compare to the 4483 straight chamber. Again as yarn count increased, additional air pressure was required to produce satisfactory splices. The improved performance was thought to be the result of a greater volume within the larger chamber, which allows more filament movement to occur, enhancing the level of intermingling.

The hybrid (increased splicing length) comparison using the 4483 straight chamber, shown in Figure 4-9, can splice yarns very well up to a count of 6600dtex, and fairly

satisfactorily up to a count of approximately 8800dtex with additional air pressure. Above 8800dtex, the chamber revealed signs of beginning to fail. It was believed that if the air pressure were to increase greater than 90psig, the SRS would continue to increase for the higher yarn count range. This was not proven due to the limitations of our experimental setup. By comparing Figures 4-7 with 4-9, it was clear that chamber cross-section was not the sole variable controlling the response of the splicer to increasing yarn count; increasing the total splicing length improved performance substantially.

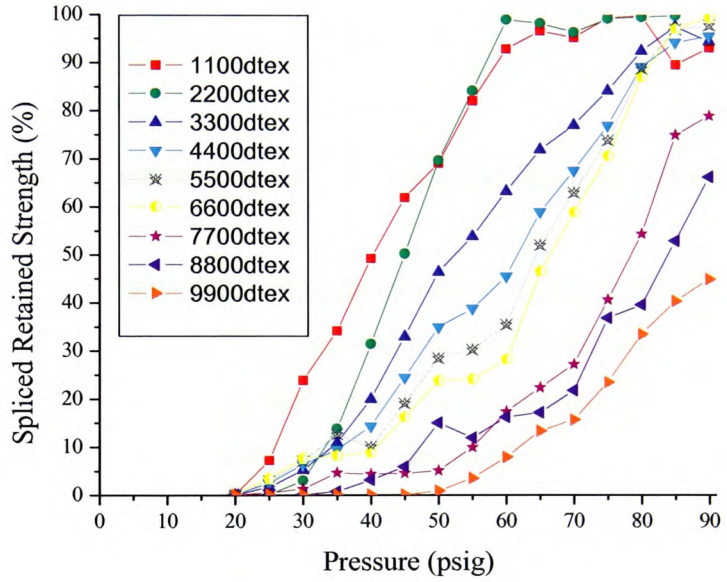

Figure 4-9. Yarn count range on 4483 straight chamber in hybrid splicer.

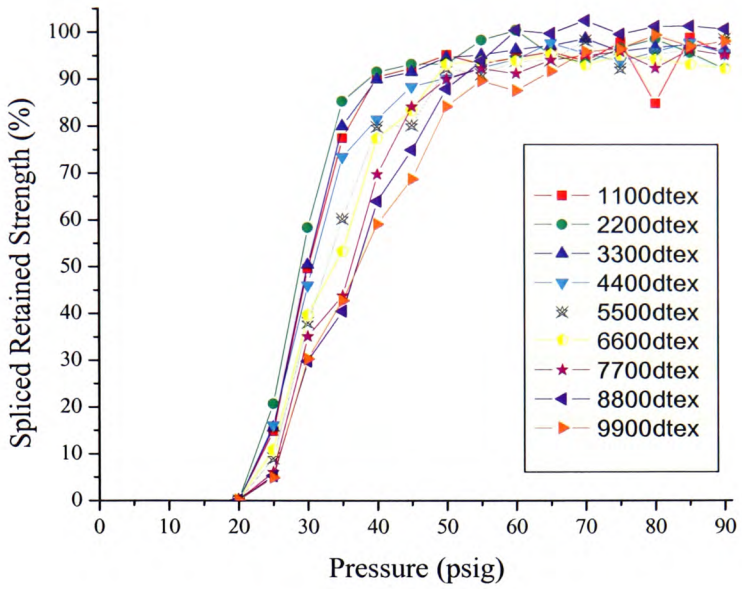

Figure 4-10. Yarn count range on 4485 straight chamber in hybrid splicer.

Figure 4-10 revealed that the 4485 straight chamber in the hybrid splicer can splice yarns very well up to a count of 9900dtex; indeed, the curves are so closely packed that it would be reasonable to deduce that much higher counts can be spliced by this configuration. As count increased, only very modest additional air pressure was required. Again, by comparing Figures 4-8 with 4-10, it was clear that increasing the total splicing length had the same effect of increased yarn count range and improved consistency.

This improved yarn count range through increased cross-sectional chamber width comes at a price. The splice strength remains consistently high but the splice appearance deteriorates. There must be a trade-off between splice strength and appearance results. These outcomes were consistent with years of field experience.

Until this point in the research, it had been assumed that, for a given splicing chamber, blast pressure was the principal determining factor in splicing performance. However, the results reported in this section showed clearly that splicer geometry must also have a

very important role. So far as is known, no published research has analysed, or even mentioned, the importance of the compound relationship between chamber profile, chamber length, and splicing length.

Each of the nine responses in the preceding charts demonstrated that, for a given splicing chamber, and a given yarn, there is a peak SRS. For any given yarn, after the peak, SRS decreased with increased pressure, presumably as filament damage occurs. In general, for any chamber and splicer geometry, it was clear that, as yarn count increased, the curves shifted along the x-axis, demonstrating that higher pressures were required as the yarns began to occupy more and more of the chamber profile. The work has yielded a multiplicity of graphs, and, as they stand, the results were not particularly easy to understand. However, close analysis eventually revealed a pattern, which relates to the behaviour of different chambers, as yarn count increases.

It was possible to represent the results in a manner which yields a clearer understanding. For each specific splicer configuration, the highest splice strength was recorded for each yarn, using an absolute, instead of a relative measure for splice strength. This yielded a series of curves, showing how each splicer configuration performed as yarn count changed, over the full yarn count range. This approach yields the curves shown in Figure 4-11.

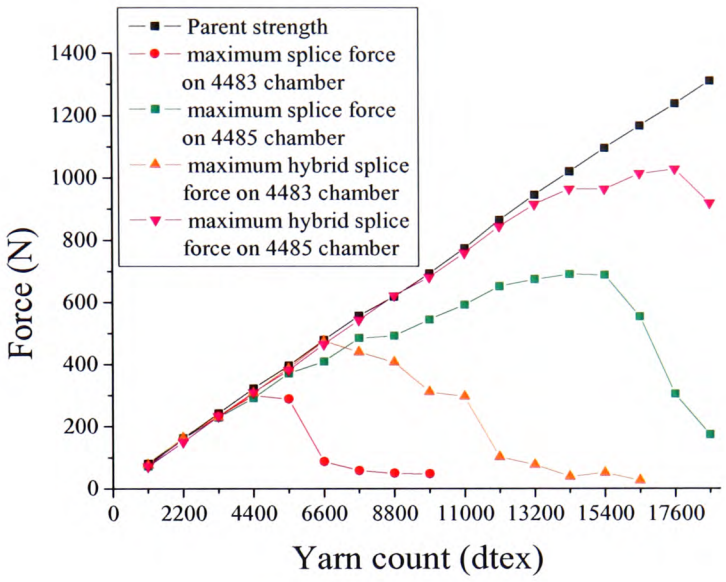

Figure 4-11. Yarn count range for both 4483 and 4485 straight chambers using the standard and hybrid splicers.

As can be seen by Figure 4-11, with the 4483 straight chamber fitted in the standard splicer, performance deteriorated markedly once the yarn count exceeded approximately 5500dtex. This chamber had a maximum SRS of approximately 98% at 65psig with a yarn count of 2200dtex. With the 4485 straight chamber, yarn count began to influence splice strength after approximately 7700dtex. However, the effect was small, meaning there was not a reduction of absolute strength, only a reduction in the rate of rise in splice strength. The real deterioration of the chambers performance only occurred above approximately 15400dtex. This chamber produced its maximum SRS of approximately 99% at 50psig with a yarn count of 2200dtex, but there was little reduction with yarn counts between 3300dtex to 5500dtex.

The performance of the hybrid splicer with the 4483 straight chamber does not begin to deteriorate until the yarn count exceeded roughly 7700dtex. Once the deterioration began, the rate of reduction was less than that of the case with the standard splicer. With the 4485 chamber, strength was barely affected at all until approximately

14300dtex. The chambers performance began to deteriorate at a rapid rate above the yarn count of 17600dtex.

Splice appearance was still degraded using the 4485 straight chamber with the hybrid splicer. Therefore the main conclusion to emerge from these results was that increased total splicing length improved all chambers' performance, thus a smaller profile chamber can be used to splice higher yarn counts to improve its appearance. Taken together, these results indicate that both chamber cross-section and total splicing length have an effect on splicing performance.

The increase in the splice performance through increasing the total splicing length was presumably due to the increased number of helix wrappings that occur between the yarn ends, therefore increasing the frictional forces between individual filaments. This was too large a subject to include here and will be analysed in greater detail in a later chapter.

The increased performance was consistent between both chamber cross-sections; therefore the hybrid splicer improves the chambers performance by a set amount, which agrees with our initial predictions that there were more helix wrappings throughout the greater splice length. These results suggest that the so called scaling effect does exist, and that it has a profound influence on splicing performance.

4.2.2 Effects of chamber length and total splicing length on splicing performance

The relationship between chamber cross-section and total splicing length for varying yarn counts was found; therefore the effect of chamber length in relation to total splicing length was examined to reveal if this factor is a significant factor in splicing performance. Only one chamber profile was selected, namely the 4485, for the following experimentation using two key yarn counts. These yarn counts were:

- 2200dtex: This yarn count was well within the splicing range of the 4485 straight chamber profile.

- 6600dtex: At this yarn count, the 4485 straight chamber profile had begun to slightly fail with the standard splicer due to the yarn count approaching its limit of its splicing range.

The experimental setup used the two chosen key yarn counts, with the range of 4485 chamber lengths in both standard and hybrid splicers. There was one exception in that only the 4485 straight and 4485 small chambers were available for experimentation in the standard splicer because of its limited size. For each yarn count, splicer and chamber configuration, the pressure was varied between 20psig and 90psig, corresponding to earlier experiments.

Figures 4-12 and 4-13 demonstrated the variations of SRS, using the allowable 4485 chamber length range with the standard and hybrid splicer, at yarn counts of 2200dtex and 6600dtex respectively.

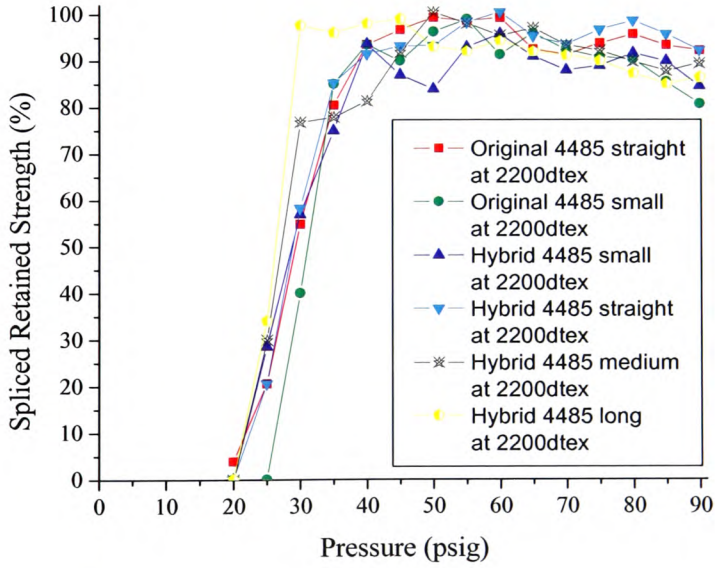

Figure 4-12. Comparison of 4485 straight chamber lengths using the standard and hybrid splicers with 2200dtex.

It was found from Figure 4-12, that using the hybrid splicer with a yarn count of 2200dtex, the 4485 straight chamber performed best at higher air pressures, improving its performance range compared to other chamber lengths. At lower air pressures, outside of the 4485 straight chambers main splicing pressure range (40 – 90psig), the longer chambers were producing satisfactory splices with the 4485 long chamber having the sharpest gradient in SRS. With the standard splicer, both the 4485 straight and 4485 small chamber lengths produced very satisfactory splices, consistently at higher pressures.

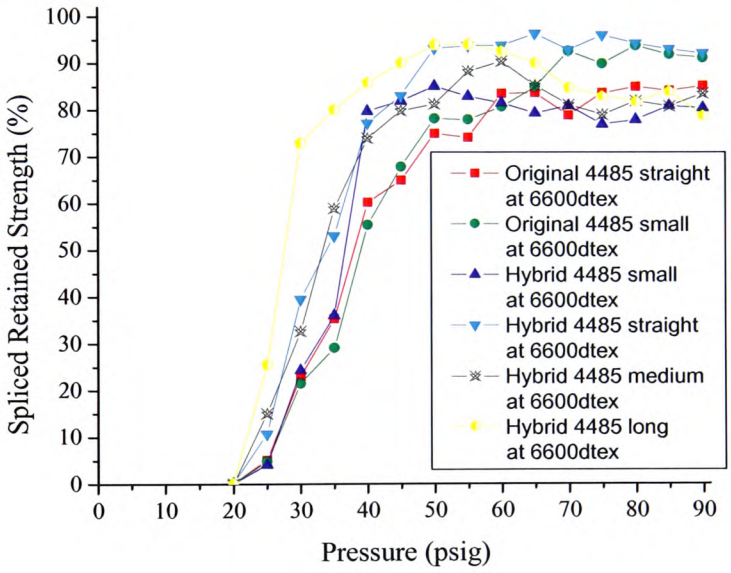

Figure 4-13. Comparison of 4485 straight chamber lengths using the standard and hybrid splicers with 6600dtex.

Figure 4-13 revealed the chamber length responses at 6600dtex. It was at this point that the chamber lengths began to reveal interesting conclusions. With the standard splicer, the 4485 straight chamber began failing to produce satisfactory splices at lower pressures. The 4485 small chamber produced better splices at higher air pressure compared with the 4485 straight chamber. With the hybrid splicer, all chamber lengths produced very satisfactory splices at higher pressures with the 4485 straight chamber

performing the best. The 4485 small chamber functioned the worst with a smaller gradient in SRS at lower air pressures. The 4485 straight and medium chambers both had similar, sharper gradients, in SRS at lower air pressures compared to the 4485 small chamber, while the 4485 long chamber produced superior splices at lower air pressures. These findings revealed that the reduction in chamber length improved splicer performance, but once a critical ratio between total splicing length and chamber length is surpassed, the reduction in chamber length becomes a limitation.

The appearance of the resulting splices over the splicing chamber length range varied slightly, with the larger chambers producing better splice appearance, but of little improvement compared to the smaller chambers. Thus the main performance increase in chamber length is towards splice strength.

Throughout the experimentation to analyse the relationship between splicing chamber length and total splicing length, taken together, it was found that the 4485 small chamber performed the greatest with the standard splicer presumably due to reduced restrictions, therefore increasing the airflow within the splicing chamber. The 4485 straight chamber performed the best in the hybrid splicer presumably due to the same reason as stated above. This reasoning was not true of the 4485 small chamber in the hybrid splicer, presumably due to the greater freedom between the loose tail ends of the yarns and the chamber ends, to maintain its control over the yarn ends. These results indicate that both splicing chamber length and total splicing length have an effect on splicing performance and the resulting relationship between them.

Overall, these observations represented powerful evidence for the existence of scaling. When count increased sufficiently, performance levels can only be maintained if:

- The splicing chamber cross-section becomes larger.
- The pressure increases.
- The total splicing length increases.

4.3 Conclusion

In this chapter, experiments were undertaken to prove if the phenomenon of scaling existed, and what affect it had on splice characteristics. A new hybrid splicer was developed that was essential in the testing of scaling. The results revealed powerful evidence for the existence of scaling. This verification of the existence of the effect called scaling is likely to be of profound importance to the design of splicers for very large yarns and tows. If a yarn was sufficiently large, it will not be sufficient merely to provide a larger splicing chamber cross-section. Splicers for such materials will probably need special provision for greatly improved air supply and an increase of total splicing length. The demands placed by the increasing yarn count in industry, will be such that splicers will almost certainly become too big to be hand-held.

Our research indicated that increasing the total splicing length vastly improved the yarn count range a given splicing chamber could handle before failing to create acceptable splices. This finding enables smaller cross-sectional splicing chambers to splice larger yarn counts thus improving the resulting splice appearance. This result has not been observed in published literature to date.

Through proving the existence of scaling, it was found that chamber length affected splicing performance but only on a smaller scale compared to total splicing length. Reducing chamber length improved splicing performance but the resulting splice appearance was slightly degraded compared with the longer chambers. Hence a hybrid splicer design has been used to prove that scaling is a major factor in splicing.

It is evident that further work is required in this area to analyse the splicing process in detail and thus the splice creation. During the splice creation, visual access to the interior of the splicing chamber is virtually impossible. Therefore, to analyse the splice formation throughout the splicing process, new methods need to be adopted that allow

us to visualise what occurs within the splicing chamber during a splice creation. This research will be described in the following chapters.

Chapter V

The use of visualisation and simulation techniques to model the pneumatic splicing process

Abstract – *Previous chapters have optimised splicer performance using indirect measures, such as blast pressure and duration. Indirect observations offer no insight into the theory behind the splicing process. Observing the splice formation with the naked eye is difficult because of the short duration and closed environment of the splicing process. This chapter reports on the application of visualisation and simulation techniques to the theoretical study of the splice formation.*

5.1 Introduction

As stated in Chapter 1, observing the splice formation with the naked eye is very difficult, because the splicing process is completed very swiftly, while enclosed in a virtually sealed environment. Various direct techniques have been used in attempts to observe the splice formation, but all have failed. Therefore different visualisation techniques have been implemented, by various researchers, with varying degrees of success, to simulate the splicing process.

This chapter reports on the application and validation of visualisation and simulation techniques to the splicing process. The visualisation and simulation techniques were utilised to analyse the splicing process in great detail, from different aspects, with the aim of yielding a theoretical model of the processes underlying splice formation. The visualisation and simulation techniques were:

1. A scaled model of a splicing chamber with consistent fluid properties.
2. The application of computational fluid dynamics (CFD) simulation software to create three dimensional (3D) models of the fluid flow within simulated chambers.

5.2 Visualisation and simulation techniques

The principal aim of the research described in this chapter was to identify and compare the airflows within a particular form of splicing chamber, using visualisation and simulation techniques, which are commonly used in many branches of research (Lamar, 2001; Haber, 1990; Daws *et al.*, 1965).

A number of visualisation techniques such as tracer filaments (Basal, 2003; Primentas and Iype, 2001), have been applied to the splicing process in the past, but they have proved inadequate for our research, yielding little new information. The constraints on direct observations, and the inadequacies of visualisation techniques used to date, have led previous researchers into using only indirect observations.

Though confronting the same constraints, the research discussed in this chapter has taken a novel approach to the use of visualisation and simulation techniques. Two methods were implemented to analyse the airflows in the specimen splicing chamber. The first method is a visualisation technique, which involved true splicing, addressed the problems of the speed of the process, and the lack of visual access to the splicing chamber by using a large scaled model of a typical splicing chamber, made of transparent plastic. The second method is a simulation technique which uses CFD software to simulate airflows in a range of different splicing chamber forms.

5.2.1 Visualisation technique – Large scale model of splicing chamber

This approach aimed to make the interior of the chamber visible, slowing the process of splice creation so that it could be seen in real time. A 10:1 scaled model of a standard 4483 trapezium chamber was manufactured, with a length equivalent to a real chamber of 10mm. It was constructed in transparent PMMA (Plexiglas, Perspex). This form of chamber was chosen because it had been used throughout the research programme, and its performance envelope was well understood, as has been documented in previous chapters. The form of the chamber is shown in Figure 5-2.

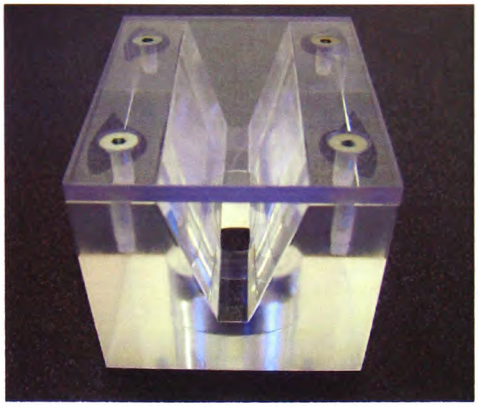

Figure 5-2. Large scale model of the 4483 straight splicing chamber.

To provide an accurate representation of the original airflow within the normal 4483 straight chamber, it was necessary to keep the Reynolds number constant. The Reynolds number is a dimensionless flow constant which characterises the airflow properties within the splicing chamber. To achieve this goal, it was necessary to change some of the splicing parameters.

The Reynolds number for the airflow within a 4483 straight chamber at 90psig was calculated from Equation 5-1 below.

$$\text{Reynolds number (Re)} = \frac{Vs \cdot L}{U_{\text{air}}} \tag{5-1}$$

Where

Vs = Mean fluid velocity (ms^{-1})
L = Characteristic length (m)
U = Kinematic fluid viscosity $(m^2 s^{-1})$

$$and\ U = \frac{\text{Absolute fluid viscosity}}{\text{Fluid density}}$$

The mean fluid velocity was calculated from the mean flow rate and chamber profile area as shown in Equation 5-2. The flow rate was obtained by connecting a flow meter to the experimental setup.

$$Vs = \frac{Volume\ flow\ rate\ (m^3 s^{-1})}{Chamber\ profile\ area\ (m^2)} \tag{5-2}$$

$$Vs = \frac{\square\ 143\,\text{ltr/min}}{10.014\,mm^2} \approx \frac{0.00239\,m^3 s^{-1}}{0.000010014\,m^2} \approx 238.75\,ms^{-1}$$

$$\therefore \text{Reynolds number (Re)} = \frac{Vs \cdot L}{U_{air}} = \frac{238.75 ms^{-1} \times 0.004m}{1.5 \times 10^{-5} m^2 s^{-1}} \approx 64 \times 10^3$$

Thus the characteristic Reynolds number for the splicing process was approximately 64000, indicating that the airflow within the splicing chamber is highly turbulent, which was determined by the following criteria:

Re < 2100 = laminar airflow

2100 < Re < 4000 = transitional flow

4000 < Re = turbulent airflow.

The size of the smallest turbulence scales is set by the Reynolds number. As Reynolds number increases, smaller and smaller scales of the flow are visible. In this sense, the Reynolds number is an indicator of the range of scales in the flow. The higher the Reynolds number, the greater the range of scales. The largest eddies will always be of the same order of size as the overall geometry, while the smallest eddies are determined by the Reynolds number (Chiang *et al.*, 1996).

To reduce flow rate while maintaining constant Reynolds number in the experimental chamber, a fluid with a higher density and a greater viscosity than air was selected.

Water was the ideal candidate, because it was transparent, easily handled, and had a combination of physical properties which yielded a Reynolds number of the right magnitude. The new fluid flow rate was calculated using Equations 5-1 and 5-2:

From Equation 5-1:

$$Vs = \frac{\mathrm{Re} \cdot U_{\text{water}}}{L_{\text{scaled model}}}$$

Where

$$\mathrm{Re} = 63661.9$$
$$U_{\text{water}} = 1.002 \times 10^{-6} m^2 s^{-1}$$
$$L_{\text{scaled model}} = 0.04m$$

$$\therefore Vs = \frac{63661.9 \times (1.002 \times 10^{-6})}{0.04}$$

$$Vs = 1.6ms^{-1}$$

Therefore, from Equation 5-2:

$$Volume\ flow rate\ (m^3 s^{-1}) = Vs\ (ms^{-1}) \cdot Chamber\ profile\ area\ (m^2)$$

$$Volume\ flow rate = 1.6ms^{-1} \times 0.0010014m^2$$

$$\therefore Volume\ flow rate \approx 1.6ls^{-1}$$

The flow rate calculated above was representative of blast pressure of 90psig, for air in the 4483 straight chamber. The experimental chamber was placed in a water tank, as shown in Figure 5-3.

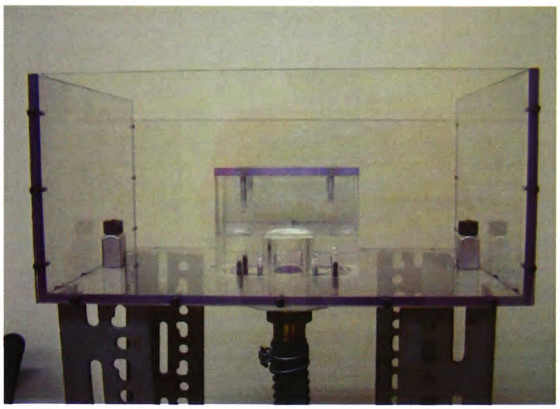

Figure 5-3. Large scale chamber mounted in water tank.

The water pump used was a Draper type SWP110. The pump was placed in a large bath of water beneath the scaled chamber, which recycled the water throughout the experiment allowing non-stop recordings of any duration. Water flow was controlled via a mechanical valve.

The scaled model was subjected with water at flow rates of $1.6ls^{-1}$ and $1.02ls^{-1}$, which were equivalent airflows at 90psig and 50psig respectively. Digital cameras were used to produce still images and videos of the flow patterns. Selections of the results over the full blast cycle are shown in Figures 5-4 and 5-5. This yielded direct comparisons on the relationship air pressure had on the fluid flow within the specimen chamber.

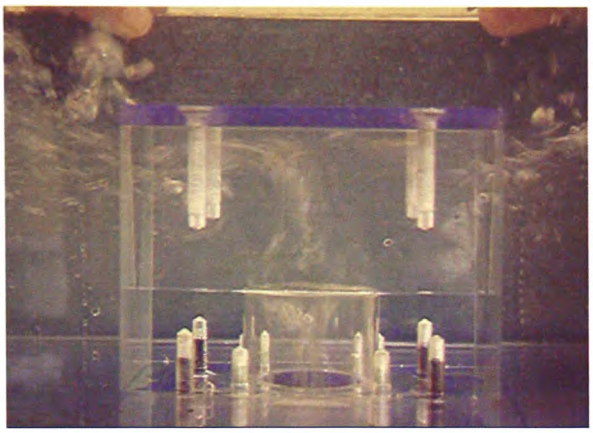

(A)

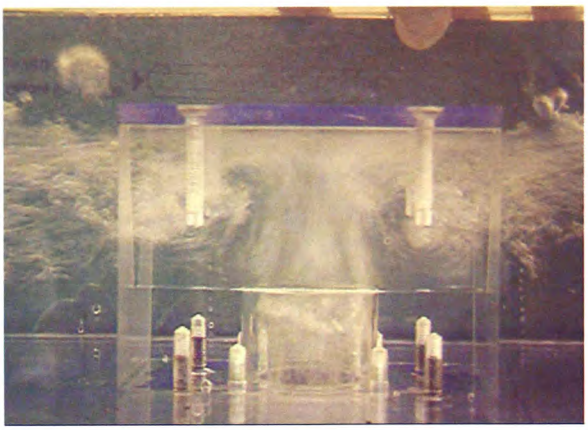

(B)

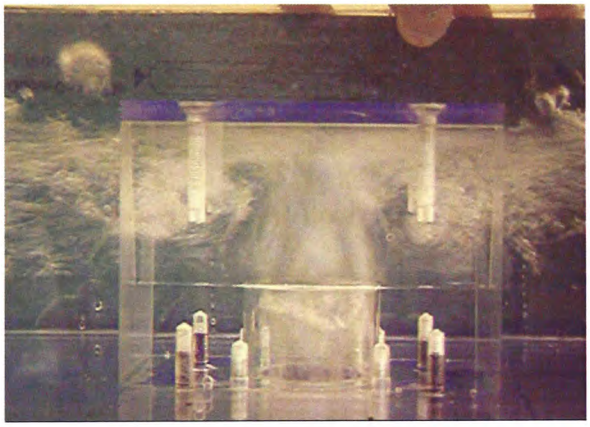

(C)

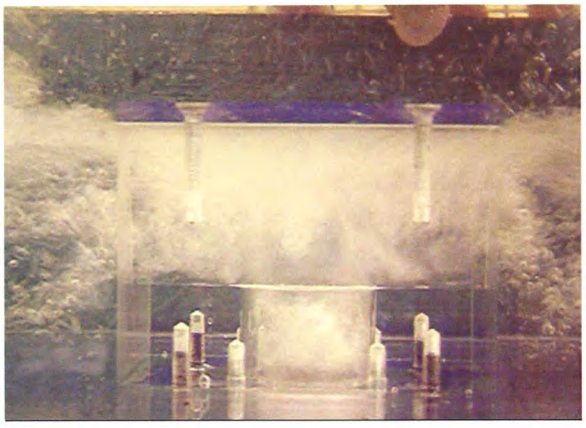

(D)

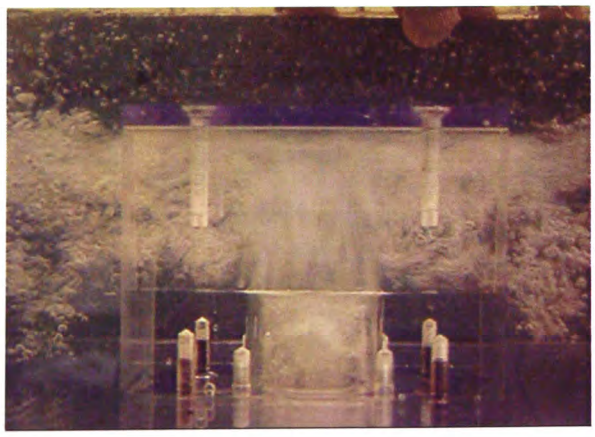

(E)

(F)

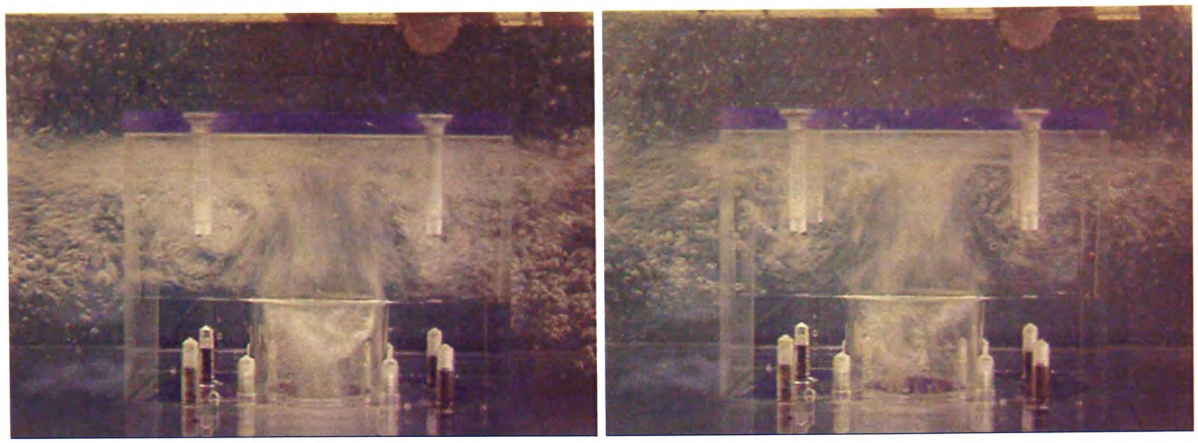

(G) (H)

Figure 5-4. Large scale model visualisation of airflow over a full blast cycle at 50psig.

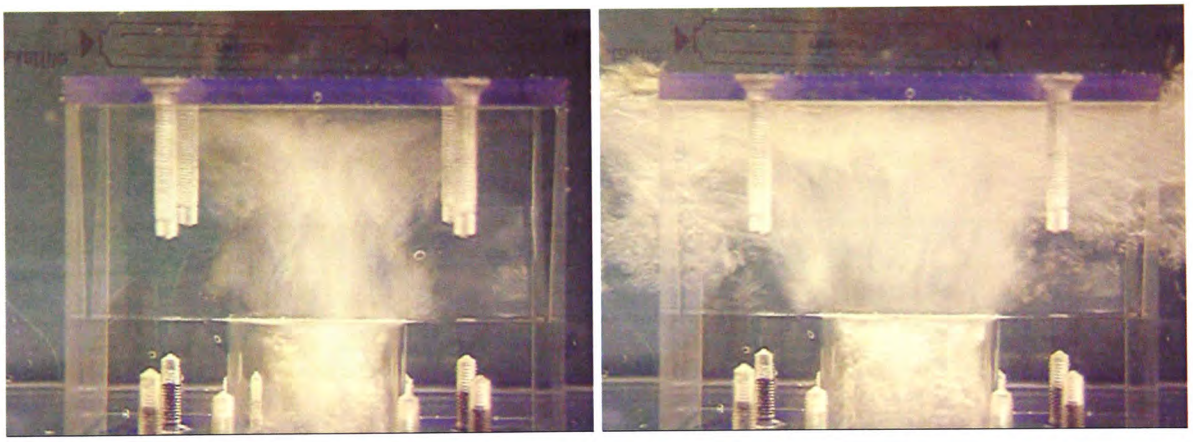

(A) (B)

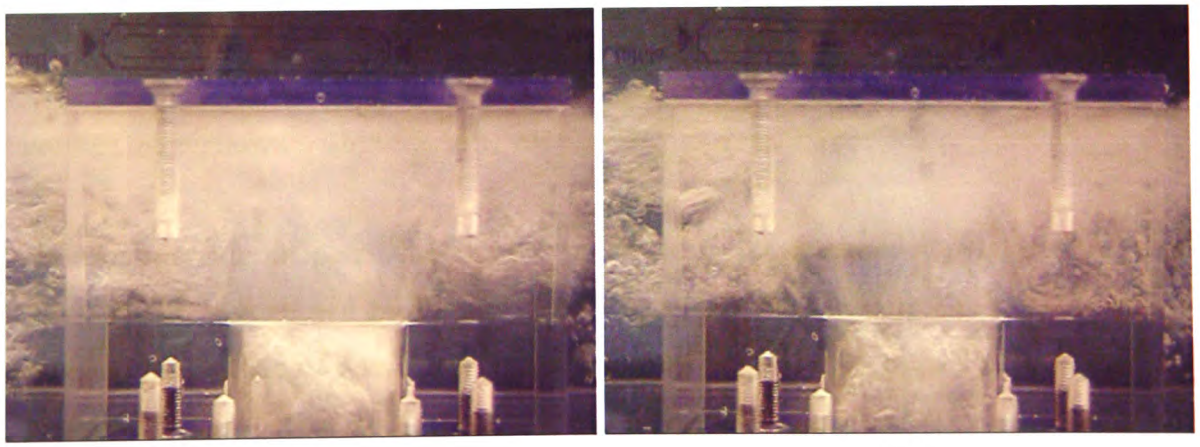

(C) (D)

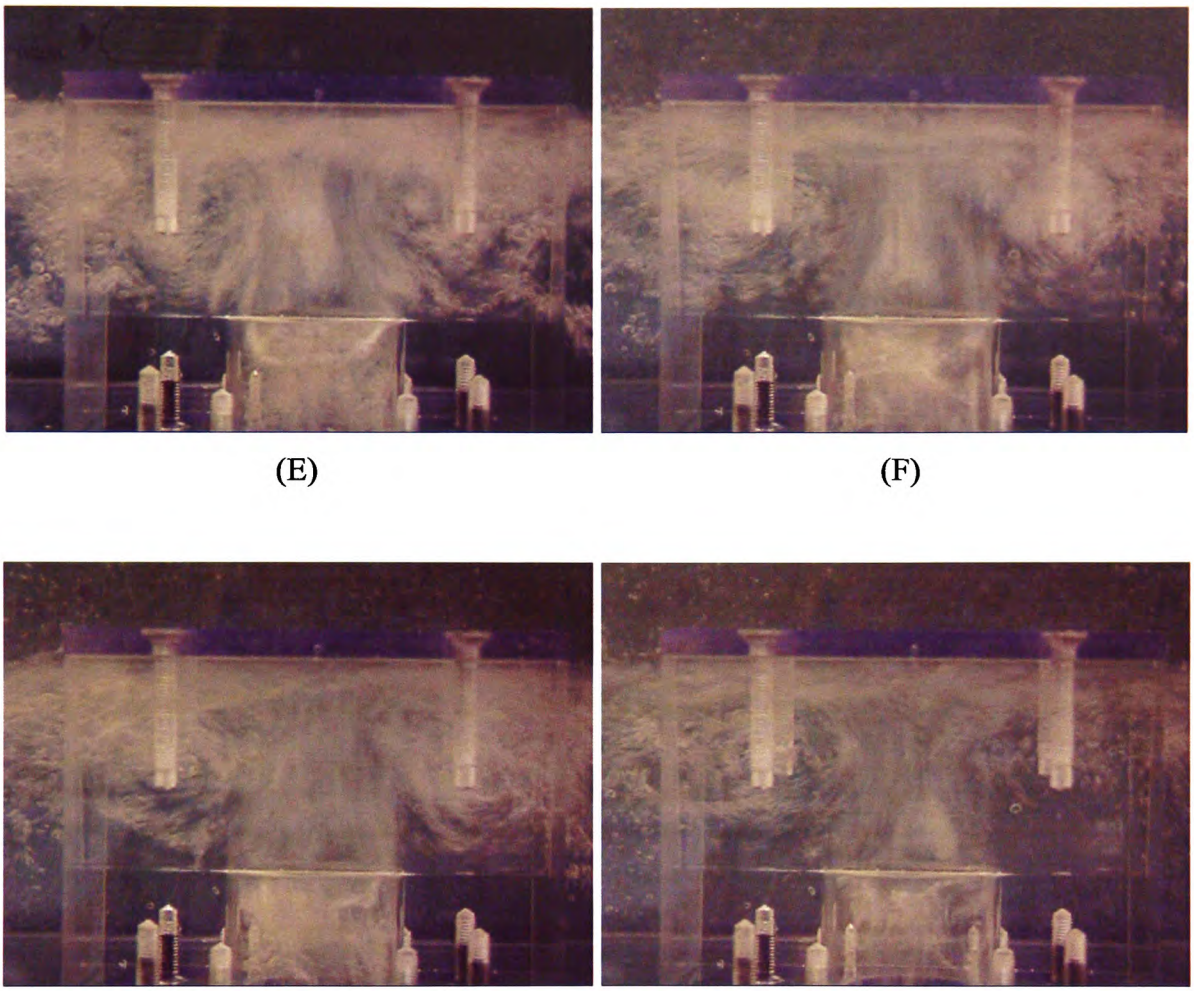

(E) (F)

(G) (H)

Figure 5-5. Large scale model visualisation of airflow over a full blast cycle at 90psig.

As can be seen the scaled model experiment reveals with some clarity the fluid flow within the splicing chamber. It reveals general similarities, and distinctive differences, between the airflows within the splicing chamber at different pressures.

The characteristic shape of the fluid flow was apparent at both 50psig ($1.02ls^{-1}$) and 90psig ($1.6ls^{-1}$) as shown by Figures 5-4 (F) and 5-5 (F) respectively. However, the scale and magnitude of the swirling vortices are larger and faster at 90psig (which was to be expected) with more of the higher velocity fluid flows residing at the roof of the chamber and flowing directly out in a direction perpendicular to that of the blast hole.

The comparison between fluid flows at different pressures was simply observational. No attempt was made at this stage to measure the velocities of individual bubbles through the chamber. This experiment was undertaken simply to establish a visual representation of the fluid motion within the chamber during a blast cycle for future reference.

Certain key fluid flow features can be seen:

- The principal vortices occupy all of the space between the outer edges of the main jet and the outer edges of the chamber.
- There is only moderate reverse flow near the base of the chamber
- There appear to be regions where the flow separates from the roof of the chamber to left and right of the blast jet, particularly visible as a white sloping "shoulder" line most clearly seen in Figure 5-5 (F).

5.2.2 Simulation technique – Computational fluid dynamics

This simulation technique used a CFD software package called Fluent and its associated computer aided design (CAD) software, Gambit. The software was applied to create a 3D computer simulation model of the airflow within a wide range of splicing chamber designs. The purpose of the work was to gain some insight into the relationship between chamber geometry and airflow.

Though relatively new, CFD has swiftly become a well-established and respected subject. However, literature on its application to splicing is sparse. Zhou and Qin (2005), used the technique, but only for observation purposes, and they made no attempt to apply their information to an understanding of the splicing process.

With the resources available, the CFD technique was not sufficiently powerful to model the behaviour of a multiplicity of individual fibres within a splicing chamber. Therefore it was necessary to ignore the presence of yarn end fibres within the chamber

space. Nevertheless, the technique made it possible to compare and contrast the airflow patterns within different chambers, thereby identifying common characteristics.

The CFD simulation is commonly accepted as the numerical solution to the governing set of Navier-Stokes equations, equation of continuity and the additional conservation equations of momentum and energy. The partial differential equations that govern fluid flow are not amenable to analytical solutions, except for very simple cases. Therefore, in order to analyse fluid flows, flow domains are split into smaller subdomains. The governing equations are then discretised and solved inside each of these subdomains. The subdomains are called cells, and the collection of all cells is called a mesh (Fluent Inc., 2005a).

To create an accurate simulation model of the airflow within the splicing chamber a number of complex steps are required:

- Create virtual entities of the fluid flow regions
- Generate a volume mesh for each region as required
- Export the mesh and apply computational fluid dynamics
- Analyse the 3D fluid flow throughout the entire entity

Firstly a 3D CAD geometry was created of the boundaries that enclose the fluid flow regions. Once the volume geometry was completed, a user defined mesh was generated automatically over the whole geometry volume with finer mesh regions created at key airflow locations, to improve accuracy. The CAD geometry and mesh generation created for a specimen chamber ready for exporting into Fluent is shown in Figure 5-6.

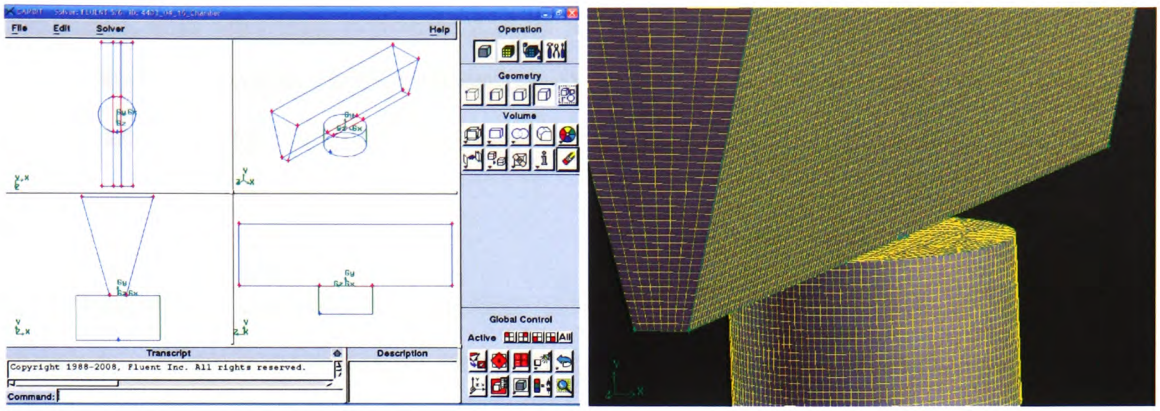

(A) (B)

Figure 5-6. (A) CAD; (B) Volume mesh generation for specimen fluid flow regions.

Once a successful volume mesh had been generated, it was exported into Fluent for the computation stage. The CFD model selected to analyse the fluid flow was the "realisable $\kappa - \varepsilon$ turbulence model" without the inclusion of fibres to simplify the fundamental study of the splicing process. A turbulence model was selected because of the very high Reynolds numbers in all known splicing processes, i.e. $Re > 4000$.

An immediate benefit of the realizable $\kappa - \varepsilon$ model over other $\kappa - \varepsilon$ models is that it more accurately predicts the spreading rate of both planar and round jets. It is also likely to provide superior performance for flows involving rotation, boundary layers under strong adverse pressure gradients, separation, and recirculation (Fluent Inc., 2005b). This was considered essential in modelling the splicing process, since high rotational airflows were known to exist in splicing chambers.

The software yielded a detailed 3D representation of the airflow properties, for the specified splicing chamber and splicing parameters. The software is powerful, generating a vast amount of information, such as velocity, mass flow rate and force magnitudes. In the first instance, however, no attempt was made to analyse this additional information. The sole purpose of the first stage was to validate the CFD technique, to determine whether it was likely to prove a useful tool for gaining an understanding of the turbulent flow structure within a chamber. With the technique

established, this was then a simple matter to run the software repeatedly, examining as many splicing chamber configurations as the experimental computers could handle. It is at this second stage that the additional material generated by the software could prove useful.

Thus, before the simulation technique could be used for analyses, it needed to be validated. Complete validation would be impossible, but a crucial first step would be to compare the output fluid flow from the CFD simulations to the results which had emerged from the scaled chamber visualisation work. A typical example of the flow within the scaled chamber is shown in Figure 5-7.

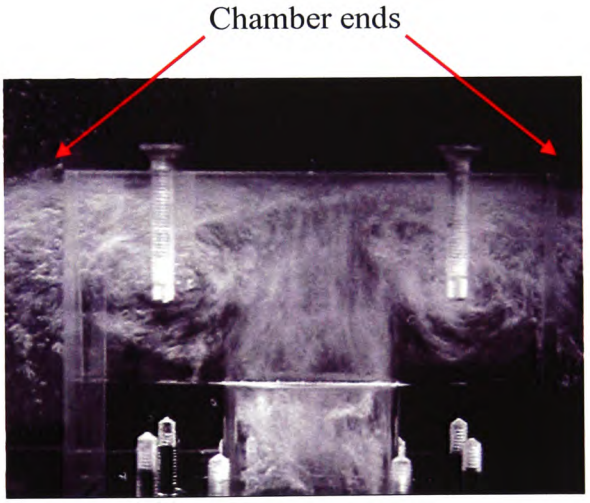

Figure 5-7. Scaled model fluid flow.

In real-life splicers, air is supplied to the splicing chambers by machined airways, which may have unusual cross-sections, or pronounced changes of direction. Figure 5-8A shows the multiple changes of direction experienced by the compressed air blast in a Model 1-11 splicer, culminating in the 4483 straight chamber, emphasised in Figure 5-8B to reveal the flow more clearly. This streamline fluid flow simulation represents the same chamber cross-section as the scaled chamber, but with a length equivalent of 16mm instead of 10mm.

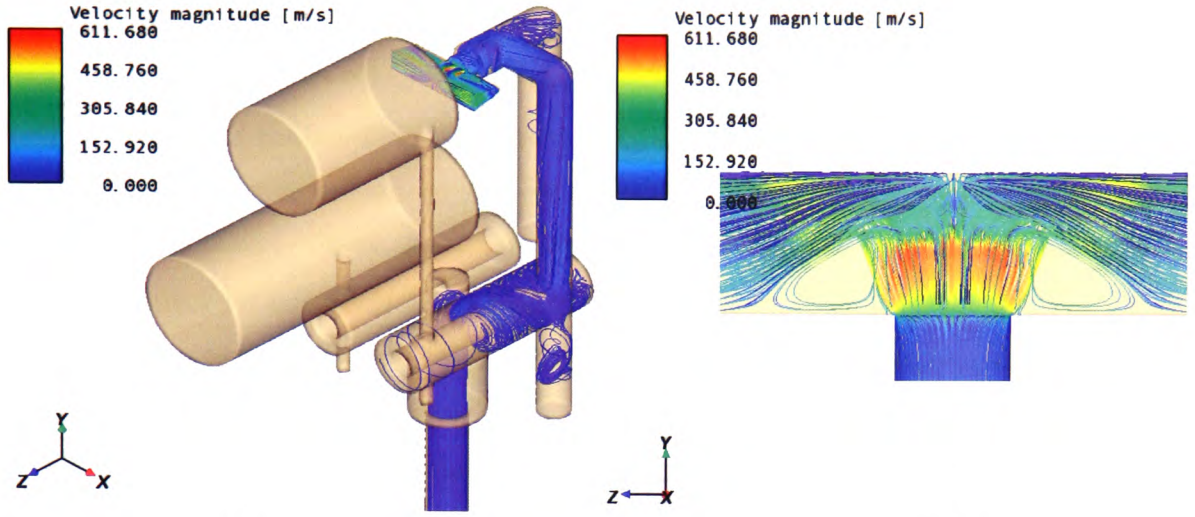

(A) (B)

Figure 5-8. CFD streamline fluid flow simulation representing (A) the whole flow path; (B) the 4483 chamber cross-section, 16mm length.

The full path flow through the Model 1-11 was simulated to develop the fluid flow so that the inlet boundary condition to the chamber was correct. All following simulations were conducted using the full path flow through the Model 1-11 splicer, but only the 3D chamber sections were shown for representation, as this is the critical area where the splicing occurs.

Some key points of difference emerged:

- The CFD simulation differs, in that the principal vortices do not occupy all of the space between the outer edges of main jet and the outer edges of the chamber.
- The CFD simulation was different, in that there is considerable reverse flow very close to the base of the chamber
- In the CFD simulation, there are regions where the flow separates from the roof of the chamber to left and right of the chamber, but in this case the flow is much more clearly defined than in the scaled chamber.

Figure 5-9 shows the second of two CFD simulations. Both 3-D realizable k-epsilon turbulence model simulations were created using a hexahedral mesh, type Cooper, with

an interval size of 0.1mm. The boundary conditions at the input (blast hole) and outputs (both exits from either side of the chamber trapezium section) were 90psig with a flow rate of 143liters/min and 0psig respectively. This streamline fluid flow simulation represents a direct equivalent in chamber cross-section and length to that of the scaled chamber. Now the correspondence between this CFD simulation and the scaled chamber visualisation is startling:

- The principal vortices of the CFD simulation look very similar to those of the scaled chamber, occupying the same portion of the chamber.
- The reverse flow near the base of the chamber is modest, as with the scaled chamber
- The region of flow separation from the roof of the chamber is almost identical to that prevailing in the scaled chamber.

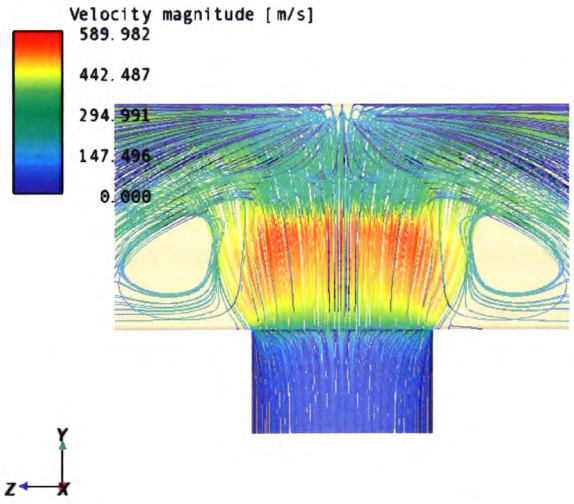

Figure 5-9. CFD streamline fluid flow simulation representing 4483 chamber cross-section, 10mm length.

The conclusions:

- There was a marked difference between the CFD simulations for a chamber of 16mm and a chamber of 10mm.

- There was a marked difference between the CFD simulation for a chamber of 16mm and the observed fluid flow in the scaled chamber.
- There was a remarkable correspondence between the CFD simulation for a chamber of 10mm and the observed fluid flow in the scaled chamber.

This series of validation experiments seem to offer compelling evidence for the general accuracy of the visualisation and simulation techniques used in this research. At first sight, the results seemed good enough to justify a substantial programme of work on CFD simulations. However, there remained one significant concern. The potential problem with the accuracy of both scaled model and simulated chambers, was the absence of yarns.

5.3 Relevance of yarn absence in the visualisation and simulation of fluid flow

In the case of CFD, it would have been impossible, with the resources available, to model the complexity of a real yarn, with a multiplicity of filaments, in a splicing chamber. Even the relatively simple simulations, of fluid flows in empty chambers, demanded much from the modest computational power, which was available. In the first instance, the simulations were run simply to gain a "feel" for the general nature of the airflows in different chamber formats. The target at the outset was merely to identify certain common characteristics between chambers of different forms, from different manufacturers.

However, as the body of CFD results grew, it became clear that the pattern of airflows within splicing chambers were very consistent and distinctive, and that the vortices were large and well defined. It also became reasonable to conclude that the only logical place for a yarn bundle to reside in a splicing chamber, once in equilibrium, would be along the "null lines" of the main vortices, which form to left and right of the blast hole and run the full length of the chamber. It seemed quite credible that the CFD simulations did, after all, have some relevance to the real world of splicing. If yarns

tend to lie along these vortex null lines, then a CFD simulation of an empty chamber can give an insight into the mechanism of splicing.

This was a hypothesis which needed to be tested, and one validation experiment was simple to perform. It had been established that there was a close correspondence between the predictions of the CFD software, and the actual flow observed in the transparent scaled chamber. The CFD results provided an incentive to use the scaled chamber to observe the formation of real splices in real time. If the scaled chamber could be shown to produce similar results to those of a normal chamber, and if the yarns could be seen to lie along the null lines of the vortices, then there would be good justification to deduce that a CFD simulation of an empty chamber is a valid representation of the airflow.

An extremely large yarn of 11000dtex was assembled from ten pieces of the 1100dtex yarn, which had been used throughout this research program. Cut by hand, lengths of this large yarn were fed into the scaled chamber, side by side, and exposed to the water flow.

Figures 5-10 revealed the splicing chamber from different angles. Comparison with the flow patterns through these figures reveals that the yarns do indeed lie in the null zones and follow the "shoulder" shape of the fluid flow as it falls away from the roof of the chamber. Much more detail can be seen in Appendix 1.

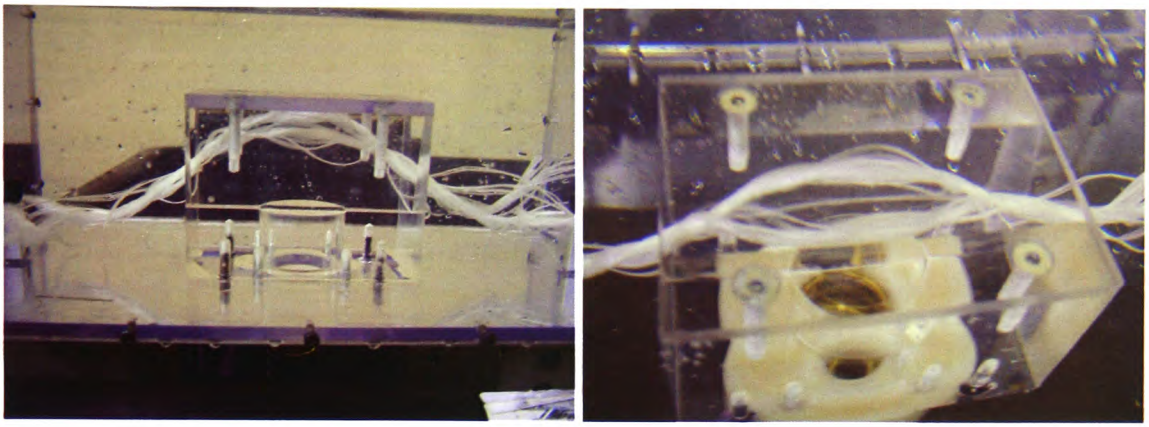

(A) (B)

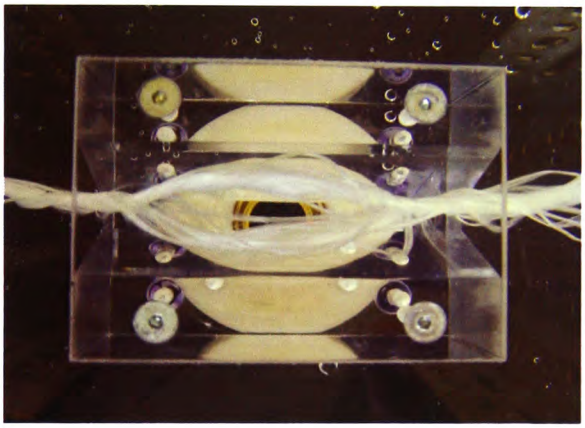

(C)

Figure 5-10. Splice creation in large scaled model.

Figure 5-10 (C), taken from above, shows clearly how bundle separation occurs directly above the blast hole, and how bundles are false-twisted, converging as the vortices lose their identity as they emerge into free air.

These results provided sufficient evidence that CFD simulations, of airflows in empty splicing chambers, were a useful tool for predicting the behaviour of air in splicing chambers, even when yarns were present. With the simulation accuracy validated, it was clear that CFD was likely to be a suitable tool for the analysis of airflow characteristics of a wide range of commercially available chambers. These simulations are analysed and discussed in the next section.

5.4 CFD Simulations

Once validated, the CFD simulations could be used to re-examine the outcomes of the earlier experiments, in which indirect observations had been used in experiments on a range of splicing chambers, under a range of conditions.

The earlier experiments had concentrated on three particular splicing chambers. Two, respectively identified as 4483 straight and 4485 straight, had simple trapezium cross-sections, but differed slightly in width of cross-section. The third, identified as 4483 bowl, was based on the 4483 profile, but had a deep bowl shape at top of the chamber above the blast hole.

CFD simulations were created for these three chamber forms. Both straight chamber simulation models were created using the same meshing scheme and interval size as the scaled model simulations (Figures 5-8 and 5-9). The 3-D realizable k-epsilon turbulence model simulation for the bowl chamber was created using a tetrahedral mesh, type TGrid, with an interval size of 0.1mm. The first of two boundary conditions at the input of the 4483 straight, 4485 straight and 4483 bowl chambers were 90psig with flow rates of 143, 159 and 132liters/min respectively. The second of two boundary conditions at the input of the 4483 straight, 4485 straight and 4483 bowl chambers were 50psig with flow rates of 108, 121 and 99liters/min. The outputs boundary condition for all models was 0psig. Each simulation produced a large body of information, too much for the main section of this document, but samples of the outputs are shown in Figures 5-11 to 5-13. Much more detail can be seen in Appendix 1. This appendix should be analysed in some detail, because the images provide a good insight into the significance of different chamber geometries.

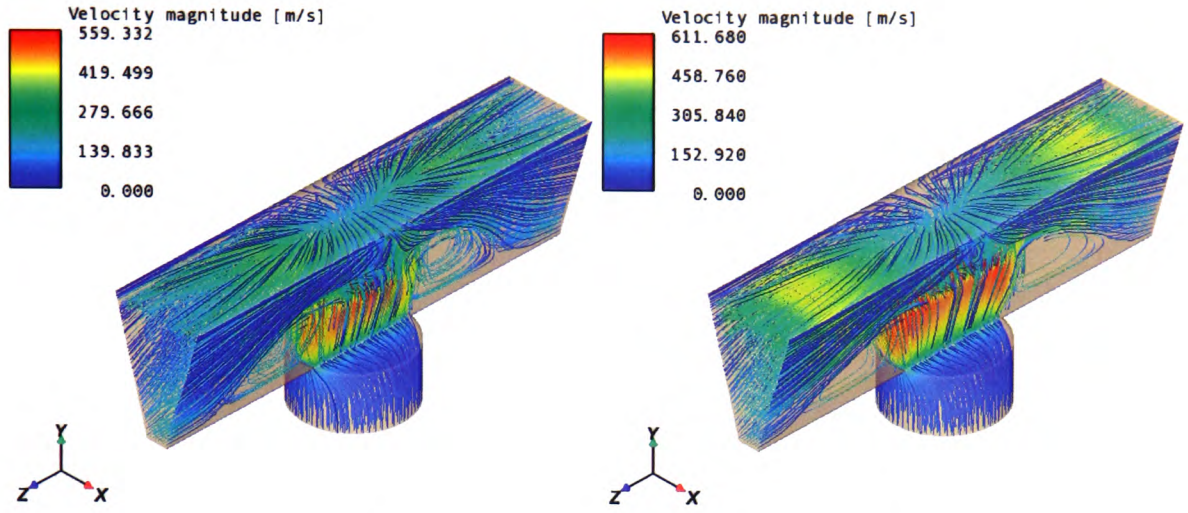

(A) (B)

Figure 5-11. 4483 straight splicing chamber: Sample CFD streamline simulation at (A) 50psig and (B) 90psig.

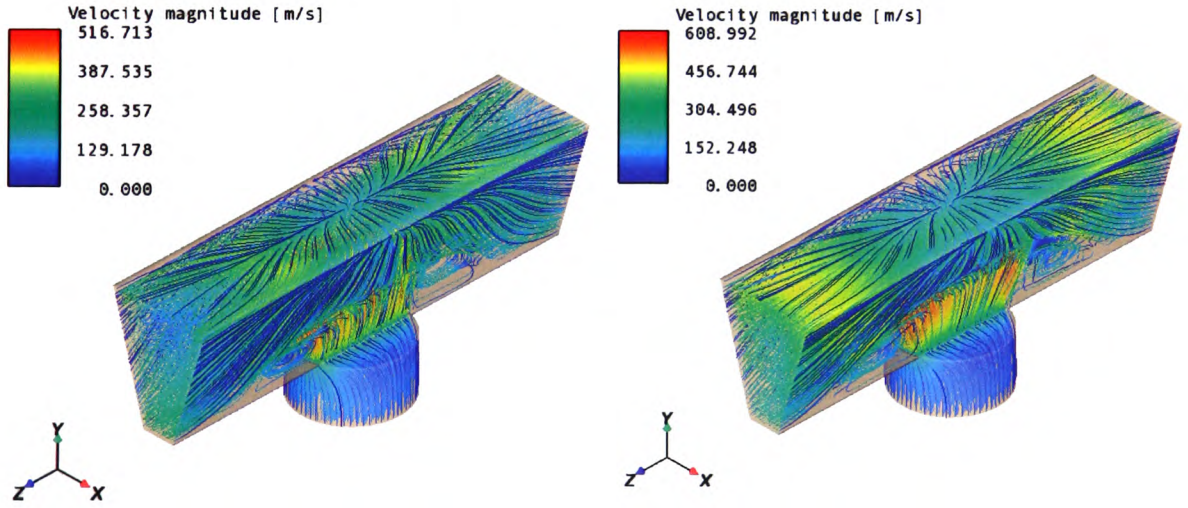

(A) (B)

Figure 5-12. 4485 straight splicing chamber: Sample CFD streamline simulation at (A) 50psig and (B) 90psig.

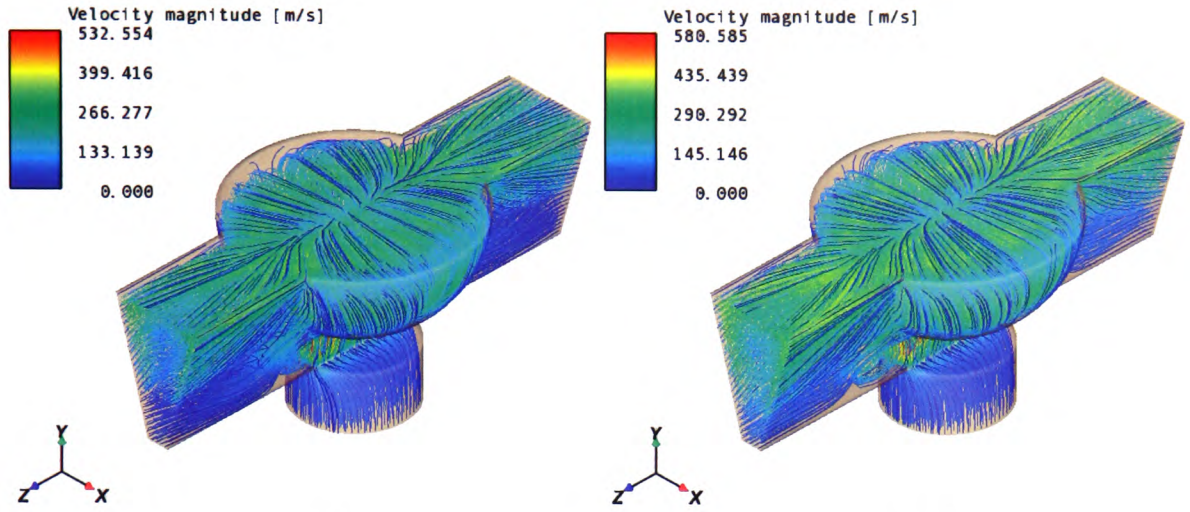

(A) (B)

Figure 5-13. 4483 bowl splicing chamber: Sample CFD streamline simulation at (A) 50psig and (B) 90psig.

All three chamber simulations indicated strong vortices in the *z* direction, on either side of the blast hole. Two significant vortices occur in the *x* direction split by the centre of the blast hole; they decay in strength towards the chamber ends. These vortices create equal but opposite rotation in the *x*-axis, which splits the yarn ends into two bundles and intermingles them throughout the length of the splice. The intermingling of the individual filaments draws the loose tails ends into the chamber, thereby slightly reducing the splice length.

The 4483 bowl chamber (Figure 5-13) seemed to function slightly different from the straight chambers; probably because it created stronger vortices in the *x*-axis. These stronger vortices improved the chambers performance by increasing the intermingling rate, producing a shorter more compact splice. There was a slight penalty in terms of appearance, because the twist-reversal zone at the centre of the splice is more conspicuous.

With all chambers, the airflow pattern remains fairly consistent as pressure varies, the principal difference being that the velocity increases with increasing pressure. With all

chambers, the yarn ends are carried to the top of the chamber, and are then separated into two approximately equal bundles, which rotate in opposite senses. It seems that the principal difference between one chamber and another lies in the efficiency of this process of separation and rotation.

5.5 Commercially available splicing chambers

The series of streamline fluid flow simulation results which follow (Figures 5-14 to 5-18), show results at varying angles, from other splicing chambers at 90psig, which are used in commercial splicers. Their simulations give weight to the proposition that, although chamber profiles differ widely, they actually produce fairly similar patterns of airflows.

The first two commercial chamber simulations (Figures 5-14 and 5-15) were created using the same meshing scheme and interval size as the 4483 bowl chamber simulation. The remaining commercial chamber simulations (Figures 5-16 to 5-18) were created using the same meshing scheme and interval size as the straight chamber simulations. The boundary conditions at the input and outputs of these simulations were 90psig with a flow rate of 143liters/min and 0psig respectively.

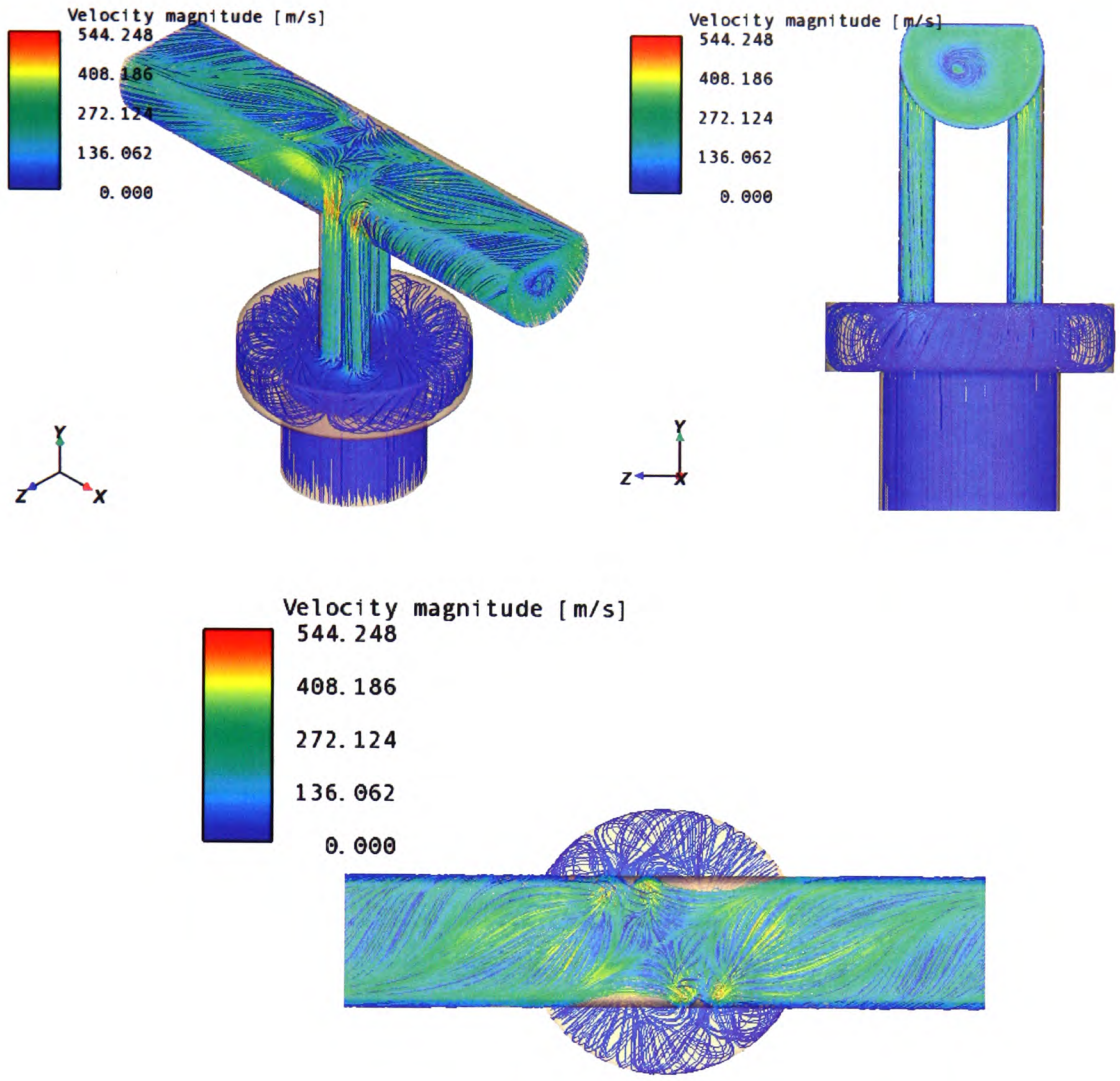

Figure 5-14. Streamline fluid flow simulation of commercially available splicing chamber.

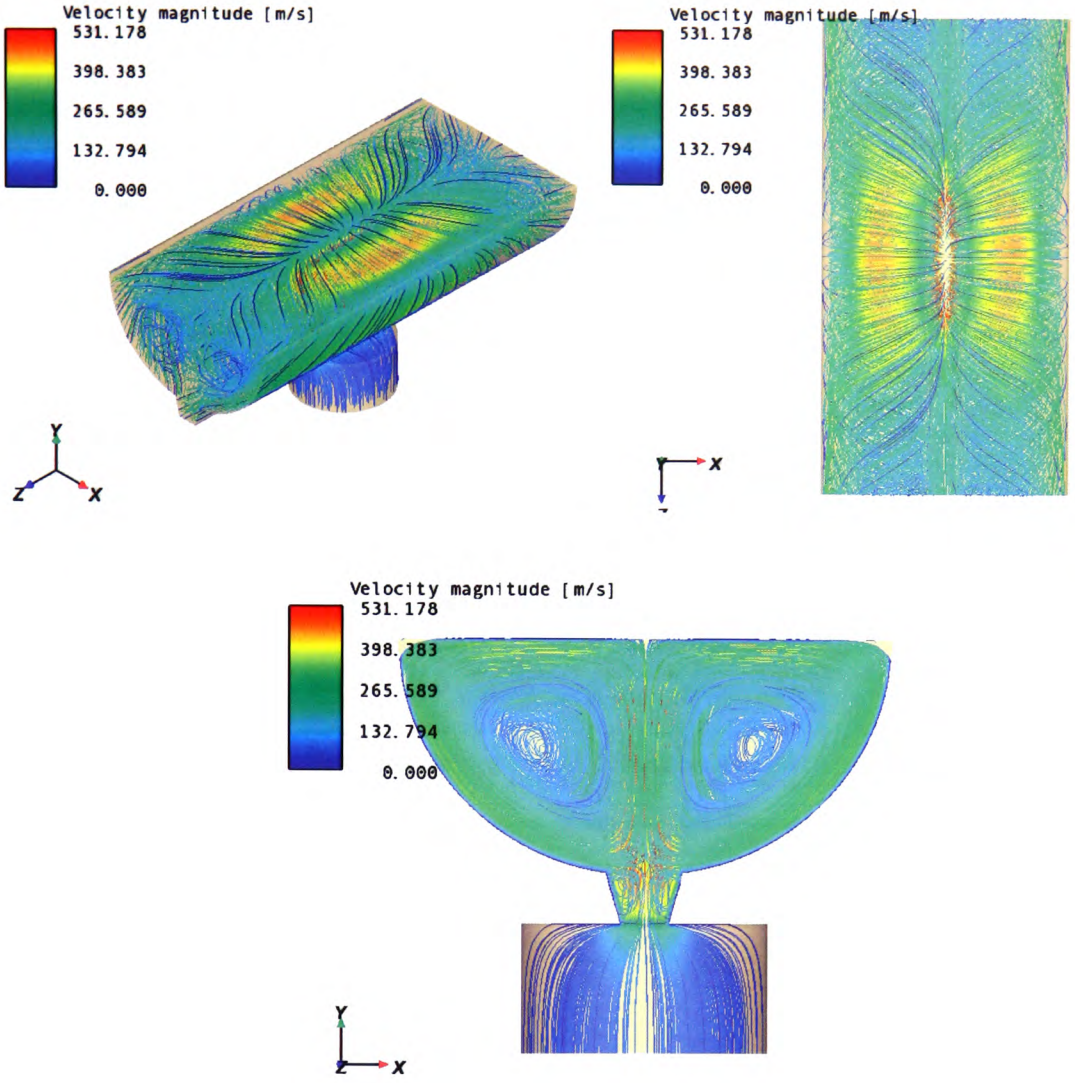

Figure 5-15. Streamline fluid flow simulation of commercially available splicing chamber.

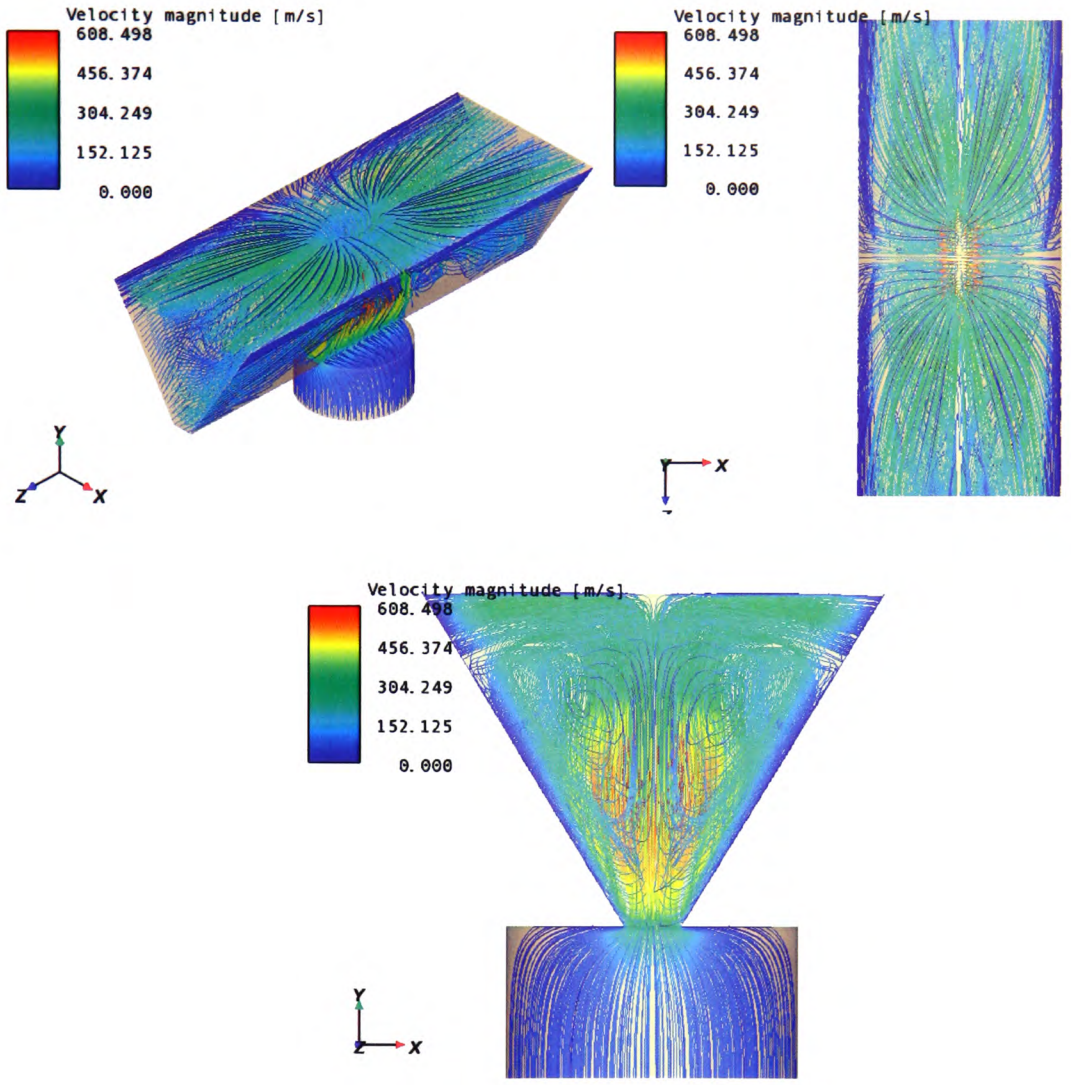

Figure 5-16. Streamline fluid flow simulation of commercially available splicing chamber.

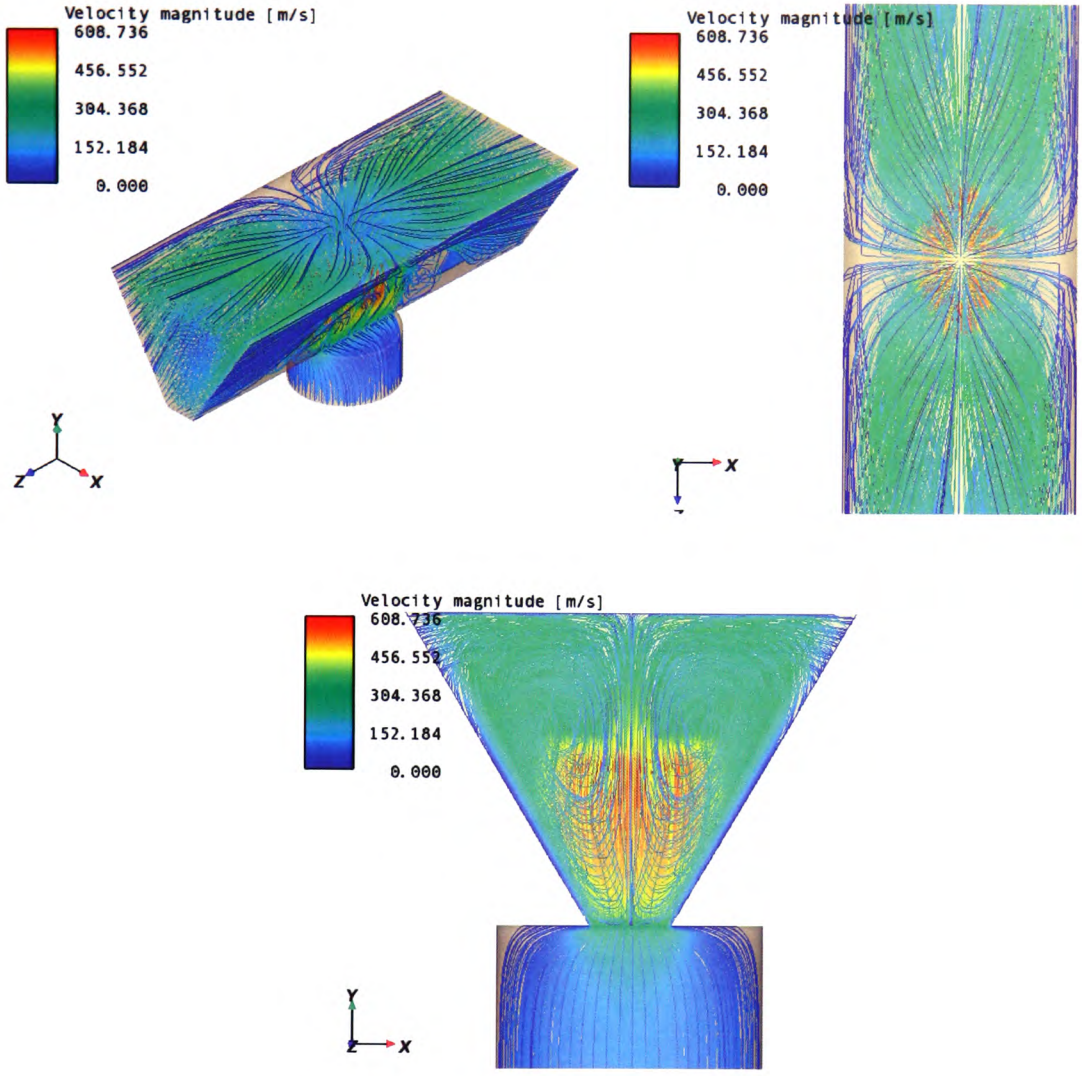

Figure 5-17. Streamline fluid flow simulation of commercially available splicing chamber.

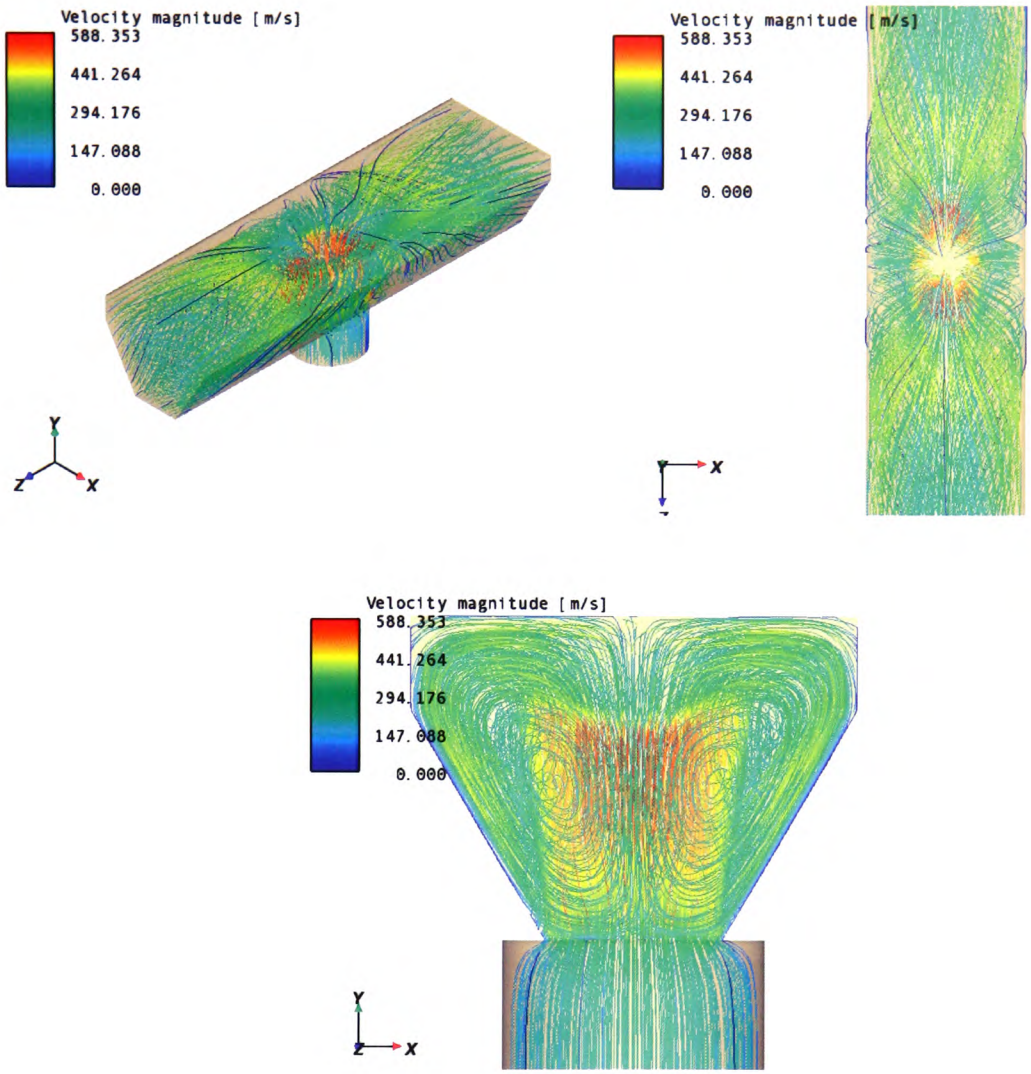

Figure 5-18. Streamline fluid flow simulation of commercially available splicing chamber.

Throughout these simulations a common characteristic airflow was revealed. All splicing chambers produce a pair of equal but opposite vortices either side of the blast hole, separating the yarn bundles for intermingling. This common airflow creates a distinctive formation of the splice. This splice structure is described in greater detail in the following chapter.

The function of all the splicing chambers is therefore broadly the same. The work seems to confirm the earlier deduction that the principal difference between all these chambers is simply their splicing efficiency.

All the preceding simulations relate to splicing chambers which are used to produce "ends-opposed" splices; this is by far the most commonly used form of joint. This form of splicing chamber was the one used throughout this programme of research, for the reasons described in Chapter 1. It is known that the processes, which control the formation of an ends-together splice, are the same as those that form an ends-opposed splice. The same characteristic general principles of airflow, apply to ends together chambers. However, in this instance the chambers are designed to drive the airflow in one direction, to produce the particular characteristics of the ends-together splice form. Since this programme of work was directed at the general principles of splicing, it was not deemed appropriate to conduct too much work on what is unquestionably a special case.

Nevertheless, it was felt appropriate, for the record, to demonstrate the similarities and differences between ends-opposed and ends-together chambers. Two ends-together chambers were simulated, as shown in Figures 5-19 and 5-20. The first ends-together chamber simulation (Figure 5-19) was created using the same meshing scheme and interval size as the straight chamber simulations, where as the second ends-together chamber simulation (Figure 5-20) was created using the same meshing scheme and interval size as the 4483 bowl chamber simulations. The boundary conditions at the inputs and outputs of both simulations were 90psig with a flow rate of 143liters/min and 0psig respectively. As can be seen, there are broad similarities between the two streamline fluid flow simulations. They share a feature, which is characteristic of many ends-together chambers – a single direction of rotation. This design feature was incorporated in these chambers to handle yarns, which have a very high twist level. The direction of rotation is chosen to remove the twist. Much more detail on ends-together splicing and ends-preparation can be seen in Appendices 3 and 4.

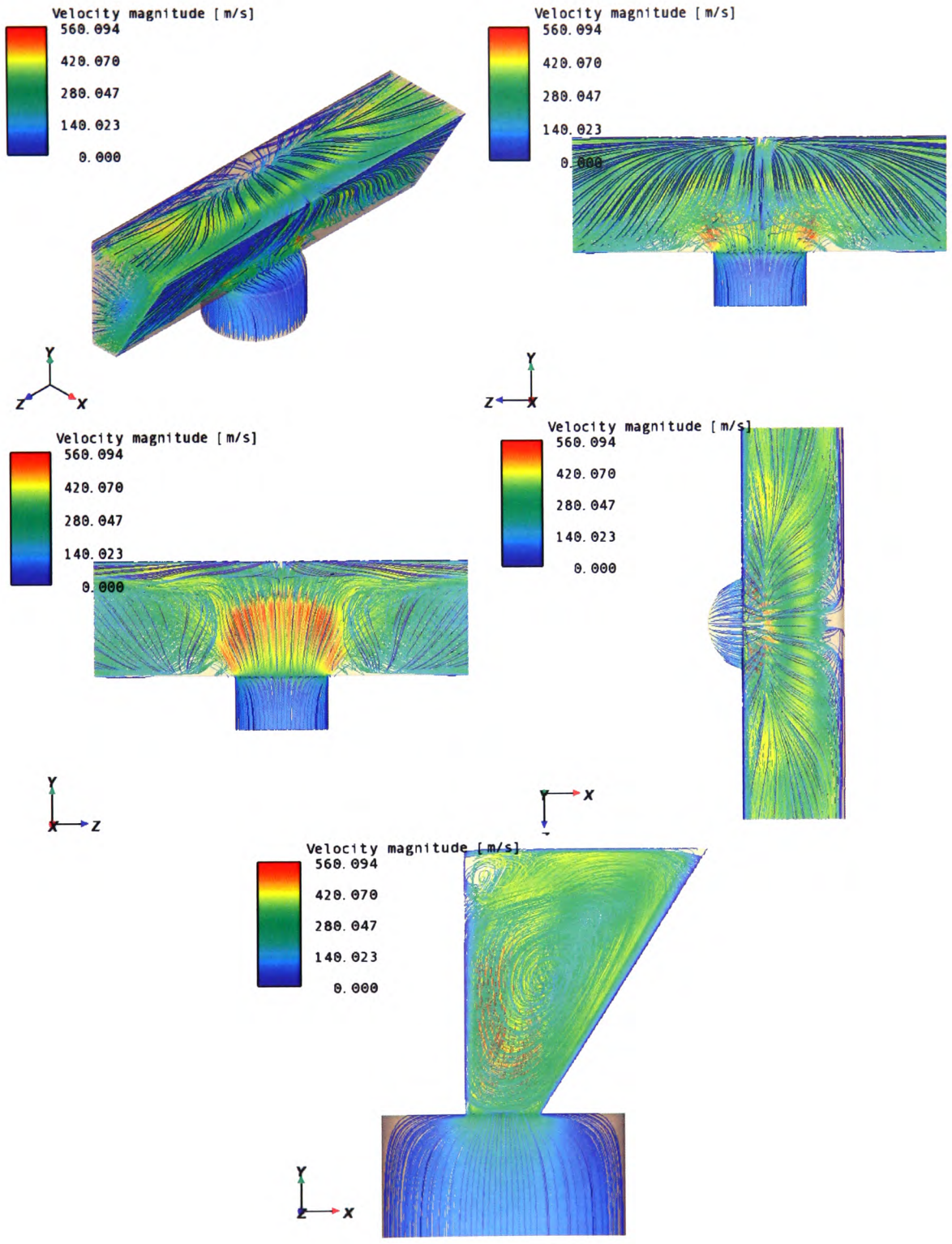

Figure 5-19. Streamline fluid flow simulation of commercially available ends together splicing chamber.

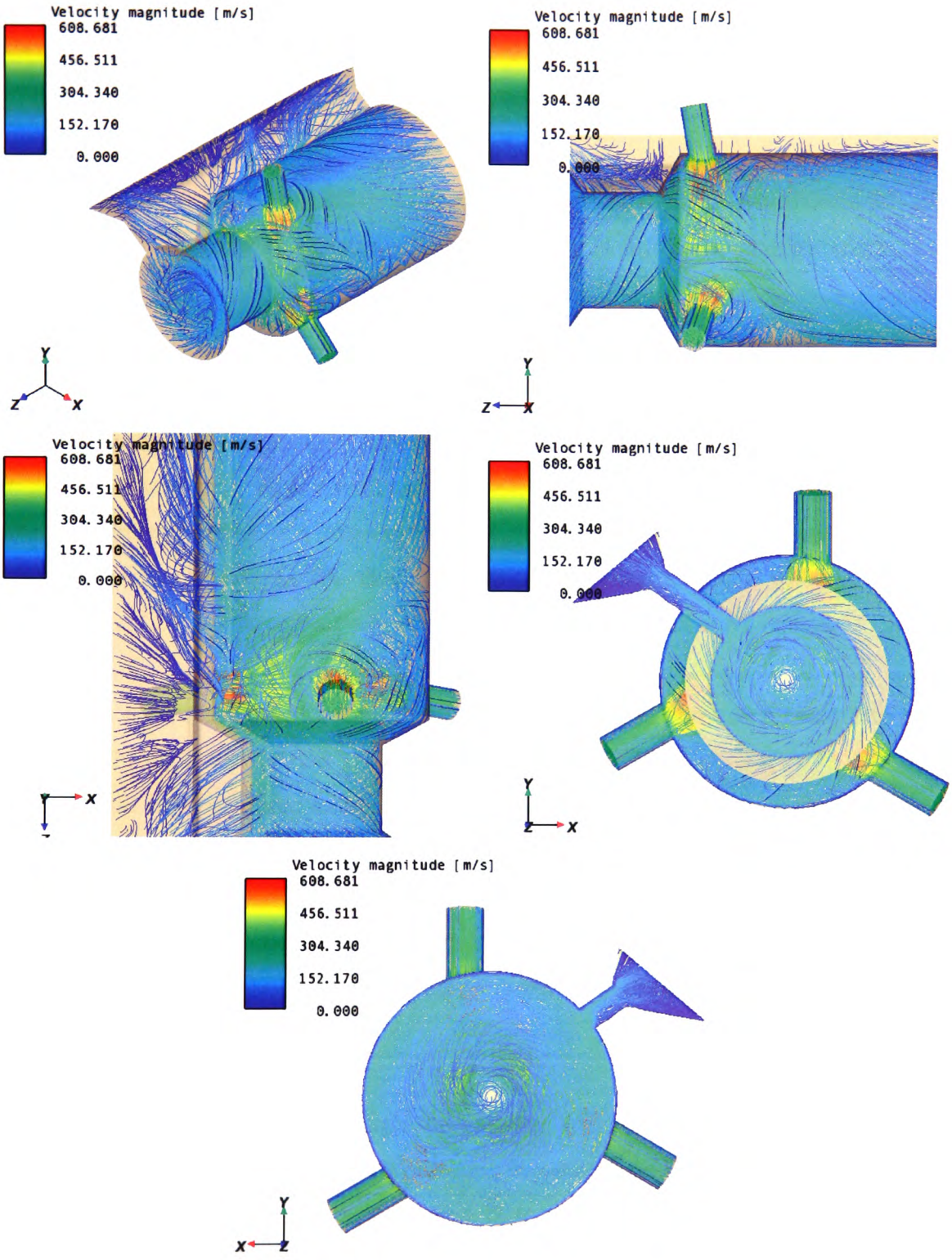

Figure 5-20. Streamline fluid flow simulation of commercially available ends together splicing chamber.

This section of the work has provided adequate proof that CFD can be used to model the airflow within any given chamber. Therefore it was highly likely that the technique can be used as a prediction tool, providing a good indication of how a new splicing chamber design might perform. This finding will eliminate much of the trial-and-error development work which has hitherto been needed when designing chambers for new yarns. It promises to reduce research time and cost in an industrial environment.

5.6 Effect of mass flow rate on splicing

One of the outputs from the CFD simulations was that of the rate of mass flow of fluid through the chamber. Examination of the mass flow data in this research has led to some interesting conclusions, and a significant change of direction in our analysis of the splicing process, involving the abandonment of air pressure as a primary process variable.

When air is compressed, and passes through a small orifice, both air velocity and mass flow rate through the orifice will, at low values, increase in line with pressure. However, the laws of aerodynamics dictate that, once the applied pressure reaches a critical value, the velocity through the orifice will reach a choked value of Mach 1, which cannot be exceeded, no matter how much the applied pressure increases. This first occurs when the ratio between outgoing pressure (in our case, the air pressure inside the splicing chamber) and incoming pressure (in our case, the compressed air line pressure) falls below 0.528.

Once this threshold is passed, though the velocity will be constant, the density of the fluid will rise in line with the applied pressure, to comply with the laws of conservation of mass. This effect is known as choked flow. There are many references in the literature to choked flow (Schmidtchen, 1994; Bar-Kohany *et al.*, 2007; O'Keefe, 2000).

Under conditions of choked flow, the dense fluid, forced to converge through the orifice, then emerges into the chamber, where it can expand very rapidly. During the fluid convergence through the orifice the flow becomes sonic, reversing the relationship between flow area and speed. As the chamber channel diverges, and expansion continues, the flow accelerates and may exceed a speed of Mach 1. The shape of the chamber profile will control the rate of expansion and the corresponding speed. There is therefore a more complex set of relationships in play than hitherto suspected. Previously, splicing was considered largely in terms of the applied pressure, the chamber dimensions, and the crudest characteristics of chamber profile such as divergence angle. It is now clear that splicing should also be considered in terms of other, more subtle features of the size of the orifice and the diverging volume of the chamber, which have a profound effect on the airflow.

The CFD work, in yielding mass flow information, revealed that under most circumstances, the splicing process operates under choked flow conditions. It was clear that, in this environment, the original convention of using air pressure as a principal splicing parameter is far from appropriate. Indeed, air pressure was an indirect measure at best, for example, it revealed nothing about differences between splicing chambers, and nothing about differences between filament counts. As a basis for formulating a theoretical model of splicing, pressure was too far removed from the actual process.

Close examination of the results obtained from the simulations suggested that the "mass flow rate" at the orifice between blast hole and chamber profile should be a more pertinent measure. Mass flow rate has the merit of being a direct measure of how the fluid is behaving, and it is easy to relate mass flow, in terms of Newtonian mechanics, to how the air may interact with the yarn filaments in the splicing chamber.
CFD results demonstrated that, for a given incoming air pressure, the mass flow rate and velocity changes markedly from chamber to chamber, because of variations of orifice diameters and diverging chamber volumes respectively. The CFD work therefore resulted in a subtle change in our approach to splicing parameters.

Instead of following the established convention of using input air pressure as the principal variable, our research was reinterpreted in terms of mass flow rate. Table 5-1 shows how the mass flow rate and velocity changes for a given pressure ratio in a 4483 straight chamber. The 'velocity at orifice' values displayed in the table are the values of the velocity at the vena contracta point, slightly ahead of the orifice. What was important to note is that choked flow occurs from approximately 13psig and above. Figures 5-21 to 5-23 reveal the variations in mass flow rate for a given pressure ratio throughout the three main experimental chambers.

Table 5-1. 4483 straight chamber.

Pressure at inlet (psig)	Pressure ratio (P_{out}/P_{in})	Velocity at orifice (m/s)	Mass flow rate at orifice (kg/s)
0	1	0	0
4	0.78	194.8	0.000626
8	0.64	265.7	0.000916
12	0.55	303.9	0.00115
16	0.47	343.2	0.00136
20	0.42	343.6	0.00156
30	0.32	343.7	0.00205
40	0.26	343.7	0.00251
50	0.22	343.7	0.00297
60	0.19	343.7	0.00342
70	0.17	343.7	0.00388
80	0.15	343.7	0.00434
90	0.14	343.7	0.00480

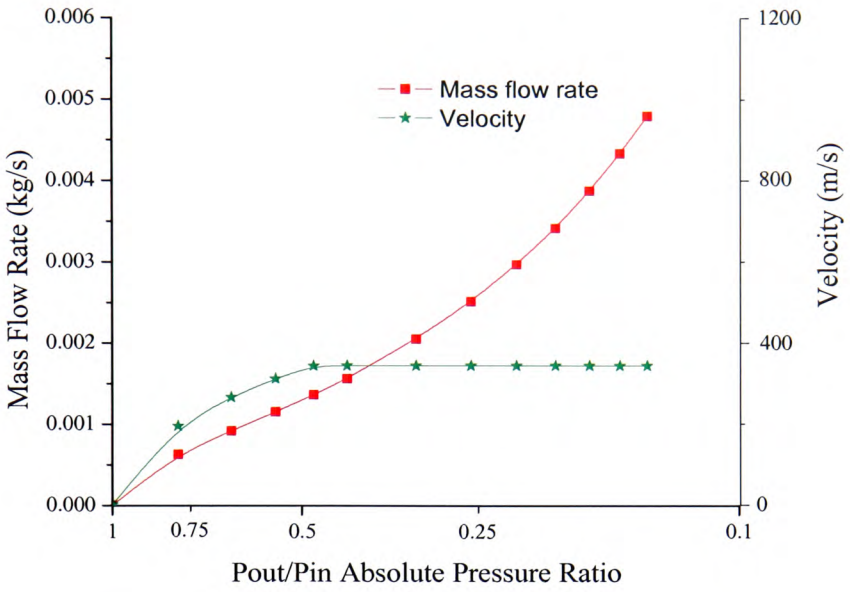

Figure 5-21. Mass flow rate for the 4483 straight chamber.

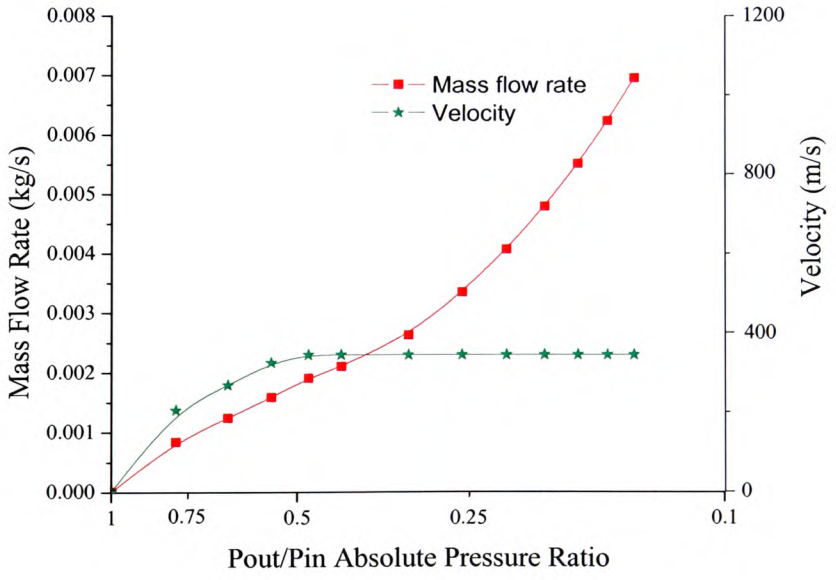

Figure 5-22. Mass flow rate for the 4485 straight chamber.

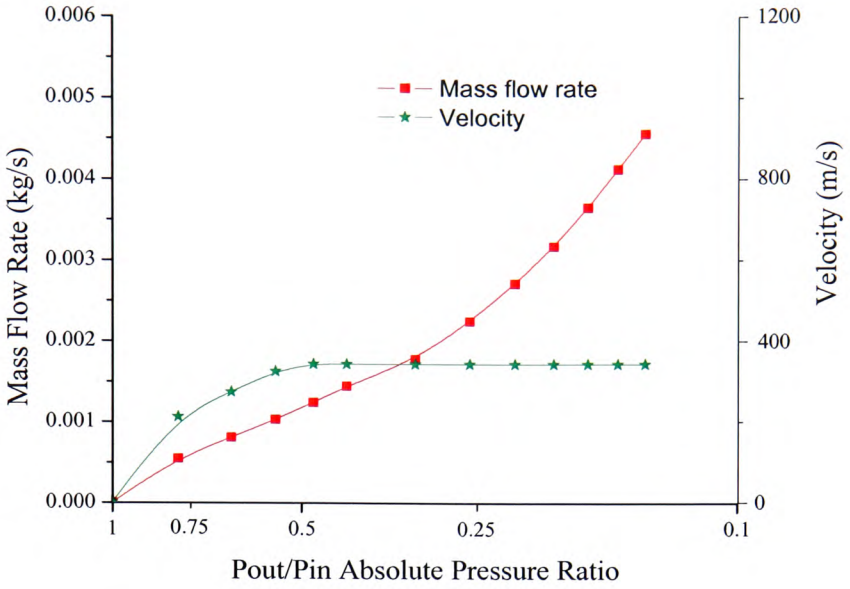

Figure 5-23. Mass flow rate for the 4483 bowl chamber.

Interesting conclusions emerged quickly from this work:

- The air velocity in the 4485 straight chamber was similar to that of the 4483 straight and 4483 bowl chambers. However, the 4485 straight chamber had a greater mass flow rate, associated with its larger diverging volume and larger orifice area. The greater mass flow rate produces stronger rotational forces along the walls of the chamber. These observations may explain why the 4485 straight chamber can handle a wider range of yarn counts than the 4483 straight, but why it also produced splices of worse appearance.
- Despite having a modest mass flow, similar to the 4483 straight, the 4483 bowl performance closely matched the 4485. This is probably related to the presence of the bowl; the chamber has a larger diverging volume than either of the other chambers, creating greater rotational forces, and producing acceptable splices at lower upstream pressures, perhaps because the splice formed much more quickly.
- The average velocity within the 4483 bowl chamber was greater than that in the straight chambers due to the greater diverging volume within the chamber by the bowl section.

The adoption of mass flow rate, instead of air pressure, as the primary process parameter, yielded a much better understanding of the splicing process, allowing easy comparison between different splicing chambers at different yarn counts.

The principal conclusion is that splicer geometry has a marked effect on splicing performance. Provided that yarn counts are within the chambers' performance envelopes, successful splices will result. But different mass flows, and hence different energy consumptions, will be needed.

5.7 Conclusion

In this chapter, a novel indirect visualisation technique and a CFD simulation technique were utilised to model the splicing process:

- A large scaled model for real-time representation of fluid flow and real splicing.
- The application of computational fluid dynamics simulation software to model 3D airflows within given chamber profiles.

The results of the CFD simulations revealed a common airflow characteristic between all chambers in industry, which leads to the conclusion that all chambers have the same general splicing process but operate with different levels of efficiency.

In general, in all splicing chambers, a blast of high velocity compressed air is produced within microseconds. This blast, interacting with the chamber surfaces, takes on the form of strong contra rotating vortices, which continue outward to the end of the chamber, fading in intensity as they move away from the centre. Yarns are swept up into these vortices, and by a complex process involving jet impact, turbulence and false-twist, swiftly become intermingled.

A new parameter of mass flow rate was introduced, to assess the efficiency of a splicing chamber. The mass flow rate clearly varies with applied air pressure, but not uniquely with pressure; it also varies according to the orifice size.

The outcome has been a new and reliable prediction method. The method uses the objective measure of mass flow in a given chamber geometry, to indicate how any splicing chamber design would perform on a given yarn count. The yarn count size determines the chamber dimensions.

Finally, it has been possible, from these new insights, to develop a completely new theoretical model of the splicing process, which explains many phenomena which have been observed, but never understood. This research is continued in the following chapter, which discusses in detail the new splicing process model, and how the characteristic structure of the splice might be formed.

Chapter VI

A proposal for a theoretical model of the pneumatic splicing process

Abstract – *In this programme of research, particular attention has been paid to the mechanical design of splicer components such as splicing chambers, and the influence of splicing parameters such as air pressure. In addition, visualisation and simulation techniques have been utilised to model the airflow within splicing chambers. The work has yielded a body of information, which suggests a broad explanation of the mechanisms which occur during the formation of a splice.*

This chapter attempts to bring the information together into one coherent whole, to propose a new theoretical model of the splicing process.

6.1 Introduction

As stated in previous chapters, pneumatic splicing is an established technique, though little research has been published in the field. Indeed, the diversity of commercial splicing chamber designs offered by different manufacturers suggests that splicer development has in most cases been conducted on an empirical basis. There is certainly little published evidence for the existence of a strong theoretical foundation.

A number of descriptive models of splicing exist in the published literature. Common to all of the descriptive models is a certain imprecision. All accounts of the splicing process are supported by drawings and illustrations which seem to bear little relation to the structures of real splices. Even the most superficial analysis shows that these models are profoundly deficient. Examples of existing unsatisfactory accounts are as follows.

As quoted in Chapter 1, Mingjie *et al.* (1999) stated that "a splice with interminglings in the middle, many small wrappings on both sides and near overlapping loopy wrappings at both ends should be ideal".

Splice structure representation by Dibble (1971), Textura AG (1967) and Shea (1981) as shown in Figures 6-1 to 6-3 respectively, did not match the reality of an actual splice.

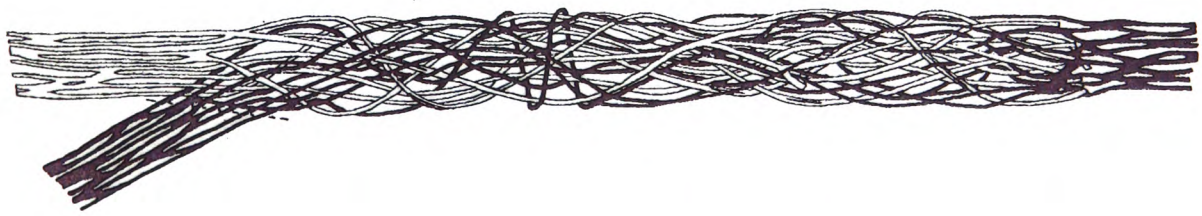

Figure 6-1. Splice structure representation.

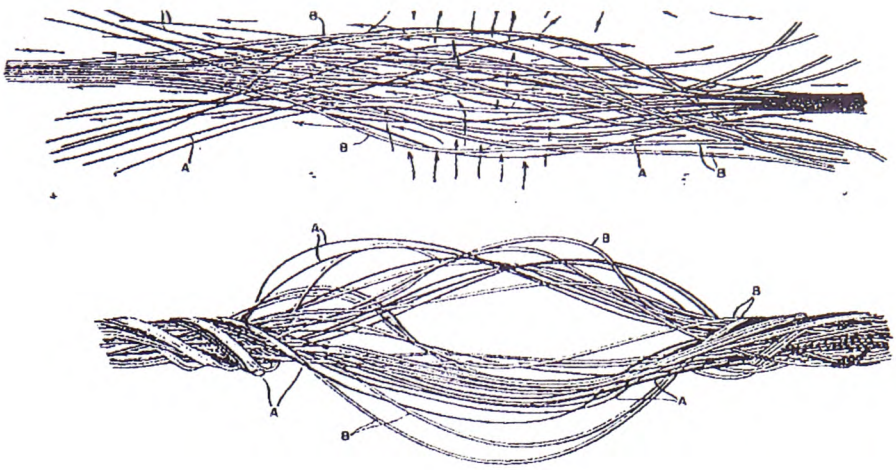

Figure 6-2. Splice structure representation.

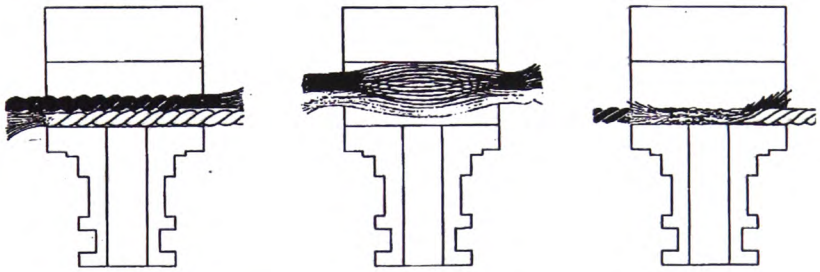

(A) (B) (C)

Figure 6-3. Basic splicing chamber with an (A) ends opposed layout; (B) separation of fibres; (C) intermingling of fibres.

These examples serve to demonstrate that the structure of a splice has not been carefully analysed at any time in the 30-year history of the technology. Even the technical manuals of splicer manufacturers sometimes represent the appearance of splices in a misleading manner.

This brief overview serves to demonstrate one of two things:

1. Manufacturers have given little priority to developing a deep understanding of the process, and are content to remain with ad-hoc solutions.

2. Manufacturers are perfectly aware of what is going on in the process, but for commercial reasons have chosen not to disclose the extent of their knowledge.

6.2 The structure of a splice

The representations of splices shown above do not relate to reality. Although random at the smallest scale, a complete splice has a distinctive and fairly reproducible structure as shown in Figure 6-4. This splice structure clearly does not conform to the structures described in the models above. The central section of the splice (which corresponds to the blast hole, the point where air enters) remains un-twisted and roughly parallel to the chamber axis. Between the central section and tail ends of the splice, the filaments are twisted, wrapped and intermingled, with the maximum amount of intermingling occurring nearest to the central section. Each end of the splice usually terminates in a small protruding "tail" where the extreme tips of the spliced yarns have not been fully bound into the structure.

Figure 6-4. Characteristic form of a splice.

The splice in the illustration has been made by joining yarns of different colours, so that the observer can gain an immediate impression of the structure of the splice. Several significant observations can be made, relating to the structure of the splice:

- Each yarn is divided into approximate two equal sections over the span of the splice with it being more evident near the centre of the splice.
- There are four zones of highly twisted filaments, above, below, to left and to right of the blast hole. The zones are mirror images of each other and, excluding the mirror symmetry, are physically essentially identical.

- There is a seemingly elliptical central section, without twist. This position corresponds to the blast hole.
- Examined closely, the central section can be seen not to be an ellipse; it consists of two distinct parts. There is a region of twist reversal between the upper left and upper right zones, and its mirror image between the lower left and lower right zones.

The two yarns start as discrete entities, but for a splice to form, their filaments must be mixed, before any intermingling takes place. If the filaments do not mix, then the yarns remain discrete, and the splicing process cannot take place. Splicing is frequently described loosely as "intermingling". However, the structure shown in Figure 6-4 clearly does not represent the simple random concepts of intermingling; it is highly ordered.

One manufacturer did develop a model of the splicing process, which was reasonably consistent with the observed splice structure. First proposed in an internal research document (Waters, 1996), it attempted to match real-life spliced joints to known physical processes. The 1996 model was founded on the established concept of filament migration and is explained in some detail in Chapter 1. The model had some appealing aspects, and for some years, it sufficed as a basic predictor of splicing chamber behaviour. It proved very useful to one splicer manufacturer, underlying a number of practical splicer designs between 1996 and 2006.

6.3 Experimental evidence emerging from this research programme

The findings from this programme of research yielded a substantial body of new information. Some of the evidence confirmed existing experience in the field, while the majority was completely new. In order to survive as a working hypothesis, the existing splicing model would have to be capable of explaining all of the new observations. The findings can be summarised as follows.

For a given yarn count, and for all chamber designs, splice strength was negligible until a certain critical lower mass flow rate was reached. Above this critical level, splice strength increased with mass flow rate, in an approximately linear relationship. Once mass flow rate reached a higher level, the linear relationship fails, and eventually strength begins to fall with increasing mass flow, presumably associated with filament damage. The critical lower mass flow rate, the gradient of the splice strength/mass flow rate curve, the critical upper mass flow rate, and the final rate of decrease of strength, all vary according to the splicing chamber design.

Splice appearance, for a certain range of mass flow rates, remained acceptable and fairly consistent, until a critical upper value of mass flow rate and blast duration was reached. Beyond this, splice appearance begins to deteriorate; its rate of decline varied, depending on the specific chamber design.

Two forms of filamentation have been identified as contributing to the degradation of appearance. The first resulted from broken filaments once the critical blast or mass flow rate has been exceeded. The point of rupture of the broken filaments corresponds closely to the position of the blast hole. The rupture mode of the broken filaments was consistent with excessive extension, in that the tips of the broken ends, when examined under the SEM, exhibited the classic appearance of local melting and is explained in greater detail in section 6.6.5.

The second form of filamentation seems to be un-related to damage. Occasionally, free floating filaments are observed, completely free at one end, and restrained in the yarn bundle at the other end. There is no evidence of excessive extension; the tips seem to be clean cut, and the filaments are straight, with a length very similar to that of the complete splice. The floating filaments seem simply to have escaped from the splicing process after being cut. This is described in greater detail in section 6.6.6.

The effect of yarn count was as expected. As yarn count increased, higher air mass flow rate was required, for all chamber designs, but some chamber designs required less mass flow rate increase than others. Also, as yarn count increased, larger cross-sections were required, for all chamber designs, but some chamber designs required less cross-sectional increase than others.

The existence of the effect known as scaling was demonstrated; it led to the concept of splicing larger yarn counts by increasing the total splicing length (the spacing between knife positions).

A scaled model of a simple splicing chamber, without yarn, replacing air with water as the fluid while maintaining a constant Reynolds number, produced a convincing visualisation of the fluid flow in a real empty splicing chamber. This scaled model visualisation technique was only implemented as a means to observe the fluid flow structure within a splicing chamber during a blast cycle. A CFD simulation of an empty chamber matched very closely the fluid flow observations of the scaled model.

When a yarn occupied the scaled chamber, the yarn took up a position which closely corresponded to the null points of the vortices predicted for empty chambers by both the scaled model and the CFD simulations. The experiments involving the scaled splicing chamber suggested that yarn bundles do not rotate in their entirety, but that individual filaments wrap repeatedly round the bundles, to produce a similar effect.

It was concluded that the scaled chamber and CFD simulations produced representative and useful results. The CFD results help to explain why some splicing chamber designs are more or less efficient than others for splice strength and appearance over a range of air mass flow rates, and why some are especially good at very low mass flow rates. The main conclusion to emerge from these simulations was that all splicing chambers produce a characteristic fluid flow pattern, suitable for producing acceptable splices, but that some chamber designs are more efficient than others.

6.4 The failure of the existing migration model of splicing

From the outset, there had been some concerns about the 1996 model as described in Chapter 1. Particularly, it required that the chamber base geometry be very closely matched to the yarn bundle diameter. There was also a concern that the number of turns of twist actually observed in a splice might be insufficient to explain the necessary level of filament migration. Nevertheless, it had proved very useful, underpinning the designs of some very efficient new forms of splicing chamber, which have been in production for over 10 years.

New observations were made during the current programme of research:

- The 1996 model predicted that optimum performance would occur when chamber base width was roughly the same as the diameter of one of the yarn bundles creating a stacking relationship; the new research indicated that the base should be twice as big as the diameter of one of the yarn bundles, placing them side by side.
- The model could not explain the occasional phenomenon of a "floating" filament, which had clearly escaped from the yarn bundle, but which had not been ruptured by the air blast.
- The model could not predict the "merging" of the filaments along the central axis of the splice, making a somewhat amorphous structure, when chambers were narrow in profile, or yarns wide.
- It could not explain why splicing performance varied with splicing chamber length.
- The notion of rotating bundles could not explain the change of performance with splicing length.

Confronted with the observations made during this research, it became inevitable that the existing model would be discredited. It was replaced by the new model which is

described in the following section, and which will function as the working hypothesis for future research.

6.5 The new model for the splicing process

All the processes described in this section were observed while using a single form of splicer design, from a single manufacturer. This splicer was chosen because it had a simple form of construction, and was easy to modify for experimental purposes. Other splicers available on the market will have more features. However, the additional functions merely enhance splice quality, or offer more consistent performance; they do not alter the principle of splicing in any way.

The operation of a yarn splicer is as follows. Two yarns are laid into the splicing chamber, from opposite ends, and are restrained by the two pairs of yarn clamps (we shall arbitrarily call our yarns "black" and "white"). Both yarns lie along the base of the splicing chamber, the filaments fairly loosely and randomly scattered, passing across the blast hole. What is destined to become the waste end of each yarn passes between a pair of cutters.

To recap the pneumatic splicing operation as described in Chapter 1, when the splicer is activated, several operations happen in very swift succession:

1. The chamber pad closes the top of the chamber, restraining the yarns so that they remain in the chamber. The knives cut off the yarn waste ends. The compressed air blast enters the splicing chamber, emerging from the blast hole as a slightly diverging jet. The blast hits the underside of the chamber pad, forcing a flow direction change to the left and right creating a system of two contra-rotating vortices.
2. The time-scale of this first stage of the splicing operation is extremely short; the chamber is about 5mm deep, and the compressed air blast enters the chamber at very high speed, typically 340m/s. So the first impact of the blast against the

pad occurs in just a few microseconds. The blast continues for approximately 1 second; when it is switched off, the chamber pad opens, and the neatly intermingled structure can be removed.

The yarn in this model during the splicing process takes a different approach to migration for intermingling as described below. Consider the first filament to move when struck by the air jet:

1. It may be a black or white filament.
2. It will be restrained at the non-cut end.
3. It will be relatively free at the cut end, but not completely free, because, being part of a bundle of filaments, it will have the rest of the filaments in close proximity.
4. The filament will be taken up to the top of the chamber, close to the chamber pad, and will then displaced sideways, an will begin to rotate, following the vortex.
5. The vortex it follows will be randomly chosen; the filament may move above or below the centre line as drawn.
6. This first filament, being quite free to move in the chamber, will not be stretched; it will probably move in a manner similar to that of a skipping rope. It may look something like Figure 6-5.

Figure 6-5. First filament in the new splicing process model.

7. Having been displaced upward and to the side, it will no longer lie in a straight line. Not restrained significantly in the chamber or at the cut end, it will compensate for the path displacement by a corresponding displacement of the

cut end. The cut end will move inward, away from the knife and towards the blast hole.

Consider the second filament to move when struck by the air jet:

1. It may be a black or white filament.
2. It will be restrained at the non-cut end.
3. Like the first filament, it will be relatively free at the cut end, but not completely free, because, being part of a bundle of filaments, it will have the rest of the filaments in close proximity.
4. Like the first one, this second filament will be taken up to the top of the chamber, close to the chamber pad, and will then be displaced sideways, and will begin to rotate, following the vortex.
5. The vortex it follows will be randomly chosen; the filament may move above or below the centre line as drawn.
6. For the purposes of this description, assume that it follows the same vortex as the first one.
7. This second filament will not be so quite free to move in the chamber as the first, since the first filament is already in residence.
8. The two filaments interact, and twist round each other to left and right of the blast hole. The resulting structure, once balanced by a similar pair rotating in the opposite direction, may represent an approximate structure to that shown in Figure 6-6.

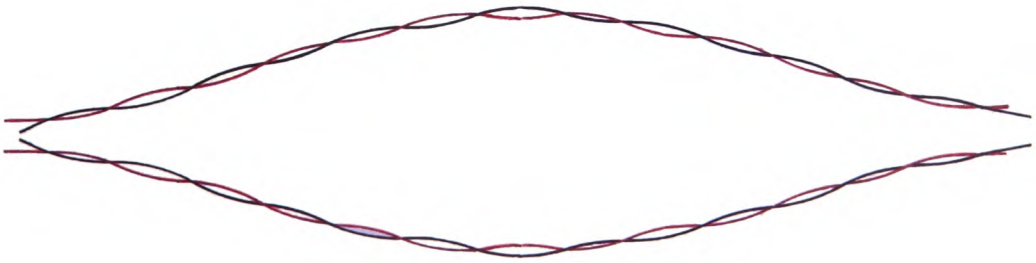

Figure 6-6. Second stage in the new splicing process model.

Since there are only two filaments in each bundle at this juncture, their twist levels will be identical, since each wraps round the other. Like the first filament, the second one, having been displaced to the side, will no longer lie in a straight line, and its cut end will move inward, away from the knife and towards the blast hole. The twist in the bundle, which is beginning to form, is false-twist. Overall there is no net twist, and the S-twist on one side is exactly matched by the Z-twist on the other.

Consider the third filament to move when struck by the air jet:

1. It may be a black or white filament.
2. It will be restrained at the non-cut end, but relatively free at the cut end (though probably slightly less free than the earlier filaments, because of the effect of the small amount of false-twist which is beginning to build up.
3. Like the others, this second filament will be taken up to the top of the chamber, close to the chamber pad, and will then displaced sideways, an will begin to rotate, following the vortex.
4. For the purposes of this description, we continue to assume that it follows the same vortex as the first and second filaments.
5. This third filament will not be less free to move in the chamber as the first two, since they have already formed a twisted bundle.
6. The third filament rotates, much as the others, but it is forced to wrap around the already-existing bundle.
7. The twist level of this third filament will not now depend on the twist level of the filaments which are already present, but will be determined more by the violence with which it is thrown round the existing bundle; the way it interacts with the blast will determine how many times it wraps round the bundle.
8. The resulting structure may represent approximately to that shown in Figure 6-7. Here, the third filament has been drawn with a higher twist level than that of the first pair,, and a second bundle has been introduced, rotating in the opposite direction.

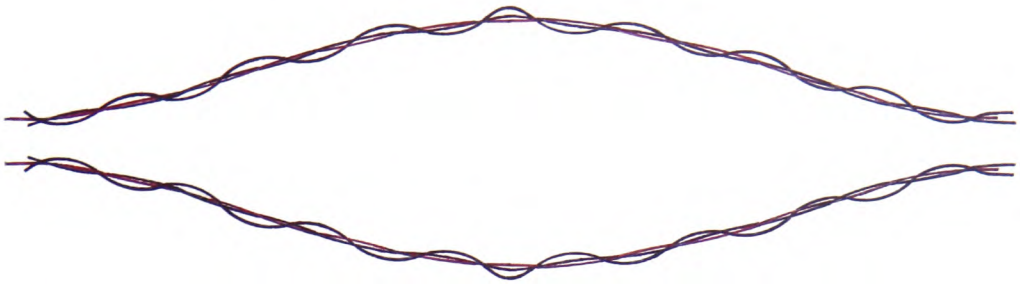

Figure 6-7. Third stage in the new splicing process model.

As with the others, the cut end of the third filament will move inward, away from the knife and towards the blast hole. It is likely to move inward less than the second filament, the false-twist which is beginning to build up is causing some filament interaction near the ends of the splice, and beginning to create the characteristic interlocking relationship at the point of filament separation. The third filament may be very slightly strained; forced to wrap round the existing bundle, exposed to the violent stream of air, and with its cut end less able to move, its length may increase slightly.

This process continues, with filament after filament wrapping round the bundle. Whether a filament is black or white, and whether it goes into the upper vortex or the lower, is a matter of chance. Overall however, there will be a roughly 50/50 split of filament types, and a roughly 50/50 split between the vortices. As each filament wraps round the bundle, the bundle radius increases, and it is likely that the number of wraps will decrease with each succeeding layer. Each cut end is now firmly bound into the structure, and cannot move; as the process continues, each succeeding filament becomes more strained, with both ends being fixed, and with the central portion being wrapped around the growing bundle. A schematic representation of this new splicing process model is shown in Figure 6-8.

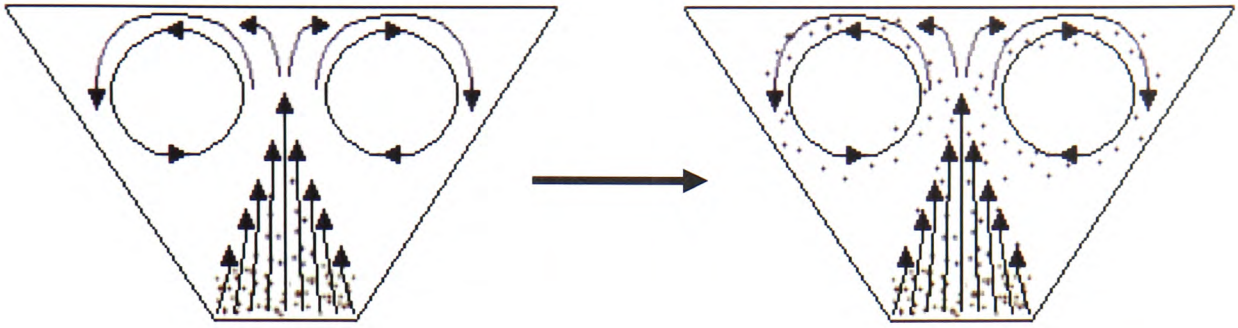

Figure 6-8. The intermingling of individual filaments

Filaments are likely to be swept up into the air stream more than once, because the zero twist region, where the reversals take place, is directly above the blast hole, so that filaments are never protected from the blast. On its next encounter with the jet, a filament may be thrown into the other, counter-rotating vortex (though this becomes increasingly unlikely as a filament becomes more tightly bound to its "parent" vortex). This structure is represented in Figure 6-9.

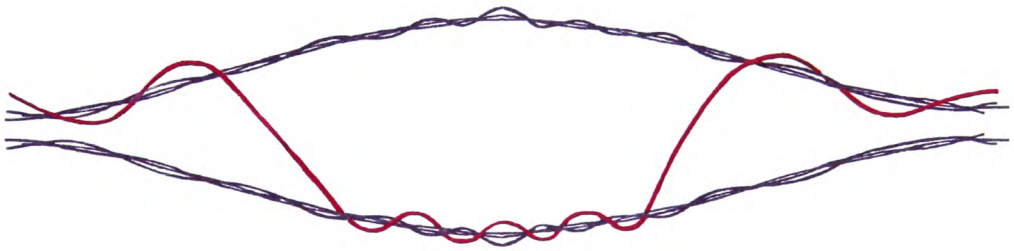

Figure 6-9. Filament crossover structure in the new splicing process model.

As this process continues, and repeats, the filaments become bound more tightly into the yarn bundles, restoring forces increase, and the structure begins to narrow as shown in Figure 6-10.

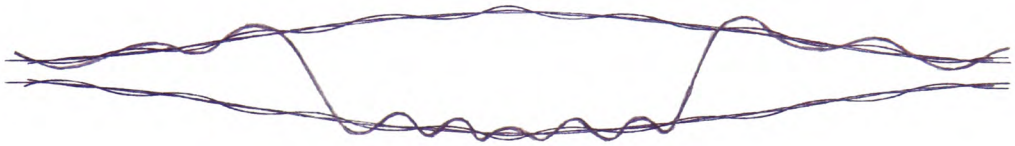

Figure 6-10. Tightening of the splice structure in the new splicing process model.

More and more filaments join the bundles, and become more and more bound into the structure. It becomes more difficult for them to move, and only the region near the blast hole, where the filaments remain free, can respond to the blast. Eventually it is likely that the system achieves some kind of equilibrium, the power of the air blast being no longer sufficient to alter the structure any further.

The whole assembly of filaments in the chamber begins to adopt the form of a flat diamond, the four sides each containing roughly equal numbers of black and white filaments. If there is an excess of mass flow rate or an excessive blast time, the forces generated will be sufficient to begin to rupture the filaments.

Figure 6-11 reveals six examples of one half of a typical fully formed splice (three with different coloured yarn for emphasis), with compacted bundles above and below the centre line, and with clear evidence that several filaments have switched during the splicing process from one bundle to the other. When the air blast ceases, some counter-rotation occurs, as the four bundles relax; but sufficient intermingling remains for the splice to become permanently consolidated. The application of a small amount of tension to the spliced yarn causes a very small amount of movement in the structure, as stresses are distributed around the structure; then the splice is complete.

(A) (B)

Figure 6-11. Examples of one half of a typical fully formed splice with (A) matching coloured yarn; (B) different coloured yarns for emphasis.

Although this description is long and detailed, the whole process happens very quickly; the whole splice is formed in less than one second, and each cycle described above probably being completed in less than a millisecond.

6.6 Real-world observations and the new model of splicing

6.6.1 Splicing chamber design

Perhaps the simplest examples, which allow for comparison between splicing chamber angles, are the simple trapezium shapes used in this research programme. A splice made using a 30° chamber is very different in form from one made on a 60° chamber. In particular, the false-twisted yarn bundles, which form the splice, are widely separated on the 60° chamber, whereas they are much closer together when made on the 30° chamber. On the 30° splice, numbers of filaments can be seen crossing the splice between the bundles; these are largely absent on the 60° splice.

With the CFD simulations validated, and the theoretical model in place, these observations are easily explained. The vortex null points are much further apart on the

60° (total included angle) chamber than on the 30° (total included angle) chamber. Since the yarn bundles take up positions, which correspond to the vortex null points, then they will form much further apart on the wider chamber. Due to this reason, as the yarn bundles rotate about centres, which are very much further apart on the wider chamber, the probability of a filament "crossing over" during one of its cycles through the blast zone is very much lower than on the narrower chamber.

The same argument applies for chambers which have the same included angle, but which differ in overall width. For a given included angle, the wider the chamber, the further apart the null points of the vortices, and the further apart the yarn bundles.

One of the splicing chamber forms which was used had a distinctive bowl profile machined out of the central section. When compared to the straight chambers, this form demonstrated certain distinctive characteristics. It made good splices at lower air pressures that the straight chambers and could handle a wider range of yarn counts without changing process parameters. The bowl chamber made splices with more filamentation than straight chambers but generally made splices with shorter "tails" than straight chambers.

These observations are easily validated through the CFD simulations and theoretical model. The bowl shape completely transforms the airflow within the splicing chamber due to the larger diverging volume of the bowl shape along with its circular profile, creating increased rotational flow in the bowl. It is certain that the yarn bundles are thrown outward due to these increased rotational vortices, increasing the sideways displacement of the yarn bundles. Increasing the sideways displacement draws in the tails more efficiently. The yarn bundles are subjected to a powerful set of vortices which, near the blast hole, are very far apart. The rotational forces are certain to be very strong. Overall, the bowl chamber is simply more aggressive in its treatment of the yarn, which makes its splicing action more efficient, but it also renders the filaments more vulnerable to damage.

6.6.2 Overall yarn count

This subject has been discussed at some length in an earlier chapter, during which the concept of "scaling" was introduced. In the new industrial applications confronted by splicer manufacturers, yarn count can be far greater than that normally encountered in the apparel environment. Compared to a normal apparel yarn, some industrial yarns have a count, which increased by a factor of perhaps 100, representing a diameter that is ten times larger.

The model requires that, for a good splice to form, a certain minimum number of helix wrappings will be required. Scaling is completely consistent with the new splicer model, because for a given splicer geometry, the increase in diameter of the yarn bundles reduces the number of helix wrappings which are possible on the subsequent individual filaments wrapping around the already existing yarn bundle located in the null vortices. Only increasing the area of the chamber profile, and increasing the total splicing distance can restore the number of helix wrappings.

6.6.3 Diameter of individual filaments

Historically, splicing has been used only in applications that relate to normal textile end-uses. Thus the construction of apparel items demands yarn whose characteristics such as filament count lie within fairly narrow limits. For a given overall count, a yarn may in principle have any number of filaments. However, as the diameter of a filament changes, so will its elastic properties. Since our splicing model is founded entirely on the elastic properties of the structural elements, specifically bending behaviour, flexibility, and extension under load, splicing performance can be expected to change with change of filament diameter.

As textile processes move away from the traditional, yarn counts and filament counts have begun to move into unfamiliar territory. This is especially the case with modern

industrial products such as heavy glass fibre. In these industrial applications, filament diameter is far greater than that normally encountered in the apparel environment. It is valid to speculate about the point at which for a given overall count, the filament diameter becomes sufficiently high to compromise the efficiency of pneumatic splicing.

As filament diameter increases, the filament as an element of the splice will become more resistant to bending. This will increase its resistance to being distorted into the characteristic splice helix, thus the helix pitch angle will decrease resulting in a decreased number of turns. Therefore the number of turns of the splice helix required for a good splice will take up a greater length.

The conclusion is that, for a given overall count, a larger filament diameter will require a longer splice length, and therefore greater knife spacing. The change of splicing performance with change of filament diameter can therefore be addressed as a particular case of the phenomenon of "scaling".

6.6.4 Reducing the number of filaments

The trials in this work have been carried out on yarns, which have 72 filaments or more. It is well known and easily understood that the pneumatic splicing method cannot be used to join monofilaments. It is valid to speculate about the point at which for a given overall count, the filament number might become sufficiently low to compromise the efficiency of pneumatic splicing. This question is closely related to the issues discussed in section 6.6.3 above relating to filament diameter.

It is relatively easy to understand how an increase of filament diameter will have some consequences. However, that discussion still assumes that the number of filaments is ample to make a satisfactory splice, given sufficient control of parameters.

The consequence of reducing filament numbers reduces the number of filament-to-filament frictional contacts per unit length of the splice structure will reduce. Since the effectiveness of the splice is a direct function of the number and nature of the frictional contacts, the strength of the splice for a given splice length will be reduced. Therefore only increasing the length of the splice, thus increasing the number of frictional contacts, can restore splice strength.

The conclusion is that reducing the number of filaments will create a need for a longer splice length, and therefore greater knife spacing. The change of splicing performance with change of filament number can therefore be addressed as another particular case of the phenomenon of "scaling".

6.6.5 Breaking of individual filaments

The images of broken filaments, captured with a SEM, reveal a classical form of rupture, well documented in the literature. The breaks are characteristic of a violent stressing of the filament, which occurs quickly and adiabatically, resulting in local melting as shown in Figure 6-12 (Hearle *et al.*, 1998, 406-415).

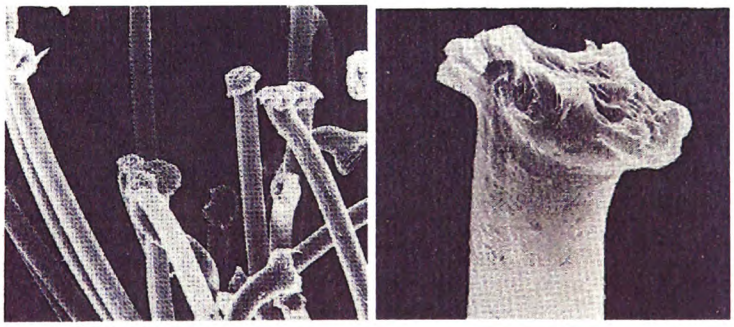

(A) (B)

Figure 6-12. Filament rupture through impact tear in (A) yarn; (B) filament.

The observations are completely consistent with the new model. The model suggests a sequence of events in which filaments are caused to whirl rapidly, in a skipping-rope

fashion, wrapping quickly and violently round the existing yarn bundles. As the splice geometry begins to become established, the filaments wrap tighter and tighter round the bundles, and become ever more constrained. The centre section of the splice, where reversals occur, remains open and positioned directly over the blast hole, so that the air jet continues to impinge violently on the filaments. Eventually, either through too violent an airflow, or too long a blast, some of the filaments will be locally stretched too far, and will break.

6.6.6 The case of "floating" filaments

This has been mentioned earlier in the text, but this section offers the opportunity to use the phenomenon as a test of the new model.

Occasionally, a splice will be formed which is, in all but one respect, perfectly normal. However, it will have one or more, always very few, completely straight filaments, which are fixed at one end, but floating completely free at the other. The length of the floating filament is such that its free end appears to correspond to the position of the cutting section. Moreover, the appearance of the end of the floating filament is clean, and neat, totally unlike the filaments which break under strain, and completely consistent with a simple cut as shown in Figure 6-13 (Hearle *et al.*, 1998, 406-415).

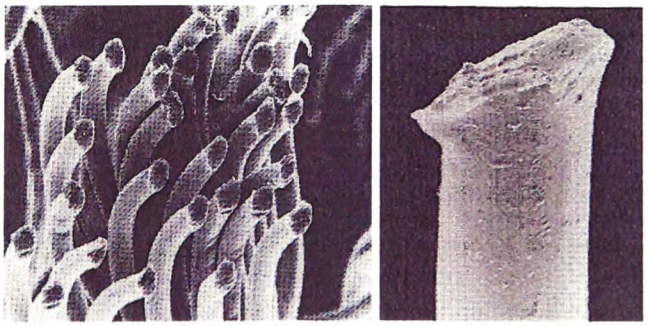

(A) (B)

Figure 6-13. Filament rupture through knife cut in (A) yarn; (B) filament.

It seems that the filament has been prepared and cut, just like its neighbours, but that it has escaped from the bundle, and has never been bound into the splice structure. The old model completely failed to explain this phenomenon, because it offered a description of the splice formation at the level of the whole yarn bundle. The new model, which works at the level of individual filaments, offers an explanation, which is easy to comprehend.

According to the model, the splice structure becomes established by filament after filament wrapping round the growing yarn bundle. The bundles converge at the ends of the splice and become ever more tightly packed. The cut ends of the filaments then become completely trapped in the structure, and cannot move at all.

However, at the start of the splice, as the first few filaments are hurled into their "skipping-rope" form, their cut ends, being largely unrestrained, are free to move. If the cut end of one of the "early" filaments were to move inward far enough, it would escape the restraints, before the converging section became properly established. Once free, the probability of recapture would be very small, and the filament would remain outside the main structure throughout.

6.6.7 Breakage of the whole splice

Splice strength is routinely tested using a tensometer. If the air pressure is very low, the failure mode of a splice is merely a gentle slipping apart of the whole splice. There has not been enough intermingling to produce a proper joint. Once properly formed, all splices, when loaded, eventually break in a characteristic manner. The splices themselves do not fail, but all filaments break at some point very close to the splice or at the critical/interlocking section of the splice due to increased tension at this point. Failure is catastrophic, with all filaments rupturing more-or-less simultaneously (depending on the yarn being spliced), at approximately the same point. Splice brake are shown in Figure 6-14.

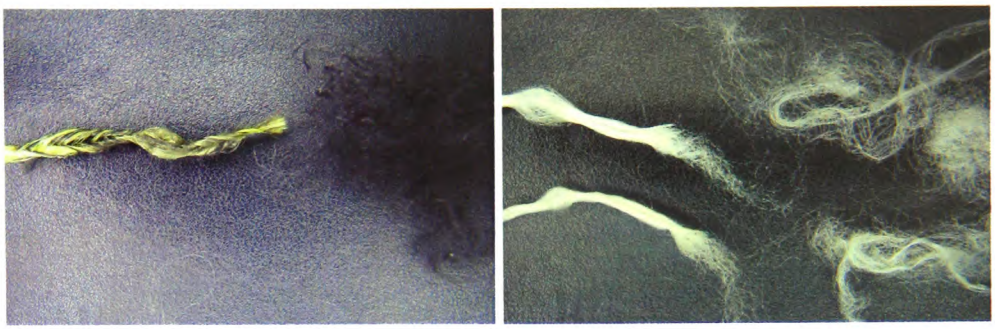

(A) (B)

Figure 6-14. Examples of splice breaks in (A) different coloured yarns; (B) matching coloured yarn.

This failure mode is easy to understand because the splice itself, if properly formed, is unlikely to break due to there is twice as much material in the splice as in either of the parent yarns. Therefore the break will always occur in one or other of the parent yarns. The new model demonstrates that the region near the tails, near the point of convergence of the yarn bundles, can be quite severely disrupted by the slight tearing action created by the diverging yarn bundles. Therefore, if any point of the parent yarn is likely to be weakened, it is probably going to be in the vicinity of the tails, and this is where the breaks always occur.

6.6.8 Effect of mass flow rate

This subject has been discussed at some length in the previous chapter. It emerged from the simulation technique and was proposed to replace blast pressure as the dominant input factor into the splicing process. Mass flow rate is unique for each chamber design and has a direct relationship with blast pressure.

The model requires that, for a good splice to form, a certain minimum number of helix wrappings will be required. We can assume from our model that the force applied to an individual filament being caught in the airflow cycles distorts the filament in a manner comparable to that of a "plucked string" scenario as shown in Figure 6-15.

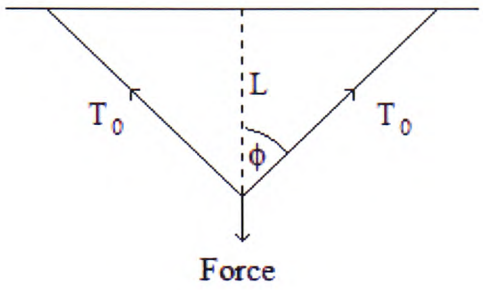

Figure 6-15. Force on a "plucked string".

As can be seen, for a given mass flow rate entering through the blast hole the filament will deflect. With greater mass flow rate, it will create greater gradients between the centre of the filaments and the non-loose ends; therefore a larger helix angle is formed, creating more helix wrappings. There is an optimum mass flow rate to create the maximum helix angle.

With a greater force and a greater helix angle, the filament will be wrapped with greater frequency round the bundle. This should result in more inter-filament contacts, and ultimately in a stronger splice. However, if this occurs in excess, the stress on the filament will eventually cause it to rupture. More detail on splicing exotic yarns can be seen in Appendix 2.

6.7 Conclusion

In this chapter, the old 1996 model of the splicing process model has been re-assessed, in the light of the evidence which has emerged from the present programme of research. Its failings have been clearly identified.

A new theoretical splicing process model has been described in detail; it has been tested against the latest experimental results, and has so far proved satisfactory.

Our account of the process is detailed, but purely descriptive; it represents merely the first step to a complete analysis, which will, with further research, enable us to develop a complete model.

Chapter VII

Conclusion

Abstract – *In this chapter the major contributions and conclusions of this thesis are summarised, and new ideas for further research are presented*

7.1 Introduction

This programme of work began by recording that, though pneumatic splicing is an established technique, little research has been published in the field, and that there is little published evidence for the existence of a strong theoretical foundation. It was shown that a number of descriptive models of splicing exist in the published literature, but that common to all of the descriptive models is a certain imprecision. All existing accounts of the splicing process are supported by drawings and illustrations which seem to bear little relation to the structures of real splices.

This thesis has described a programme of work on the splicing process. The research combined traditional indirect systems of measurement with visualisation and simulation techniques; it identified the shortcomings of existing theoretical models of the splicing process, and developed a new theoretical splicing process model.

It is particularly important that the new splicing model be validated, because the introduction of new materials over the past decade, such as carbon, has posed significant challenges for the designers of splicing equipment. The different compositions and mechanical properties of the fibres mean that existing splicing systems are no longer adequate. Novel splicer design and more sophisticated control measures will be required to make satisfactory joints in these new materials. The increasing rate of adoption of these new fibres requires effective, novel technical splicing solutions, founded on a sound theoretical basis.

7.2 The development of the new splicing process model

It was essential in evaluating the mechanism behind the pneumatic splicing process, to initially experiment on all aspects of splicing, by improving on work conducted by earlier researchers, using conventional measures such as chamber design and blast pressure.

In this thesis, Chapters 2 and 3 describe the validation of the Taguchi DOE method, when applied to the splicing process. Specifically the Taguchi method was used to optimise splice strength and splice appearance. Finally it was used to identify process conditions which would deliver a splice which represented an adequate compromise between splice strength and splice appearance.

The body of work described in Chapters 2 and 3 had been conducted on a single yarn count, but it was known that, in real splicing environments, splicing performance deteriorated when the count was increased substantially. The research discussed in Chapter 4 records how the work was extended to analyse the effect of different yarn counts on the splicing process. Chapter 4 examined a new hypothesis, called "scaling", which suggested that large changes of yarn count should require corresponding changes not only in the splicing chamber, but also in the geometry of the entire splicer. Research revealed that increasing the total splicing length vastly improved the yarn count range performance of a given splicing chamber. This finding enables smaller cross-sectional splicing chambers to splice larger yarn counts with greater appearance. The work revealed powerful evidence for the existence of "scaling"; a conclusion which is likely to be of profound importance to the design of splicers for very large yarns and tows.

Chapter 5 addressed the problem that the splicing process cannot be observed directly. New methods were needed to represent the splicing process in a convincing manner. A novel indirect visualisation technique and a CFD simulation technique were utilised to model the splicing process:

- A large scaled model for real-time representation of fluid flow and real splicing.
- The application of CFD simulation software to model 3D airflows within given chamber profiles.

From the visualisation and simulation work, new insights were gained into the fundamentals underlying the splicing process. The results of the CFD simulations

revealed a common airflow characteristic between all chambers in industry, which leads to the conclusion that all chambers have the same general splicing process but operate with different levels of efficiency.

Another significant outcome from the simulation technique was the discovery that the use of air pressure as the most important splicing control parameter was based on flawed logic. A new parameter of mass flow rate was introduced, to assess the efficiency of a splicing chamber. The mass flow rate clearly varies with applied air pressure, but not uniquely with pressure; it also varies according to the detailed profile of the splicing chamber design. A reliable prediction method emerged, which uses the objective measure of mass flow in a given chamber geometry, to indicate how any splicing chamber design would perform on a given yarn count, with the yarn count size determining the chamber geometry.

In Chapter 6, the analyses conducted in previous chapters were brought together, and were first used to test the validity of the old model of splicing, which had been in use for many years. The old model was found to be severely deficient. The analyses were then used as the basis of a completely new theoretical model of the splicing process. This model has succeeded in explaining a number of phenomena which had been observed but never understood. The formation of the characteristic structure of the splice was discussed in detail. The new model has been validated against a wide range of practical situations, to evaluate its performance in real textile environments.

The new model if proves adequately resilient, the process of design and development of future splicers will become more logical, and less ad-hoc. This new model represents a novel contribution to the splicing technology.

This descriptive model is only the first step. So far, the model has been successful, but like all hypotheses, it remains to be tested more rigorously in the future.

7.3 Future work

The work described in this thesis appears to represent an advance in the understanding of the splicing process. Satisfactory explanations have been offered for phenomena which can be observed, at a macro-level, during the splicing process. A theoretical model of the process has been developed and described. It is likely that this model will be of some use in the design and development of real yarn splicers in the future.

Certain questions remain, however. Quite simply, there is a remarkable variation of detailed structure, at the level of the individual splice. The starting conditions are simple, known, and easily controlled. In the simplest case:

- Two yarns, usually of the same yarn and filament count, are placed in the splicing chamber of a splicer.
- The splicer has a known and constant geometry.
- The splicing chamber has a known and constant geometry.
- The fluid medium is supplied at a known and constant pressure.
- With constant pressure and constant geometry, fluid mass flow rate is constant.

Even though all these parameters can be kept constant, the output in terms of the individual splice is clearly and measurably variable. Figures 7-1 and 7-2 reveal splices which have all been produced under identical conditions. Even to the lay observer, it is clear that there is a wide variation of splice appearance and structure.

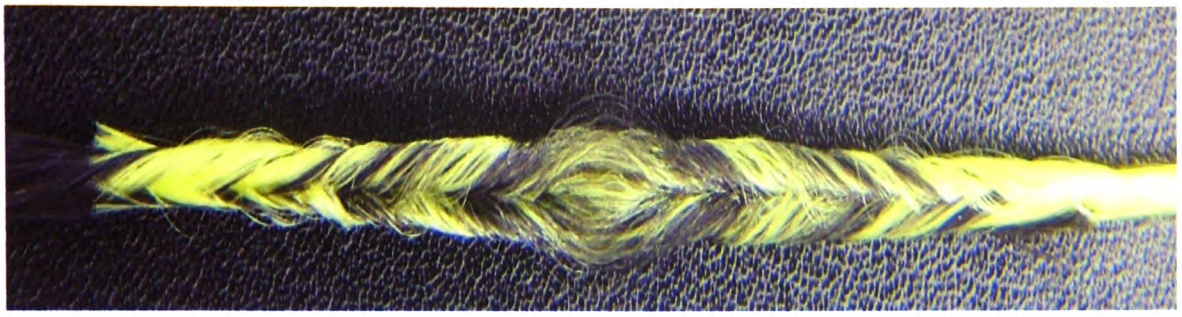

(A)

(B)

Figure 7-1. Splice produced under optimum settings as (A) a whole; (B) close up.

(A)

(B)

Figure 7-2. Splice produced under optimum settings as (A) a whole; (B) close up.

The variability is not of a magnitude which has any major effect on splice quality, and is sufficiently uniform to be useful in the real world of a textile factory. Though the variability of splicing is not of sufficient magnitude to cause problems for textile manufacturers, it is of real interest to researchers attempting to understand the detailed mechanisms of the process.

The next stage of splicing research should concern itself with a quest for the understanding of the elements of local variation which govern the construction of an individual splice. The description of the proposed model, in Chapter 6, has a single central proposition, namely that the splice is formed filament-by-filament. The path of an individual filament is easy to visualise at a qualitative level. A force is applied to the filament at a point corresponding to the blast hole. Any individual filament traces a helical path through the splice bundle, generally being confined to one half of the splice, but occasionally straying from one half to another. The helix pitch varies along its length. The geometry of the helix will be defined by the "capstan effect", determined by the magnitude of the force applied by the blast, and the friction between the filament and the bundle around which it wraps.

The forces to which any individual filament will be exposed should therefore be relatively easy to analyse, especially if it remains on one half of the splice throughout.

In addition, the proposed model touches upon the variable elements present in the process splice formation:

- As the splice bundle is built up from individual filaments, the "next" filament in the sequence can be from either of the two yarns.
- The "next" filament in the sequence can be thrown in either of two directions.
- The "next" filament in the sequence may have already entered the splice bundle, but may now be being picked up by the blast for a second or third or even fourth time.

- The filament which is picked up by the blast for a second or third time may occasionally switch at random from its original bundle to the one opposite.

Taking these issues into account, the concepts lying behind splice formation become very much less clear. There is a demonstrable statistical element at work, which will certainly involve the detail of the local air turbulence at any instant, and the manner, and sequence, in which individual filaments are drawn into the splice structure. This statistical element is far too advanced; therefore any statistical analysis was disregarded. If splicing is to be understood at the level of the individual splice, and individual filament, it will be necessary to undertake a closer examination of the mixing ratio between opposite yarn end filaments. This can perhaps be done by freezing the splice and dissecting it sliver-by-sliver, building up a visual representation to reveal the exact path individual filaments take throughout the splicing process.

It is this individual filament analysis method which will form the basis of future work.

References

Antony, J. and Antony, F.J., 2001. *Teaching the Taguchi method to industrial engineers*, Work Study, **50**(4), 141-149.

Bar-Kohany, T., Sher, I. and Sher, E., 2007. *Choked Flow of a Bubbly Mixture Through an Effervescent and Flash-Boiling Atomizer: A Theoretical Approach*, Journal of the International Institutes for Liquid Atomization and Spray Systems, **17**(5), 431-449.

Basal, G., 2003. *The Structure and Properties of Vortex and Compact Spun Yarns*, Raleigh, North Carolina State University, Thesis, 115-123.

Bendell, A., Disney, j. and Pridmore, W.A., 1989. *Taguchi methods – application in world industry*, IFS publications, London, England.

Cheng, S. & Fung, W.Y., 2004. *Joining yarn ends together by pneumatic splicing*, ATA Journal, **15**(3), 40-45.

Cheng, K.P.S. & Lam, H.L.I., 1997. *Pneumatic splicing*, Textile Asia, **7**, 66-69.

Cheng, K.P.S. & Lam, H.L.I., 2000a. *Strength of Pneumatic Spliced Polyester/Cotton Ring Spun Yarns*, Textile Research Journal, **70**(3), 243-246.

Cheng, K.P.S. & Lam, H.L.I., 2000b. *Physical Properties of Pneumatic Spliced Cotton Ring Spun Yarns*, Textile Research Journal, **70**(12), 1053-1057.

Cheng, K.P.S. and Lam, H.L.I., 2003. *Evaluating and Comparing the Physical Properties of Spliced Yarns by Regression and Neural Network Techniques*, Textile Research Journal, **73**(2), 161-164.

Chiang, T.P., Sheu, W.H. and Hwang, R.R., 1996. *Effect of Reynolds number on the eddy structure in a lid-driven cavity*, International Journal for Numerical Methods in Fluids, **26**(5), 557-579.

Coleman, D.E. and Montgomery, D.C., 1993. *A systematic approach to planning for a designed industrial experiment*, Technometrics, **35**(1), 1-27.

Daws, L.F., Penwarden, A.D. and Waters, G.T., 1965. *A Visualization Technique for the Study of Air Movement in Rooms*, Journal of the Institution of Heating and Ventilating Engineers, **33**, 24-28.

Dibble, M.L., 1971. *Splicing of multifilament strands by turbulent gaseous fluid*, Patent No: US 3581486.

Dogu, I., 1972. *The Distribution of Transverse Pressure in a Twisted Yarn Allowing for the Fiber Migration and Variation of Fiber Packing Density*, Textile Research Journal, **42**(12), 726-733.

Fibre2fashion, 2008. *yarn glossary*, Available at: http://www.fibre2fashion.com/glossary/glossary14.htm.

Fluent Inc., 2005a. *Fluent 6.2 User's Guide*, 155-223.

Fluent Inc., 2005b. *Fluent 6.2 User's Guide*, 719-806.

Fox, R.T. and Lee, D., 1990. *Optimization of metal injection molding: experimental design*, The International Journal of Powder Metallurgy, **26**(3), 233-243.

Gebald, G., 1982. *Splicing technology in auto winding*, Textile Month, 26-29.

Ghosh, A., Ishtiaque, S.M. and Rengasamy, R.S., 2005. *Stress-strain characteristics of different spun yarns as a function of strain rate and gauge length*, Journal of the Textile Institute, **98**(2), 99-104.

Haber, R.B., 1990. *Visualization techniques for engineering mechanics*, Computing Systems in Education, **1**(1), 37-50.

Hassen, M.B., Jaouachi, B., Sahnoun, M. and Sakli, F., 2008. *Mechanical properties and appearance of wet-spliced cotton/elastane yarns*, Journal of the Textile Institute, **99**(2), 119-123.

Hearle, J.W.S., Lomas, B. and Cooke, W.D., 1998. *Atlas of Fibre Fracture and Damage to Textiles*, The Textile Institute, Woodhead publishing, Cambridge, England.

Hearle, J.W.S. and Wilkins, A.H., 2006. *Movement of fibers in assemblies*, Journal of the Textile Institute, **97**(1), 1-9.

Iwnicki, K., 1964. *Process and apparatus for Joining Yarns or Tows*, Patent No. GB956992.

Kadolph, S.J. and Langford A.L., 2001. *Textiles – Ninth edition*, London, Prentice Hall.

Kaushik, R.C.D., Hari, P.K., Sharma, I.C. and Sarkar, A.K., 1987*a*. *Performance of spliced yarn in warping and weaving*, Textile Research Journal, **57**, 670-673.

Kaushik, R.C.D. & Sharma, I.C., 1988. *Mechanism of the Splice*, Textile Research Journal, **58**(5), 263-268.

Kaushik, R.C.D., Sharma, I.C. and Hari, P.K., 1987b. *Effect of Fiber/Yarn Variables on Mechanical Properties of Spliced Yarn*, Textile Research Journal, **57**(8), 490-494.

Kothari, V.K., Sengupta, A.K., Rengasamy, R.S. and Goswami, B.C., 1989. *Influence of Interfilament Friction on Structure and Properties of Air Textured Yarns*, Textile Research Journal, **59**(6), 317-323.

Lam, H.L.I. and Cheng, K.P.S., 1997. *Pneumatic splicing*, Textile Asia, **7**, 66-69.

Lamar, J.E., 2001. *Flow-Visualization Techniques Used at High Speed by Configuration Aerodynamics Wind-Tunnel-Test Team*, Technical Report: NASA/TM-2001-210848.

Lappage, J., 2005. *End breaks in the spinning and weaving of weavable singles yarns*, Textile Research Journal, **75**(6), 512-517.

Lewandowski, S. and Drobina, R., 2004. *Strength and geometric sizes of pneumatic spliced combed wool ring spun yarns*, Fibres & Textiles in Eastern Europe, **12**, 2(46), 31-37.

Lewandowski, S. and Stanczyk, T., 2005. I*dentification and classification of spliced wool combed yarn joints by artificial neural networks. Part II: Interpretation of identification and classification results of the unknotted spliced yarn joints*, Fibres & Textiles in Eastern Europe, **13**, 2(50), 16-19.

Lochner, R.H., 1991. *Pros and cons of Taguchi*, Quality Engineering, **3**(4), 537-549.

Logan, F.E., 2001. *Air entanglement yarn splicer*, Patant No: US 6185922 B1.

Logothetis, N., Atkinson, C.J., Salmon, J.P. and Best, K.F., 1990. *Development of newly installed processes*, The International Journal of Advanced Manufacturing Technology, **5**, 256-274.

Merati, A.A., Konda, F., Okamura, M. and Marui, E., 1998. *Filament Pre-tension in Core Yarn Friction Spinning*, Textile Research Journal, **68**(4), 254-264.

Mingjie, X., Peijie, H., Shihua, S., Bingchang, Q. & Tao, L., 1999. *Study on Pneumatic Splice*, Journal of China Textile University, **16**(2), 109-112.

Morrison, M. E., 2005. *Split splicing*, Available at: http://morcatknits.typepad.com/spitsplicing/2005/03/or_how_to_join_.html.

Nair, V.N., 1992. *Taguchi's parameter design: A panel discussion*, Technometrics, **34**(2), 127-161.

Nikolic, M., Stjepanovic, Z., Lesjak, F. and Stritof, A., 2003. *Compact spinning for improved quality of ring-spun yarns*, Fibres & Textiles in Eastern Europe, **11**, 4(43), 30-35.

Oinuma, R., Narisawa, I. and Koyama, K., 1995. *Mechanism of end breakage due to knots in plain-weft knitting zone*, Journal of the Textile Machinery Society of Japan, **48**(7), 43-52.

O'Keefe controls co., 2003. *Choked Flow of Gases*, 48.

Oxenham, W. and Basu, A., 1993. *Effect of Jet design on the properties of air-jet spun yarns*, Textile Research Journal, **63**(11), 674-678.

Paliwal, M.C. and Patel, R.S., 1989. *Assessment of yarn splicing in Indian mills*, 30th Technological conference, 24.1-24.5.

Pan, N., 1993. *Prediction of statistical strengths of twisted fibre structures*, Journal of Materials Science, **28**(22), 6107-6114.

Peace, G.S., 1993. *Taguchi methods – a hands-on approach*, Addison-Wesley publishing company, Wokingham, England, 13-311.

Primentas, A. and Iype, C., 2001. *The Configuration of Textile Fibres in Staple Yarns*, Journal of Textile and Apparel, Technology and Management, **1**(2), 1-8.

Ropers Knots Page, 1997. Available at: http://www.realknots.com.

Rowlands, H., Antony, J. and Knowles, G., 2000. *An application of experimental design for process optimisation*, TQM Magazine, **12**(2), 78-83.

Satapathy, B.K. and Bijwe, J., 2004. *Performance of friction materials based on variation in nature of organic fibres Part I. Fade and recovery behaviour*, Wear, **257**, 573-584.

Schlafhorst, 1998. *Yarn end preparation device for cheese-producing textile machines*, Patent No: US 5829706.

Schmidtchen, U., 1994. *Choked flow of helium II through phase separators*, Journal of Low Temperature Physics, **97**(5-6), 365-392.

Sengupta, S., 2000. *Retained strength of air-spliced yarn – Rupture process and effect of test length*, Indian Journal of Fibre & Textile Research, **25**, 277-283.

Shea, R.J., 1981. *Developing a splicer that works*, Textile Horizons, **2**, 16-18.

Sreprateep, K. and Bohez, E.L.J., 2006. *Computer Aided Modelling of Fiber Assemblies*, Computer-Aided Design & Applications, **3**(1-4), 367-376.

Suber, P., 2004. *Knots on the Web*, Earlham Collage, Available at: http://www.earlham.edu/~peters/knotlink.htm.

Taguchi, G., 1989. *Introduction to Quality Engineering*, UNIPUB, New York.

Textura AG., 1969. *Method and apparatus for splicing yarns*, Patent No: US 1175621

The Textile Institute, 1963. *Textile Terms and Definitions – 5th Edition*, Textile Institute, Manchester, England.

The Textile Institute, 1970. *Textile Terms and Definitions – 6th Edition*, Textile Institute, Manchester, England.

Thomas, A.J. and Antony, J., 2003. *An integrated approach to improving the adhesive bond strength of honeycomb composite joints*, Work Study, **52**(5), 244-255.

Thomas, A.J. and Antony, J., 2005. *A comparative analysis of the Taguchi and Shainin DOE techniques in an aerospace environment*, Productivity and Performance Management, **54**(8), 658-678.

Wagner, H. D., Gallis, H. E. and Wiesel, E., 1993. *Study of the interface in Kevlar 49-epoxy composites by means of microband and fragmentation tests: effect of materials and testing variables*, Journal of Materials Science, **28**, 2238-2244.

Waters, G.T., 1996. *Improvement in Yarn Splicing*, Application for S.M.A.R.T. award, Welsh office.

Waters, G.T., 1998. *Pneumatic yarn splicer*, Patent No: US 5809761.

Waters, G.T., 2007. *Splicing history*, Internal document of GTW Developments, Pontypool.

Webb, C.J., Waters G.T., Thomas, A.J., Liu, G.P. and Thomas, C., 2007a. *The use of the Taguchi Design of Experiment method in optimising splicing conditions for a Nylon 66 yarn*, Journal of the Textile Institute, **98**(4), 327-336.

Webb, C.J., Waters G.T., Thomas, A.J., Liu, G.P. and Thomas, E.J.C., accepted 2007b. *Optimising splicing parameters for splice aesthetics for a continuous filament synthetic yarn*, Journal of the Textile Institute.

Webb, C.J., Waters G.T., Thomas, A.J., Liu, G.P. and Thomas, E.J.C., 2009. *The influence of yarn count on the splicing of simple continuous filament synthetic yarns*, Textile Research Journal, **97**(3), 195-204.

Webb, C.J., Waters G.T., Thomas, A.J., Liu, G.P. and Thomas, E.J.C., accepted 2008. *The use of visualisation and simulation techniques to model the splicing process*, Journal of the Textile Institute.

Wei, Q.F. and Wang, X.Q., 2003. *Dynamic characterisation of industrial textiles using an environmental scanning electron microscope*, Journal of Industrial Textiles, **33**(2), 101-110.

Wei, Q. F. and Wang, X. Q., 2004. *AFM Characterisation of Technical Fibres*, Journal of Industrial Textiles, **34**(1), 51-60.

Wei, Q.F., Wang, X.Q., Mather, R.R. and Fotheringham, A.F., 2004. *New Approaches to Characterisation of Textile Materials Using Environmental Scanning Electron Microscope*, Fibres & Textiles in Eastern Europe, **12**, 2(46), 79-83.

Witkowska, B. and Frydrych, I., 2004. *A Comparative Analysis of Tear Strength Methods*, Fibres & Textiles in Eastern Europe, **12**, 2(46), 42-47.

Wojtysiak, J., 2003. *System Approach to the Research Process in Problems of Textile Engineering and Technology*, Fibres & Textiles in Eastern Europe, **11**, 4(43), 86-89.

Wood, J.I., 1982. *The Development of Air-splicing Techniques for the Jointing of Woollen-spun Yarns for Tufted-carpet Manufacture*, Journal of the Textile Institute, **2**, 71-79.

Wu, C.M., Black, J.T. and Jiang, B.C., 1991. *Using Taguchi methods to determine/ optimize robot process capability for path following*, Robotics & Computer-Integrated Manufacturing, **8**(1), 9-25.

Zeng, Y.C., Wan, Y., Yu, C.W. and He, J., 2005. *Controlling the Air Vortex Twist in Air-Jet Spinning*, Textile Research Journal, **75**(2), 175-177.

Zhou J. and Qin, P., 2005. *Air Flow in a Pneumatic Splicer by CFD*, Textile Research Journal, **75**(2), 106-110.

Appendix 1

Compilation of pictures from visualisation and simulation techniques

---

Scaled model splice creation

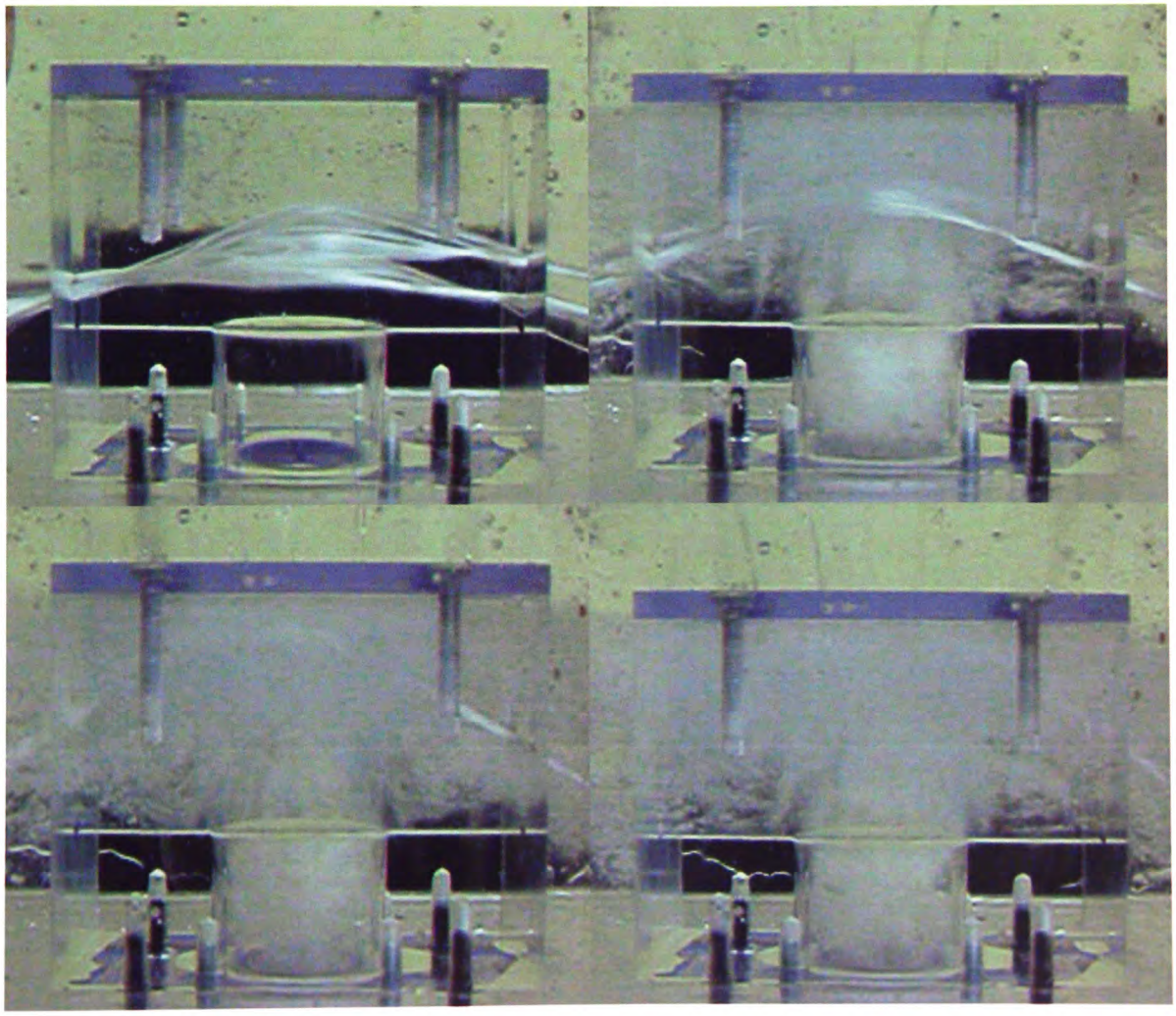

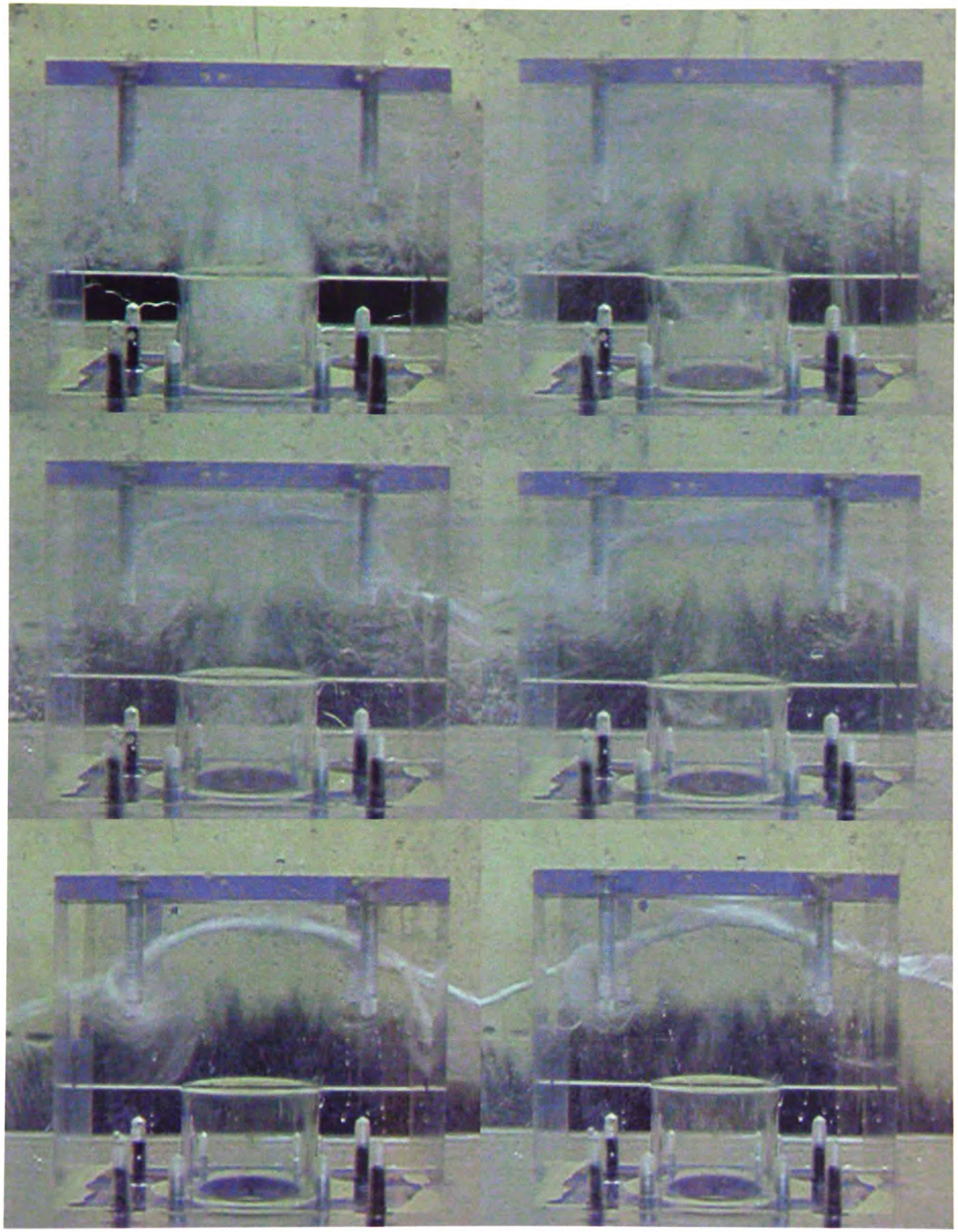

CFD simulations

The 4483 straight chamber 3-D realizable k-epsilon turbulence model simulations were created using a hexahedral mesh, type Cooper, with an interval size of 0.1mm. The boundary conditions at the input (blast hole) ranged from 0 to 90psi and with flow rates of 0 and 143liters/min respectively. The boundary conditions at the outputs (both exits from either side of the chamber trapezium section) were 0psi. Various angles of the 4483 straight chamber streamline airflow simulation at 50psi with a flow rate of 108liters/min are as follows:

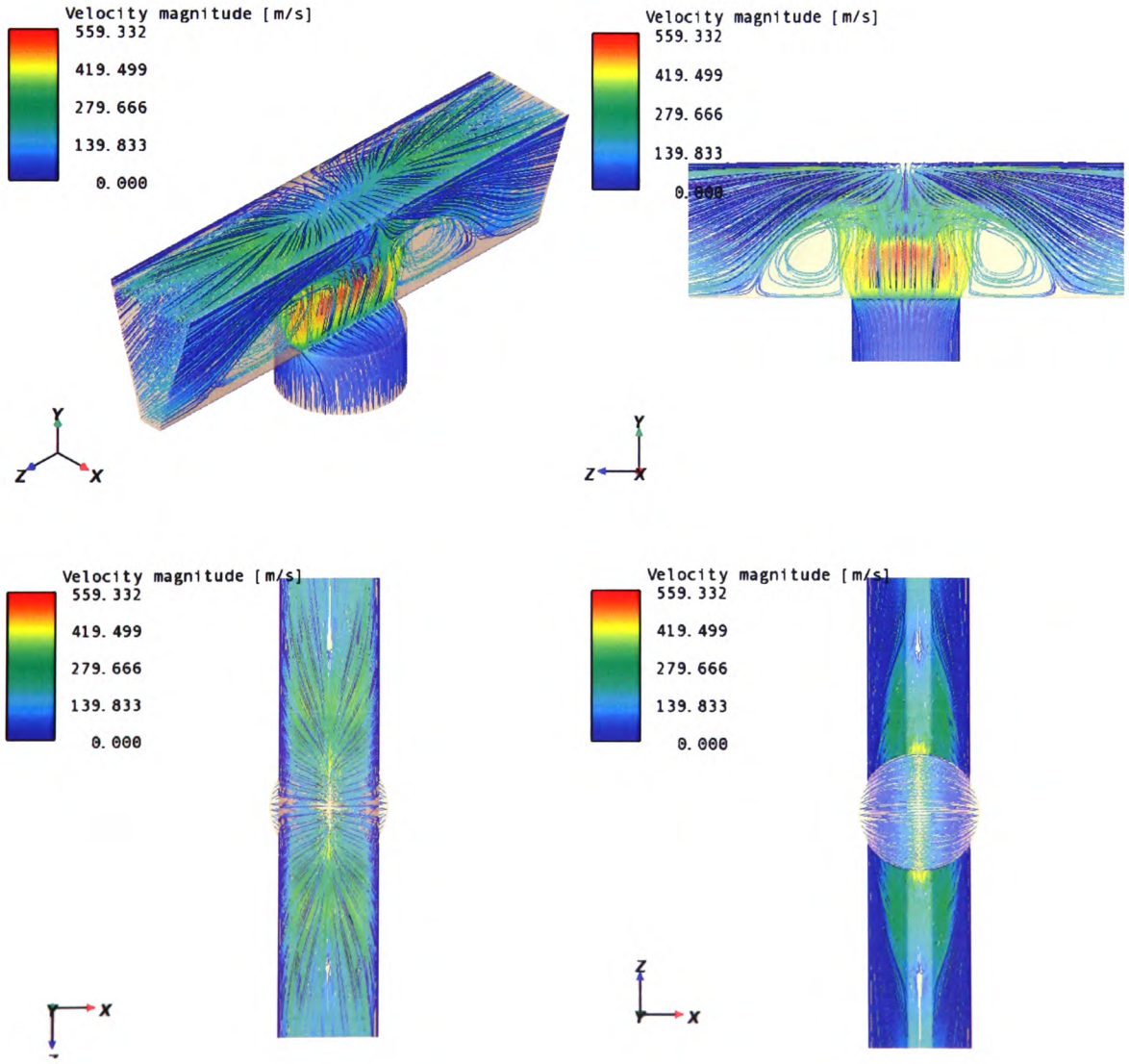

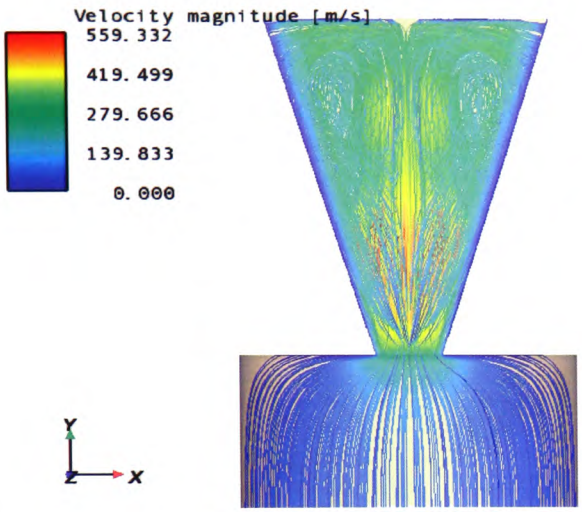
Velocity magnitude [m/s]
559.332
419.499
279.666
139.833
0.000
Y
Z
X

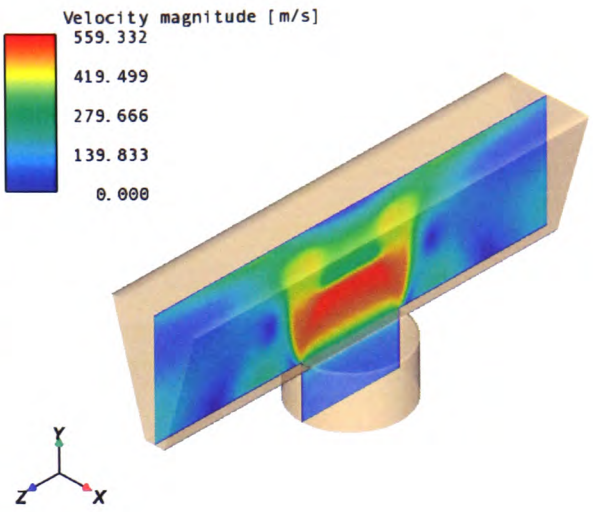
Velocity magnitude [m/s]
559.332
419.499
279.666
139.833
0.000
Y
Z
X

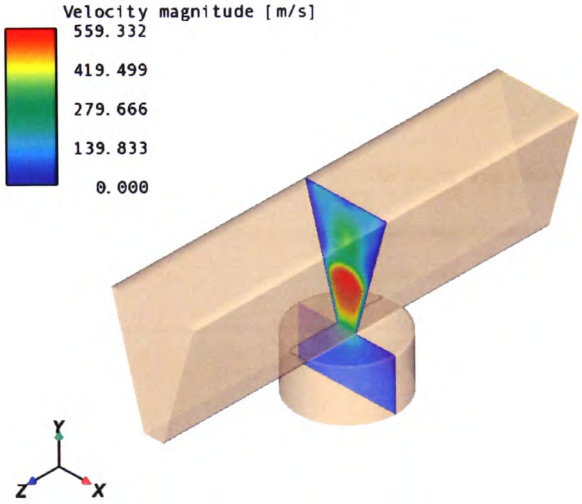
Velocity magnitude [m/s]
559.332
419.499
279.666
139.833
0.000
Y
Z
X

Various angles of the 4483 straight chamber streamline airflow simulation at 90psi with a flow rate of 143liters/min are as follows:

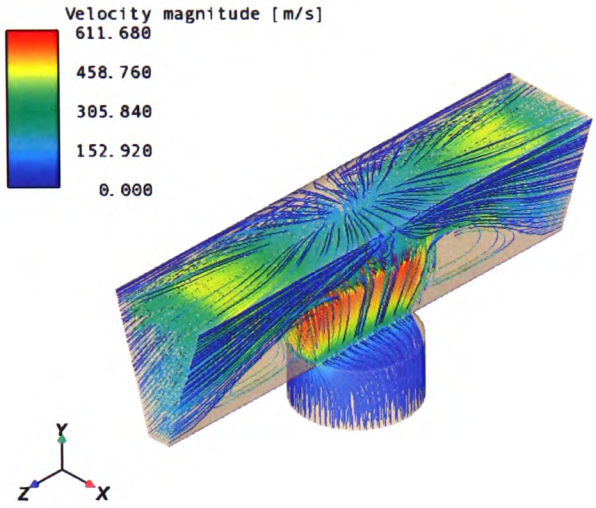

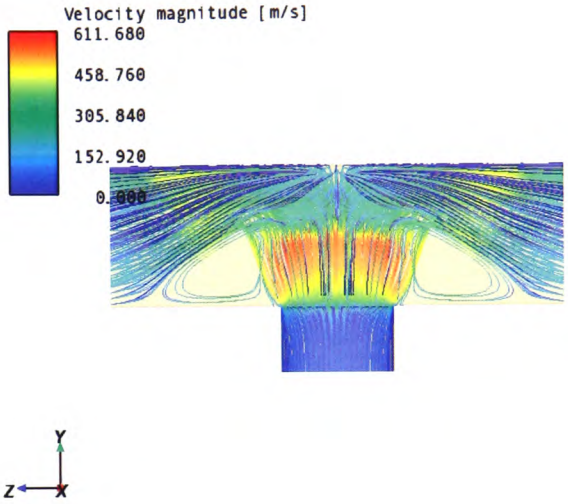

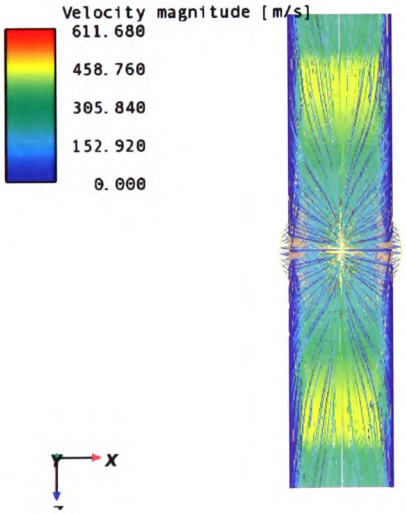

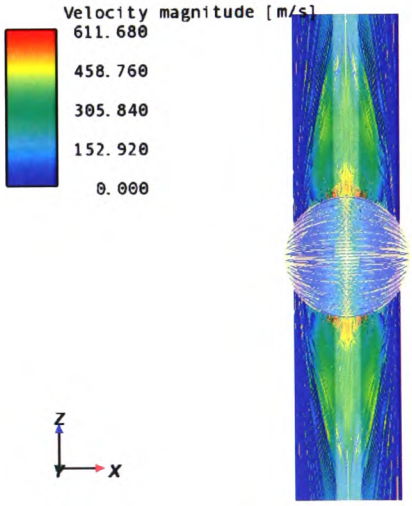

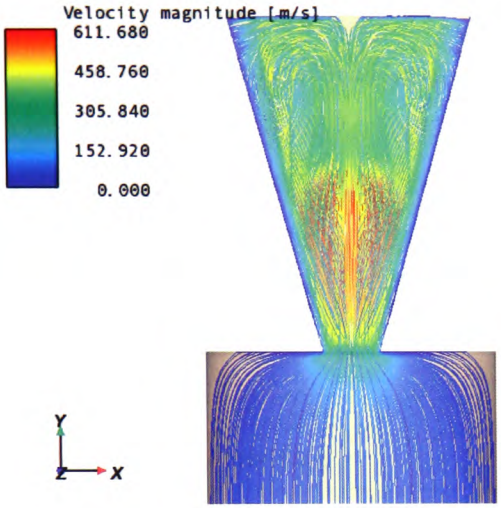
Velocity magnitude [m/s]
611.680
458.760
305.840
152.920
0.000
Y
Z
X

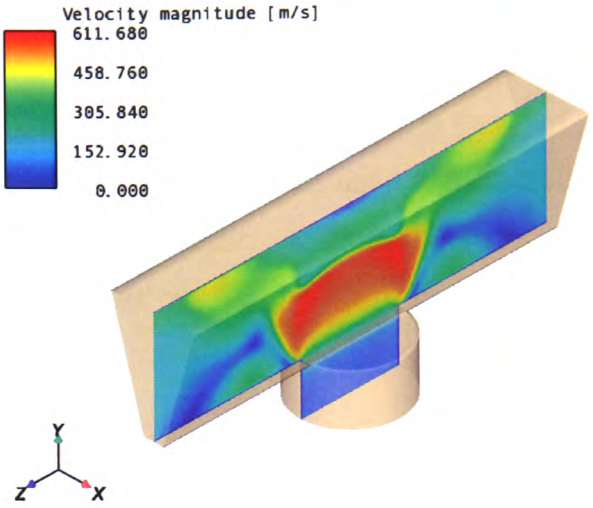
Velocity magnitude [m/s]
611.680
458.760
305.840
152.920
0.000
Y
Z
X

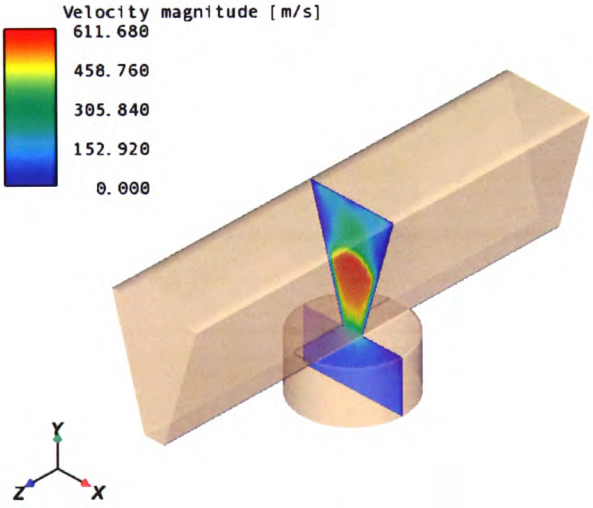
Velocity magnitude [m/s]
611.680
458.760
305.840
152.920
0.000
Y
Z
X

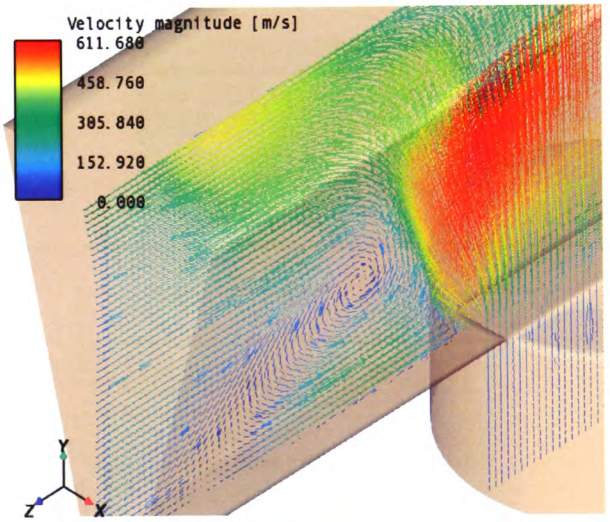
Velocity magnitude [m/s]
611.680
458.760
305.840
152.920
0.000
Y
Z
X

The 4485 straight chamber 3-D realizable k-epsilon turbulence model simulations were created using a hexahedral mesh, type Cooper, with an interval size of 0.1mm. The boundary conditions at the input (blast hole) ranged from 0 to 90psi and with flow rates of 0 and 159liters/min respectively. The boundary conditions at the outputs (both exits from either side of the chamber trapezium section) were 0psi. Various angles of the 4485 straight chamber streamline airflow simulation at 50psi with a flow rate of 121liters/min are as follows:

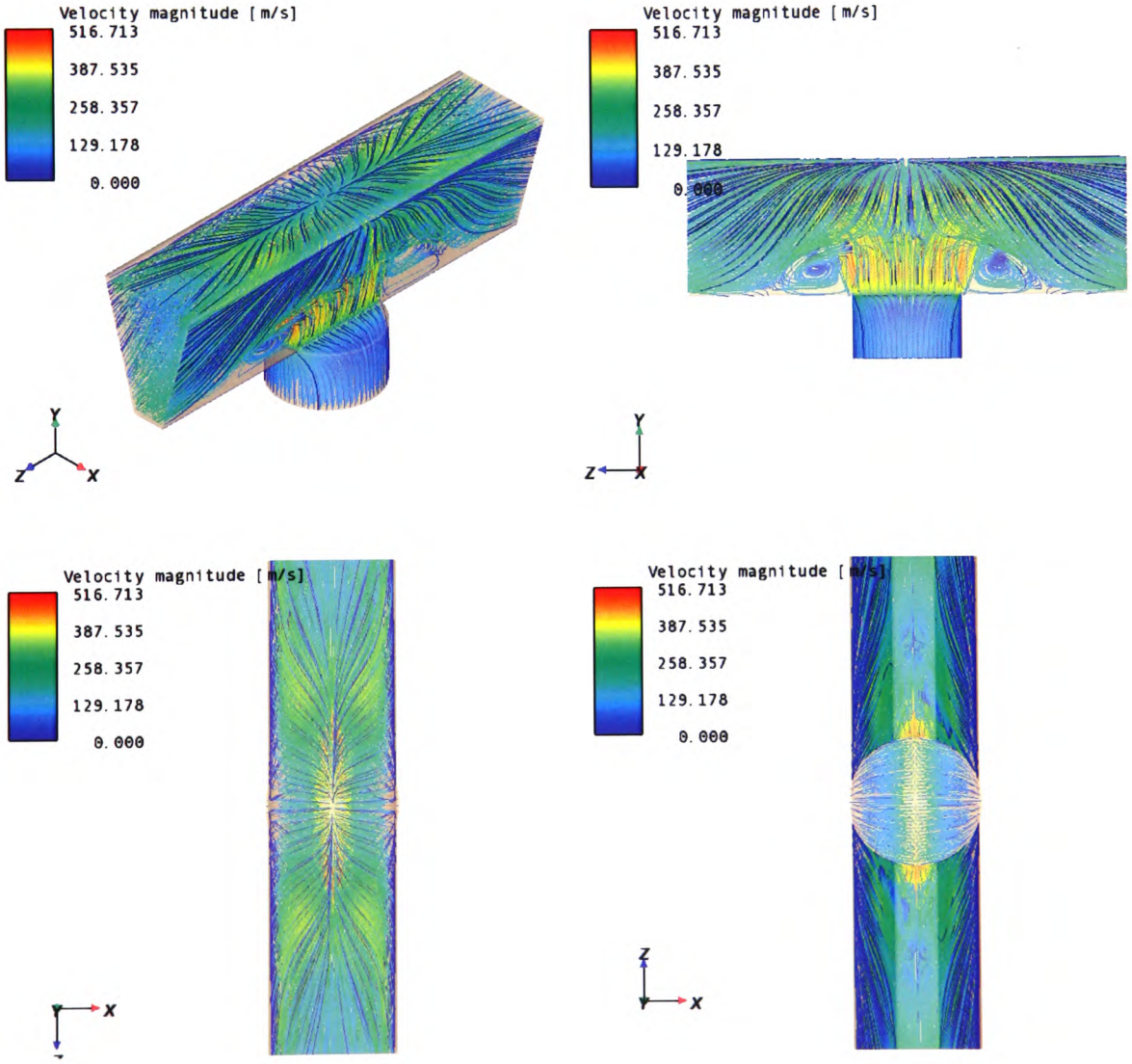

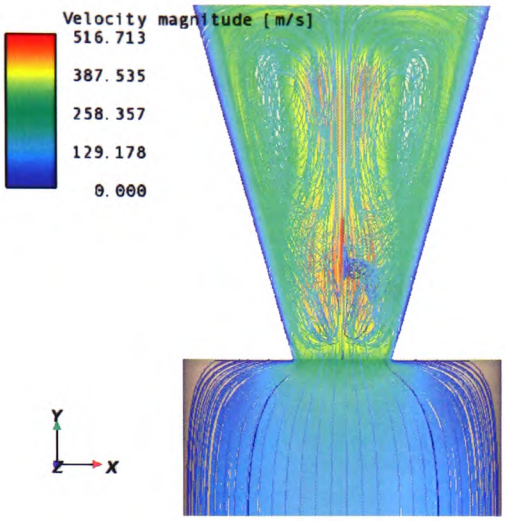
Velocity magnitude [m/s]
516.713
387.535
258.357
129.178
0.000
Y
Z
X

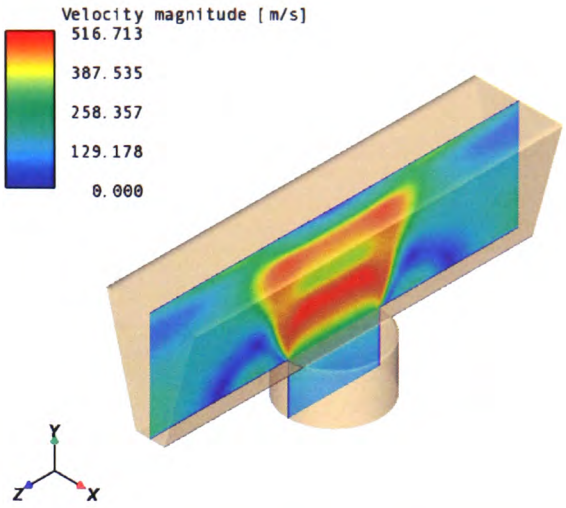
Velocity magnitude [m/s]
516.713
387.535
258.357
129.178
0.000
Y
Z
X

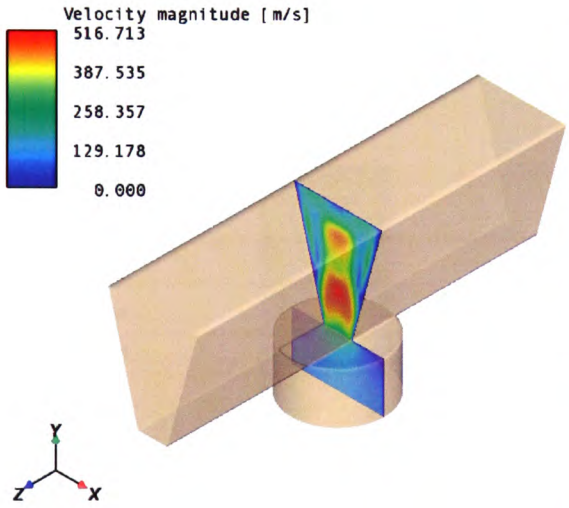
Velocity magnitude [m/s]
516.713
387.535
258.357
129.178
0.000
Y
Z
X

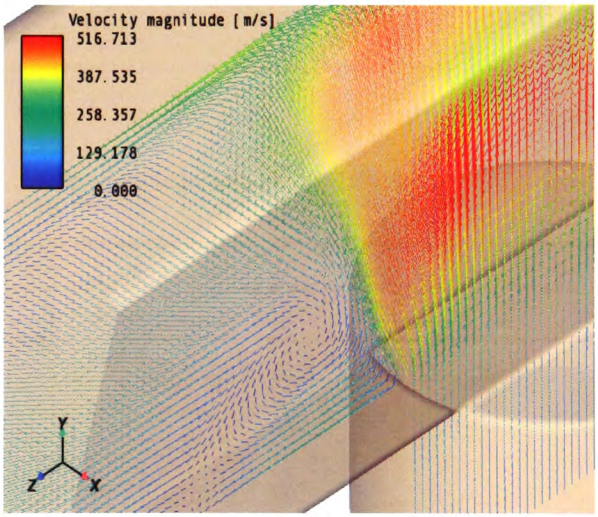
Velocity magnitude [m/s]
516.713
387.535
258.357
129.178
0.000
Y
Z
X

Various angles of the 4485 straight chamber streamline airflow simulation at 90psi with a flow rate of 159liters/min are as follows:

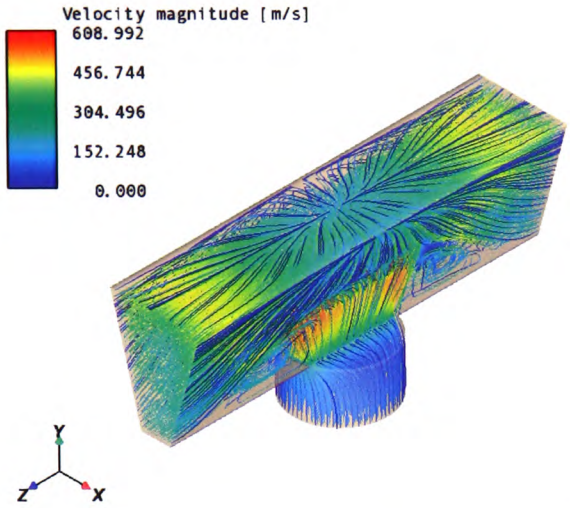

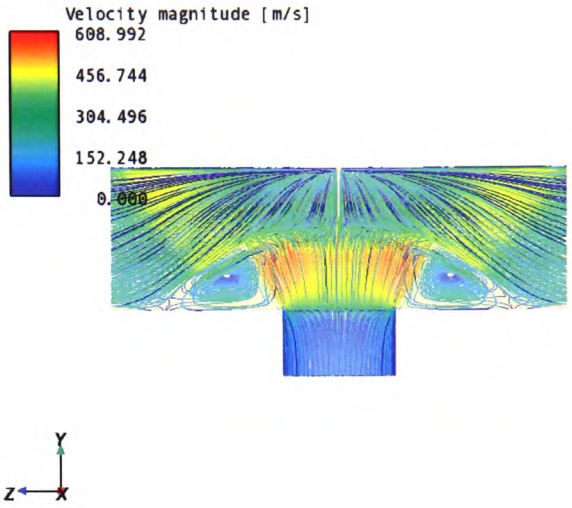

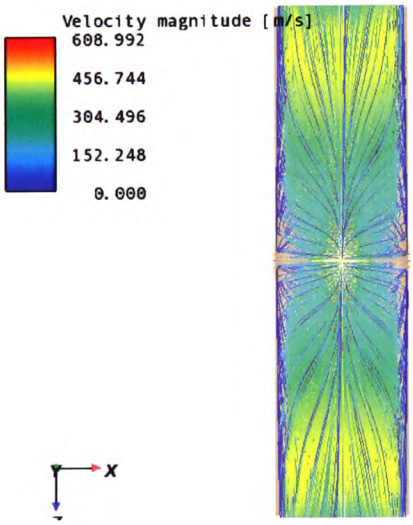

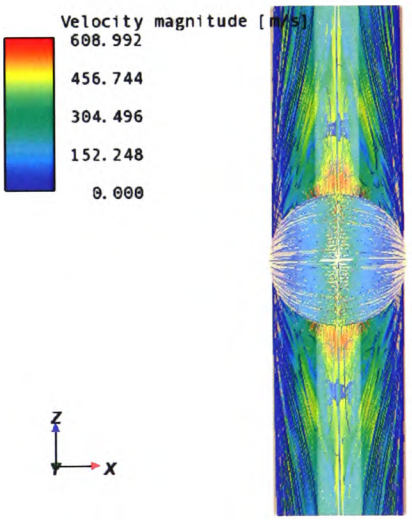

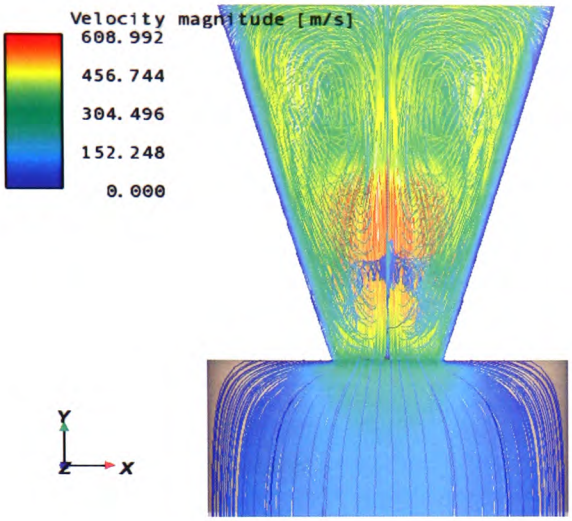
Velocity magnitude [m/s]
608.992
456.744
304.496
152.248
0.000
Y
Z
X

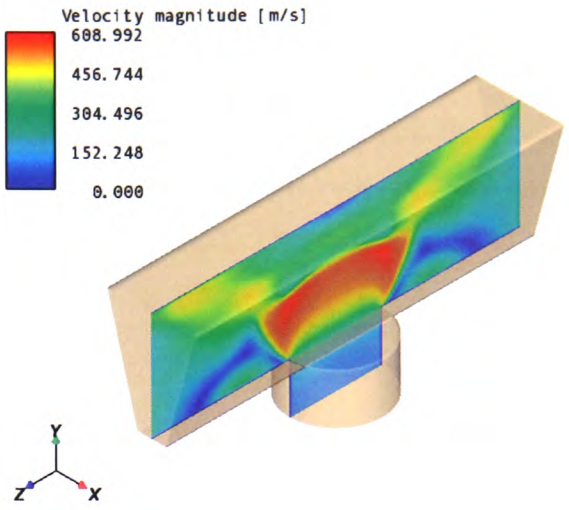
Velocity magnitude [m/s]
608.992
456.744
304.496
152.248
0.000
Y
Z
X

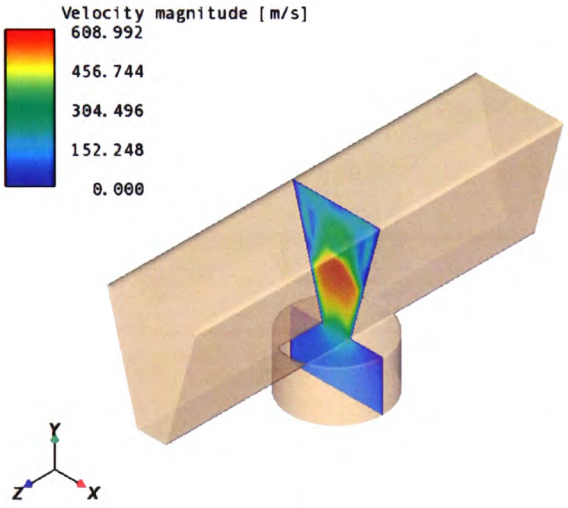
Velocity magnitude [m/s]
608.992
456.744
304.496
152.248
0.000
Y
Z
X

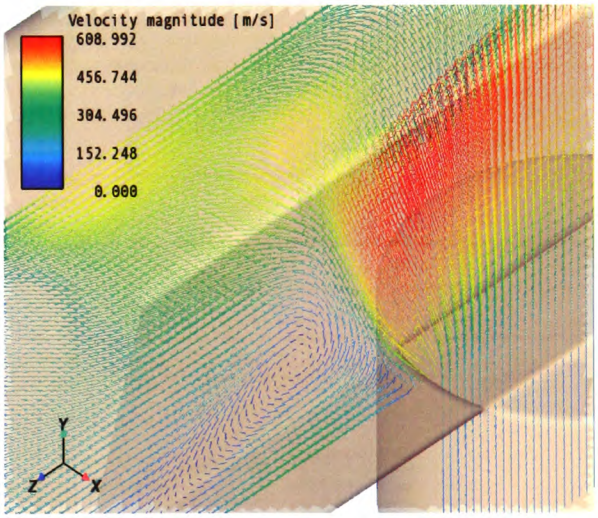
Velocity magnitude [m/s]
608.992
456.744
304.496
152.248
0.000
Y
Z
X

The 4483 bowl chamber 3-D realizable k-epsilon turbulence model simulation were created using a tetrahedral mesh, type TGrid, with an interval size of 0.1mm. The boundary conditions at the input (blast hole) ranged from 0 to 90psi and with flow rates of 0 and 132liters/min respectively. The boundary conditions at the outputs (both exits from either side of the chamber trapezium section) were 0psi. Various angles of the 4483 bowl chamber streamline airflow simulation at 50psi with a flow rate of 99liters/min are as follows:

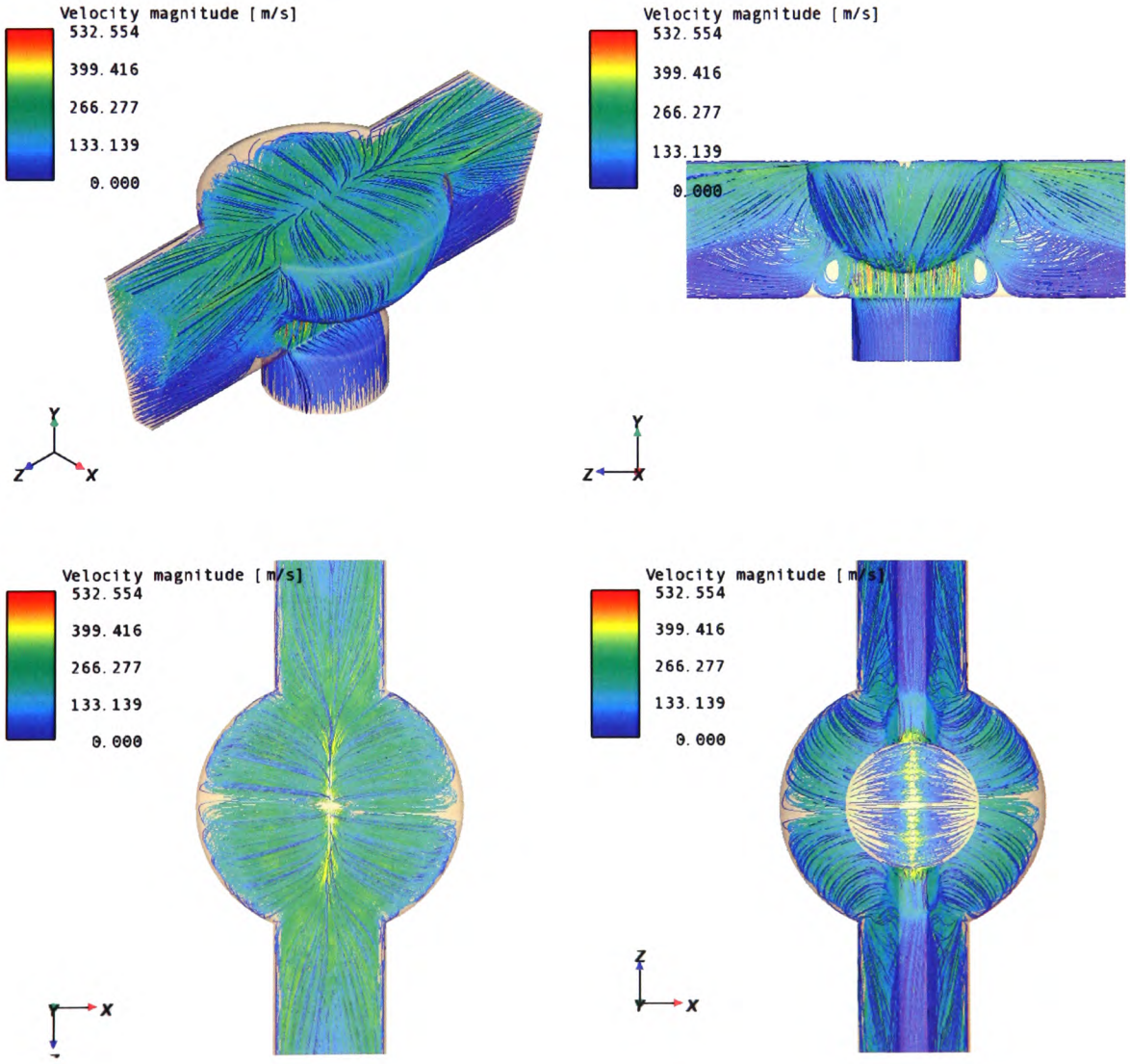

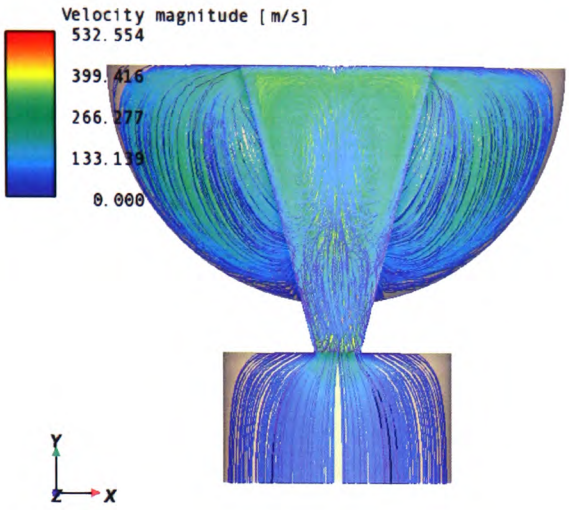
Velocity magnitude [m/s]
532.554
399.416
266.277
133.139
0.000
Y
Z
X

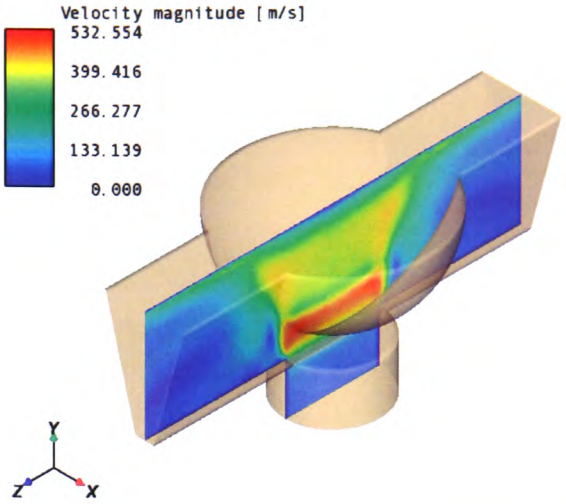
Velocity magnitude [m/s]
532.554
399.416
266.277
133.139
0.000
Y
Z
X

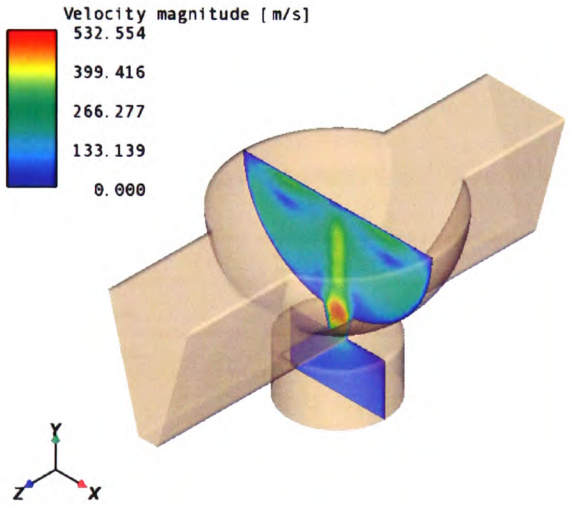
Velocity magnitude [m/s]
532.554
399.416
266.277
133.139
0.000
Y
Z
X

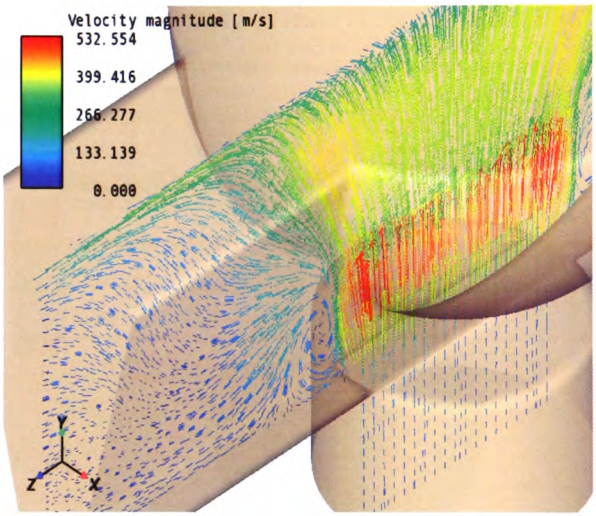
Velocity magnitude [m/s]
532.554
399.416
266.277
133.139
0.000
Y
Z
X

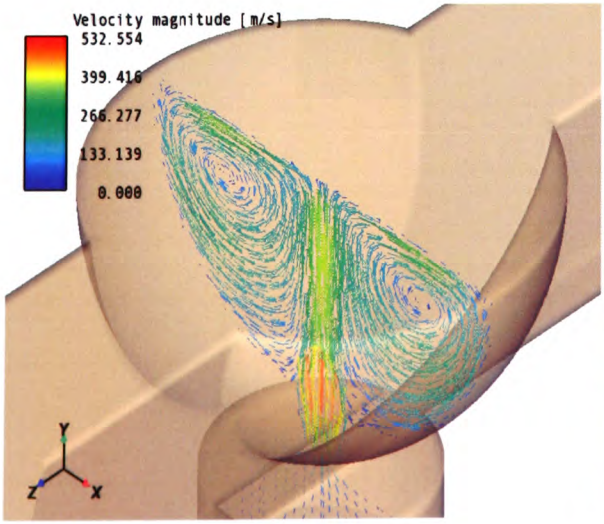
Velocity magnitude [m/s]
532.554
399.416
266.277
133.139
0.000
Y
Z
X

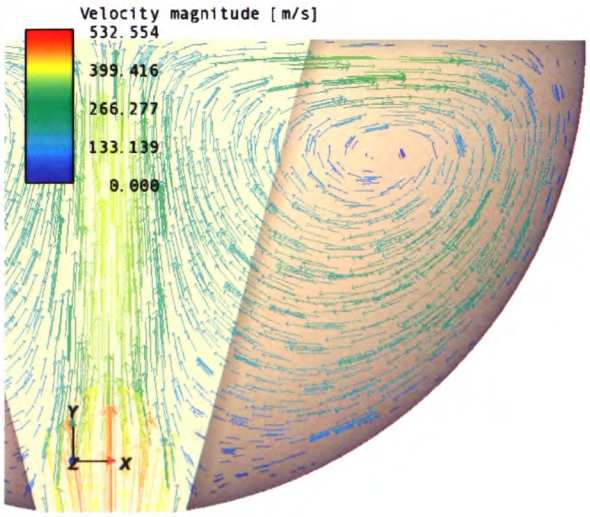
Velocity magnitude [m/s]
532.554
399.416
266.277
133.139
0.000
Y
Z
X

Various angles of the 4483 bowl chamber streamline airflow simulation at 90psi with a flow rate of 132liters/min are as follows:

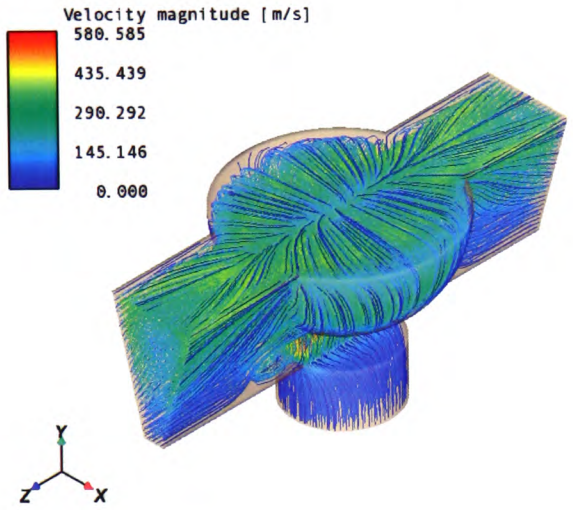

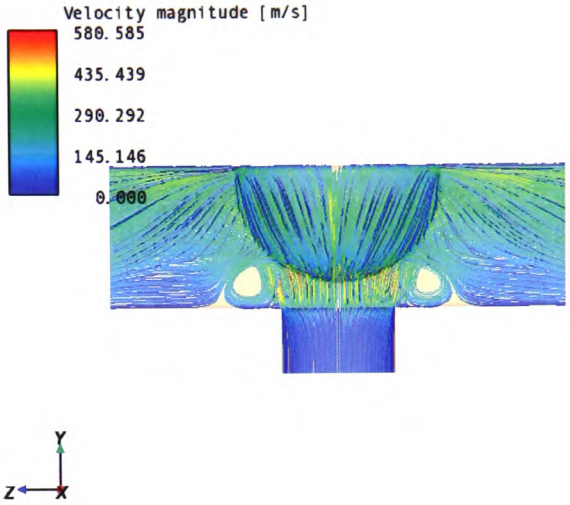

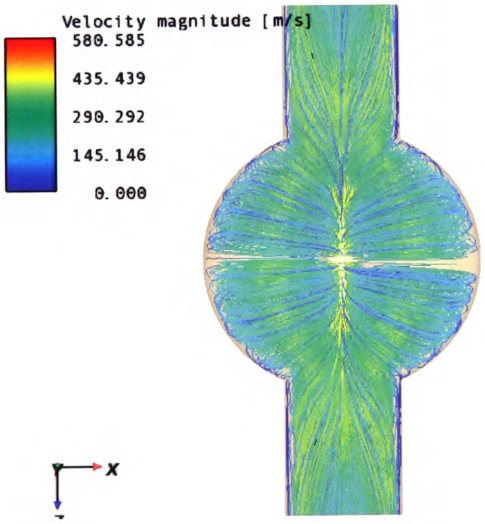

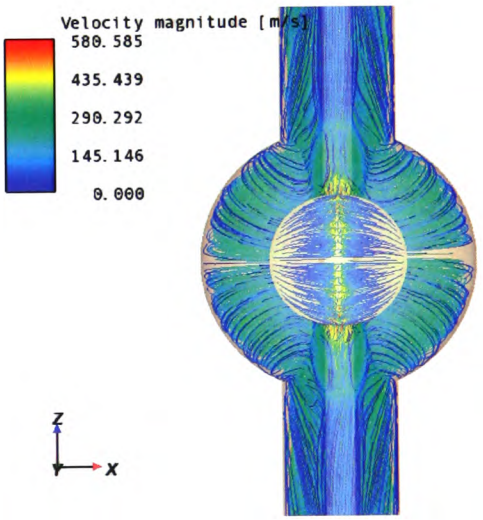

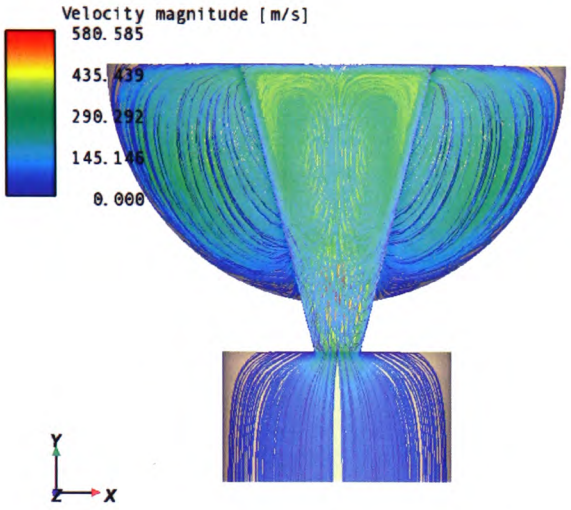
Velocity magnitude [m/s]
580.585
435.439
290.292
145.146
0.000
Y
Z
X

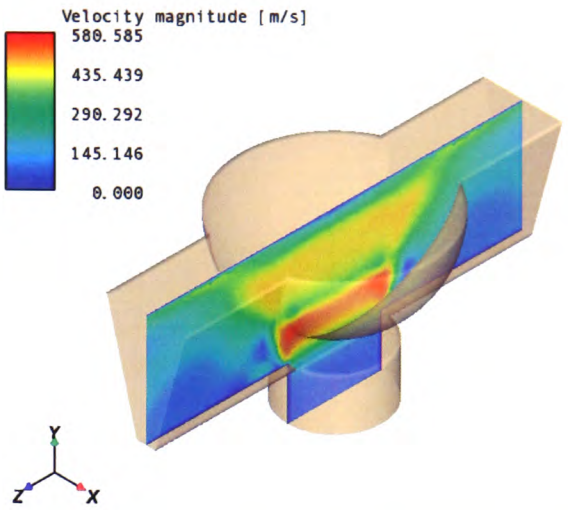
Velocity magnitude [m/s]
580.585
435.439
290.292
145.146
0.000
Y
Z
X

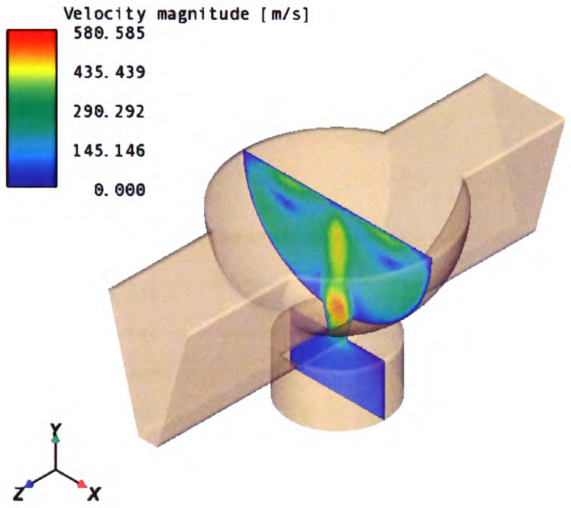
Velocity magnitude [m/s]
580.585
435.439
290.292
145.146
0.000
Y
Z
X

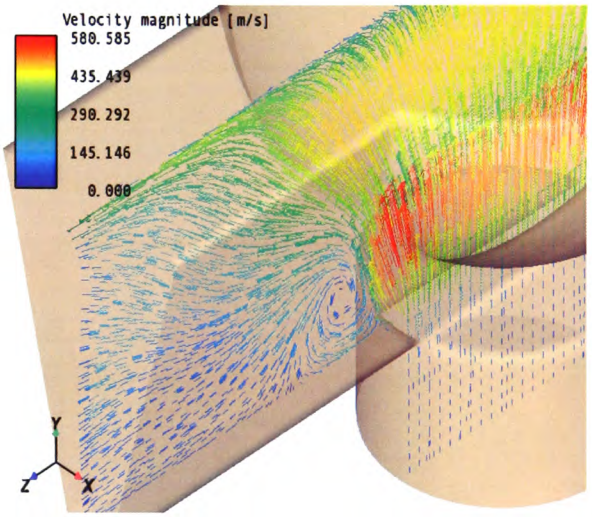
Velocity magnitude [m/s]
580.585
435.439
290.292
145.146
0.000
Y
Z
X

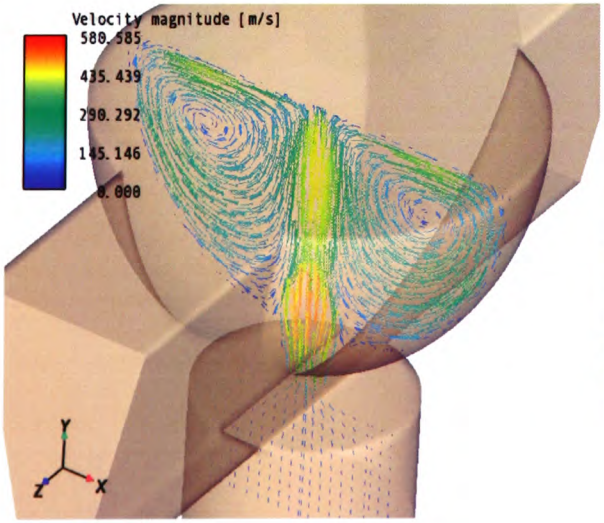
Velocity magnitude [m/s]
580.585
435.439
290.292
145.146
0.000
Y
Z
X

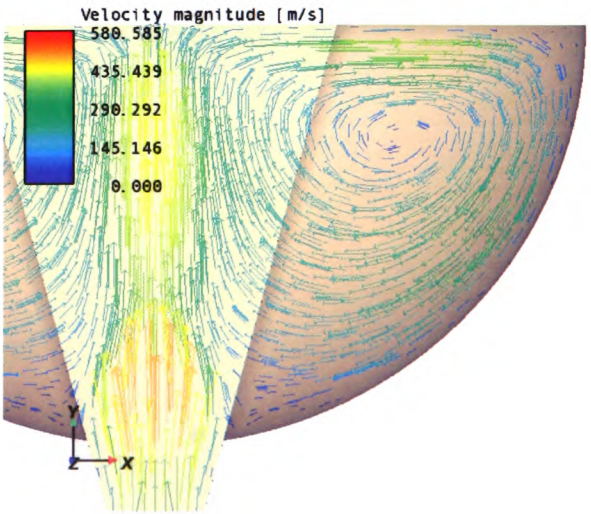
Velocity magnitude [m/s]
580.585
435.439
290.292
145.146
0.000
Y
Z
X

Streamline airflow simulation of 4483 straight chamber over the whole experimental pressure range:

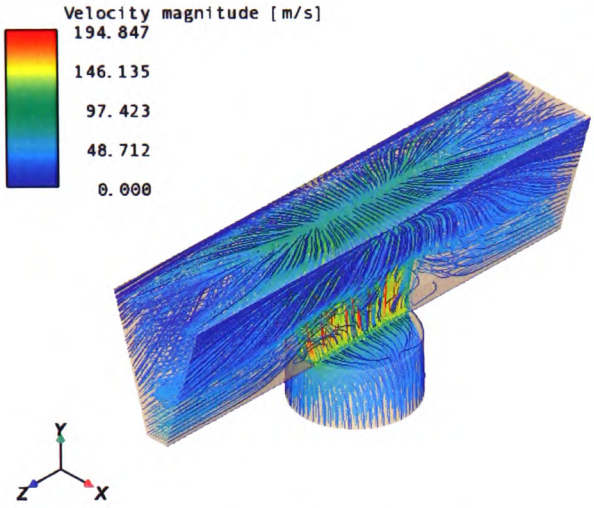

4psi (42liters/min)

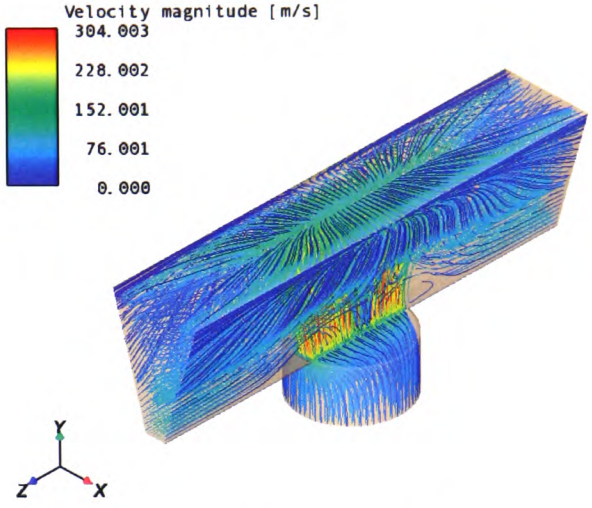

12psi (68liters/min)

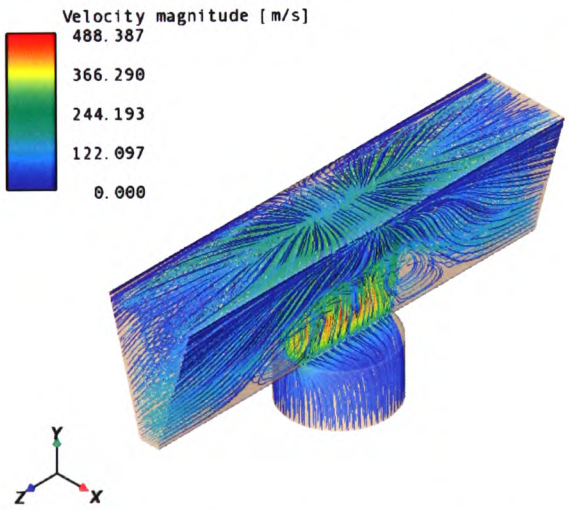

30psi (92liters/min)

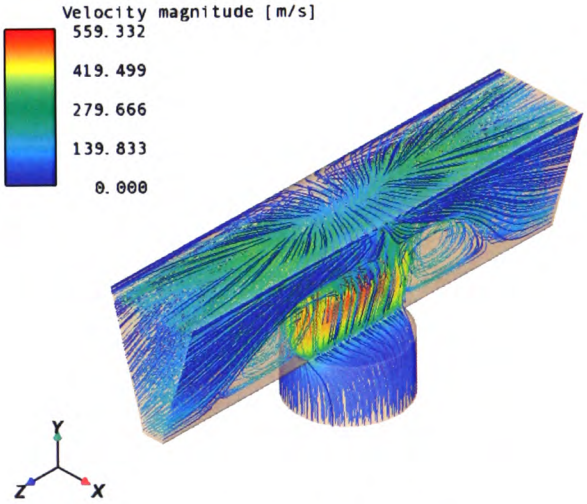

50psi (108liters/min)

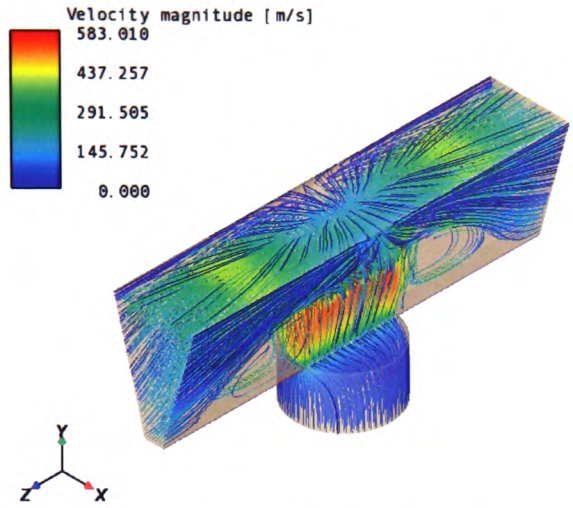

70psi (130liters/min)

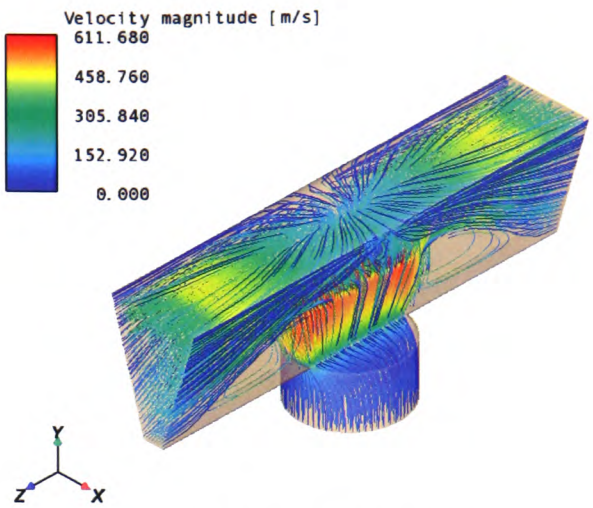

90psi (143liters/min)

Table A1-1. 4483 straight chamber.

Pressure at inlet (psig)	Pressure ratio (P_{out}/P_{in})	Velocity at orifice (m/s)	Mass flow rate at orifice (kg/s)
0	1	0	0
4	0.78	194.8	0.00063
8	0.64	265.7	0.00092
12	0.55	303.9	0.00115
16	0.47	343.2	0.00136
20	0.42	343.6	0.00156
30	0.32	343.7	0.00205
40	0.26	343.7	0.00251
50	0.22	343.7	0.00297
60	0.19	343.7	0.00342
70	0.17	343.7	0.00388
80	0.15	343.7	0.00434
90	0.14	343.7	0.00480

Streamline airflow simulation of 4485 straight splicing chamber over the whole experimental pressure range:

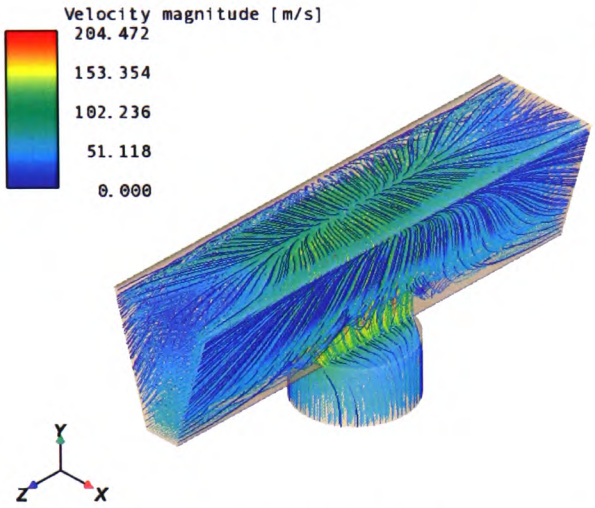

4psi (56liters/min)

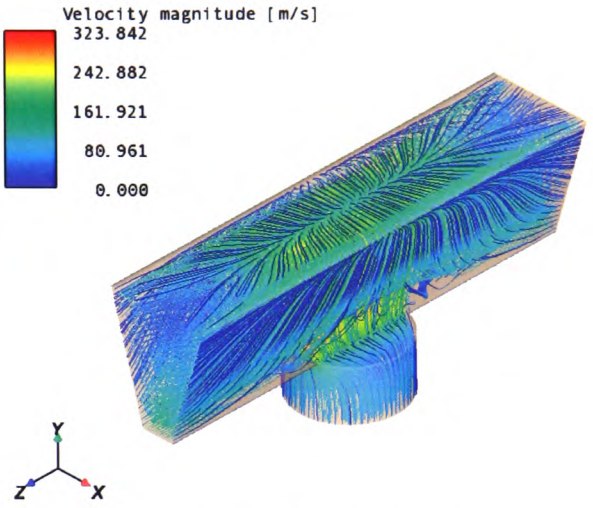

12psi (79liters/min)

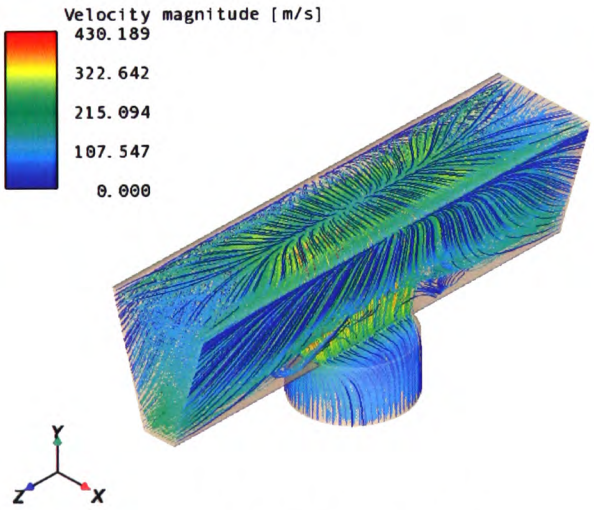

30psi (106liters/min)

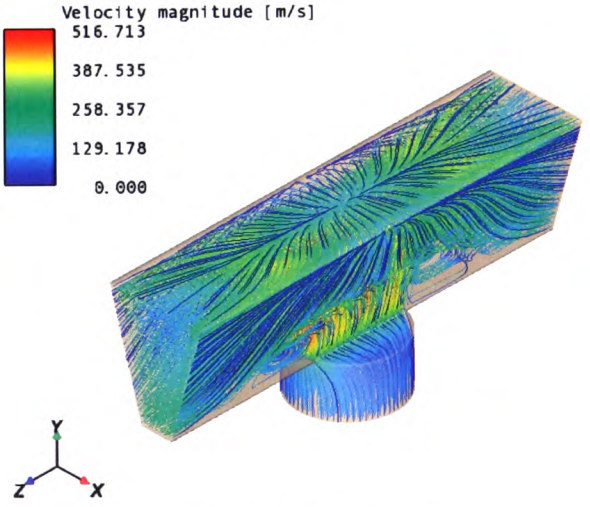

50psi (121liters/min)

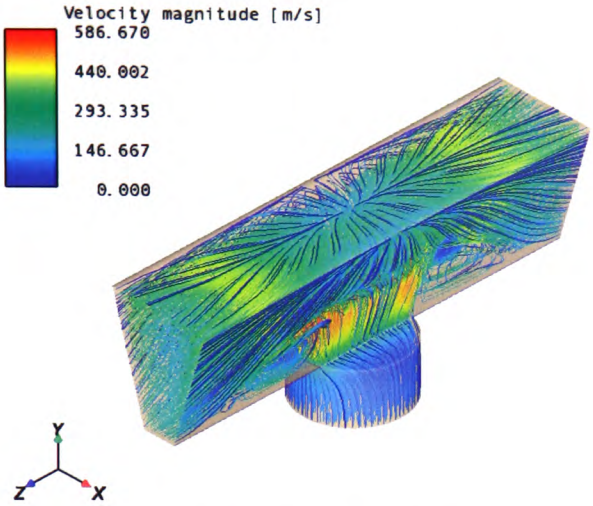

70psi (140liters/min)

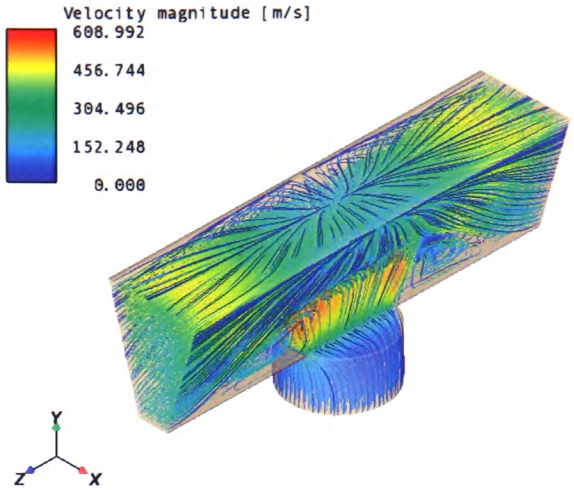

90psi (159liters/min)

Table A1-2. 4485 straight chamber.

Pressure at inlet (psig)	Pressure ratio (P_{out}/P_{in})	Velocity at orifice (m/s)	Mass flow rate at orifice (kg/s)
0	1	0	0
4	0.78	204.5	0.00084
8	0.64	267.4	0.00124
12	0.55	323.8	0.00158
16	0.47	343.5	0.00191
20	0.42	343.6	0.00210
30	0.32	343.7	0.00263
40	0.26	343.7	0.00335
50	0.22	343.7	0.00407
60	0.19	343.7	0.00479
70	0.17	343.7	0.00551
80	0.15	343.7	0.00623
90	0.14	343.7	0.00696

Streamline airflow simulation of 4483 bowl splicing chamber over the whole experimental pressure range:

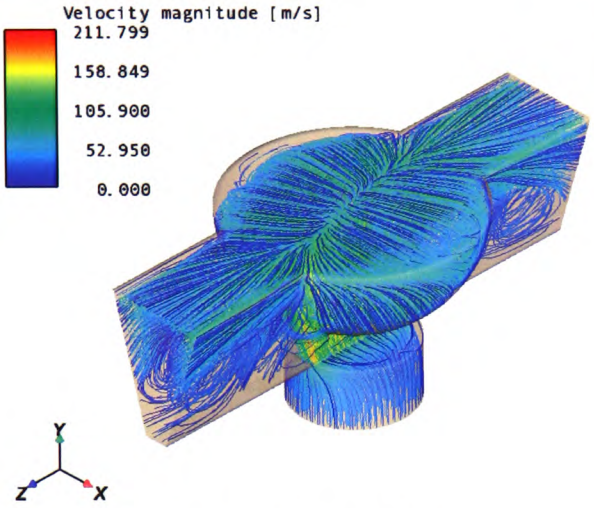

4psi (35liters/min)

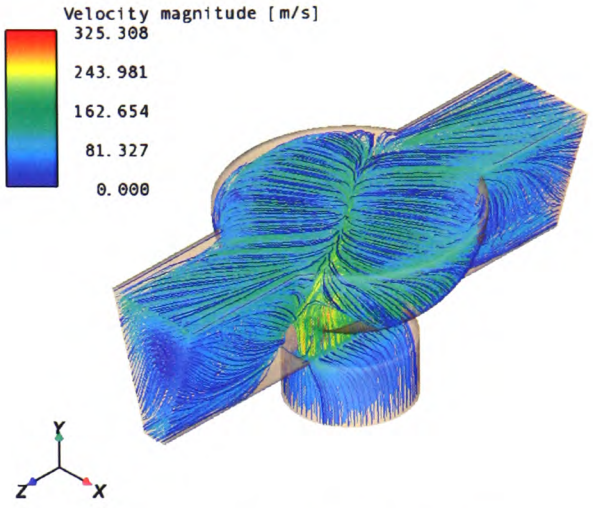

12psi (60liters/min)

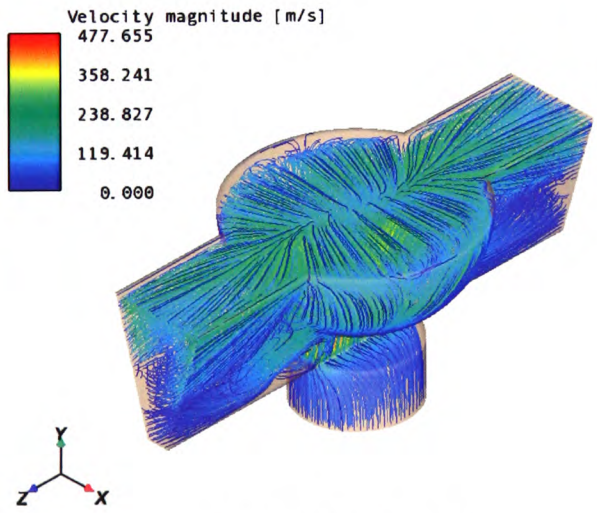

30psi (81liters/min)

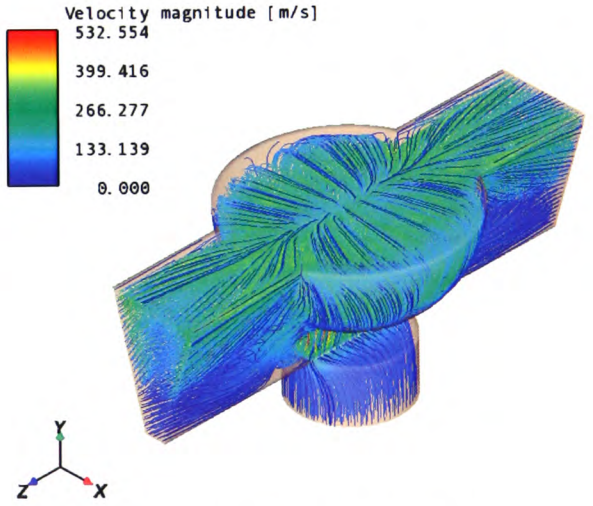

50psi (99liters/min)

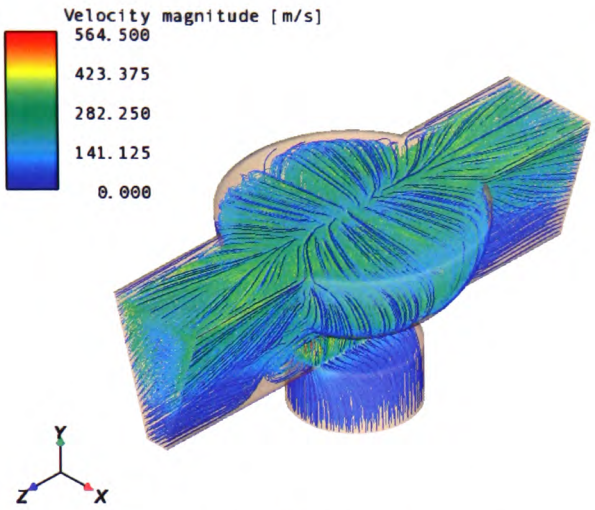

70psi (116liters/min)

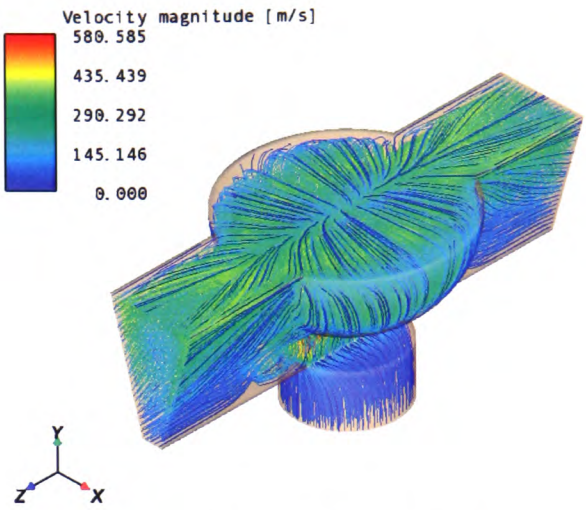

90psi (132liters/min)

Table A1-3. 4483 bowl chamber.

Pressure at inlet (psig)	Pressure ratio (P_{out}/P_{in})	Velocity at orifice (m/s)	Mass flow rate at orifice (kg/s)
0	1	0	0
4	0.78	211.8	0.00055
8	0.64	273.8	0.00080
12	0.55	325.3	0.00103
16	0.47	343.6	0.00124
20	0.42	343.6	0.00145
30	0.32	343.7	0.00178
40	0.26	343.7	0.00225
50	0.22	343.7	0.00272
60	0.19	343.7	0.00318
70	0.17	343.7	0.00366
80	0.15	343.7	0.00413
90	0.14	343.7	0.00457

Appendix 2

Splicing more exotic yarns

Splicing of tough yarns

In recent years, new, tough fibres have been introduced to the market. These fibres, such as aramids, are distinctive in that they have a very high strength-to-weight ratio. Their applications of pressure vessels, flak jackets, etc., are now very familiar.

Such materials pose special problems, in that they are very difficult to cut. Failure to cut the waste ends reliably and cleanly certainly can make splicing performance unreliable, and this issue is a perennial headache for splicer manufacturers and users. However, the business of cutting is purely an engineering problem, which has no direct relevance to the mechanisms of splicing, and the new splicer model. For the purposes of this section, therefore we shall be concerned only with the issues raised by these special fibres, in terms of how they react to the splicing process.

In many respects, the new fibres behave just like nylon or polyester. They are continuous filament yarns, and generally have a negligible twist level and might therefore be considered to ideal candidates, of cutting problems, excepted for splicing. All other things being equal, an aramid splice should be very similar to a nylon splice.

Certainly that statement should be made with some reservations:

- The extensibilities of nylon and aramid are different.
- The frictional characteristics are somewhat different.
- The values of bending modulus are somewhat different.

Despite these caveats, the practical reality is that a splice in polyester and a splice in an aramid of similar count, are remarkably similar, and that have a reasonably similar strength, because splicing is a process which has its origins in friction, and the capstan effect.

Therefore, apart from the cutting problem, another major issue exist for splicing aramid. The absolute breaking load of an aramid splice, and the absolute breaking load of a nylon splice, are not that much different. But when the breaking load is reported as a proportion of the parent yarn strength, an aramid splice looks very poor, and this fact displeases the users. Knowing that the fibre is being used in extreme environments, they are concerned that a "weak" splice will fail in service.

Whatever the actual merit of such an argument, it needs to be accepted that it inhibits willingness of aramid users to accept the application of splicers to their operations.

The technical solution is simply to make the splice longer. As splice length increases:

- The helix angles will remain much the same.
- The helix pitch will remain much the same.
- Each filament will experience more helix cycles.
- Each filament will experience a greater "capstan" wrap angle.
- Each filament will be exposed to more points of contact with others increasing its friction between filaments.

The conclusion is that, when splicing an inherently strong yarn, maintaining an acceptable percentage of parent yarn strength will require a longer splice length, and therefore greater knife spacing. The change of splicing performance with change of yarn strength can therefore be addressed as a particular case of the phenomenon of "scaling".

Splicing of partially oriented yarn (POY)

A fairly satisfactory definition of POY is given in the web site http://www.fibre2fashion.com/glossary/glossary14.htm.

"A continuous-filament yarn made by extruding a synthetic polymer so that a substantial degree of molecular orientation is present in the resulting filaments, but further molecular orientation is possible.
Notes:

1. *The resulting yarn will usually require a positive draw-ratio in subsequent processing in order to orient fully the molecular structure and optimize tensile properties.*
2. *Yarns of this type made by high-speed spinning are commonly used as a feedstock for producing draw-textured yarns."*

It is well known that POY is particularly difficult to splice, and specially modified splicers have been designed to address the problem. The poor performance of POY is easily explained in terms of the new model. Since the yarn is not fully drawn, that it will require further extension before it will perform as a normal textile yarn. Under tension, it extends easily, so that its stress against strain behaviour is completely different from its fully-drawn counterpart. Since the efficiency of the splicing process is heavily dependent upon the reaction of individual filaments to strain, POY behaves in an anomalous fashion, by extending without resistance. Filament tensions remain very low, and filament mixing does not occur with the required efficiency. Poor splices result.

POY can only be spliced if there is a preliminary stage, in which the yarn is extended to the point where it behaves as a normal, fully drawn, textile yarn.

Splicing of fancy yarns

Fancy yarns usually consist of two or more components. A core yarn is an essential element, and one or more outer yarns are wrapped or pneumatically intermingled around the core. The core yarn bears any load imposed by processing, or when the yarn is incorporated into a garment. The wrapper or outer yarn gives a textured or fancy effect, conferring a distinctive appearance on resulting fabric.

It will be clear that the overall length of the effect yarn is therefore always greater than the length of the core yarn. Such a construction is difficult to splice. Generally, once the yarn is cut as part of the splicing process, the cut end of the effect yarn is free to move, and the yarn is certainly too long to come under any significant tension, as it is extended by the blast. The outcome is that, while the core yarn may be spliced quite satisfactorily, the effect yarn generally behaves independently, "rubbing back" to form an ugly slub which is not in keeping with the overall appearance of the fancy yarn.

The only option for such yarns is to use that ends-together technique. Generally, using this approach, both core yarn and effect yarn become bound into the splice, and the "tail" which is produced adequately resembles the original appearance.

Splicing of elastomeric "stretch" yarn

Like fancy yarns, elastomeric yarns have a core/wrapper construction. In detail, however, their constructions are very different. While both consist of two or more components, and both have a wrapper element enclosing the core, the elastomeric core of a "stretch" yarn does not act as a strong backbone. Instead, its elastic properties allow the whole structure to stretch and to recover after loading. Such materials have their application in "support" garments, which apply a modest compressive force to chosen parts of the body. The elastomeric core yarn provides the stretch, and physical support when the yarn is incorporated into a garment.

The wrapper or outer yarn has the sole function of hiding the core from view. Elastomers have a strange shiny, translucent appearance, and an unpleasant waxy "feel", and would be unacceptable to users if not disguised. It will be clear that the elastomeric core has a very low modulus, and the material is therefore a poor candidate for splicing, especially as the effect yarn, being wrapped around the outside, itself has little or no resistance to extension.

Such a construction is extremely difficult to splice. Generally, once the yarn is cut as part of the splicing process, the core shrinks, and springs back, away from the knife. The splicer is left to join only the wrapper yarn, which is itself (because of its length) a poor candidate for splicing.

Elastomeric core yarns cannot be spliced by conventional methods, even the ends-together method fails miserably. Only special splicers, with additional features designed to overcome this particular set of problems, will join such products.

The only option for such yarns is to use that ends-together technique. Generally, using this approach, both core yarn and effect yarn become bound into the splice, and the "tail" which is produced adequately resembles the original appearance.

Appendix 3

The special case of "ends-together" splices

Appendix 4 of this document, relating to "ends-preparation", touches on the issue of high twist levels, specifically how splicers can be made to produce adequate splices in twisted spun staple yarns. However, there are some yarns, which are virtually impossible to splice by conventional methods – their twist level is so high, or so stable, that it is impossible to reduce the twist sufficiently to make a splice. The problem is acute with heat-set twisted synthetics; the heat-setting process confers a degree of stability of the twisted structure, so that no amount of ends preparation will persuade the filaments to take a parallel form.

Theoretically, it is possible to design a splicer with a splicing chamber which, using a suitable cross-sectional profile and a suitable airflow, can de-twist both yarn ends. However, such a design, with contra-rotating vortices, is very difficult to accomplish within the tight geometry of a splicing chamber. For all practical purposes, difficult materials such as heat-set twisted synthetics and tyre cord cannot be spliced by conventional methods.

It is also possible to make a splicer, which physically de-twists the components, then splices them, then re-introduces the twist. Indeed, such splicers exist, for applications such as tyre cord. However, they are complex and expensive, and can only be justified for applications in which performance and appearance are sufficiently important to override cost considerations.

For less critical applications, a simpler form of splice has been developed. This is described in Chapter 5 as the "ends-together" form. In the conventional ends-opposed splice, the tarns to be joined are introduced to the splicer from opposite sides of the splicing chamber. When an ends-together splice is made, the two ends of yarn are introduced via the same side of the chamber. To facilitate the removal of twist, the chamber profile is designed to impart reverse twist. As an example, Figure A3-1 shows a simulation of the rotational airflow induced by a commercial ends-together splicing chamber. The high air velocities achieved in such a splicing chamber, seen in the legend at the side, expose the yarns to a high level of local stress. Both yarns spin rapidly together in the airflow, and once the majority of the twist has been removed, the filaments become intermingled.

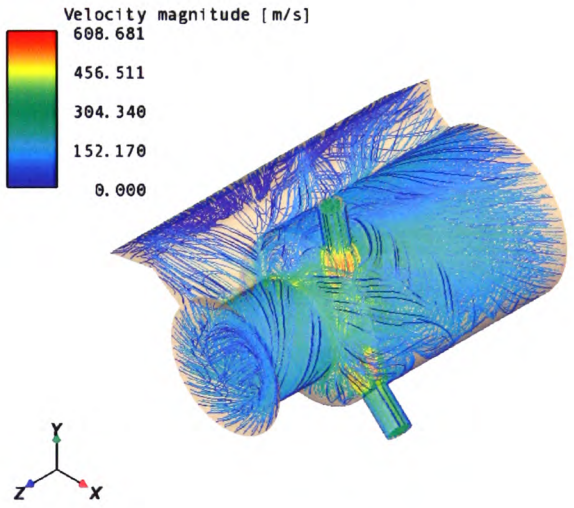

Figure A3-1. Commercial ends-together splicing chamber

The technique is powerful, it can handle highly twisted yarns with ease, but there are penalties. In particular, the splice projects outward at 90° to the thread line when the yarns are removed from the chamber. Compared to the conventional form, the splice is usually of an unattractive appearance. Figures A3-2 and A3-3 show, in schematic form, the essential differences between this splice and the standard "ends-opposed" joint respectively.

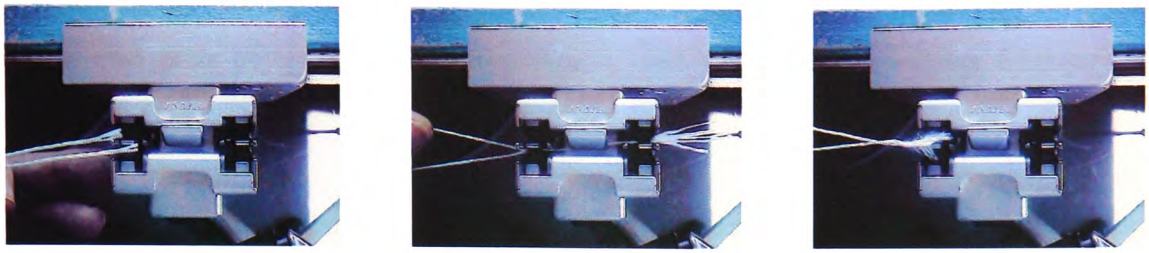

Figure A3-2. Ends together splicing

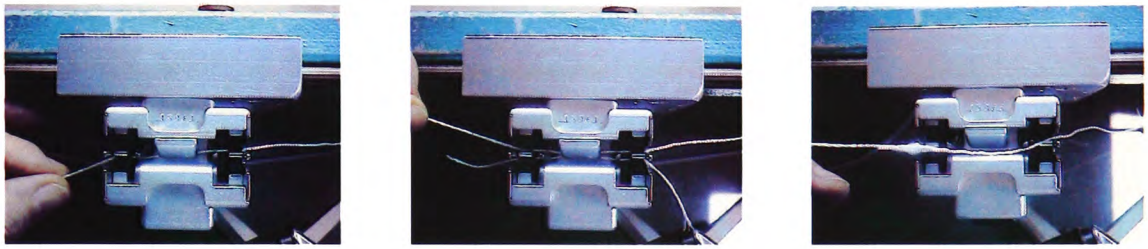

Figure A3-3. Ends opposed splicing

Sometimes, however, this is the only possible solution, and if the textile application is not critical, the ends together form of splice will suffice.

Used widely in the carpet industry, joining yarns of wool, wool/nylon, and other blends, the splice format is important. The significance of the ends-together splice form to the industry is such that it is necessary for this report to explain the distinctive appearance of the ends-together splice, especially if its structure can be shown to be consistent with the new model.

At first sight, it would seem that the splicing model and the form of an ends-together splice are not compatible. The model of splicing proposed in this report describes a structure, which is symmetrical about both the blast hole and the chamber axis, and it explains the formation of the four essentially identical sub-structures of the splice. The ends-together splice does not appear to conform; its structure seems to challenge the

accuracy of the model. Instead of four clearly defined sections, it has two ill-defined zones; one area of tightly entangled fibres, and another area where filaments are separate, and opened into "tail" of a parallel or conical form.

In fact, the mechanisms, which form an ends-together splice, can easily be shown to be essentially identical to those relating to its counterpart.

This assertion can be tested very simply. The ends-together splice is most frequently used for rough-structured staple yarns, such as 80/20 wool/nylon blends for carpets. However, examining the detailed structure and formation of such a splice does not offer much insight, because in the splicing process many of the fibres are blown away. The final joint may contain no more than 50 per cent of the original material.

The test was best done by making an ends-together splice in a strong continuous filament yarn. This material will be sufficiently tough to resist the damaging effects of the blast, so that virtually all of the fibres will survive the splicing action. In addition, the splice is made using a conventional symmetrical-section splicing chamber, to avoid the confusion caused by the twisting action of an asymmetric chamber.

The outcome was a structure of the appearance shown in Figure A3-4. Note that the two component yarns have been opened out to form the distinctive "tail"

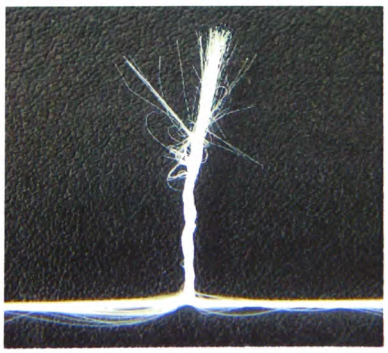

Figure A3-4. Ends-together splice

The structure, which is revealed is essentially identical to the one described during the analysis of the ends-opposed splice. All that is missing is the continuation of one of the yarns, off to the right of the image.

- The four contra-rotated sections are visible
- The tight clusters of twisted filaments are visible
- The open section of twist reversal, at the point which was above the blast hole is visible

This outcome is not what is generally seen in real ends-together splices. However, this is easily explained, because, as noted above, in a normal splice, much of the fibre is usually blown away; it has survived here only because of the use of a tough yarn. The only real difference between the splice in this picture and a conventional ends-opposed one is that the filaments at the right-hand, cut end appears rather more untidy that their counterparts on the left. This is not a surprising conclusion. All of the filaments on the left are tightly constrained during the blast, while all the fibres on the right, having been cut, are free to move.

There remains one caveat; the splice shown above was made using a symmetrical splicing chamber, which creates the now-familiar pattern of two pairs of helices on opposing senses. In general, ends-together splices are made using asymmetric splicing chambers, which, by their design, remove twist. This does not invalidate the experiment described above, however; the splicing chamber simply makes a splice equivalent to the top or bottom half of what was shown.

So it is proposed that an ends-together splice is formed by the same mechanisms as an ends-opposed splice. If the new splicing model stands for one splice form, it will stand for both.

Appendix 4

The splicing process and "ends-preparation"

All of the work reported in this thesis relates to the splicing of continuous filament yarns, which, within the scale of the splicing chamber, have essentially no real twist. The examination and analysis of such simple yarn constructions was a necessary simplification, bearing in mind that the splicing process itself is surprisingly complex. It could be argued that this approach was too simplistic, because most real yarns have significant levels of twist. Attempts to splice spun staple yarns by simple methods are generally unsuccessful. Commonly, weak or failed splices result, and there are thin, weak central sections, with large fluffy "tails" at each end of the splice.

The reasons for poor splicing performance with spun yarns, especially short-staple yarns, are not difficult to understand. Firstly, with fairly high twist levels, the yarns initially behave somewhat like monofilaments when placed in a splicer. Secondly, the discontinuous structure of a staple yarn is such that stresses cannot be distributed in the simple manner seen with continuous filament yarns.

In simple splicers, attempt to improve performance on spun yarns typically involve increasing the blast pressure, or the blast duration, but with staple yarns this simply results in severe disruption of the fibres, and a poor splice with fluffy tails which have not been drawn into the splice structure. In the limit, if excessive blast time or blast pressure is used, the fibres will in effect be drafted from the splice structure, becoming free to be blown away in the air stream. This effect produces the distinctive thin weak central section.

Most published literature addresses this problem, because most yarns in real life are spun staple. Literature routinely refers to an additional technique known as "ends-preparation". Examples of ends-preparation are particularly conspicuous in patent submissions, which describe a wide variety of devices. A description of ends-preparation, which is accurate and relatively brief, is given by Schlafhorst (1998):

> "[in ends-preparation] the yarn twist is undone and loose fibres are blown away, so that the result is a so-called opened yarn end with as many parallel fibres as possible, which are spliced pneumatically to the fibres of the other yarn end."

In other words, in yarn splicing, the purpose of ends-preparation is to return the fibres as far as possible to the state in which they all lie parallel. Only then will effective splicing be possible.

Thus the technique of ends-preparation is simply a preliminary process step. The formulation of a model of the splicing process need take no account of ends-preparation techniques, since they are not relevant to a discussion of the mechanism of the splicing process.

Appendix 5

Published papers

Taylor & Francis
Taylor & Francis Group

The use of the Taguchi design of experiment method in optimizing splicing conditions for a Nylon 66 yarn

Date Submitted 23 February 2006, Date Accepted 24 August 2006 doi:10.1080/00405000701489255

C. J. Webb[1], G. T. Waters[1], A. J. Thomas[2], G. P. Liu[3] and C. Thomas[2]

[1] *GTW Developments Ltd., Pontypool, Newport, United Kingdom*
[2] *Cardiff University, Cardiff, Wales, United Kingdom*
[3] *University of Glamorgan, Trefforest, Wales, United Kingdom*

Abstract: Yarn splicing joins two yarns by applying a blast of compressed air into a profiled device called a splicing chamber. Splicing is a mature technology, but there is little published work on its fundamental principles. The current research program addresses these principles. However, the research confronts many variables such as yarn count and construction. The Taguchi design of experiment method can simplify the research, by reducing the amount of testing. This article presents a record of controlled testing to establish the validity of the Taguchi method in this context. The tests were performed using an industry-standard synthetic yarn as a base line for the research. The article reports on the Taguchi analysis of results and its effectiveness in optimizing splicer parameters to produce a strong splice with minimum variation. Later, articles will apply the technique to results of work on different yarns, assessing splice aesthetics, yarn characteristics, and splicing chamber geometry with the objective of yielding a mathematical model for the splicing process.

Key words: Taguchi, design of experiment, splicing, parameter optimisation, spliced retained strength.

INTRODUCTION

Before splicing was developed, companies in the textile industry joined two separate yarns by various forms of knotting. This solution was adequate in most cases, although occasionally the knot caused a jam in the textile machine, which resulted in machine stoppages and cost penalties (Oinuma *et al.*, 1995).

The pneumatic splicing technique overcomes the deficiencies of knotting. The process involves introducing two multifilament yarns into a chamber, held side by side in an overlapping relationship, which are subjected to a high-pressure turbulent flow of compressed air from a jet that agitates the filaments. As a result, a neat strong bond between the yarns is produced (Cheng and Fung, 2004; Iwnicki, 1964). This process significantly improves the joint quality and factory productivity.

Corresponding Author:
Carwyn Webb
University of Glamorgan
Trefforest, Wales, UK
Email: cjwebb@glam.ac.uk

Spliced yarns are expected to meet the same performance characteristics as the parent material (Lewandowski and Drobina, 2004). However, splicing is a complicated and variable process that can lead to unpredictable characteristics of strength and appearance. The air within the splicing chamber is that of high turbulence (Reynolds number typically of the order of 10^5). The violent small-scale disturbances radically disrupt the arrangement of the fibres in the splicing chamber, producing twisting and intermingling. The resulting splice has a characteristic and reproducible form (Fig. 1). The central section, which corresponds to the air entry point, appears unchanged, with the majority of the fibres lying untwisted and roughly parallel to the chamber axis. Either side of this central section, the fibres lie in dense clusters, highly twisted and intermingled together. Each cluster usually terminates in a small 'tail' where the extreme tips of the spliced yarns have not been fully bound into the structure.

To date, little theoretical knowledge has been published about what actually occurs within the splicing chamber. Therefore, the optimization of the splicing performance is difficult to achieve since it is difficult to identify the major parameters, which affect joint strength and appearance. This limits the ability of a user to produce consistently high splice strengths with acceptable aesthetics.

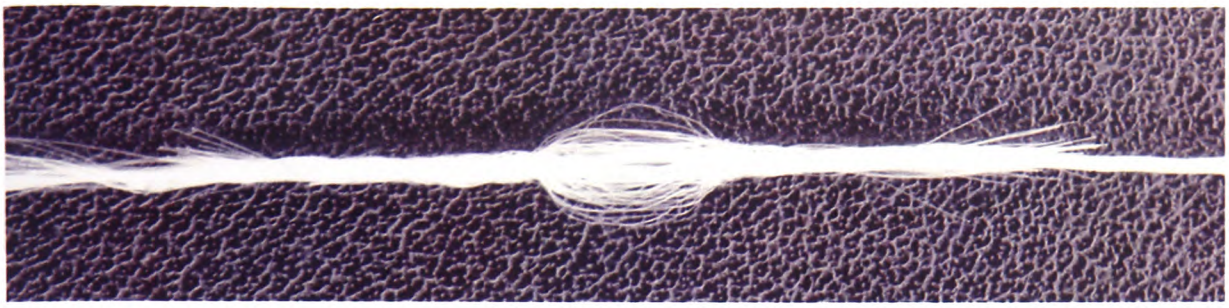

Figure 1 Characteristic form of a splice.

Table 1 **Comparison of Taguchi versus full-factorial DOE**

	Replications	Number of levels	Orthogonal array	Dominant factors within a group	Tests
Taguchi DOE	20	3	L27	12	540
Full-factorial DOE	20	3	...	12	10628820

To meet the requirement of achieving high and consistent joint strength from a spliced joint, an understanding of all critical control and noise variables along with their effect on the splicing process needs to be addressed (Peace, 1993). This understanding of all the parameters will allow various methods for estimating the contribution of each of the critical variables toward the strength and variability of the splice.

Due to the large number of critical variables, it would be too time-consuming to conduct a full-factorial analysis (Table 1). The Taguchi method is a powerful design of experiment (DOE) technique (Fox and Lee, 1990; Logothetis *et al.*, 1990; Thomas and Antony, 2003), which can increase the productivity and quality of a product with a minimum amount of testing. Therefore, the Taguchi DOE technique was considered as an experimental tool. The technique performs a partial factorial analysis set by the orthogonal array chosen. The main disadvantage of this method is the potential loss of accuracy due to the partial factorial analysis and effective implementation of the Taguchi method (Lochner, 1991).

This article addresses solely the input parameters that affect splice strength, as a simple means of assessing the utility of the Taguchi method for splicing performance. Once the relevance of the method to the splicing process has been established and the simpler set of input parameters better understood, later work will deal with the less tractable variables such as yarn type and count, and outcomes such as splice aesthetics.

EXPERIMENTAL METHOD

The splicing process itself is known to be complex, but the analysis of the process is made more difficult by the multiplicity of yarns, which may be spliced in practical situations. For example, yarns may be composed of synthetic continuous filament, synthetic staple filament or natural staple fibre, or from blends of all three.

At the outset, it was necessary to establish certain baseline performance characteristics, against which other results may be assessed. The first stage of work was, therefore, concerned only in simple industry standard yarn, chosen as a suitable baseline. This yarn was a 1,100 decitex, continuous filament Nylon 66 with low twist, consisting of 72 filaments, as used in the manufacturing of standard motor vehicle safety belts.

A brainstorming session was undertaken by an interdisciplinary team. This identified the factors that were expected to have an effect on the tensile strength of the splice. Figure 2 shows the cause and effect diagram resulting from the brainstorming session. There were a minimum of 18 possible factors found which were prioritised in terms of their likely effect on splice strength.

Due to the difficulty and cost of controlling certain parameters in practical production scenarios, some have been discarded as noise factors Coleman and Montgomery, 1993. The noise factors identified were temperature, humidity, fibre density (the structure of the filaments), splice length, procedures, blast hole (or holes) position, testing and recording equipment tolerances.

Splice strength is measured by its spliced retained strength (SRS). SRS is the strength of the spliced yarn expressed as the percentage of the parent yarn in which the splice was inserted Sengupta, 2000. Equation 1 illustrates this relationship.

$$\text{SRS} = \frac{\text{Spliced yarn strength}}{\text{Parent yarn (non-spliced)}} \times 100 \qquad (1)$$

A Pareto analysis was conducted on the possible control factors to identify major causes that affect the SRS, resulting in the factor selection for Taguchi experimentation Table 2.

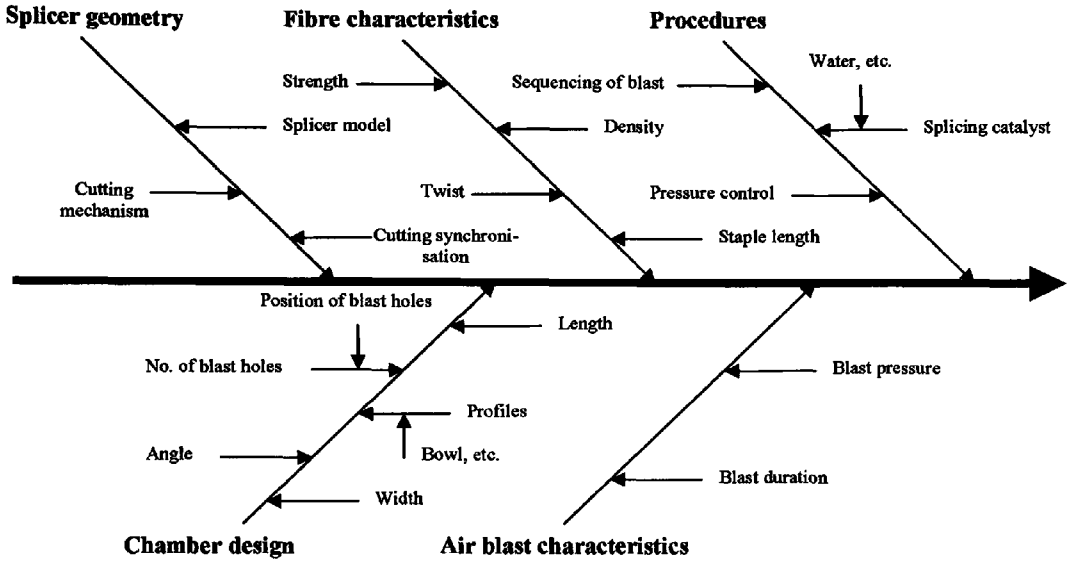

Figure 2 Cause and effect diagram revealing possible factors affecting the splice strength.

Table 2 **Selected splicing parameters**

Parameter	Factor
Blast pressure	A
Blast duration	B
Chamber design	C
Cutting synchronization	D

Preliminary testing confirmed that each of the chamber designs subsections (width, profile, angle, etc.) had an individual effect on the SRS although not major. However, all of the factors, when pooled together in a particular chamber design, had a major overall effect on the splice strength. Chamber design was, therefore, included as a main factor for the experiment.

Before factor selection of the levels for the Taguchi experiment, individual experiments were conducted on blast pressure, blast duration and chamber design to reveal how they each contributed to the SRS of the yarn.

The blast pressure was varied from 0 psi to 90 psi on all chamber designs whilst maintaining all other parameters constant. Each recording was taken at intervals of 2.5 psi to 5 psi.

Blast duration tests were conducted at four key pressures, namely 20, 40, 60 and 80 psi. At each pressure, tests were conducted with blast durations of 0.5, 1, 2 and 3 seconds.

Another parameter, known as cutting synchronisation, was factored into the experiment. Splicers can be designed so that the air blast and cutting action may be separately controlled; this technique expands the range of performance of a splicer. On the experimental splicer, the range of cutting synchronisation was defined by an arbitrary scale ranging from 0 to 6. With the scale set at 0, the knives cut the yarns before the initial air blast, releasing the yarn ends filaments to move freely around the chamber from the outset. With the scale set at 3, the air blast and yarn cutting are simultaneous. With the scale set at 6, the yarns are cut after the initial blast.

MATERIALS AND EQUIPMENT

Three representative chamber designs were used in the experiments. Two of these have the same basic V-shaped geometry (Fig. 3) with only the width at the bottom of the splicing chamber differing. These were 0.8 mm (identified as 4483 straight) and 1.25 mm (identified as 4485 straight), respectively. The third chamber design considered (identified as 4483 bowl) is of the same general profile as the 4483 straight chamber, but it has a hemispherical bowl machined out at the centre of the chamber (Fig. 4). These three chamber designs represent the most common chambers developed by GTW Developments (Waters, 1998).

The chamber designs described above were made on a milling machine with an accuracy of ± 0.01 mm and $0.1°$. The specifications of the chamber that were not varied during this set of experiments were 4.8 mm depth, 16 mm length, 30° chamber angle, and 4 mm blast hole diameter at the centre of the chamber.

The splices were prepared on one type of 1,100 decitex, 72 filament, Nylon 66 fibre, with test samples being taken from a single bobbin to minimise variability.

The joints were made using a GTW Developments splicer, type 1–11. The compressed air was dried and filtered to create consistent air properties, using an air drier followed by an air filter (type AW30-F03D) and mist separator (type AFM30-F03D) with a 0.3-μm 95% filtered particle size.

Pressure was controlled using an electro-pneumatic regulator (type ITV2050-312BS3-Q) which supplies a user-specified constant pressure with an accuracy of ± 0.03 psi.

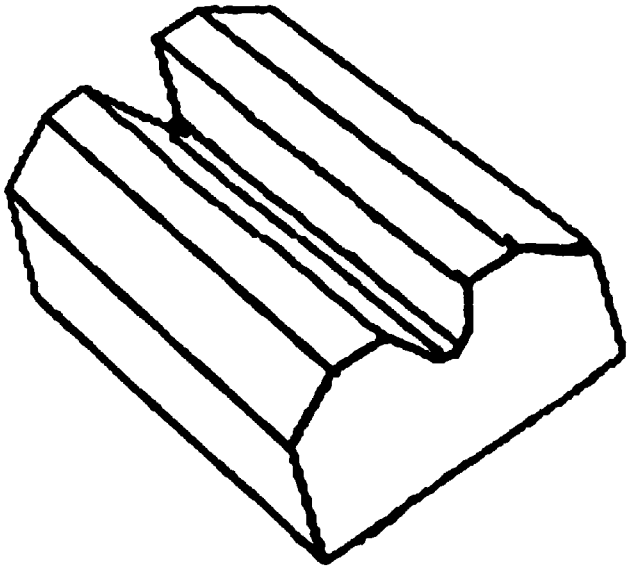

Figure 3 Straight chamber design.

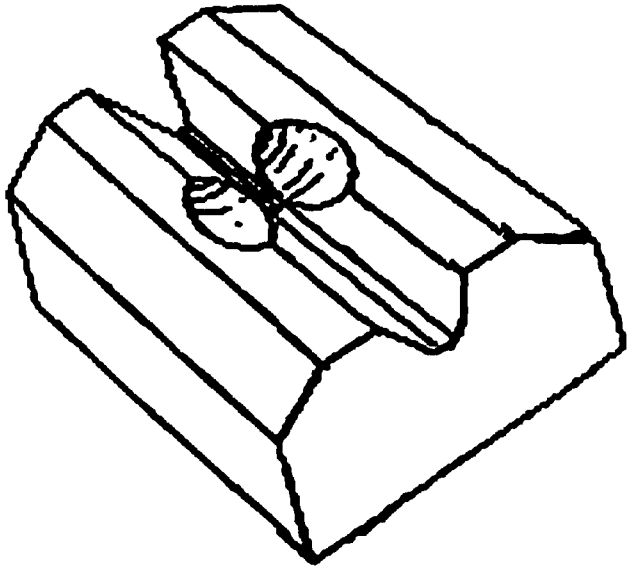

Figure 4 Bowl chamber design.

The tensile strength of the test samples was measured using a Lloyd Instruments tensile testing machine (type T5000) with a 100 mm/min crosshead speed.

To obtain accurate result with the least amount of noise variation, all the equipment was controlled and results were collected electronically using an ARM7 control board and a PC. The experimental set-up used is shown in Figure 5.

RESULTS

During the initial experimentation on the reference yarn, it was discovered that there was a substantial variation between individual values of SRS under the same experimental conditions as shown in Figure 6. It is possible that this variation is present because spliced bonds are unpredictable and consequently no two splices are the same because the filaments are packed randomly throughout the yarn (Kaushik *et al.*, 1987, 1988; Rowlands *et al.*, 2000; Wei *et al.*, 2004). The variation described above increases the complexity in discovering a correlation between the splicing parameters and strength. Therefore, to minimise experimental error and assess variability of performance, a repetition of 20 tests was executed for each experimental condition.

Once the factor test levels were selected, the Taguchi experiment was executed. Thereafter, an analysis of variance (ANOVA) was conducted to reveal if any of the factors chosen were statistically significant. A confirmatory run was then conducted using the optimum parameter settings found, as a result of the Taguchi experiment, to verify that the results achieved using these settings provided the maximum SRS with the greatest robustness (i.e. minimum variation between readings)(Antony and Antony, 2001; Bendell *et al.*, 1989).

Figure 7 shows the strength (SRS) versus pressure response plot ranging from 0 to 90 psi on a 4483 bowl chamber design. The strength versus pressure responses of the 4483 and 4485 simple chamber designs are shown in Figure 8 and 9, respectively.

Only specific test set-ups were chosen to be tested with blast duration to determine the output response profile. The span of the profile was covered and noticeably only selected pressures at key levels needed testing. Therefore, linear approximation was used to eliminate redundant results. Figures 10–12 show the output responses of the blast duration experimentation across the four selected pressures on each of the three chamber designs.

The strength versus pressure curves (Figures 7, 8 and 9) are all consistent with the blast duration test results as shown in Figures 10–12.

DISCUSSION

All three chamber designs with various blast durations produce strength versus pressure response plots of the same general form. The general form can be represented schematically as shown in Figure 13.

The standard strength versus pressure curve splits into the following four regions.

1. A region where no splice is formed. There is insufficient pressure to force the individual fibres of the yarn to intermingle sufficiently to create a splice. The splice slips apart as soon as any load is applied.
2. A small region when SRS increases slowly with pressure. Once the pressure has exceeded a critical level P_0, the SRS increases as the intermingling process begins. This cannot be seen with the bowl chamber, but is very clear in the other two cases.
3. A region when SRS progressively increases at a faster rate with pressure. Once the pressure has exceeded a critical level P_1, the SRS increases roughly linearly with pressure, reflecting an increase in the degree of intermingling.

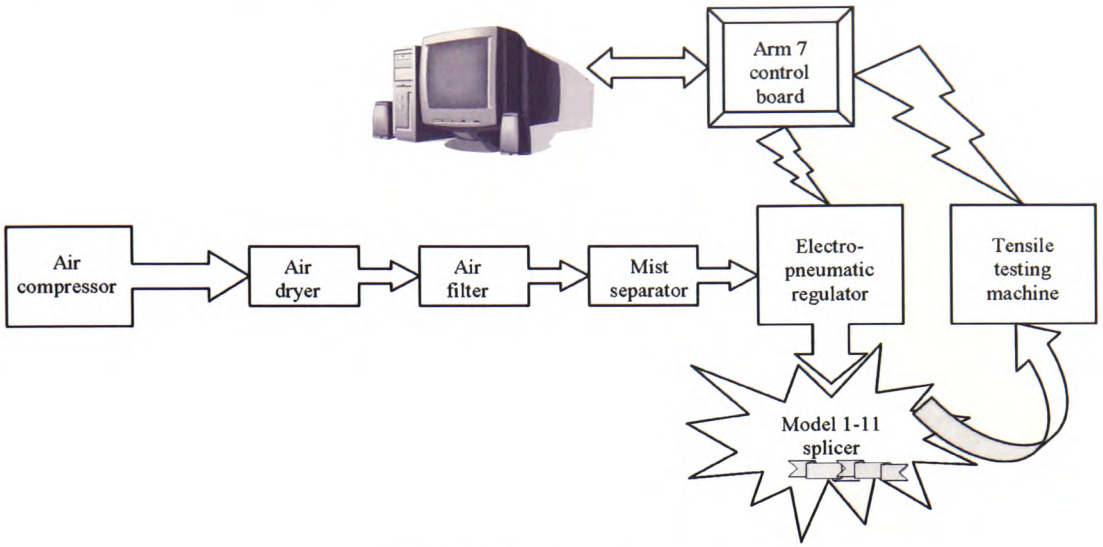

Figure 5 Experimental set-up.

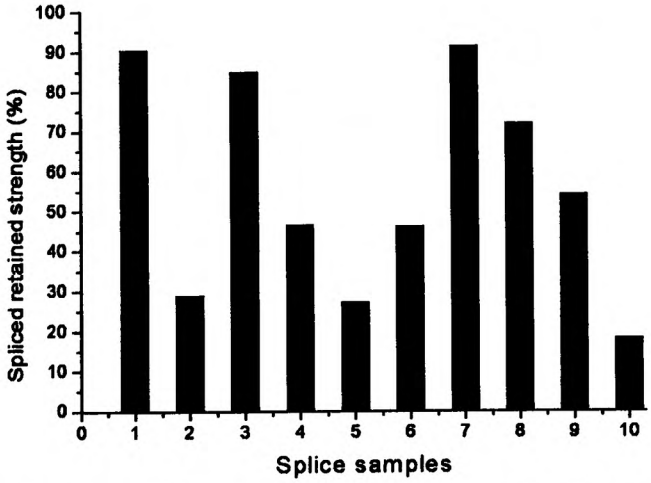

Figure 6 First 10 samples at 35 psi on a 4485 straight chamber.

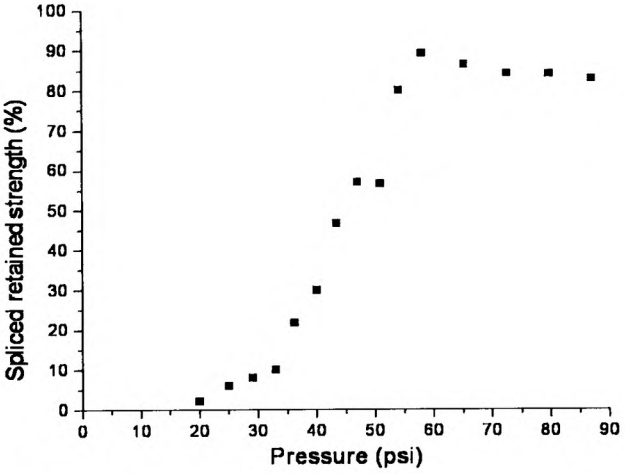

Figure 8 4483 straight chamber.

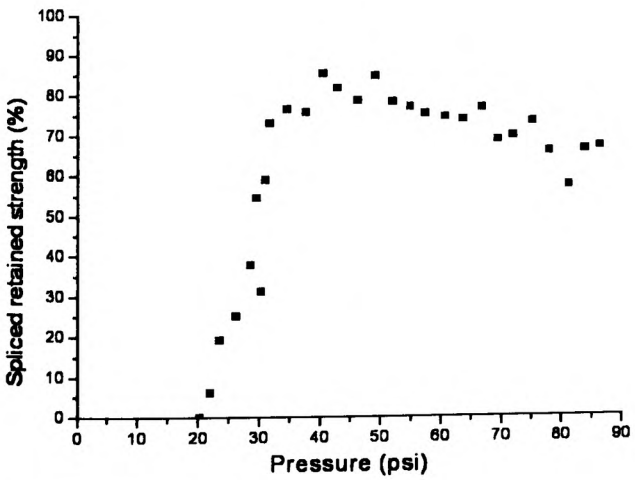

Figure 7 4483 bowl chamber.

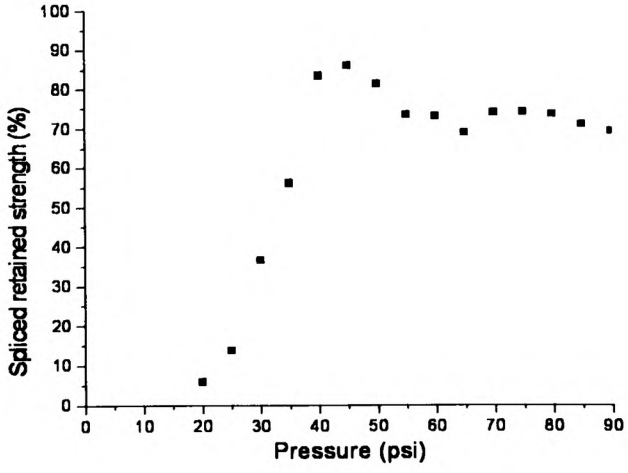

Figure 9 4485 straight chamber.

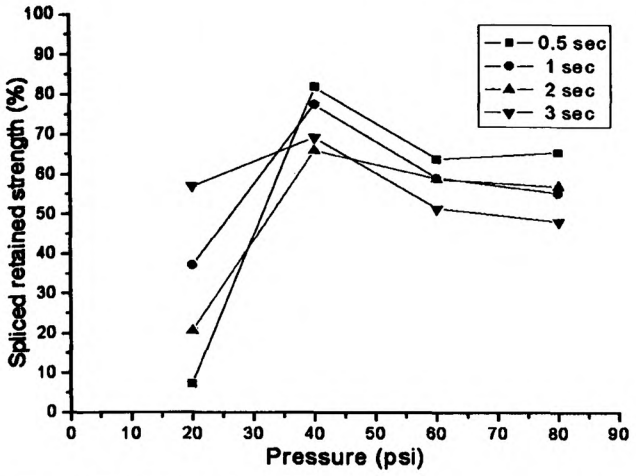

Figure 10 4483 bowl chamber.

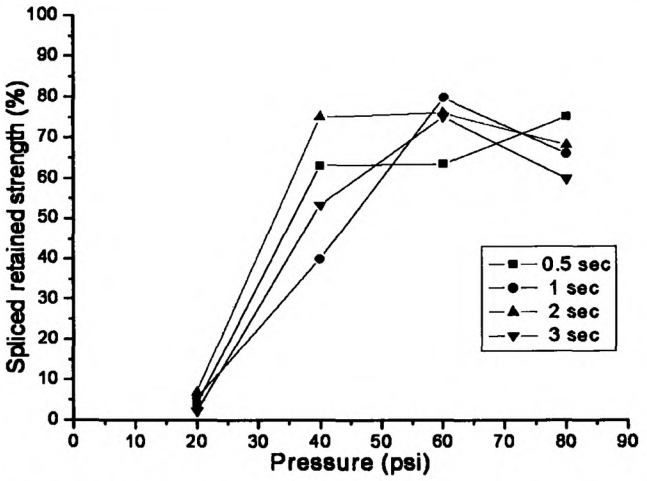

Figure 12 4485 straight chamber.

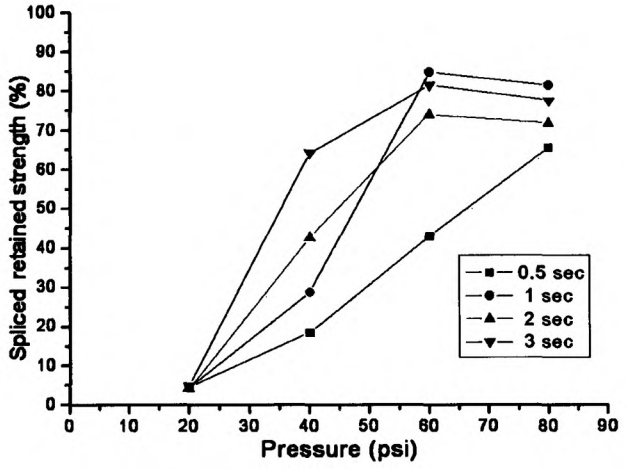

Figure 11 4483 straight chamber.

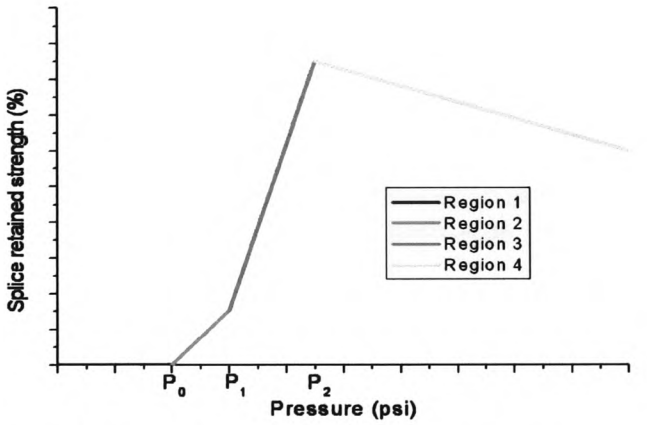

Figure 13 Standard strength versus pressure curve.

4. A region where the SRS reaches a maximum and then begins to decrease as shown at pressure P_2. It is likely that the decrease in SRS is associated with filament damage within the chamber resulting from excessive pressure. The rate of decline is roughly constant.

Although the general form of the strength/pressure curve is similar for all splicing chambers, there are some significant differences that need to be addressed:

1. The 4485 straight chamber produced splices of measurable strength only after about 35 psi, at which pressure the 4483 bowl chamber was already producing strong splices.
2. The 4483 straight chamber did not begin to produce strong splices until approximately 45 psi.
3. The 4483 straight chamber produced splices of maximum strength (89%) at about 60 psi, whereas the 4483 bowl and 4485 straight chambers reached their maximum (85% and 86%, respectively) at the much lower figure of 45 psi.
4. After the maximum, the rate of decrease was faster with the 4483 bowl than with the 4483 straight and 4485 straight chambers.

Some understanding of the mechanisms lying behind these differences can be gained by examining a computational fluid dynamics representation of the straight chamber design, created by fluent, as shown by Figure 14.

A splice is created in the chamber by a transverse air blast entering the chamber at very high speed through the blast hole. This directly hits two discrete yarns at the bottom of the chamber, displacing them to the chamber roof, separating them in approximately equal bundles. The two equal bundles are then exposed to two contra-rotating vortices of air and the mixed bundles are separated, twisted in opposite senses, and intermingled. In the small straight chamber (4483), the vortices of air near the blast hole are constrained within the relatively narrow confines of the chamber cross section. In the bowl and large straight (4485) chambers, there is much more room for the vortices to form, and the bundles are separated to a much greater degree.

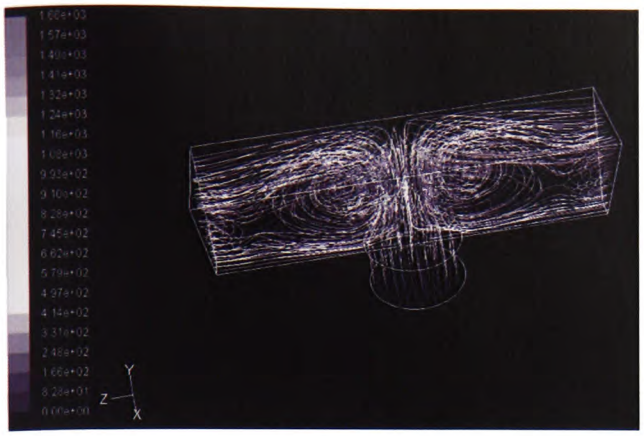

Figure 14 Computational fluid dynamics representation.

Therefore, it is arguable that the larger cross-sectional chamber design creates stronger vortices at the centre, thus drawing more filaments into the centre of the splice at an earlier stage in the splicing process; this results in increased intermingling and wrapping near the centre and a reduced tail at the ends of the splice.

The large cross-sectional chambers have an adverse effect at higher pressures or blast durations because the splice is forced outward by the big vortices, especially those of the bowl chamber, which at high pressures leads inevitably to damage.

Table 3 **Selected splicing parameters**

Factor	Level 1	Level 2	Level 3
A (psi)	40	50	60
B (sec)	1	1.5	2
C	4483 straight	4485 straight	4483 bowl
D	0	3	6

The blast duration tests revealed that 0.5 second is too short to form a splice and 3 seconds is too long at 60 psi or higher. This is probably because of increased filament damage and therefore fewer filaments are available for intermingling, thus producing weaker splices. Overall, there is not a great difference in tensile strength due to blast duration at optimum pressure once the critical blast duration value has been reached (i.e. the splice has formed at approximately 1 second).

Following the preliminary investigation, approximate optimum settings for the Taguchi DOE were established. These parameter settings are shown in Table 3. Three levels were considered due to the non-linearity of the splicing functions; therefore, an L27 orthogonal array (OA) was

	Main factors and interactions										
Run	A	B	AB	AB	C	AC	AC	D	AD	AD	SRS (%)
1	1	1	1	1	1	1	1	1	1	1	51.629
2	1	1	1	1	2	2	2	2	2	2	73.238
3	1	1	1	1	3	3	3	3	3	3	81.418
4	1	2	2	2	1	1	1	2	2	2	79.177
5	1	2	2	2	2	2	2	3	3	3	78.942
6	1	2	2	2	3	3	3	1	1	1	77.775
7	1	3	3	3	1	1	1	3	3	3	70.822
8	1	3	3	3	2	2	2	1	1	1	76.392
9	1	3	3	3	3	3	3	2	2	2	76.077
10	2	1	2	3	1	2	3	1	2	3	82.328
11	2	1	2	3	2	3	1	2	3	1	88.102
12	2	1	2	3	3	1	2	3	1	2	74.513
13	2	2	3	1	1	2	3	2	3	1	76.695
14	2	2	3	1	2	3	1	3	1	2	86.269
15	2	2	3	1	3	1	2	1	2	3	73.652
16	2	3	1	2	1	2	3	3	1	2	77.845
17	2	3	1	2	2	3	1	1	2	3	77.945
18	2	3	1	2	3	1	2	2	3	1	68.459
19	3	1	3	2	1	3	2	1	3	2	78.197
20	3	1	3	2	2	1	3	2	1	3	60.562
21	3	1	3	2	3	2	1	3	2	1	65.518
22	3	2	1	3	1	3	2	2	1	3	71.980
23	3	2	1	3	2	1	3	3	2	1	80.517
24	3	2	1	3	3	2	1	1	3	2	87.861
25	3	3	2	1	1	3	2	3	2	1	54.269
26	3	3	2	1	2	1	3	1	3	2	71.723
27	3	3	2	1	3	2	1	2	1	3	65.574

Factor A		
L1	L2	L3
73.941148	78.423145	68.466859

Factor C		
L1	L2	L3
71.438087	77.076699	72.316396

Factor B		
L1	L2	L3
72.833949	76.985393	71.01181

Factor D		
L1	L2	L3
73.055578	73.318447	74.457127

Largest is best:	Factors	A2	B2	C2	D3

Interaction AB			
	B1	B2	B3
A1	68.761939	78.631237	74.430369
A2	81.647778	78.872069	74.749588
A3	68.092231	73.452872	63.855474

Interaction AC			
	C1	C2	C3
A1	67.20918	76.190804	78.42346
A2	78.956124	84.105211	72.208101
A3	68.148899	70.934051	66.317629

Interaction AD			
	D1	D2	D3
A1	68.598451	76.18436	77.860633
A2	77.974851	77.751963	79.542621
A3	72.593432	68.039019	68.766127

Figure 15 L27 Orthogonal array and optimum factor identification.

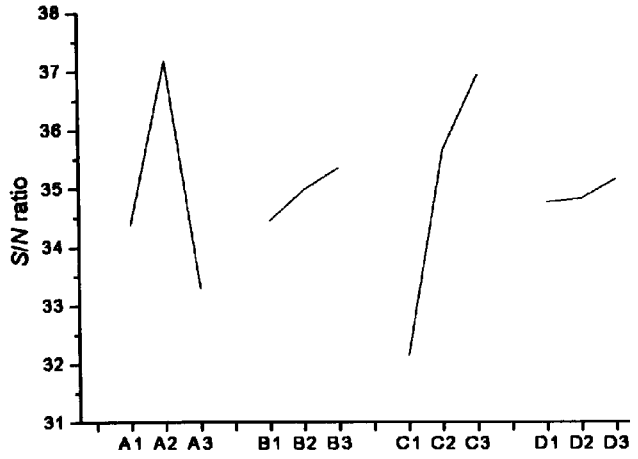

Figure 16 Signal-to-noise ratio response plot.

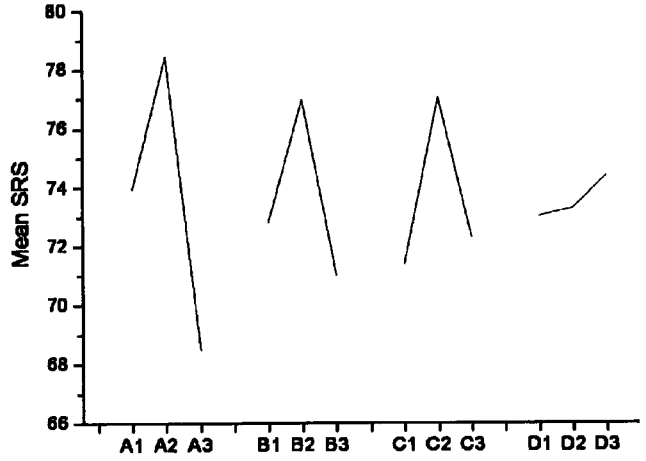

Figure 17 SRS response plot.

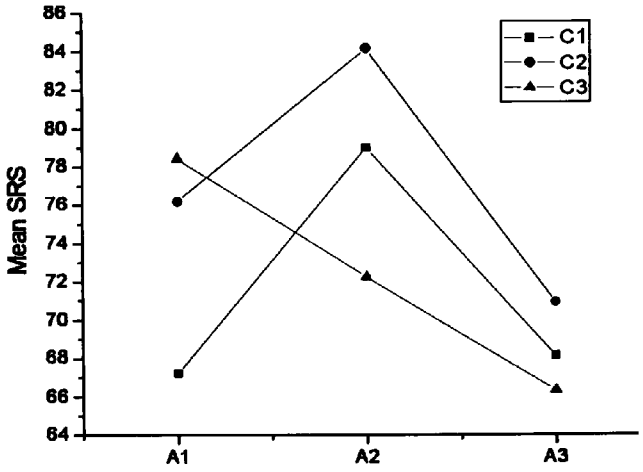

Figure 18 Interaction AC.

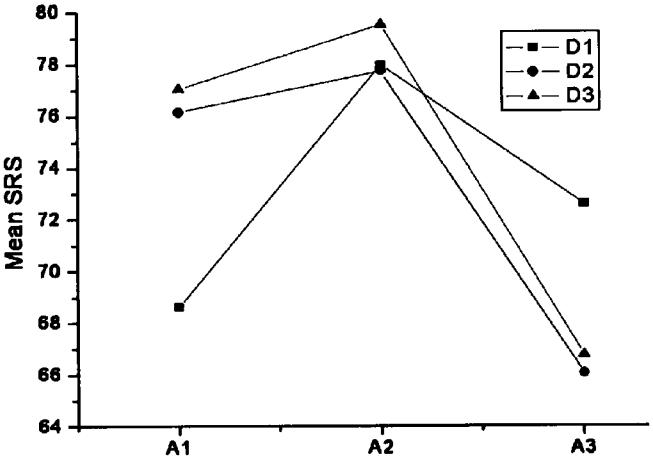

Figure 19 Interaction AD.

chosen for the experiment. Figure 15 shows the L27 OA and the factor identification results.

The main signal-to-noise ratio (SNR) that will be of interest in the splicing process is the 'largest is best' as shown by Equation 2. Largest is best SNR and it was selected because the purpose of this experiment was to acquire the maximum splice strength (Wu *et al.*, 1991):

$$S/N_{\text{Largestisbest}} = -10\log\left(\frac{1}{n}\sum\left(\frac{1}{y_i}\right)^2\right) \qquad (2)$$

where n is the number of values at each test condition and y_i is each observed value.

The results of the ANOVA revealed that factor A (blast pressure) was statistically significant. Factors B, C and D were found to be statistically insignificant.

Figures 16 and 17 illustrate the SNR and the mean response of the SRS respectively at each level of the selected factors.

Factors B and C gave us the largest mean SRS at level 2, even though the largest SNR was at level 3. Therefore, since both factors are not statistically significant, the level is chosen in favour of the mean response (Bendell *et al.*, 1989a).

Table 4 Confirmatory run

	Before	After	Increase/decrease (%)
Tensile strength	77.21	88.04	14.03
Variance	0.2	0.089	55.5

The strength of the interactions AC and AD required further investigation (Figure 18 and 19) (Nair *et al.* 1992). The interaction plots revealed intersections indicating strong interactions. As A is a dominant factor, it was logical to select the other factors at levels where the maximum SRS point resides. The four factors were, therefore, selected as A2, B2, C2 and D3. A confirmatory run was conducted to validate the data collected, and the results are shown in Table 4 (Antony and Antony, 2001; Bendell *et al.*, 1989).

The confirmatory run was undertaken using the same experimental set-up as the Taguchi experimentation, and

with the same number of replications. Table 4 compares the results obtained from the parameter combination deduced from the Taguchi experiment with the results normally achieved using standard industry practice.

The result of the confirmatory run reveals that the splice strength increased by 14% and the variance decreased by 55.5%.

CONCLUSION

The Taguchi DOE method was applied to determine the optimum splicing parameter set up to achieve the greatest SRS. The results of the experiment revealed that blast pressure was the most important factor.

Chamber design and cutting synchronisation (parameters C and D) had an influential interaction with blast pressure. These factors were logically chosen to coincide with the maximum SRS of factor A at its optimum setting, level 2, due to factor A being statistically significant.

Blast duration (factor B) tests revealed that durations in the range 1.0–2.0 seconds were required to form satisfactory splices. The optimum setting for maximising splice strength was established approximately 1.5 seconds.

Therefore, optimum parameter settings achieved on the reference yarn were as follows.

Factor A: Level 2 = 50 psi
Factor B: Level 2 = 1.5 seconds
Factor C: Level 2 = 4485 straight chamber
Factor D: Level 3 = 6

A confirmatory run was carried out using these factors shown above resulting in a maximum SRS of 88%, with a variance of 0.089. This represents an increase of 14% in tensile strength and a decrease of 55.5% in variance compared to previously recommended optimum levels.

The results indicate that the strength of the splice on the reference yarn is influenced by the design of the splicing chamber profile. This result has not been observed in published literature. However, this is no great surprise; the absence of such information is probably because splicer manufacturers have been protective of their intellectual property. The wide variation in splicing chambers observed in real splicers serves to suggest that much work on chamber designs has been done, but remains unpublished in the interest of company confidentiality.

Improved strength and robustness of the splicing process on the reference yarn has, therefore, been demonstrated. Hence, the Taguchi DOE method is a valid statistical tool in this context that can be used efficiently and effectively to achieve the optimum parameter settings of any specific target output with using only a truncated number of test samples.

The simple experiments described in this article established the validity of the Taguchi DOE technique while applied to this method. However, to gain a greater insight into the process, it will be necessary to expand significantly the range of splicing parameters investigated. Therefore, later articles will include the results of work on different variables such as yarn type, characteristics, count and splicing chamber geometry, while assessing splice aesthetics and strain repeatability. The main resolution of this work is that it may yield a mathematical model for the splicing process.

REFERENCES

ANTONY, J. and ANTONY, F. J., 2001. Teaching the Taguchi method to industrial engineers, *Work Study*, 50(4), 141–149.

BENDELL, A., DISNEY, J. and PRIDMORE, W. A., 1989a. *Taguchi Methods: Applications in World Industry*, IFS Publications, London, England, pp. 39–56.

BENDELL, A., DISNEY, J. and PRIDMORE, W. A., 1989b. *Taguchi Methods: Application in World Industry*, IFS Publications, London, England, pp. 99–112.

CHENG, S. and FUNG, W. Y., 2004. Joining yarn ends together by pneumatic splicing, *ATA J.*, 15(3), 40–45.

COLEMAN, D. E., MONTGOMERY, D. C., GUNTER, B. H., HAHN, G. J., HAALAND, P. D., O'CONNELL, M. A., LEON, R. V., SHOEMAKER, A. C. and KWOK-LEUNG, T., 1993. A systematic approach to planning for a designed industrial experiment, *Technometrics*, 35(1), 1–27.

FOX, R. T. and LEE, D., 1990. Optimization of metal injection molding: Experimental design, *Int. J. Powder Metallurgy*, 26(3), 233–243.

IWNICKI, K., 1964. Process and apparatus for Joining Yarns or Tows, Patent No. GB956992.

KAUSHIK, R. C. D., HARI, P. K. and SHARMA, I. C., 1988. Mechanism of the splice, *Text. Res. J.*, 58(5), 263–268.

KAUSHIK, R. C. D., SHARMA, I. C. and HARI, P. K., 1987. Effect of fiber/yarn variables on mechanical properties of spliced yarn, *Text. Res. J.*, 57(8), 490–494.

LEWANDOWSKI, S. and DROBINA, R., 2004. Strength and geometric sizes of pneumatically spliced combed wool ring spun yarns, *Fibres Text. Eastern Eur.*, 12, 2(46), 31–37.

LOCHNER, R. H., 1991. Pros and cons of Taguchi, *Qual. Eng.*, 3(4), 537–549.

LOGOTHETIS, N., ATKINSON, C. J., SALMON, J. P. and BEST, K. F., 1990. Development of newly installed processes, *Int. J. Adv. Manufact. Technol.*, 5, 256–274.

NAIR, V. N., ABRAHAM, B., MACKAY, J., NELDER, J. A., BOX, G., PHADKE, M. S., KACKER, R. N., SACKS, J., WELCH, W. J., LORENZEN, T. J., SHOEMAKER, A. C., TSUI, K. L., LUCAS, J. M., TAGUCHI, S., MYERS, R. H., VINING, G. G. and JEFF WU, C. F., 1992. Taguchi's parameter design: A panel discussion, *Technometrics*, 34(2), 127–161.

OINUMA, R., NARISAWA, I. and KOYAMA, K., 1995. Mechanism of end breakage due to knots in plain-weft knitting zone, *J. Text. Eng.*, 48(7), 43–52.

PEACE, G. S., 1993. *Taguchi Methods: A Hands-on Approach*, Addison-Wesley, Wokingham, England, pp. 13–22.

ROWLANDS, H., ANTONY, J. and KNOWLES, G., 2000. An application of experimental design for process optimisation, *TQM Mag.*, 12(2), 78–83.

SENGUPTA, S., 2000. Retained strength of air-spliced yarn—Rupture process and effect of test length, *Ind. J. Fibre Text. Res.*, 25, 277–283.

THOMAS, A. J. and ANTONY, J., 2003. An integrated approach to improving the adhesive bond strength of honeycomb composite joints, *Work Study*, 52(5), 244–255.

WATERS, G. T., 1998. *Pneumatic Yarn Splicer*, Patent No. US5809761.

WEI, Q. F., WANG, X. Q., MATHER, R. R. and FOTHERINGHAM, A. F., 2004. New approaches to characterisation of textile materials using environmental scanning electron microscope, *Fibres Text. Eastern Eur.*, 12, 2(46), 79–83.

WU, C. M., BLACK, J. T. and JIANG, B. C., 1991. Using Taguchi methods to determine/optimize robot process capability for path following, *Robotics Computer-integrated Manufact.*, 8(1), 9–25.

Accepted and being published in The Journal of the Textile Institute

Optimising splicing parameters for splice aesthetics for a continuous filament synthetic yarn

C. J. Webb, G. T. Waters (GTW Developments Ltd.), A. J. Thomas,
G. P. Liu, E.J.C. Thomas (University of Glamorgan)

Abstract: Pneumatic yarn splicing is a well established technique for joining two yarn ends together by means of a blast of compressed air in a device known as a splicing chamber. Earlier research has addressed the effect of variables such as air pressure and splicing chamber design upon easily-quantifiable outputs such as splice strength. This paper continues the work on splice strength done by Webb *et al.* (accepted 2006), in this instance addressing the issue of optimising splice appearance. The research uses the same statistical methods of Taguchi analysis which were established in the earlier work. By combining the results from the splice strength experiments with this new work on splice appearance, it has been demonstrated that the strongest splice does not in general correspond with the best appearance. In general therefore it is necessary to establish an overall optimum splicer configuration, offering an acceptable compromise between splice strength and splice appearance.

Keywords: Taguchi, Splicing, Parameter optimisation, Spliced retained strength, Retained yarn appearance.

INTRODUCTION

In the textile industry, knotting in various forms was traditionally used to join yarn ends together. Knotting was not especially satisfactory, being operator-sensitive and variable in quality. Inconsistent knotting produced faulty fabric and sporadic machine stoppages; both problems were unacceptable to the end user, Cheng and Fung (2004).

Pneumatic splicing was developed to overcome the problems associated with knotting. It is used worldwide, and has been responsible for improved quality and efficiency. The splicing process involves introducing two multifilament yarns into a splicing chamber, and subjecting them to a high pressure turbulent flow of compressed air; the filaments become intermingled, and the two yarn ends are combined into one, making a neat strong joint whose strength closely matches that of the original yarn, Paliwal and Patel (1989), Mingjie *et al.* (1999). Due to the random nature of the individual filament positions throughout the yarn, no two splices are exactly the same at the microscopic, filament level, Wei *et al.* (2004), Wei and Wang (2003), but at the scale of the entire splice, there is only slight variation in performance and appearance between splices.

For acceptable performance, manufacturers require a spliced joint to perform well and to resemble closely the appearance of the original yarn, Lam and Cheng (1997). Thus the two most important splice characteristics are splice strength and appearance, Lewandowski and Drobina (2004). As air pressure or blast duration is progressively increased from a low level, splice strength increases; however, when a critical pressure is exceeded, filament damage begins to occur and splice strength begins to diminish.

Because of the large number of critical variables it would be too time-consuming to conduct a full factorial analysis. The Taguchi method is a powerful design of experiment (DOE) technique, Thomas and Antony (2003), which can increase the productivity and quality of a product with a minimum amount of testing and can be applied to the splicing process as proven in previous work by Webb *et al.* (accepted 2006). The technique performs a partial factorial analysis set by the orthogonal array chosen, where in this case an L27 orthogonal array is used. There is one main disadvantage associated with this method, which is the potential loss of accuracy due to the partial factorial analysis, which is why confirmatory runs were undertaken to prove the splicing process optimisation.

Previous work in this research programme done by Webb *et al.* (2007), has been carried out on assessing solely the effect that individual parameters have on the splice strength alone. Analysis was simplified by using the Taguchi robust parameter design approach, Taguchi (1989), Thomas and Antony (2005), to record only a select number of test samples, focussing on a small number of splicing processing variables.

However, although splice strength is a necessary outcome, it is not the case. Filamentation is relevant to splice strength, but it is also critically important to processing efficiency. Broken filaments may run back, getting caught in components of the machinery, making the splice unacceptably bulky and in extreme circumstances the entire yarn may break. An ugly splice with high levels of filamentation will be no better than a poor knot and ultimately the machine efficiency and fabric quality will be unacceptable.

Before this programme of work was undertaken, there already existed a general understanding of how splice parameters affected splice strength and splice appearance but not combined. In order to meet the combined requirements of achieving high joint strength and consistent quality of appearance, the effect of the combination of splicing parameters needs to be understood, characterised and finely tuned, Peace (1993, pp. 23-54). This paper addresses the input parameters which affect the two parameters of splice strength and splice appearance together. The aim of the work was to identify a compromise between strength and appearance, so that process parameters could be identified to maximise the overall acceptability of the splices in a specific yarn.

The tests performed in this research were all done on a simple continuous filament yarn that was chosen as a suitable baseline in previous work by Webb *et al.* (2007). This yarn was an 1100dtex, continuous filament Nylon 66 with low twist, consisting of 72 filaments, as used in the manufacture of standard motor vehicle safety belts. Future work will be carried out in a later

paper, to assess if the results obtained for the given yarn count will remain generally valid for other different yarn types and counts.

EXPERIMENTAL METHOD

In order to ensure consistency with earlier work by Webb et al. (2007), which examined only splice strength; the same experimental test setup was retained. A microscope with embedded digital camera was added to record the splice appearance.

The experiments were designed to subject the standard yarn to a wide range of experimental conditions, measuring strength and appearance for each condition, using a sampling method defined by the Taguchi Design of Experiment (DOE). From the Taguchi factor identification and level optimisation analysis, would emerge an optimised set of processing conditions, giving a compromise between splice appearance and strength, Antony and Antony (2001). The independent and compromised optimal sets of splicing parameters (factor levels) are then confirmed through a set of individual confirmatory runs.

For the experiments to have any validity, acceptable and reproducible measures of splice strength and appearance were needed.

Splice Retained Strength (SRS), was simple. It could be expressed as a simple percentage (Equation 1) –

$$SRS = \frac{Spliced\ yarn\ strength}{Parent\ yarn\left(non-spliced\right)} \times 100 \quad \text{(Eq. 1)}$$

This measure is well documented, and is within the normal limits of experimental error, completely objective, Sengupta (2000).

Splice appearance was more difficult to assess. Unlike SRS, appearance is a subjective measure. In principle, appearance could be assessed by using a device such as an Uster, but the detailed structure of a splice is not completely analogous to that which is defined as yarn hairiness, Nikolic *et* al. (2003). The notion of using hairiness as a measure was soon rejected for the simple fact that a splice made in a continuous filament yarn, with just a few broken filaments, would score quite well on a hairiness test and yet such a splice could prove very disruptive to yarn processing. A method of assessment of appearance was therefore required, which would have some relevance to processing efficiency.

Consider the general characteristics of a splice. In general, all splices have a characteristic and broadly reproducible form as indicated in Figure 1 below.

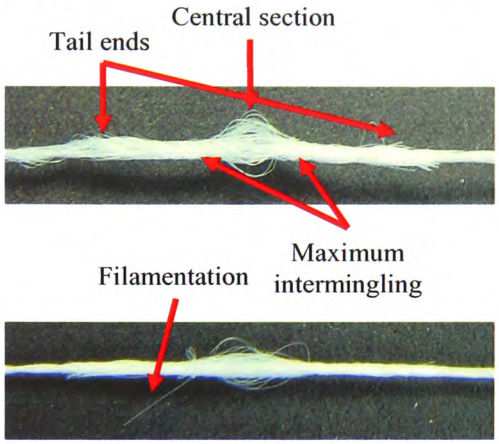

Figure 1 - Characteristic form of a splice

The central section of the structure remains untwisted and roughly parallel to the chamber axis. These pictures were taken on a "bowl" chamber, and the spreading of the filaments at the centre is very marked. Had a simple straight-section chamber been used, the filaments would be much flatter, nearly parallel, but the bowl form has been chosen to show the central section more clearly.

These two chambers have the same general V shaped profile (identified as straight chamber) with only a hemispherical bowl machined out at the centre of the chamber differing (identified as bowl chamber). These chamber designs represent the most common chambers developed by GTW Developments, Waters (1998), Wood (1982) and are described in more detail in the following materials and equipments section.

Between the central section and the ends of the splice, the yarns are intertwined, with the maximum amount of intermingling occurring nearest to the central section. In the main section of the splice, the fibres lie in dense clusters, therefore, there is an increase in yarn diameter in the splice, since two yarns occupy the space normally occupied by one. The increase in diameter is generally modest, because the fibres

Table I – Splice appearance scale

	Splice appearance scale									
Appearance features	1	2	3	4	5	6	7	8	9	10
Slight diameter increase			■	■	■	■	■	■	■	■
Large diameter increase	■	■	■	■	■	■				
Slight filamentation				■	■	■	■	■		
Large filamentation	■	■	■	■	■					
No tail ends								■	■	■
Slight tail ends		■	■	■	■	■	■	■	■	
Large tail ends	■	■								
Slight central section increase				■	■	■	■	■	■	■
Large central section increase	■	■	■	■						

in the splice are generally more tightly packed than in the parent yarn. At each end, the splice usually terminates in a small 'tail' where the extreme tips of the spliced yarns have not been fully bound into the structure.

In certain circumstances, the splice may demonstrate filamentation. This will occur if some aspect of the splicing process, interacting with the mechanical properties of the yarn, has led to one or more filaments being broken or not being fully bound into the splice. As filamentation increases, appearance is degraded, and processing efficiency falls.

To describe the aesthetics of a splice, the Retained Yarn Appearance (RYA) scale was devised and validated through the inspection and grading of hundreds of splices, Cheng and Lam (2000). A subjective scale from 1-10 was finally used, based upon the appearance of each spliced joint as summarised in Table I.

If a splice scored 10, it has no visible filamentation, and has a well-ordered structure in the main section of the splice. All the fibres are bound into the structure. There are no "tails".

If a splice scored 5, it has a medium level of filamentation with a less ordered structure in the main section of the splice. The splice is still acceptable in terms of appearance and processability.

If a splice scored 1, it has extreme filamentation, and the characteristic appearance of a splice is disrupted. The splice is completely unacceptable in terms of appearance and processability.

Obviously there is going to be a diameter increase when splicing because there are two yarn ends joining together. The difference between slight and large diameter increase is that in some splices, the filaments are not bound in a tight structure and therefore cover a greater volume. Slight diameter increase is equal or less than three times the diameter of a single yarn end while large diameter increase is anything above this.

If the yarn ends are not fully bound into the splice then we get tail ends and filamentation. The protrusion of tail ends are assessed by the following criteria, Slight tail ends is equal or less than the diameter of splice and greater than that for large tail ends. Filamentation is assessed by the number of filaments that are protruding from the splice either by stray filaments not being bound into splice or through filaments close to blast hole being damaged through excessive air velocity. Slight filamentation is equal or less than 10% of total filaments protruding from splice.

The final grade of RYA was a combination of various attributes but not of the same weight. Larger weight or higher preference was given to tail ends and filamentation because these areas are most problematic in industry. Therefore double the weighting was given to these.

Figure 2 shows three examples A, B and C with each obtaining a RYA of 9, 6 and 1 respectively. In greater detail splice example B was obtained by placing the sample under controlled tension and assessing the yarn diameter, tail ends, breakage and filamentation. Splice B had a diameter of 2.5mm (4.2mm at centre) with a tail end of 1.7mm which obtains a score of 3 out of 4. Also there was only a slight diameter increase and therefore obtains a score of 1 out of 2. There were 4 damaged/broken filaments and 6 loose filaments that remained unbound into the splice therefore when pooled together equates to 7% filamentation and a resulting score of 2 out of 4. Therefore splice sample B has an overall RYA score of 6.

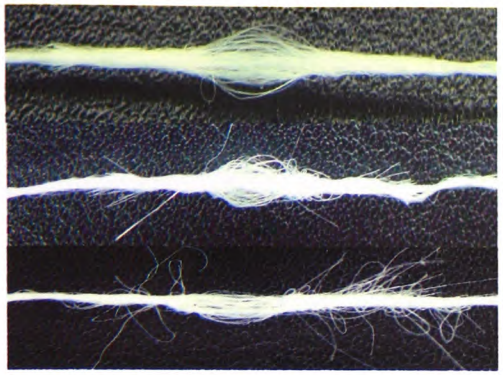

Figure 2 – Splice appearance grade: (A) 9, (B) 6 and (C) 1.

With acceptable and reproducible measures of strength and appearance defined, the main experiment could be designed.

In the previous study, a Pareto analysis was conducted to identify the factors most likely to play a dominant role in the splicing process, Peace (1993, pp. 70-96), Coleman and Montgomery (1993). Table II shows the four parameters that were identified. The first study addressed these factors in terms of their effect on SRS, and then optimised these four parameters using the Taguchi DOE method. This method improved the absolute value of strength and reduced variability.

Table II – Selected splicing parameters

Parameter	Factor
Blast pressure	A
Blast duration	B
Chamber design	C
Cutting synchronisation	D

Since three of the output parameters had a big affect on the output response with blast pressure being statistically significant at 99%, it was concluded that they were also likely to affect other splice characteristics such as splice appearance. That approach was the basis of this paper.

The test parameters were varied over the same ranges, using the same intervals, as in previous studies:

- Blast pressure was varied from 0 to 90psi, at intervals of 5psi.
- Four blast durations were used at four key blast pressures of 20, 40, 60 and 80psi: 0.5, 1, 2 and 3 seconds.
- A system of cutting synchronisation was used, defined by an arbitrary scale ranging from 0 – 6:
  0 – With the control set at 0, the knives cut the yarns before the start of the air blast, releasing the yarn ends filaments to move freely around the chamber from the outset.
  3 – With the scale set at 3, the air blast and yarn cutting are simultaneous.
  6 – With the scale set at 6 the yarns are cut after the start of the air blast.

Cutting synchronisation was factored into the experiment because it is known to have an effect on the appearance of the splice, specifically on the 'tail' sections at each end of the splice. In greater detail splicers can be designed so that the air blast and cutting action may be separately controlled to release or hold the yarn in the chamber to the users preference; this technique expands the range of performance of a splicer. On the experimental splicer, the range of cutting synchronisation was defined by an arbitrary scale ranging from 0 – 6.

For each experimental condition, 20 splice repetitions were undertaken, subjected and assessed under the same controlled tension to reduce variability. The average splice appearance was assessed using results from 5 independent engineers under each experimental condition, on the RYA scale from 1 to 10. Splice strength was measured using the same techniques as employed in the earlier experiments by Webb *et al.* (2007).

MATERIALS AND EQUIPMENT

The same three representative chamber designs were used as in the work conducted earlier by Webb *et al.* (2007). All three chamber profiles utilised the same general geometry. All were 4.8mm deep, 16mm long, with a 30° chamber angle and a blast hole of 4 mm diameter at the centre.

- The smallest, the 4483 straight, had a width at the base of 0.8 mm.
- The largest, the 4485 straight, had a width at the base of 1.25 mm.
- The 4483 bowl chamber was essentially the same as the 4483 straight, but it had hemispherical profile machined out at the centre of the chamber (Figure 3 inset).

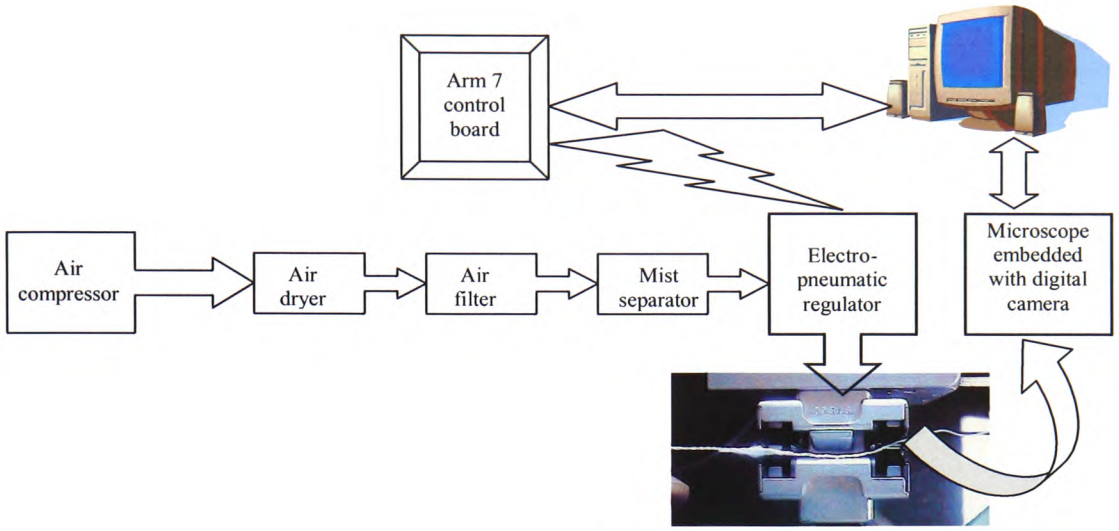

Figure 4 – Experimental setup

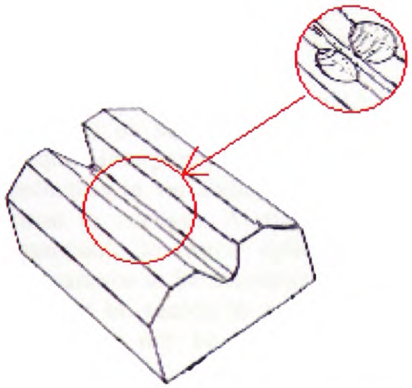

Figure 3 - Standard 'V' shaped chamber – "inset shows the "bowl""

One type of 1100dtex, 72 filament, continuous filament Nylon 66 with low twist fibre was used throughout, all from the same bobbin to minimise variability.

The splices were prepared on a Model 1-11 splicer, from GTW Developments Ltd.

The compressed air used was filtered and dried before reaching the splicer to create consistent air properties. The equipment used was an air drier followed by an air filter, (type AW30-F03D) and mist separator, (type AFM30-F03D) with a 0.3µm 95% filtered particle size. The air pressure was controlled with an accuracy of +/- 0.03psi using an electro-pneumatic regulator, (type ITV2050-312BS3-Q).

Splice appearance of the test samples, measured under controlled tension, were assessed by examining digital photographs, taken on a digital camera at 2016x1512 resolution embedded into a microscope and images taken from a scanning electron microscope.

To minimise human error, all the equipment was controlled and results collected electronically using an ARM7 control board, digital camera and a PC.

The experimental setup used is shown schematically in Figure 4.

RESULTS

At the outset of the earlier work on splice strength by Webb *et al.* (2007), individual splice strengths varied quite widely, and it was only after the optimisation using the Taguchi method that the variability was reduced.

The RYA rankings were converted into percentages, therefore, could be plotted against the corresponding individual results for SRS.

Initial tests were conducted at 4 key pressures, namely 20, 40, 60 & 80psi over the 4 blast durations 0.5, 1, 2 & 3sec. These initial tests were conducted to reveal if appearance did have the same output response to that of strength. Figure 5 shows the responses using the 4483 bowl chamber.

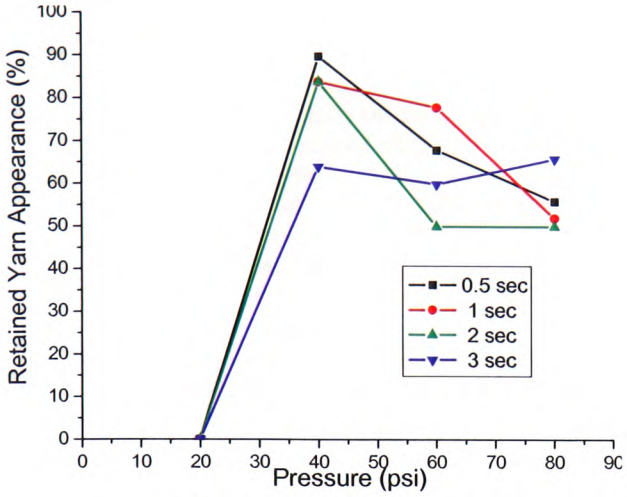

Figure 5 – 4483 bowl chamber

As can be seen, the output responses are similar to their SRS equivalent which also stands true for the 4483 and 4485 straight chambers. Therefore, they can be analysed in greater detail using one configuration.

These results, at the level of the individual splice, require interpretation, because there was a slight reduction in variability between results in comparison to strength. At first sight it might seem reasonable to expect splice strength and splice appearance to be intimately linked. There may however be reason to argue that the two parameters may not be as closely linked as originally thought.

Yarn damage was proven by subjecting a continuous filament yarn to the same stresses as the splicing process under different splicing conditions and recorded via a scanning electron microscope (SEM). This was done to reveal a distinction between a broken filament and a loose tail end filament when assessing splice appearance but in the grand scheme of things it is not relevant because any filamentation whether broke or loose ends will cause problems in industrial practice, Hearle and Wilkins (2006). The SEM recordings for both filament ends are shown in Figure 6.

Splice appearance is a function of filament damage, i.e. the greater the number of filaments which break on exposure to the air blast, the poorer the appearance. However, at least when the damage is moderate, most of the visible damage concerns only those filaments which lie on the outside and close to the centre of the splice; those which are at the core are largely protected from the blast. So the hypothesis is that, at moderate levels of filamentation, appearance is a feature of the outside of the bundle.

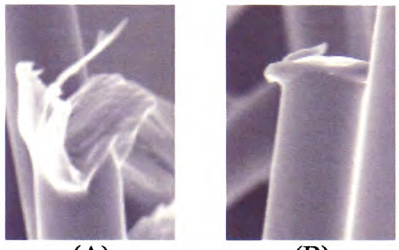

(A) (B)

Figure 6 – (A) Broken filament; (B) Cut tail end filament

Splice strength seems to be different. Others have shown that spliced joints are inherently unpredictable, Kaushik *et al.* (1987*a*), i.e. no two splices are the same, because the filaments are packed randomly throughout the yarn. This randomness may result in a wide range of filament geometry from splice to splice. Thus, the filaments may intertwine differently from splice to splice, Kaushik *et al.* (1988), Kaushik *et al.* (1987*b*), Rowlands *et al.* (2000). The implication of this work is that, again at moderate levels of filamentation, strength is a feature of the manner in which filaments interact in the body of the splice.

This point needs to be addressed more completely in later work. However, for the purposes of these experiments, experimental error was once more minimised by executing 20 tests for each experimental condition. In the graphs which follow, each point represents the mean of 20 observations.

Figures 7, 8 & 9 show how SRS and RYA vary with air pressure, with the three chosen experimental splicing chambers. In these graphs, the results relate specifically to splices made with blast durations of 1 second. A compromise between the two spliced characteristics was considered with greater preference toward splice strength due to this being the critical component in industry. The compromise was obtained by joining the two SRS & RYA percentages to reveal the overall optimum. This compromise is also included on the graph plots to reveal where the optimum compromise occurs that produces a strong splice with acceptable appearance.

In Figure 7 (4483 bowl chamber), it can be seen that the SRS increases sharply after the air pressure reaches 20psi, reaching a maximum at around 40-50psi. It then falls off fairly uniformly as the air pressure is increased further. The RYA begins at approximately 80%, reaching a maximum at around 30psi. It then falls off fairly uniformly as the air pressure is increased further. The rate of decrease is broadly similar to the corresponding drop of SRS.

In Figure 8 (4483 straight chamber), it can be seen that the SRS increases after the air pressure reaches 20psi. The rate of increase thereafter is much more gradual in comparison with the bowl chamber, reaching a maximum at around 55-60psi. It then falls off fairly uniformly as the air pressure is increased further. The RYA begins at approximately 60%, but it does not reach a well defined maximum. After the initial steep increase, the gradient moderates from 30 to 75psi. In fact, it is probably reasonable to conclude (bearing in mind the subjective nature of the assessment) that RYA is constant across the range from 45-75psi. It then falls off fairly sharply as the air pressure is increased further.

On comparing both splice characteristics, it revealed that the maximum appearance approximately coincides when the maximum splice strength configuration seemed to form.

In Figure 9 (4485 straight chamber), it can be seen that the SRS increases sharply after the air pressure reaches 20psi, reaching a maximum at around 40-50psi. It then falls off fairly uniformly as the air pressure is increased further. The RYA begins at approximately 70%, reaching a maximum at 30psi. It then falls off fairly uniformly as the air pressure is increased further. The rate of decrease is somewhat faster than the corresponding drop of SRS.

The most startling observation is that, whereas, for the 4483 bowl chamber, SRS and RYA are broadly in step, there are noticeable differences between the two in the 4485 straight chamber, and startling differences between the two in the 4483 straight chamber.

The Taguchi experiment was executed with the selected factor levels from the initial experimentation to optimise the splice appearance alone. An analysis of variance (ANOVA) was conducted to reveal if any of the factors chosen were statistically significant.

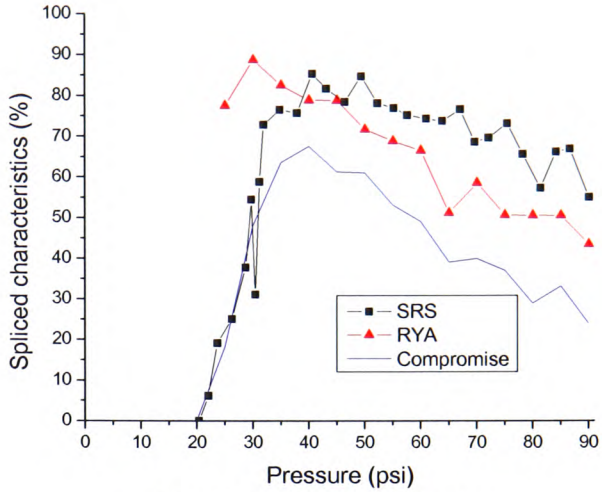

Figure 7 – 4483 bowl chamber

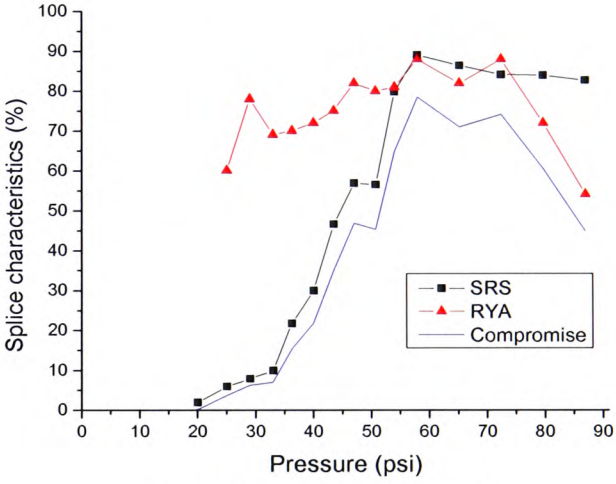

Figure 8 – 4483 straight chamber

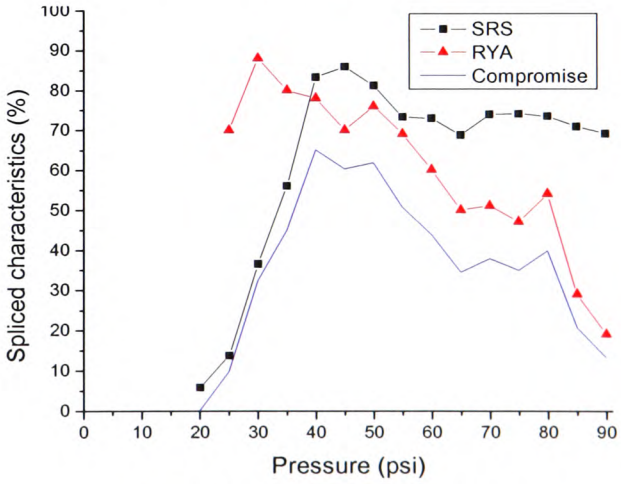

Figure 9 – 4485 straight chamber

A confirmatory run was then conducted using the optimum parameter settings found to verify that the optimum splicer setting found provided the maximum RYA with the greatest robustness (i.e. minimum variation between readings), Bendell *et al.* (1989).

Once the optimum splicer setting for maximum RYA was found and confirmed then a compromise between the two optimums (RYA and SRS) was conducted, giving preference to the statistically significant factors and their relative levels to find an overall optimum splicer setting which provides the greatest splice appearance with the maximum strength.

DISCUSSION

The 4483 bowl chamber (Figure 7) forms its maximum RYA of approximately 90% at approximately 35psi and then decreases gradually with increasing air pressure. This is likely due to the violent vortices that are created within the chamber at high pressures which in turn agitates the filaments extensively to cause damage or force them not to get bound into the splice.

The 4483 straight chamber (Figure 8) forms average to high splice appearance until the optimal pressure was achieved at approximately 60psi resulting in a maximum RYA of 88%. This is the point where the optimum amount of intermingling takes place with the least amount of filamentation. Once the maximum RYA was reached, it began to decreases rapidly due to increasing filamentation.

The 4483 bowl and 4485 straight chambers (Figure 7 & 9) both have very similar RYA characteristics with the only difference being, that the latter chamber having a greater decline of RYA once the maximum was reached.

It is arguable that with the straight chamber, after the maximum splice strength formation has occurred i.e. filaments fully intermingled, the violent air pressure causes a very miniscule amount of outer filaments to not get bound into the splice or begin to 'fray'. Where as with the bowl chamber, the airflow within, naturally draws the outer filament to wrap around the splice resulting in a better appearance splice with less filamentation, Oxenham and Basu (1993).

The optimum compromise on all three chamber designs are approximately at their maximum SRS. With this in mind the maximum SRS and below, has more variability than splices created at higher pressures due to a more violent airflow within the chamber increasing the consistency of stronger intermingling, resulting in greater frictional forces.

Only at 60psi or greater for the 4483 bowl and 4485 straight chambers and at 80psi or greater for the 4483 straight chamber does the appearance become constantly unacceptable. Below these pressures, very few splices are aesthetically unacceptable and the consistency increases until the maximum RYA is achieved.

The maximum compromise is obtained using the 4483 straight chamber (Figure 8) at approximately 60psi. The greatest appearance splices are created in the chamber with the smallest volume which restricts the movement of the individual fibres thus reducing the filamentation. With this in mind due to the small volume, it requires a greater amount of compressed air pressure to sufficiently intermingle the fibres resulting in a consistently strong splice.

The blast duration tests revealed that 0.5 and 1 seconds were very similar in splice appearance but 0.5 seconds from previous experimentation by Webb *et al.* (2007), it was found that it was too short to form a strong splice, whereas 2 seconds and above was too long especially at higher pressures resulting in worse splice appearance but stronger. This is probably because at 0.5 seconds the filament have not had time to intermingle sufficiently to create a strong splice but have had enough time to create the appearance that of a characteristic splice.

The opposite can be said about longer blast durations, in that the maximum amount of intermingling takes place to form the splice before the blast has finished and therefore the remaining blast duration begins to damage the filaments at the centre of the splice creating filamentation which ultimately is the cause for poor splice appearance and a reduction in strength.

The blast duration curves Figure 5, 4483 and 4485 straight chambers are all consistent with the RYA test results shown in Figures 7, 8 and 9 respectively.

Table III – Selected splicing parameters

Factor	Parameter	Level 1	Level 2	Level 3
A	Blast pressure	40psi	50psi	60psi
B	Blast duration	1sec	1.5sec	2sec
C	Chamber design	4483 straight	4485 straight	4483 bowl
D	Cutting synchronisation	0	3	6

The preliminary investigation revealed that the approximate optimum compromise between SRS and RYA was between 40 to 60psi. The parameter levels for the Taguchi DOE was established and shown in Table III. Three levels were considered due to the nonlinearity of the splicing functions. An L27 orthogonal array (OA) was chosen for the experiment, Peace (1993, pp. 114-166).

The L27 OA and the factor identification results for RYA are shown in Figure 10 along with the SRS results and optimum selected factors found from the previous study by Webb *et al.* (2007).

The signal to noise ratio (SNR) that will be of interest in the splicing process is the 'largest is best' because the output response of this experiment is to acquire the maximum splice characteristics, Wu *et al.* (1991), Peace (1993, pp. 292-311).

Equation 2 below shows the SNR for 'larger is best'.

$$S/N_{larger\,is\,best} = -10\log\left(\frac{1}{n}\sum\left(\frac{1}{y_i}\right)^2\right) \qquad \text{(Eq. 2)}$$

Where:
n = number of values at each test condition,
y_i = each observed value.

The results of the Analysis of Variance (ANOVA) for appearance, as shown in Table IV, revealed that all factors were statistically significant at 95% and factors B, C and D were statistically significant at 99%.

	Main Factors and Interactions											
Run	A	B	AB	AB	C	AC	AC	D	AD	AD	SRS (%)	RYA (%)
1	1	1	1	1	1	1	1	1	1	1	51.63	92
2	1	1	1	1	2	2	2	2	2	2	73.24	90
3	1	1	1	1	3	3	3	3	3	3	81.42	88
4	1	2	2	2	1	1	1	2	2	2	79.18	86
5	1	2	2	2	2	2	2	3	3	3	78.94	74
6	1	2	2	2	3	3	3	1	1	1	77.77	56
7	1	3	3	3	1	1	1	3	3	3	70.82	80
8	1	3	3	3	2	2	2	1	1	1	76.39	54
9	1	3	3	3	3	3	3	2	2	2	76.08	70
10	2	1	2	3	1	2	3	1	2	3	82.33	80
11	2	1	2	3	2	3	1	2	3	1	88.10	80
12	2	1	2	3	3	1	2	3	1	2	74.51	88
13	2	2	3	1	1	2	3	2	3	1	76.70	84
14	2	2	3	1	2	3	1	3	1	2	86.27	64
15	2	2	3	1	3	1	2	1	2	3	73.65	62
16	2	3	1	2	1	2	3	3	1	2	77.85	82
17	2	3	1	2	2	3	1	1	2	3	77.94	62
18	2	3	1	2	3	1	2	2	3	1	68.46	84
19	3	1	3	2	1	3	2	1	3	2	78.20	80
20	3	1	3	2	2	1	3	2	1	3	60.56	64
21	3	1	3	2	3	2	1	3	2	1	65.52	92
22	3	2	1	3	1	3	2	2	1	3	71.98	84
23	3	2	1	3	2	1	3	3	2	1	80.52	58
24	3	2	1	3	3	2	1	1	3	2	67.86	48
25	3	3	2	1	1	3	2	3	2	1	54.27	62
26	3	3	2	1	2	1	3	1	3	2	71.72	49
27	3	3	2	1	3	2	1	2	1	3	65.57	64

Factor A		
L1	L2	L3
76.67	76.22	66.78

Factor C		
L1	L2	L3
81.11	66.11	72.44

Factor B		
L1	L2	L3
83.78	68.44	67.44

Factor D		
L1	L2	L3
64.78	**78.44**	76.44

Selected Factors - SRS	A2	B2	C2	D3

Selected Factors - RYA	A1	B1	C1	D2

Interaction AB			
	B1	B2	B3
A1	**90**	72	68
A2	82.67	70	76
A3	78.67	63.33	58.33

Interaction AC			
	C1	C2	C3
A1	**86**	72.67	71.33
A2	82	68.67	78
A3	75.33	57	68

Interaction AD			
	D1	D2	D3
A1	67.33	82	80.67
A2	68	**82.67**	78
A3	59	70.67	70.67

Figure 10 – L27 Orthogonal array and optimum factor identification for RYA

The ANOVA from Webb *et al.* (2007), revealed that A was the only statistically significant factor with factors B and C marginally close to being 95% statistically significant. Table IV shows the ANOVA of both strength and appearance experiments.

Figures 11 and 12 illustrate the SNR and the mean response of the SRS and RYA at each level of the selected factors respectively. Factors A, B and C gave us the largest mean RYA at level 1, while factor D gave us the largest mean RYA at level 2. From the mean response plot you can see that factors B and C are the most influential in obtaining the greatest splice appearance. At closer inspection factor A could be selected at level 1 or 2 due to the almost equal mean response plot. All the mean response plots coincide with the SNR plot.

After analysis of interaction AB it was considered that AB could be omitted because it was not considered significant in the trials.

Table IV – ANOVA of each splice characteristic

Spliced Retained Strength (SRS)				
Factors	**DOF**	**SS**	**MS**	***F* ratio**
A	2	8951.03	4475.51	7.71 **
B	2	3374.30	1687.15	2.91
C	2	3313.55	1656.78	2.85
D	2	199.80	99.90	0.17
AB1	2	523.64	261.82	0.45
AB2	2	3267.37	1633.68	2.81
AC1	2	4143.59	2071.80	3.57 *
AC2	2	1691.38	845.69	1.46
AD1	2	1749.43	874.71	1.51
AD2	2	2306.67	1153.33	1.99
Error	519	301388.98	580.71	N/A
Total	539	330909.75	N/A	N/A
Retained Yarn Appearance (RYA)				
A	2	15009.26	7504.63	4.42 *
B	2	44787.04	22393.42	13.18 **
C	2	30398.15	15199.07	8.95 **
D	2	28703.70	14351.85	8.45 **
AB1	2	4453.70	2226.85	1.31
AB2	2	2064.81	1032.41	0.61
AC1	2	1398.15	699.07	0.41
AC2	2	4592.59	2296.30	1.35
AD1	2	564.81	282.41	0.17
AD2	2	37.04	18.52	0.01
Error	519	881566.52	1698.59	N/A
Total	539	1014575.78	N/A	N/A

Notes:
* Indicates factor/interaction is statistically significant at 5% level of significance - $F(0.05,2,519) = 3.01$
** Indicates factor/interaction is statistically significant at 1% level of significance - $F(0.01,2,519) = 4.65$

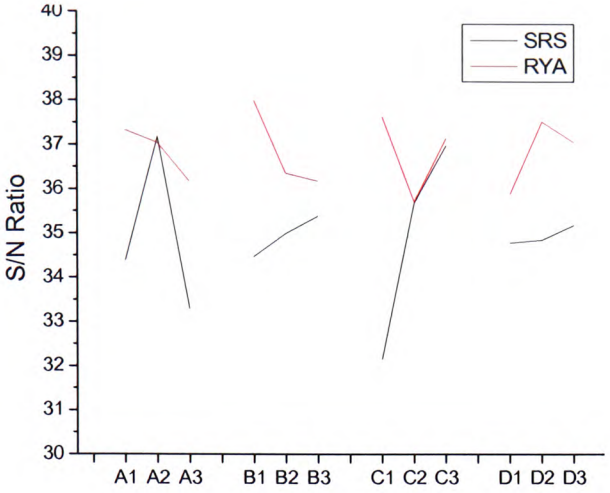

Figure 11 – SNR response plot

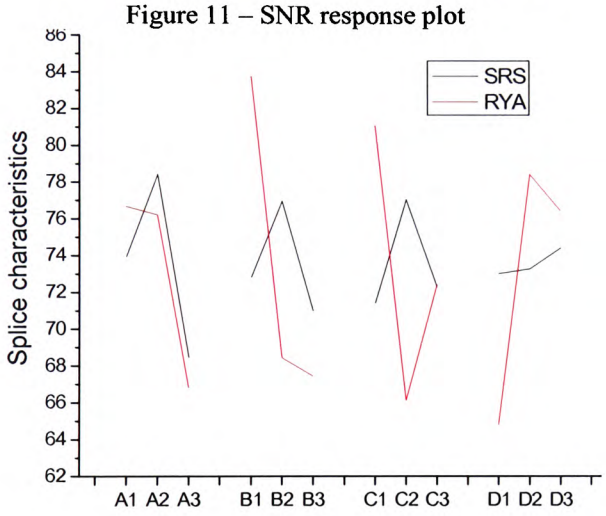

Figure 12 – Mean response plot

A confirmatory run was undertaken with the same experimental setup and number of replications to validate the data collected. The results are shown in Table V which compares the combination of levels deduced from the Taguchi experiment with the results normally achieved using standard industry practice.

Table V - Confirmatory run

	Before	After	Increase/ Decrease (percent)
Splice appearance	53.64	92	71.51%
Variance	1.27	0.63	50.39%

81.5% of the Taguchi experimentation resulted in acceptable splice appearance, where 60% of them resulted in near identical splice appearance compared with unspliced appearance (bar a slightly increased central section). The RYA with the confirmatory parameter settings was 92% with a variance of 0.63, which is an increase in splice appearance of 71.5% with a decrease in variance of 50.4% compared to normal industry practice.

The optimum parameter settings for each individual Taguchi experiment were 2,2,2,3 and 1,1,1,2 for SRS and RYA respectively. In industry a compromise between the two is required, therefore the statistically significant factors obtained from the ANOVA analysis (Table IV), were chosen from each experiment along with the better understanding of individual parameter achieved on the different effect of splice performance, to provide an optimum compromise.

In the SRS experiment, blast pressure (factor A) was the only statistically significant factor with chamber design (factor C) and blast duration (factor B) being extremely close. In the RYA experiment blast duration, chamber design and cutting synchronisation (factor D) were statistically significant at 99% with blast pressure only marginally being 95% statistically significant.

Therefore factors B, C and D can be altered without a great significant change in strength and factor A can be changed without a major significant change in appearance. Over the two Taguchi analyses all four factors are statistically significant with only factor A competing for the dominant factor level, which was chosen as the most statistically significant level. Merging these factors together, produced a splicer parameter setting of 2,1,1,2 as shown below:

Blast pressure = 50psi
Blast duration = 1sec
Chamber design = 4483 straight chamber
Cutting synchronisation = 3

Having obtained the optimal factor settings for the combined output responses of strength and appearance confirmatory runs was conducted which are shown in Table VI.

Table VI - Confirmatory run

	Before	After	Increase/ Decrease (percent)
Splice Strength	88	66.25	24.72%
Variance	0.089	0.86	866.29%
Splice appearance	92	85	7.61%
Variance	0.63	0.85	34.92%

Due to the different chamber design (4483 straight) that was deduced from Taguchi analysis to produce the best splice appearance it has had consequential negative affect on the splice strength. From the experimentation (Figure 8) on the 4483 straight chamber, at 50psi the splice strength is relatively low in comparison to industry requirements. Therefore it can be seen that if the pressure is raised to 60psi then the splice strength is greatly improved with a negligible difference in appearance. A confirmatory run of these results are shown in Table VII.

Table VII - Confirmatory run

	Before	After	Increase/ Decrease (percent)
Splice Strength	66.25	84.18	27.06%
Variance	0.86	0.33	61.63%
Splice appearance	85	89.67	5.49%
Variance	0.85	0.48	43.53%

CONCLUSION

The Splicing parameter setup was optimised for the reference yarn by applying the Taguchi DOE method to obtain the maximum SRS and RYA. The splicer setup for SRS and RYA were 2,2,2,3 and 1,1,1,2 respectively. The ANOVA revealed that for SRS, factor A (blast pressure) was the only statistically significant factor at 99%, while all factors for RYA were statistically significant at 95% level and factors B, C and D (blast duration, chamber design and cutting synchronisation) were statistically significant at 99%. Therefore factor A is the most important factor for SRS while factor C is for RYA.

Confirmatory runs were carried out on the individual optimum parameter settings 2,2,2,3 and 1,1,1,2 for strength and appearance respectively. The results of the confirmatory runs gave a maximum spliced retained strength (SRS) of 88%, with a variance of 0.089 and a retained yarn appearance (RYA) of 92% with a variance of 0.63. This represents a very acceptable splice appearance with an increase of 71.51% in RYA and a decrease of 50.39% in variance compared to previously recommended optimum levels.

After the Taguchi experimentation, ANOVA and observations of the mean response and the SNR ratios, an optimum splice setting was derived that produced a good splice appearance with maximum strength for the reference yarn. This optimum splicer setting was 2,1,1,2

Factor A: Level 2 = 50psi
Factor B: Level 1 = 1sec
Factor C: Level 1 = 4483 straight chamber
Factor D: Level 2 = 3

Using the new combined optimum factor settings a confirmatory run was completed resulting in an overall SRS of 66.25%, with a variance of 0.86 and a RYA of 85% with a variance of 0.85. This represents a very acceptable splice appearance with a decrease of 24.72% in tensile strength and an increase of 866% in variance compared to individual optimisation levels.

The lower the blast duration the better the appearance with the optimum being approximately 1sec but a splice needs approximately 1.5 seconds to form properly to create a strong splice.

Due to the different chamber design (4483 straight) and reduced blast duration, which was deduced from Taguchi analysis to produce the best splice appearance, it has had consequential negative affect on the splice strength. From the experimentation (Figure 8) on the 4483 straight chamber at 50psi the splice strength is relatively low in comparison to industry requirements. Therefore if the pressure is increased to 60psi then the splice strength is greatly improved with a negligible difference in appearance.

A confirmatory run was carried out using the increased pressure setting resulting in an overall SRS of 84.2%, with a variance of 0.33 and a RYA of 89.7% with a variance of 0.48. This represents a slight increase in appearance of 5.5%, with a decrease of 43.5% in variance and an increase of 27% in tensile strength and an decrease of 61.6% in variance.

Hence an improved overall splicer design has been established that maximises appearance and strength that is required in industry worldwide.

REFERENCES

Antony, J. and Antony, F.J., 2001. *Teaching the Taguchi method to industrial engineers*, Work study, **50**, 4, 141-149.

Bendell, A., Disney, j. and Pridmore, W.A., 1989. *Taguchi methods – application in world industry*, IFS publications, 39-56.

Cheng, K.P.S. and Lam, H.L.I., 2000. *Physical properties of pneumatically spliced cotton ring spun yarns*, Textile research journal, **70**, 12, 1053-1057.

Cheng, S. and Fung, W.Y., 2004. *Joining yarn ends together by pneumatic splicing*, ATA Journal, **15**, 3, 40-45.

Coleman, D.E. and Montgomery, D.C., 1993. *A systematic approach to planning for a designed industrial experiment*, Technometrics, **35**, 1, 1-27.

Hearle, J.W.S. and Wilkins, A.H., 2006. *Movement of fibers in assemblies*, Journal of the textile institute, **97**, 1, 1-9.

Kaushik, R.C.D., Hari, P.K. and Sharma, I.C., 1988. *Mechanism of the Splice*, Textile Research Journal, **58**, 5, 263-268.

Kaushik, R.C.D., Hari, P.K., Sharma, I.C. and Sarkar, A.K., 1987*a*. *Performance of spliced yarn in warping and weaving*, Textile research journal, **57**, 670-673.

Kaushik, R.C.D., Sharma, I.C. and Hari, P.K., 1987*b*. *Effect of Fiber/Yarn Variables on Mechanical Properties of Spliced Yarn*, Textile Research Journal, **57**, 8, 490-494.

Lam, H.L.I. and Cheng, K.P.S., 1997. *Pneumatic splicing*, Textile Asia, **7**, 66-69.

Lewandowski, S. and Drobina, R., 2004. *Strength and geometric sizes of pneumatic spliced combed wool ring spun yarns*, Fibres & textiles in Eastern Europe, **12**, 2(46), 31-37.

Mingjie, x., Peijie, H., Shihua, S., Bingchang, Q. and Tao, L., 1999. *Study on pneumatic splice*, Journal of China textile university, **16**, 2, 109-112.

Nikolic, M., Stjepanovic, Z., Lesjak, F. and Stritof, A., 2003. *Compact spinning for improved quality of ring-spun yarns*, **11**, 4(43), 30-35

Oxenham, W. and Basu, A., 1993. *Effect of Jet design on the properties of air-jet spun yarns*, Textile research journal, **63**, 11, 674-678.

Paliwal, M.C. and Patel, R.S., 1989. *Assessment of yarn splicing in Indian mills*, 30th Technological conference, 24.1-24.5.

Peace, G.S., 1993. *Taguchi methods – a hands-on approach*, Addison-Wesley publishing company, Wokingham, England, 23-311.

Rowlands, H., Antony, J. and Knowles, G., 2000. *An application of experimental design for process optimisation*, **12**, 2, 78-83.

Sengupta, S., 2000. *Retained strength of air-spliced yarn – Rupture process and effect of test length*, Indian Journal of Fibre & Textile Research, **25**, 277-283.

Taguchi, G., 1989. *Introduction to Quality Engineering*, UNIPUB, New York.

Thomas, A.J. and Antony, J., 2003. *An integrated approach to improving the adhesive bond strength of honeycomb composite joints*, Work Study, **52**, 5, 244-255.

Thomas, A.J. and Antony, J., 2005. *A comparative analysis of the Taguchi and Shainin DOE techniques in an aerospace environment*, **54**, 8, 658-678.

Waters, G.T., 1998. *Pneumatic yarn splicer*, Patent No: US5809761.

Webb, C.J., Waters G.T., Thomas, A.J., Liu, G.P. and Thomas, E.J.C., 2007. *The use of the Taguchi Design of Experiment method in optimising splicing conditions for a Nylon 66 yarn*, Journal of the Textile Institute, **98**(4), 327-336.

Wei, Q.F. and Wang, X.Q., 2003. *Dynamic characterisation of industrial textiles using an environmental scanning electron microscope*, Journal of industrial textiles, **33**, 2, 101-110.

Wei, Q.F., Wang, X.Q., Mather, R.R. and Fotheringham, A.F., 2004. *New Approaches to Characterisation of Textile Materials Using Environmental Scanning Electron Microscope*, Fibres & Textiles in Eastern Europe, **12**, 2(46), 79-83.

Wood, J.I., 1982. *The Development of Air-splicing Techniques for the Jointing of Woollen-spun Yarns for Tufted-carpet Manufacture*, Journal of the Textile Institute, **2**, 71-79.

Wu, C.M., Black, J.T. and Jiang, B.C., 1991. *Using Taguchi methods to determine/ optimize robot process capability for path following*, Robotics & computer-integrated manufacturing, **8**, 1, 9-25.

Textile Research Journal | Article

The Influence of Yarn Count on the Splicing of Simple Continuous Filament Synthetic Yarns

Abstract Pneumatic splicing is a complex process, its efficiency being dependent on many variables. The research reported in this paper relates to the relationship between splicing performance and yarn count. The tests were performed using an industry-standard synthetic yarn, which was used as a baseline in previous research on the splicing process. This paper reports on the change in performance of industry-standard and experimental splicers with various configurations as yarn count was varied. The report offers an explanation for the change of splicing performance with yarn count.

Key words parameter optimization, scaling, spliced retained strength, splicing

Carwyn James Webb[1] **and Graham Thomas Waters**
GTW Developments, Pontypool, NP4 6NF, Wales

Guo Ping Liu and Clive Thomas
Faculty of Advanced Technology, University of Glamorgan, Pontypridd, CF37 1DL, Wales

Pneumatic splicing is a common technique used in the textile industry to join two yarn ends together. Two multifilament yarns are introduced into a splicing chamber from opposing ends in an overlapping relationship, and are subjected to a blast of compressed air. Once the air blast enters the splicing chamber, it creates two contra-rotating vortices, which displace the individual filaments of the yarns, causing them to intermingle in a distinctive and reproducible manner. As a result, a neat strong bond between the yarns is produced [1].

In industry, manufacturers require certain splicing characteristics from a spliced joint [2, 3]. The principal requirement is for splice strength, however, good splice appearance may also be required in specific cases where the resulting product needs to be snag-free to be accepted by the end user [4].

In real pneumatic splicers, increase of yarn count usually demands an increase of the cross-sectional area of the splicing chamber. The relevance of variation of splicing chamber cross-section can be understood very simply. Consider a splicing chamber, which is optimized for a particular yarn. If the yarn dtex increases, then the characteristic diameter of the yarn will increase. At some point, the cross-section of the chamber may be such that there is simply not enough room in the chamber for free fiber intermingling to take place. Indeed, if the yarn count increases sufficiently, fibers will become so closely packed in the chamber that there will be essentially no filament motion. In these circumstances, the logical option is to use a chamber of larger cross-section to accommodate the increased yarn size.

This approach may yield a strong splice, but it frequently degrades the splice appearance, an effect which may be critical in some textile processes. It may increase the filamentation in the splice, and may yield more prominent tail ends [5]. This aspect of splicing has been addressed in some detail by us in earlier papers [6, 7].

Merely increasing chamber cross-section therefore is not a complete solution to splicing of high-count yarns. There is a further and ultimately more important factor which needs to be considered when considering increasing yarn count. This factor is the fixed geometry of the splicer itself and limits the splicing performance regardless of changes in chamber design. Total splicing length is controlled by the separation of the splicer knives. Therefore, 'knife separation' will be used hereafter to represent the total splicing length. In a simple continuous filament yarn in which the individual filaments remain largely intact during the splicing operation, the length of the splice corresponds very closely to the knife separation, as shown in

[1] Corresponding author: e-mail: cjwebb@glam.ac.uk

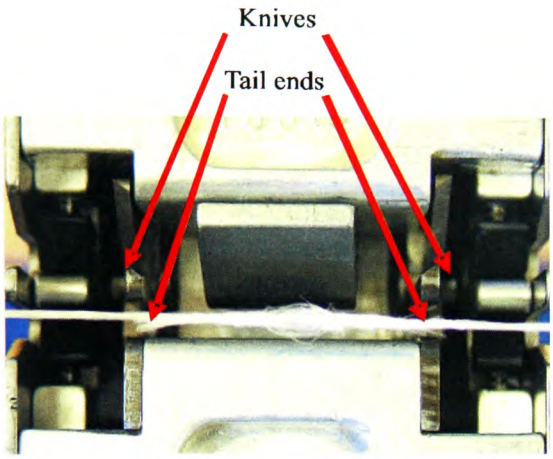

Figure 1 Comparison between knife separation and splice length.

Figure 1. Thus, the absolute splice length is approximately constant, irrespective of yarn count.

For simple engineering reasons, on a commercial splicer, knife separation is fixed. Once a splicer design is finalized, then the splice length for that particular splicer cannot be altered. As the yarn count increases, the cross-section of the yarn will increase, while the splice length remains constant. Therefore, the ratio between splice length and splice diameter decreases. So as yarns get bigger, the absolute splice length remains constant, but the relative splice length is reduced, as shown in Figure 2.

At some point, this reduction of relative splice length might be expected to have an adverse effect on the splice quality. For the purposes of this report, the phenomenon will be described as 'scaling'. It should be noted that the word 'scaling' is an arbitrarily selected term. It has no quantitative significance, but is merely used as a shorthand device throughout this paper; it attaches a convenient name to the hypothesis that there is a necessary relationship between the physical scale of the whole splicer and the physical size of the yarn.

There has been little or no published work on the subject of scaling, therefore, an analysis of the relevance of scaling the splicer geometry and chamber parameters may prove fruitful.

This paper addresses the input parameters which affect splice strength, as the yarn count is changed, specifically knife separation, splicing chamber cross-section, and splicing chamber length. It confirms that the scaling phenomenon exists, and that it is a powerful factor in determining the performance of pneumatic yarn splicers.

Figure 2 Comparison of relative splice lengths using 1100 and 11000 dtex yarn counts.

Materials and Equipment

An industry-standard polyester fiber was used starting from 1100 dtex, 72 filaments increasing uniformly in steps of 1100 dtex over the full experimental yarn count range. The test samples for a given dtex were taken from a single bobbin to minimize variability [6].

The requirements of the experimentation demanded the following:

- Variation of knife separation distance.
- Variation of splicing chamber cross-sections.
- Variation of splicing chamber lengths.

There were two variations of knife separation distance:

- The standard splicer design, with a knife separation distance of 32 mm.
- A hybrid splicer design, with a knife separation distance of double the standard splicer design, of 64 mm.

The hybrid splicer design is shown in Figure 3. The increased length was achieved by the use of large splicer body extensions, which can clearly be seen in the illustration.

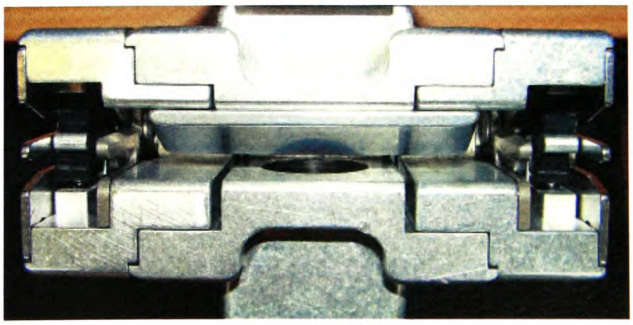

Figure 3 Hybrid splicer design.

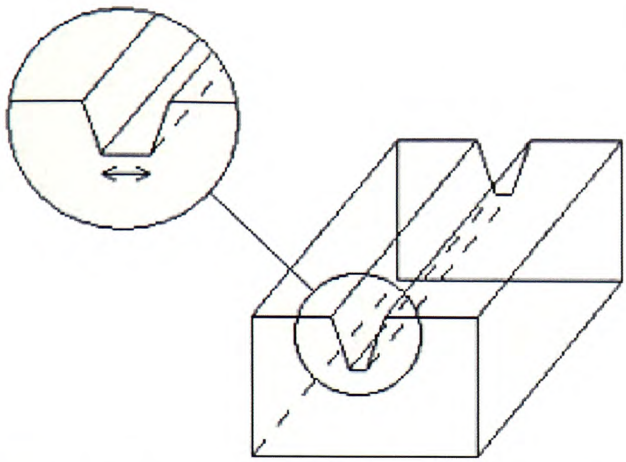

Figure 4 Chamber width design variations (increased width shown by inset).

An infinite number of splicing chamber cross-sections are possible. Our earlier work used some comparatively simple trapezium sections, therefore, the same chambers were used for this series of experiments to enable direct comparisons with the previous baseline research [7]. These chambers were (Figure 4):

- Chamber 4483 – a chamber with a simple 30° profile, 4.8 mm deep, and with a width diverging from 0.8 mm at the base.
- Chamber 4485 – a chamber with a simple 30° profile, 4.8 mm deep, and with a width diverging from 1.25 mm at the base.

Four key splicing chamber lengths were used, as shown in Figure 5. The chamber lengths were based on the straight splicing chamber of 16 mm, in the 4483 and 4485 profiles as specified above. The normal 16 mm production chambers, described in this report as '4483 straight' and '4485 straight', were used throughout to represent existing splicing practice. In most experiments, the chosen chamber was fitted to the standard commercial splicer, but in some cases it was used in the hybrid splicer for direct comparisons. From previous studies, both chambers performed consistently, therefore, only the 4483 profile was used for comparisons in chamber length.

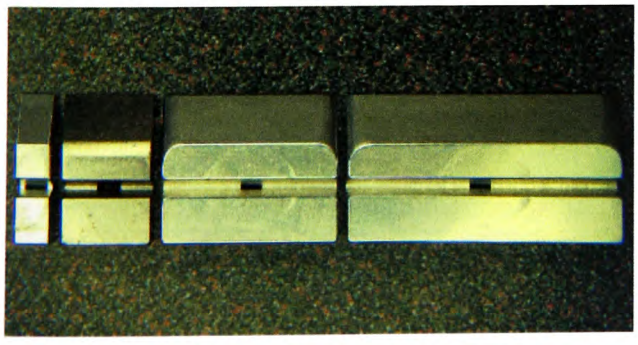

Figure 5 Variation on chamber lengths from left to right are 4483 small, straight, medium, and long, respectively.

The three variations on the straight chamber length were:

- A chamber of double the standard length, of 32 mm with a 4483 profile. This chamber, described in the report as '4483 medium', was selected so that, when it was fitted into the hybrid splicer, it maintained the same ratio between chamber length and knife separation as that which prevailed on the original splicer and chamber configuration.
- A chamber of three times the standard length, of 48 mm with a 4483 profile. This chamber, described in the report as '4483 long', was selected for use on the hybrid splicer to maintain the same distance between the chamber ends and knife assemblies to that which prevailed on the standard splicer and straight chamber configuration.
- A very short chamber with overall length of 6 mm, with a 4483 profile. This chamber, described in the report as '4483 small', was not designed to maintain any particular spatial relationship. It was the shortest possible chamber which could be manufactured to fit the splicer. It was selected to illustrate an extreme case of the effect of splicing chamber length on splicing performance.

The compressed air supply was dried via a Dominick Hunter Dryer (type CRD refrigeration dryer), and filtered by an air filter (type AW30-F03D) and mist separator (type AFM30-F03D). This air preparation was used to create consistent air properties, improving the reliability of the experimental results.

Compressed air pressure was controlled using an electro-pneumatic regulator (type ITV2050-312BS3-Q).

All the spliced yarn joints were prepared on the GTW Developments Model 1–11 and its hybrid variation, pneumatic splicing devices [8].

Tensile strength of the test samples was measured using a Lloyd Instruments tensile testing machine (Type T5000) with a 100 mm/min crosshead speed.

Splice appearance of the test samples, measured under controlled tension, was assessed by examining digital photographs taken on a digital camera at 2016x1512 resolution embedded into a microscope.

All the equipment was controlled and results collected electronically using an ARM7 control board and a PC to minimize human error. The experimental set-up used is shown in Figure 6.

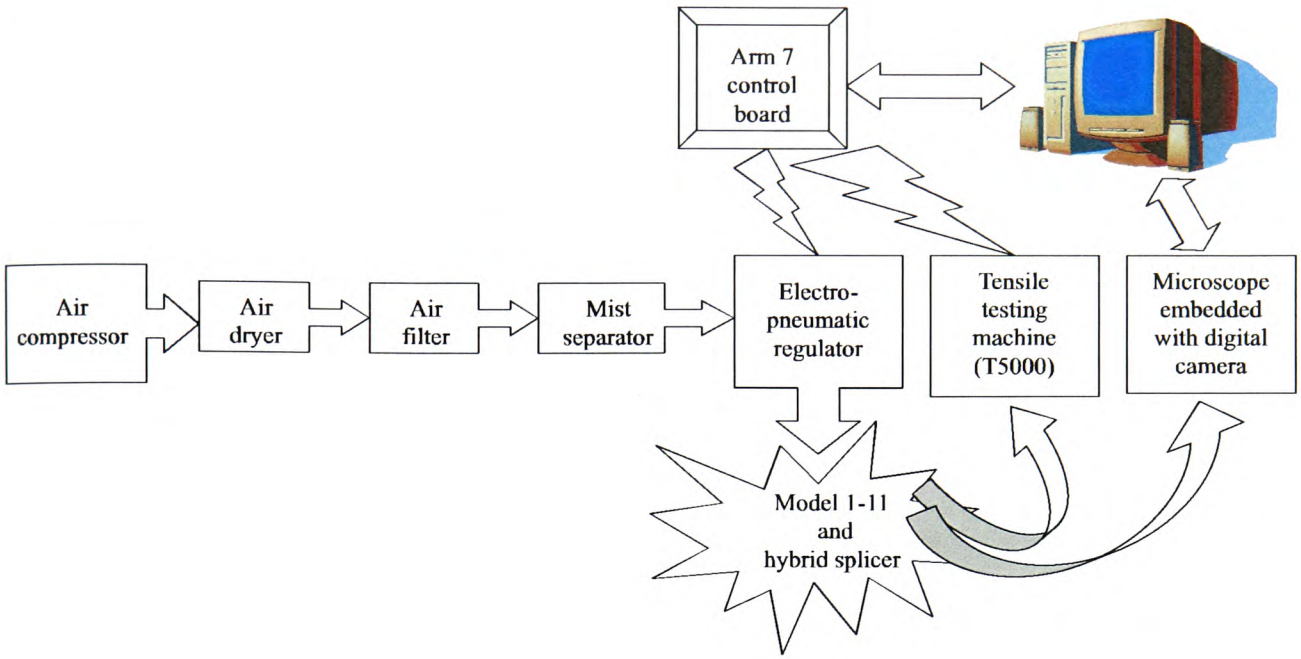

Figure 6 Experimental set-up.

Experimental Method

Earlier work by us [7] identified a number of factors thought to have an effect on the tensile strength and appearance of the splice and determined an optimum compromise between the two [9]. Work reported in these papers was conducted on a specific yarn of a specific count using a specific splicer. No account was taken of the effect on splicing performance due to varying yarn count, although it was suggested at the time that yarn count could have an effect. This paper addresses this point while expanding the range of observations.

In order to ensure consistency with the earlier work stated above, the same experimental test set-up was retained. For the purpose of the experiment, a polyester yarn of 1100 dtex, 72 filaments was used as the base product.

It was necessary to choose a means of achieving higher yarn counts. With a standard continuous-filament yarn, count can be changed by altering a number of parameters. For example:

- Keeping the filament dtex constant and doubling the number of filaments can double count.
- Keeping the number of filaments constant and doubling the dtex of each filament can double count.

In this research, yarn count was increased by increasing the number of filaments. This approach simplified the analysis by keeping the bending stiffness of each filament constant. So multiples of the 1100 dtex yarn count were assembled over the full range of yarn counts experimented with.

The principal aim of the experimentation described in this report was to identify the relationship between splice quality and yarn count, with particular attention being paid to the following three major variables, splicing chamber cross-section, splicing chamber length, and knife separation. Two experimental methods were undertaken to analyze these major variables individually.

The first experiment dealt with splicing chamber cross-section and knife separation. The experimental splicing chambers of different cross-sections were used to determine how splicing performance deteriorated as yarn count increased to a point where the scaling factor became too large for a particular section. Once the performance of splicing chambers in a standard splicer had been assessed, the changes of splicing performance in the hybrid splicer were measured.

The second experiment dealt with splicing chamber length and knife separation. The experimental splicing chambers of different lengths were used to determine whether chamber length had any significant effect on splice characteristics. Knife separation distance was altered, thereby

Table 1 Selected splicing parameters.

Factor	Parameter	Level 1	Level 2	Level 3	Level 4
A	Chamber length	6 mm	16 mm	32 mm	50 mm
B	Blast pressure	40 psi	55 psi	70 psi	85 psi
C	Chamber cross-section	0.80 mm	1.25 mm	N/A	N/A
D	Yarn count	2200 dtex	6600 dtex	N/A	N/A
E	Knife separation	32 mm	64 mm	N/A	N/A

examining the relationship between varying chamber length and knife separation.

The experimental set-up was consistent with that used in our earlier work to maintain a level of consistency among all elements of the research [6, 7]. As before, the principal measure of splice quality was taken as the splice strength. Splice strength was measured by its 'spliced retained strength' (SRS). SRS is the strength of the spliced yarn expressed as the percentage of the parent yarn in which the splice was inserted [10]. Equation (1) illustrates this relationship.

$$SRS = \frac{Spliced\ yarn\ strength}{Parent\ yarn\ (non\text{-}spliced)} \times 100 \qquad (1)$$

Splice appearance was measured on an arbitrary scale and was only recorded as acceptable or not due to splice strength being the dominant factor analyzed throughout the experimentation [11, 12]. Blast duration and cutting synchronization were consistent throughout the experimentation and were therefore disregarded.

The first experimental set-up was undertaken with a 4483 straight chamber in a standard splicer, to splice yarn counts over the full range. For each yarn count, splicer and chamber configuration, the pressure was varied between 20 psi and 90 psi with SRS and appearance recordings taken at intervals of 5 psi.

The same experimental set-up was subjected to the same range of experimental conditions, but with a 4485 straight chamber fitted into the standard splicer.

To compare splicing chamber cross-section and knife separation, the standard splicer was now replaced with the hybrid splicer and was subjected to the same range of experimental conditions with using both the 4483 and 4485 straight chambers.

It had been established throughout the first experiment that both chamber cross-section and knife separation were directly associated with splicing performance as yarn count varied. The next stage sought to examine whether splicing chamber length was a significant factor, therefore, only the 4483 chamber profile was selected for experimentation over two key yarn counts. These yarn counts were:

- 2200 dtex – both the 4483 and 4485 chambers performed satisfactorily.
- 6600 dtex – the 4483 chamber had begun to fail, but the 4485 chamber continued to perform well.

The second experimental set-up was undertaken using the chosen two key yarn counts with the range of 4483 chamber lengths in a hybrid splicer. For each yarn count, splicer and chamber configuration, the pressure was varied between 20 psi and 90 psi with SRS and appearance recordings taken at intervals of 5 psi.

To compare splicing chamber length and knife separation, the same experimental set-up with the standard splicer replacing the hybrid splicer, was subjected to the same range of experimental conditions with one exception. Only the 4483 straight and 4483 small chambers were available for experimentation due to the knife separation restriction of the standard splicer.

A Taguchi design of experiment (DOE) was implemented to distinguish the dominant factor levels and the statistically significant factors. The factor levels selected for the Taguchi analysis are displayed in Table 1.

Results

Figures 7 and 8 show the variations of SRS for the first experimental set-up, using the 4483 and 4485 straight chamber, respectively, in a standard splicer over a yarn count range of 1100 to 9900 dtex in steps of 1100 dtex. Only a range of 9900 dtex has been shown due to the 4483 straight chamber failing and not producing any splices of significant quality at higher yarn counts. This range was displayed for all results for direct comparisons.

To analyze the effect knife separation had on splice quality, the experimental method was repeated, but with the standard splicer being replaced with the hybrid splicer. The results for the 4483 and 4485 chambers using the hybrid splicer are shown in Figures 9 and 10, respectively.

Each of the nine curves in the preceding charts demonstrated that, for a given splicing chamber and a given yarn, there was a peak SRS. For any given yarn, after the peak, SRS decreased with increase of pressure (as filament dam-

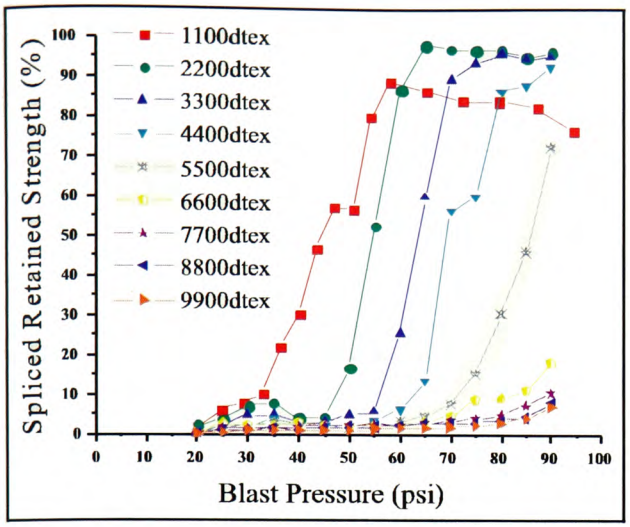

Figure 7 Variation of SRS with air pressure and yarn count using standard splicer and 4483 straight chamber.

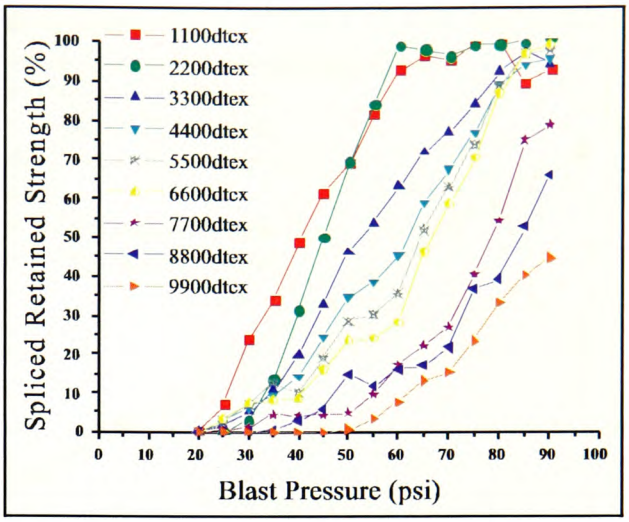

Figure 9 Variation of SRS with air pressure and yarn count using hybrid splicer and 4483 straight chamber.

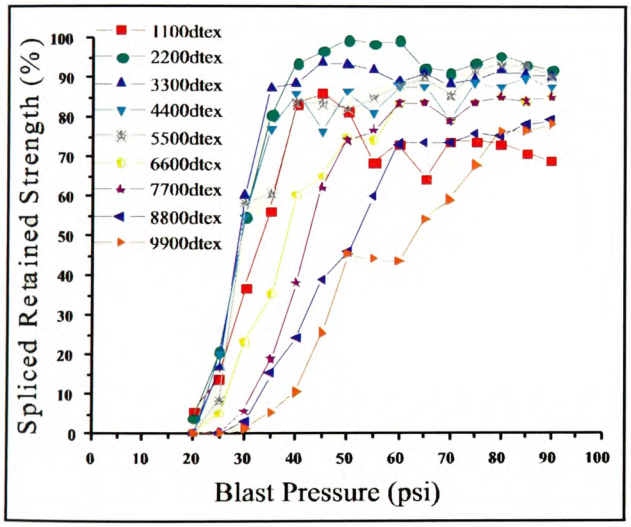

Figure 8 Variation of SRS with air pressure and yarn count using standard splicer and 4485 straight chamber.

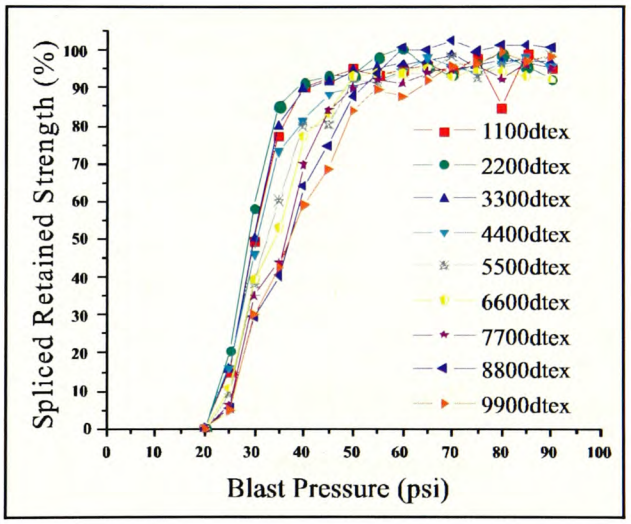

Figure 10 Variation of SRS with air pressure and yarn count using hybrid splicer and 4485 straight chamber.

age occurred). As yarn count increased, the curves shifted along the x-axis, demonstrating that higher pressures were required as the yarns began to occupy more and more of the chamber profile. As they stand, these results were not particularly easy to understand. However, close analysis eventually revealed a pattern, which related to the behavior of different chambers, as yarn count increased.

It was possible to represent the results in a manner which yielded a clearer understanding. For each specific splicer configuration, the highest splice strength was recorded for each yarn using an absolute instead of a relative measure for splice strength. This yielded a series of curves, showing how each splicer configuration performed as yarn count changed over the full yarn count range experimented with. This approach yielded the curves shown in Figure 11.

It was clear that knife separation had an effect on the splicing performance, but was only analyzed at a constant

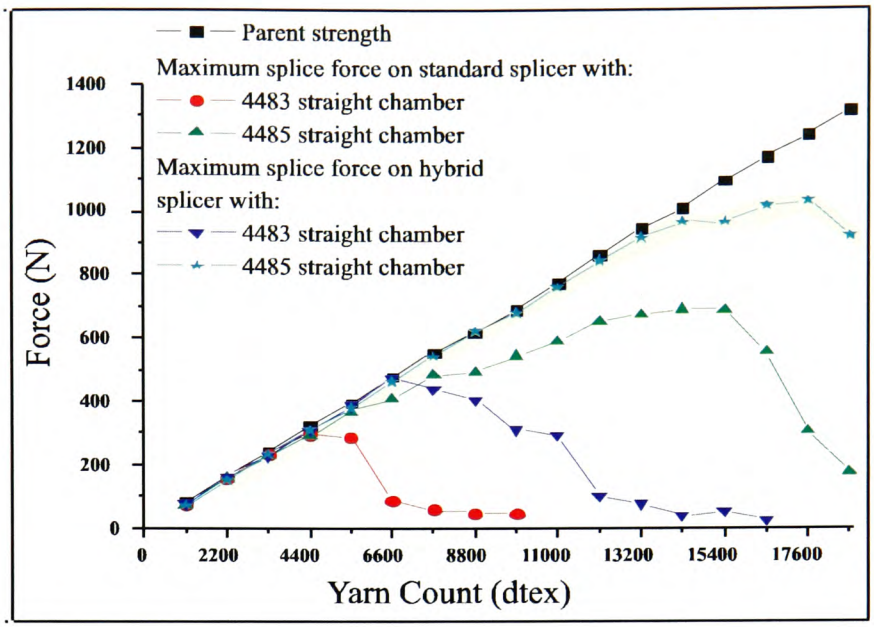

Figure 11 Yarn count range for both 4483 and 4485 straight chambers using the standard and hybrid splicers.

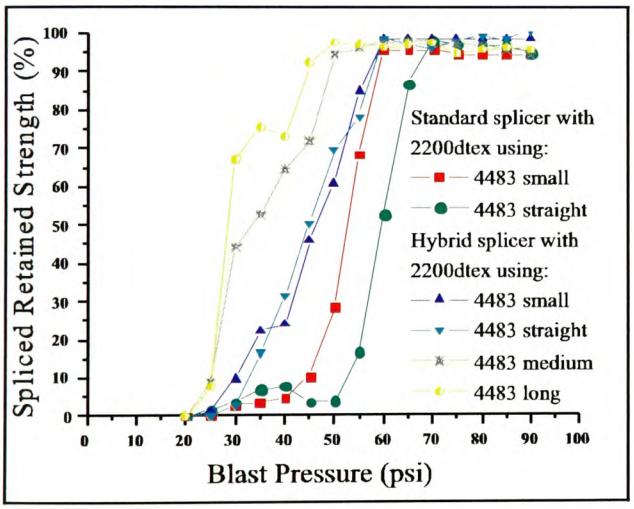

Figure 12 Comparison of 4483 chamber length range using hybrid splicer with 2200 dtex.

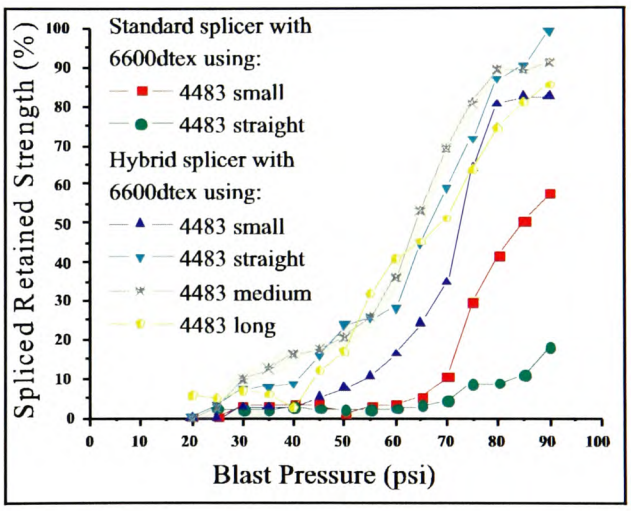

Figure 13 Comparison of 4483 chamber length range using hybrid splicer with 6600 dtex.

chamber length. Therefore, splicing chamber length was analyzed using both splicers. Figures 12 and 13 show the variations of SRS for the second experimental set-up using the 4483 chamber length range with the standard and hybrid splicer, respectively.

Figure 14 reveals the outcome of the Taguchi DOE analysis. As can be seen, the dominant factor levels were:

Factor A: Level 1 = 6 mm.
Factor B: Level 3 = 70 psi.
Factor C: Level 2 = 1.25 mm.
Factor D: Level 1 = 2200 dtex.
Factor E: Level 2 = 64 mm.

The results of the analysis of variance (ANOVA), as shown in Table 2, revealed that factors A, B, and E were statistically significant at 95%, with factors B and E being statistically significant at 99%.

Table 2 ANOVA of each splice characteristic.

Spliced retained strength (SRS)

Factors	DOF	SS	MS	*F* ratio
A	3	19088.57	6362.86	3.83*
B	3	129982.39	43327.46	26.08**
C	1	1864.62	1864.62	1.12
D	1	4956.18	4956.18	2.98
E	1	158294.91	158294.91	95.30**
AE1	3	9364.98	3121.66	1.88
AE2	3	11549.36	3849.79	2.32
Error	307	509953.83	1661.09	*******
Total	319	836839.85	*******	*******

*Indicates factor/interaction was statistically significant at 5% level of significance – $F(0.05,1,307) = 3.87$; $F(0.05,3,307) = 2.63$.
**Indicates factor/interaction was statistically significant at 1% level of significance – $F(0.01,1,307) = 6.72$; $F(0.01,3,307) = 3.85$.
DOF = degrees of freedom; SS = sum of the squares of deviation; MS = mean square error; *F* ratio = the ratio used to determine whether the variances in two independent samples are equal.

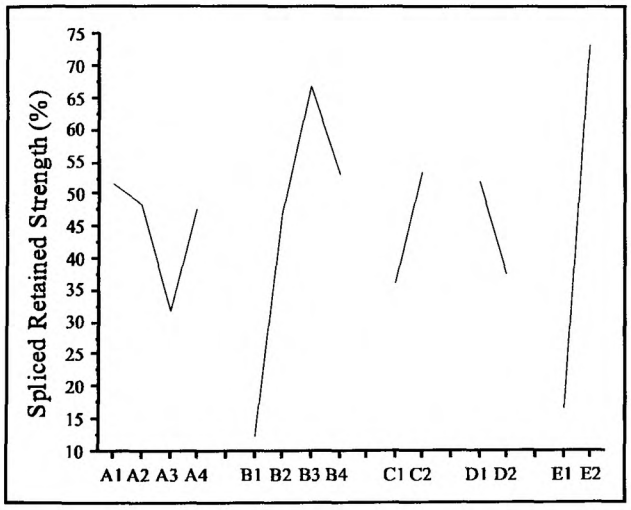

Figure 14 Mean response plot.

Discussion

At the outset of this work, long field experience had shown that as yarn count increased, it was necessary to increase splicing chamber cross-sectional area. However, everyday experience also seemed to show that cross-sectional area provided only limited benefit; once yarn count increased beyond a certain point, increasing cross-sectional area offered no further improvement. Put simply, very large yarns proved impossible to splice, even when splicing chamber cross-sections became very large. This was counter-intuitive in that chambers which comfortably accommodated the largest of yarns, failed to produce a satisfactory splice.

Therefore, it was clearly necessary to determine whether this ultimate failure of splicer performance was real, and whether splicer design characteristics other than chamber cross-section could be playing a part.

The results from the first experimental set-up revealed some interesting factors on how splicing chamber cross-section and knife separation had an effect on splicing performance. Figure 7 indicates fairly clearly that results on the 4483 chamber were acceptable up to 4400 dtex, provided that air pressures were increased as yarn count rose. It also reveals that the performance of the 4483 became completely unacceptable above 5500 dtex. This was thought to be the result of the yarn simply becoming too big for the chamber, so that little or no filament movement could occur.

Figure 8 reveals that the larger 4485 chamber cross-section coped much better with the larger yarn counts and produced greater SRS at lower air pressures. Up to yarn counts of 7700 dtex, the chamber still reproduced consistently strong splices, whereas above this yarn count, the chamber began to falter as splice strength progressively decreased as yarn count increased. This improved performance was thought to be the result of a greater volume within the chamber to accommodate the larger yarn counts, enabling filament movement and thus intermingling to occur.

This improved yarn count range through increased cross-sectional chamber width came at a price. The splice strength remained consistently high, but consequently the splice appearance was deteriorating, as shown in Figure 15. This was presumably due to the same reason as previously

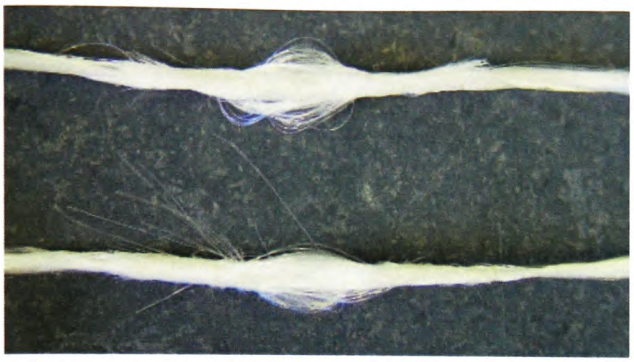

Figure 15 Splice appearance comparison between chamber cross-sections of 0.80 mm (top) and 1.25 mm (bottom).

described. Therefore, a trade-off between splice strength and appearance will occur. These results were consistent with years of field experience.

The hybrid comparison using the 4483, shown in Figure 9, revealed that the increase in knife separation drastically improved the chamber's performance and increased its yarn count range to approximately double. The rise in SRS of yarn counts, as air pressure was increased, was consistent with the standard splicer up to the point where the standard splicer failed. It was believed that if the air pressure was to increase to more than 90 psi, the SRS would continue to increase for the higher yarn counts. This was not proven due to the limitations of our experimental setup. Figure 10 revealed that the increased knife separation had the same effect on the 4485 straight chamber, increasing its yarn count range and improving consistency.

As can be seen from Figure 11, with the 4483 straight chamber fitted in the standard splicer, performance deteriorated markedly once the yarn count exceeded approximately 5500 dtex. Splice strength was actually reduced, presumably because the yarn was too big for the chamber, and filaments could no longer move freely. With the 4485 straight chamber, yarn count began to influence splice strength after approximately 7700 dtex. However, the effect was small, meaning there was not a reduction of absolute strength, only a reduction in the rate of rise of splice strength. The real deterioration of the chamber's performance only occurred above approximately 15400 dtex.

The performance of the hybrid splicer with the 4483 straight chamber fitted did not begin to deteriorate until the yarn count exceeded roughly 7700 dtex. Once the deterioration started, the rate of reduction was less than that of the case with the standard splicer. With the 4485 chamber, strength was barely affected at all until approximately 14300 dtex. The chamber's performance began to deteriorate at a rapid rate above a yarn count of 17600 dtex.

Splice appearance was still degraded using the 4485 straight chamber with the hybrid splicer. Therefore, the main conclusion to emanate from these results was that increased knife separation improved the chamber's performance and, therefore, a smaller profile chamber could be used at a higher yarn count to improve its appearance. Taken together, these results indicated that both chamber cross-section and knife separation had an effect on splicing performance.

The increase in the splice performance through increasing the knife separation was presumably due to the increased number of crossovers that occurred between the yarn ends, therefore, increasing the frictional forces between individual filaments. This was too large a subject to include here and will be analyzed in greater detail in a future paper.

The increased performance was consistent between both chamber cross-sections. Therefore, the hybrid splicer improved the chamber's performance by a set amount, which concurred with our initial predictions that there was an increased number of crossovers throughout the increased splice.

It was found from Figure 12 that with a yarn count of 2200 dtex, the 4483 straight chamber performed the greatest at higher air pressures, while using the hybrid splicer, improving its performance range compared to other chamber lengths. At lower air pressures, the 4483 long had the sharpest incline in SRS. With the standard splicer, both 4483 straight and small chamber length performed consistently at higher pressures, with the 4483 small chamber producing splices at lower air pressures.

It was not until the 6600 dtex yarn count was analyzed (Figure 13) that the chamber lengths began to reveal interesting conclusions. With the standard splicer, the 4483 straight chamber failed at this yarn count, but what was astonishing was that the 4483 small chamber produced acceptable splices at higher air pressures. Therefore, the reduction in chamber length improved splicer performance. The hybrid results were similar compared with the 2200 dtex results in that the 4483 medium had the greatest incline in SRS and the 4483 straight produced the maximum SRS at the higher air pressures. From these findings and the Taguchi analysis, it was clear that there was an optimum ratio between chamber length and knife separation.

The appearance of the resulting splices over the splicing chamber length range varied slightly with the larger chambers, producing better splice appearance, but of little improvement compared to the smaller length chambers, as shown in Figure 16. Thus, the main performance increase in chamber length was towards the splice strength.

Throughout the experimentation to analyze the relationship between splicing chamber length and knife separation, taken together, it was found that the 4483 small performed the greatest with the standard splicer. This was presumably due to reduced restrictions on the airflow, therefore, increasing the airflow within the splicing chamber. The 4483 straight produced the best in the hybrid

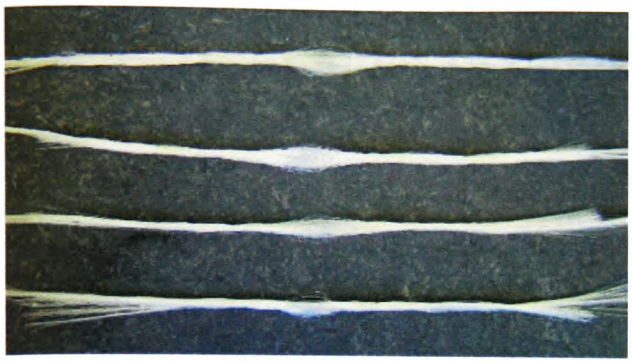

Figure 16 Splice appearance comparisons over the whole tested chamber length range of 6 mm (bottom) to 50 mm (top).

splicer, presumably due to the same reasons as in the standard splicer, but with the acceptation of the 4483 small being too large a gap between the tail ends of the yarns and the chamber ends to maintain the yarn ends under control. These results indicated that both splicing chamber length and knife separation had an effect on splicing performance.

Overall, these observations represent powerful evidence for the existence of scaling. When count increases sufficiently, performance levels can only be maintained if:

- The splicing chamber cross-section becomes larger.
- The airflow increases.
- The knife separation increases.

Conclusion

The results of our experimentation observations revealed powerful evidence for the existence of scaling. This verification of the existence of the effect called scaling is likely to be of profound importance to the design of splicers for very large yarns and tows. If a yarn is sufficiently large, it will not be sufficient merely to provide a larger splicing chamber cross-section. Splicers for such materials will probably need special provision for greatly improved air supply and increasing knife separation. The demands placed by the vastly increasing yarn geometry in industry will be such that splicers will almost certainly become too big to be hand-held. These results have not been observed in published literature to date.

Our research indicated that increasing the knife separation vastly improved the yarn count range a given splicing chamber could handle before failing to create acceptable splices. This finding enabled smaller cross-sectional splicing chambers to splice larger yarn counts, thus improving the resulting splice appearance. The comparative smaller chamber (to a certain degree) in both splicers improved splicing performance, but the resulting splice appearance was slightly degraded compared with the longer chambers. It is evident that further work is required in this area to analyze the splicing process in detail and thus the splice creation. This work will be presented in a future paper.

Literature Cited

1. Cheng, S., and Fung, W. Y., Joining Yarn Ends Together by Pneumatic Splicing, *ATA J.* **15**(3), 40–45 (2004).
2. Lam, H. L. I., and Cheng, K. P. S., Pneumatic Splicing, *Textile Asia* **7**, 66–69 (1997).
3. Lappage, J., End Breaks in the Spinning and Weaving of Weavable Singles Yarns, *Textile Res. J.* **75**(6), 512–517 (2005).
4. Lewandowski, S., and Drobina, R., Strength and Geometric Sizes of Pneumatic Spliced Combed Wool Ring Spun Yarns, *Fibres Textiles East. Eur.* **12**, 31–37 (2004).
5. Mingjie, X., Peijie, H., Shihua, S., Bingchang, Q., and Tao, L., Study on Pneumatic Splice, *J. China Textile Univ.* **16**(2), 109–112 (1999).
6. Webb, C. J., Waters, G. T., Thomas, A. J., Liu, G. P., and Thomas, C., The Use of the Taguchi Design of Experiment Method in Optimising Splicing Conditions for a Nylon 66 Yarn, *J. Textile Inst.* **98**(4), 327–336 (2007).
7. Webb, C. J., Waters, G. T., Thomas, A. J., Liu, G. P., and Thomas, C., Optimising Splicing Parameters for Splice Aesthetics for a Continuous Filament Synthetic Yarn, *J. Textile Inst.* (in Press).
8. Waters, G. T., Pneumatic Yarn Splicer, Patent No: US5809761 (1998).
9. Hassen, M. B., Jaouachi, B., Sahnoun, M., and Sakli, F., Mechanical Properties and Appearance of Wet-spliced Cotton/Elastane Yarns, *J. Textile Inst.* **99**(2), 119–123 (2008).
10. Sengupta, S., Retained Strength of Air-spliced Yarn – Rupture Process and Effect of Test Length, *Indian J. Fibre Textile Res.* **25**, 277–283 (2000).
11. Cheng, K. P. S., and Lam, H. L. I., Physical Properties of Pneumatically Spliced Cotton Ring Spun Yarns, *Textile Res. J.* **70**(12), 1053–1057 (2000).
12. Lewandowski, S., and Stanczyk, T., Identification and Classification of Spliced Wool Combed Yarn Joints by Artificial Neural Networks, Part II: Interpretation of Identification and Classification Results of the Unknotted Spliced Yarn Joints, *Fibres Textiles East. Eur.* **13**, 16–19 (2005).

The use of visualisation and simulation techniques to model the splicing process

C. J. Webb[1], G. T. Waters[2], G. P. Liu[1], E. J. C. Thomas[1]
[1]*University of Glamorgan, Trefforest, Wales, United Kingdom*
[2]*GTW Developments Ltd., Pontypool, Newport, United Kingdom*

Abstract: Pneumatic yarn splicing is a well-established technique for joining two yarn ends together by means of a blast of compressed air in a device known as a splicing chamber. Earlier research done by Webb *et al.* (2007) optimised external splicer parameters, such as air pressure and duration, for maximum splice strength, using experimental data only. Indirect observations such as air pressure offer no insight into the theory behind the splicing process. Observing the splice formation with the naked eye is difficult because of the short duration and sealed environment of the splicing process. This paper reports on the application of visualisation and simulation techniques to the theoretical study of the splice formation.

Keywords: Splicing, Chamber design, CFD, Visualisation, Simulation, Modelling.

INTRODUCTION

Companies in the textile industry traditionally joined yarns from two bobbins by various forms of knotting. As consumer quality requirements became ever more demanding, knotting as a solution proved inadequate. Pneumatic splicing was devised to overcome the deficiencies of knotting.

Splicing is simple in principle but is very complex when investigated in detail. The splicing process involves introducing two staple or multifilament yarn ends into a device known as a splicing chamber, usually from opposing ends, in an overlapping relationship. Splicing chambers come in a variety of forms; a common chamber profile, model 4483 straight, is shown in Figure 1. The 4483 straight has a basic V shaped geometry with the following dimensions:

- 30 degree profile
- 4.8 mm deep
- 0.8mm width diverging the base

Once the yarn ends are placed in the chamber, they are secured in place by closing the chamber lid. The chamber lid prevents the yarns from escaping and creates the confined space needed for the splicing process to take place. The yarns are then subjected to a high pressure turbulent flow of compressed air (Reynolds number typically of the order of 10^5). The compressed air excites the filaments into intermingling through a complex aerodynamic process of contra rotating vortices and small scale disturbances. As a result, a neat strong bond between the yarns is produced (Cheng and Fung, 2004).

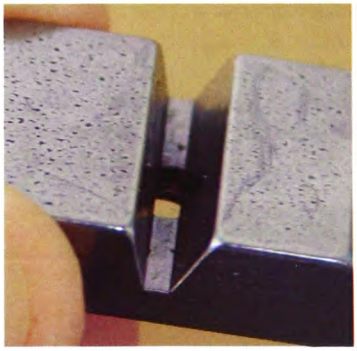

Figure 1 – 4483 straight chamber

Previous works by Webb *et al.* (2007, accepted 2007), revealed that splice consistency and strength are closely associated with the design of the splicing chamber and the pressure of the air supply (Mingjie *et al.*, 1999). In the textile industry, manufacturers require spliced

yarns to resemble closely the characteristics of the original yarn (Lewandowski and Drobina, 2004). This is made even more difficult by the fact that splices made under the same conditions have a certain amount of variation within them.

The processes involved in pneumatic splicing are far more complex than first appears. Moreover, the small scale of the splicing chamber and the very high levels of turbulence, make direct observation of the splicing process almost impossible. Most research into splicing has therefore avoided direct observation, relying instead on a more indirect approach, and concentrating on external parameters, which are simple to measure. For example, work done by Cheng and Lam (2003), addressed the effect of variables such as air pressure upon splice strength and appearance to optimise the splicing process. However, they did not offer any theory behind how a splice is formed or offer any comment about how splicing parameters interact to produce splice characteristics.

Such indirect observation on experimental data only, is valuable up to a point, in that it does at least allow operators to establish optimum splicing conditions for a particular application. However, indirect observation offers no insight into the mechanism of how a splice is formed, and of the detailed processes, which produce splice characteristics such as strength. Understanding of the process of splicing has failed to move beyond the qualitative. To date, little or no theoretical knowledge has been published about what actually occurs within the splicing chamber during the splicing process.

This conclusion is to some extent borne out by the wide diversity of splicing chamber designs used by various companies in the industry. It is interesting to note that all these different forms of splicing chambers produce results that are broadly similar, i.e. splices of adequate strength and appearance that perform well in the textile environment. The inference must be that all the diverse chamber designs create similar splices by somehow producing comparable key airflows within the splicing chamber.

Observing the splice formation with the naked eye is difficult, because the splicing process is completed quickly, and is enclosed in a sealed environment. Various direct techniques have been used in attempts to observe the splice formation, but all have failed. Therefore different visualisation and simulation techniques have been implemented, with varying degrees of success, to simulate the splicing process.

A typical splice structure looks random at first but when analysed in greater detail, an underlying order emerges, with certain key process components contributing specifically to splice characteristics. The airflow within the splicing chamber is the most important single component in deciding the resulting splice formation (Oxenham and Basu, 1993).

The principal aim of the work described in this paper was to identify and compare the airflows within a particular form of splicing chamber, using visualisation and simulation techniques, which are commonly used in many branches of research (Lamar, 2001; Haber, 1990; Daws *et al.*, 1965). These visualisation and simulation techniques were used to analyse the airflows in the specimen splicing chamber.

The visualisation technique, which involved true splicing, addressed the problems of the speed of the process, and the lack of visual access to the splicing chamber by using a scaled model of a typical splicing chamber, made of transparent plastic.

The simulation technique used CFD software to model airflows in a range of different splicing chamber forms.

EXPERIMENTAL METHOD

Visualisation technique – Large scale model of splicing chamber

This visualisation technique used a model of a standard 4483 trapezium chamber, manufactured to a scale of 10:1 with a length equivalent of 10mm. This form of chamber was chosen, because it has been used throughout this research programme, and its performance envelope was well understood (Webb *et al.*, 2007). The form of the chamber is shown in Figure 2.

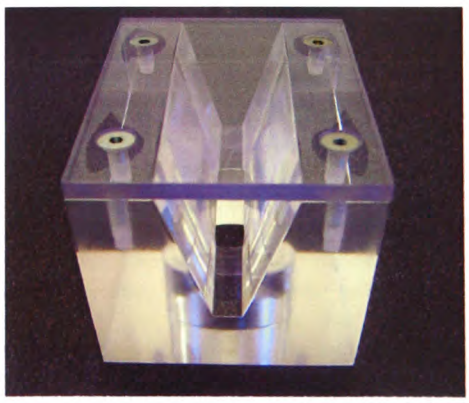

Figure 2 – Scaled model of the 4483 straight splicing chamber

As mentioned previously, the airflow within a splicing chamber is highly turbulent, with a Reynolds number typically of the order of 10^5. The Reynolds number is a dimensionless flow constant which characterises the airflow properties within the splicing chamber. The change of chamber dimensions had an effect on the Reynolds number, but it was necessary to keep the number constant, if the scaled chamber were to give an accurate representation of the original airflow within the normal 4483 straight chamber. To achieve this goal, it was necessary to change some of the splicing parameters.

A more accurate value for Reynolds number for the airflow within a 4483 straight chamber at 6.33kgf/cm^2 was approximately 64000, calculated from Equation 1 below.

$$\text{Reynolds number (Re)} = \frac{Vs \cdot L}{U_{air}} \qquad \text{(Eq. 1)}$$

Where

Vs = Mean fluid velocity

L = Characteristic length (diameter if tube)

U = Kinematic fluid viscosity

$$and\ U = \frac{\text{Absolute fluid viscosity}}{\text{Fluid density}}$$

The simplest way to maintain constant Reynolds number in the experimental chamber was to use a fluid, which had a higher density and viscosity than air. Water was the ideal candidate, because it was transparent, easily handled, and had a combination of physical properties which yielded a Reynolds number of the right magnitude. The new fluid flow rate was calculated using Equations 1 and 2:

$$Vs = \frac{\text{Re} \cdot U_{water}}{L_{scaled\,model}}$$

Where

$$U_{water} = 1.002 \times 10^{-6} m^2 s^{-1}$$

$$\therefore Vs = 1.6 ms^{-1}$$

Therefore

$$Vs = \frac{Volume\ flow\ rate\ (m^3 s^{-1})}{Chamber\ profile\ area\ (m^2)} \qquad \text{(Eq. 2)}$$

$$\therefore Volume\ flow\ rate \approx 1.6 ls^{-1}$$

The flow rate calculated above was representative of blast pressure of 6.33kgf/cm^2, for air in the 4483 straight chamber.

Simulation technique – Computational fluid dynamics

This simulation technique used a CFD software package called Fluent along with its brother computer aided design (CAD) software, Gambit. The software was applied to create a 3D computer simulation model of the airflow within a wide range of splicing chamber designs. The purpose of the work was to gain some insight into the effect that chamber geometry had on the resulting airflow.

CFD and literature on its application to splicing is sparse. Zhou and Qin (2005), used the technique, but only for observation purposes, they made no attempt to apply their information to an understanding of the splicing process.

At this stage of the work, the CFD technique was not sufficiently powerful to model the behaviour of a multiplicity of individual fibres within a splicing chamber. Therefore it was necessary to ignore the presence of yarn end fibres within the chamber space. Nevertheless, the technique made it possible to compare and contrast the airflow patterns within different chambers, thereby identifying common characteristics.

The CFD simulation is commonly accepted as the numerical solution to the governing set of Navier-Stokes equations, equation of continuity and the additional conservation equations of momentum and energy. The partial differential equations that govern fluid flow are not amenable to analytical solutions, except for very simple cases. Therefore, in order to analyse fluid flows, flow domains are split into smaller subdomains. The governing equations are then discretised and solved inside each of these subdomains. The subdomains are called cells, and the collection of all cells is called a mesh (Fluent Inc., 2005a).

To create an accurate simulation model of the airflow within the splicing chamber a number of complex steps are required as described below:

- Create virtual entities of the fluid flow regions
- Generate a volume mesh for each region as required
- Export the mesh and apply computational fluid dynamics
- Analyse the 3D fluid flow throughout the entire entity

Firstly a 3D CAD geometry is created of the boundaries that enclose the fluid flow regions. Once the volume geometry is completed, a user defined mesh is generated over the whole geometry volume with a finer mesh created at key airflow locations, to improve accuracy. The CAD geometry and mesh generation created for a specimen chamber ready for exporting into Fluent is shown in Figure 3.

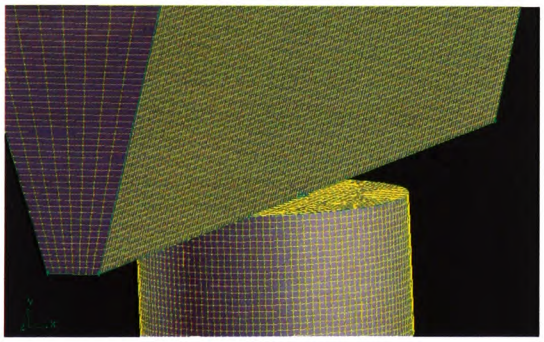

Figure 3 – CAD design and volume mesh generation for specimen fluid flow regions

Once the mesh had been generated, it was exported into Fluent for the computation stage. The result is an accurate 3D representation of the airflow properties, for the specified splicing chamber and splicing parameters.

The software is powerful, generating a great deal of information, such as velocity, mass flow rate and force magnitudes. It proved a useful tool for gaining an understanding of the turbulent flow structure. The application of CFD was very successful, which aids that this method could be used in any future study of pneumatic splicing. As will be described later in this paper, the CFD results were an essential element in the development of a new physical model of the splicing process.

The CFD model selected to analyse the fluid flow was the realisable $\kappa - \varepsilon$ turbulence model without the inclusion of fibres to simplify the fundamental study of the splicing process. A turbulence model was selected because of the very high Reynolds numbers in all known splicing processes.

An immediate benefit of the realizable $\kappa - \varepsilon$ model over the standard and Re-Normalisation Group (RNG) models is that it more accurately predicts the spreading rate of both planar and round jets. It is also likely to provide superior performance for flows involving rotation, boundary layers under strong adverse pressure gradients, separation, and recirculation. This was considered essential in modelling the splicing process, since high rotational airflows were known to exist in splicing chambers. The detailed arithmetical description of the selected turbulence model is shown in detail in Appendix 1 (Fluent Inc., 2005b)

Before the simulation results could be used for analyses, it needed to be validated. The CFD technique was first applied to the 4483 straight splicing chamber used in earlier work. The chamber had the same form as the large scaled model described earlier. The results of the simulation were compared with the flows observed in the scaled chamber, and shown to be very similar.

With the simulation accuracy validated, a range of chambers manufactured by leading industrial splicing companies were modeled. This permitted easy comparison between fluid flows in different splicing chamber designs, revealing how different designs achieved consistent splicing performance.

MATERIALS AND EQUIPMENT

Earlier splicing process research by Webb *et al.* (2007) had used a range of splicing chambers, including the chamber identified as 4483 straight (Figure 1).

The experimental splicing chamber was a 10:1 scaled version of the 4483 straight chamber with a length equivalent of 10mm, constructed in PMMA (Plexiglas, Perspex).

The scaled chamber was placed in a water tank, as shown in Figure 4.

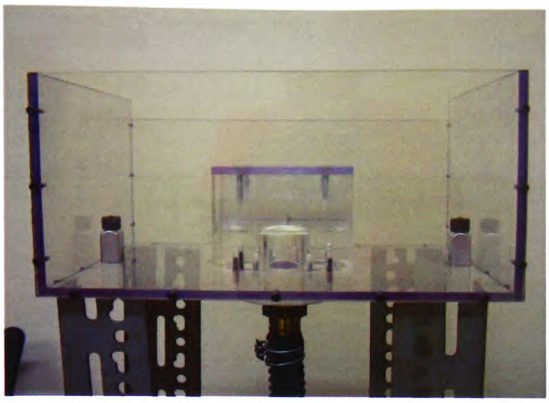

Figure 4 – Scaled chamber mounted in water tank

The water pump used was a Draper type SWP110. The pump was placed in a large bath of water beneath the scaled chamber. Water flow was controlled via a mechanical valve.

A high-resolution digital video camera was used to record the splicing process in both real time and still shots.

The CFD simulations and analysis of the digital video were conducted on a PC.

RESULTS AND DISCUSSION

The results that follow compare the representations of fluid flows, which emerged from the visualisation and simulation techniques.

Figure 5 shows the water flow within the large scaled chamber model, at conditions representative of air at 6.33kgf/cm^2 in a standard chamber.

As can be seen key fluid flow features emerge as follows:

- The principal vortices occupy all of the space between the outer edges of main jet and the outer edges of the chamber.
- There is only moderate reverse flow near the base of the chamber
- There appear to be regions where the flow separates from the roof of the chamber to left and right of the blast jet, particularly visible as a white sloping "shoulder" line on the left.

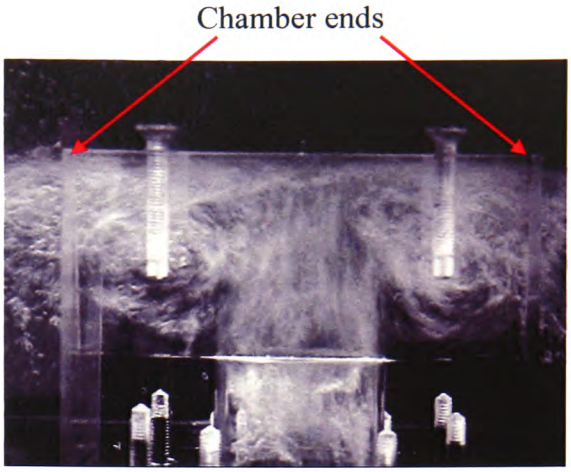

Figure 5 – Scaled model fluid flow

The first of two CFD simulations is shown in Figure 6. It represents the same chamber cross-section as the scaled chamber, but with a length equivalent of 16mm instead of 10mm. These key fluid flows emerged:

- The principal vortices do not occupy all of the space between the outer edges of main jet and the outer edges of the chamber.
- There is considerable reverse flow close to the base of the chamber
- There appears to be regions where the flow separates from the roof of the chamber to left and right of the chamber, but in this case the flow is much more clearly defined than in the scaled chamber.

Figure 7 shows the second of two CFD simulations. It represents a direct equivalent in chamber cross-section and length to that of the scaled chamber. Now the correspondence between this CFD simulation and the scaled chamber visualisation is startling:

- The principal vortices look very similar, occupying the same portion of the chamber.
- The reverse flow near the base of the chamber is modest
- The region of flow separation from the roof of the chamber is almost identical.

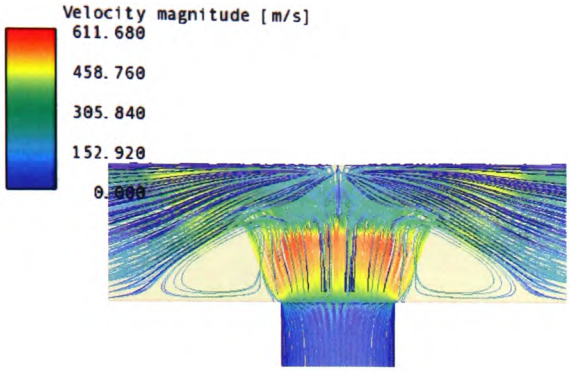

Figure 6 – CFD simulation representing 4483 chamber cross section, 16 mm length

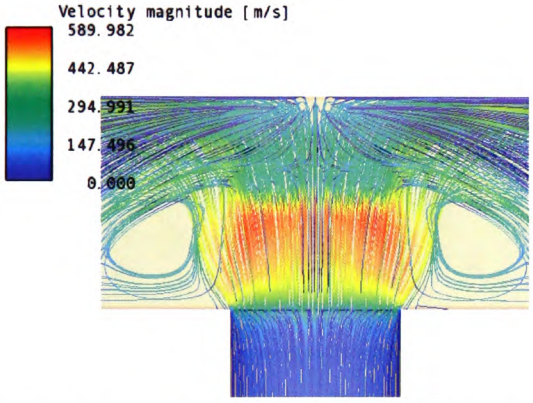

Figure 7 – CFD simulation representing 4483 chamber cross section, 10 mm length

As can be seen the CFD simulations for equivalent chamber lengths of 16mm and 10mm are significantly different from each other, whereas, the CFD simulation for 10mm is remarkably similar to flows observed in the scaled splicing chamber.

This series of validation experiments seem to offer compelling evidence for the general accuracy of the simulation technique used in this work. At first sight, the results seemed good enough to justify a substantial programme of work on CFD simulations. However, there remained one significant concern. The potential problem with the accuracy of all of the experiments, both scaled and simulated, was the absence of yarns.

Effect of yarn absence in visualisation of fluid flow

In the case of CFD, it would have been impossible, with the resources available, to model the complexity of a real yarn, with a multiplicity of filaments, in a splicing chamber. Even the relatively simple simulations, of fluid flows in empty chambers, demanded high computational power. In the first instance, the simulations were run simply to gain a "feel" for the general nature of the airflows in different chamber formats. The target at the outset was merely to identify certain common characteristics between chambers of different forms, from different manufacturers.

However, as the body of CFD results grew, it became clear that the pattern of airflows within splicing chambers were very consistent and distinctive, and that the vortices were large and well defined. It also became reasonable to conclude that the only logical place for a yarn bundle to reside in a splicing chamber, once in equilibrium, would be along the "null lines" of the main vortices, which form to left and right of the blast hole and run the full length of the chamber. It seemed quite credible that the CFD simulations did, after all, have some relevance to the real world of splicing. If yarns tend to lie along these vortex null lines, then a CFD simulation of an empty chamber can give an insight into the mechanism of splicing.

This was a hypothesis, which needed to be tested, and one validation experiment was simple to perform. It had been established that there was a close correspondence between the predictions of the CFD software, and the actual flow observed in the transparent scaled chamber. The CFD results provided an incentive to use the scaled chamber to observe the formation of real splices in real time. If the scaled chamber could be shown to produce similar results to those of a normal chamber, and if the yarns could be seen to lie along the null lines of the vortices, then there would be good justification to deduce that a CFD simulation of an empty chamber is a valid representation of the airflow.

An extremely large yarn of 11000dtex was selected with consistent properties as the 1100dtex yarn, which had been used in previous optimisation experiments (Webb *et al.*, 2007; Webb *et al.*, accepted 2007). Cut to length by hand, they were then fed into the scaled chamber, side by side, and exposed to the water flow. The results are shown in the Figures 8 and 9.

Figure 8 shows the splicing chamber at a slight angle. Comparison with the flow patterns in Figure 9 shows that the yarns do indeed lie in the null zones and follow the "shoulder" shape of

the fluid flow as it falls away from the roof of the chamber.

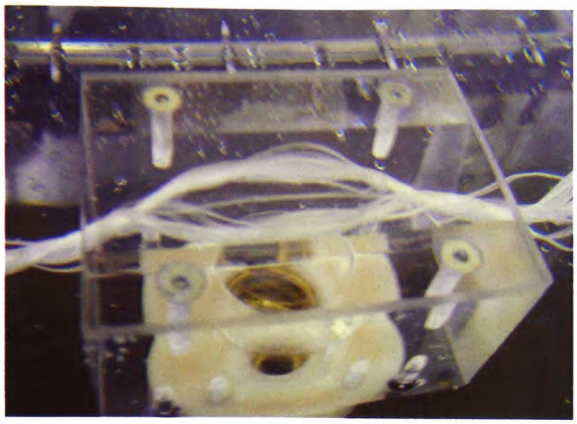

Figure 8 – Splice creation in large scaled model

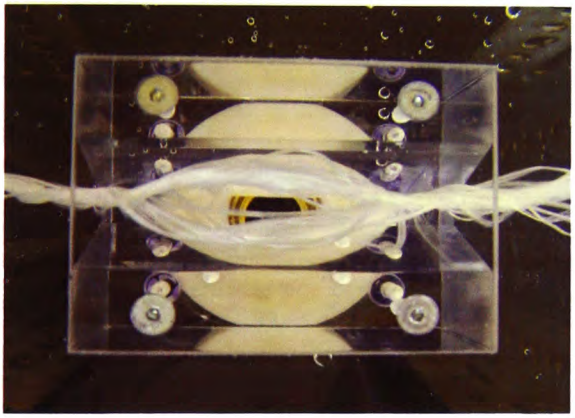

Figure 9 – Splice creation in large scaled model

Figure 9, taken from above, shows clearly how bundle separation occurs directly above the blast hole, and how filaments are twisted, converging as the vortices lose their identity as they emerge into free air.

These results provided sufficient evidence to use CFD simulations of airflows in empty splicing chambers. It was clear that CFD was a suitable tool for the analysis of airflow characteristics of a wide range of commercially available chambers.

Computational fluid dynamics simulations

The CFD simulations were now used to re-examine the outcomes of the work previously conducted by Webb *et al.* (2007, accepted 2007), on splice strength, splice appearance, and "scaling".

The earlier experiments had concentrated on three particular splicing chambers. Two, respectively identified as 4483 straight and 4485 straight, had simple trapezium cross-sections, but differed slightly in width of cross-section. The third, identified as 4483 bowl, was based on the 4483 profile, but had a deep bowl shape at top of the chamber above the blast hole. The results of the CFD simulations are shown in Figures 10 to 12.

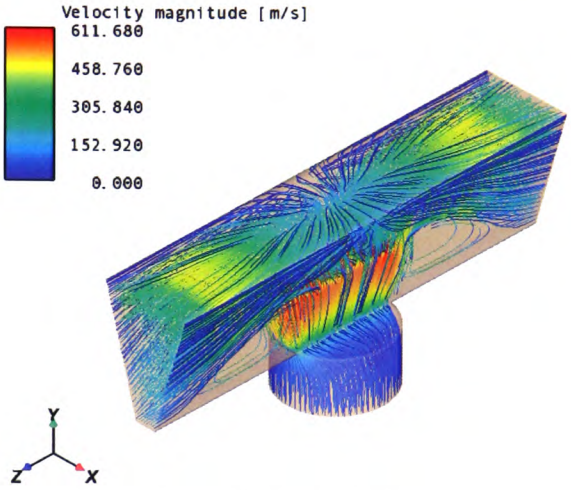

Figure 10 – 4483 straight simulation

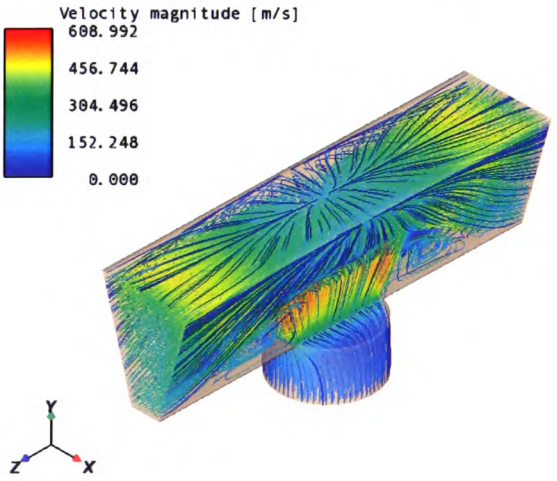

Figure 11 – 4485 straight simulation

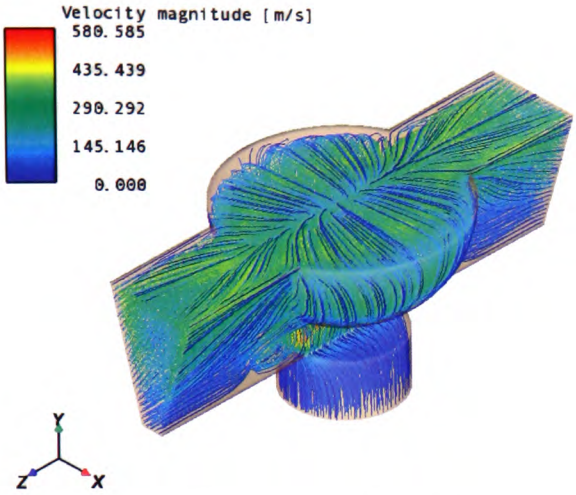

Figure 12 – 4483 bowl simulation

All three chamber simulations produced strong vortices in the z direction, on either side of the blast hole. Two significant vortices occur in the x direction split by the centre of the blast hole; they decay in strength towards the chamber ends. These vortices create equal but opposite rotation in the x-axis, which acts as the catalyst for splitting the yarn ends into two bundles and intermingling them throughout the length of the splice. The intermingling of the individual filaments draws the loose tails ends into the chamber, thereby reducing the splice length.

The 4483 bowl chamber (Figure 12) seems to function slightly differently from the straight chambers; probably because it creates stronger vortices in the x-axis. These stronger vortices improve the chamber performance by increasing the intermingling rate, producing a shorter more compact splice, though there is a slight penalty in terms of appearance, because the twist-reversal zone at the centre of the splice is more conspicuous.

These simulations confirm what was previously hypothesized to happen during the splicing process by blasting the yarn ends up to the top of the chamber then separating them into 2 approximately equal bundles and the rotation of these bundles draws in the yarn ends by reducing its length through twisting, until it reaches a point when no more twisting can occur and the splice is locked into its structure.

The series of simulation results, which follow (Figures 13 to 15) show results from other splicing chambers, which are used in commercial splicers. Their simulations give weight to the proposition that, although chamber profiles differ widely, they actually produce fairly similar patterns of airflows.

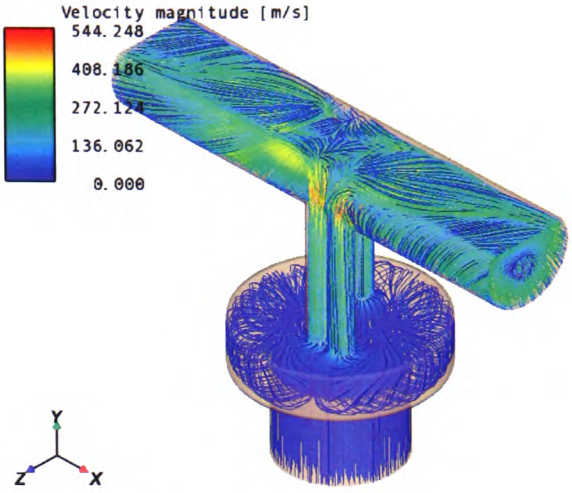

Figure 13 – Commercially available splicing chamber simulation

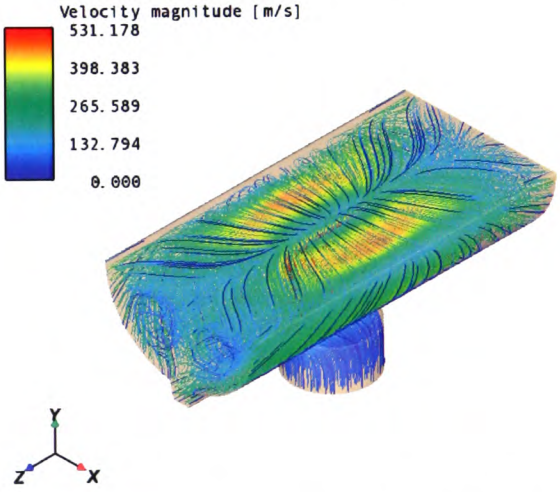

Figure 14 – Commercially available splicing chamber simulation

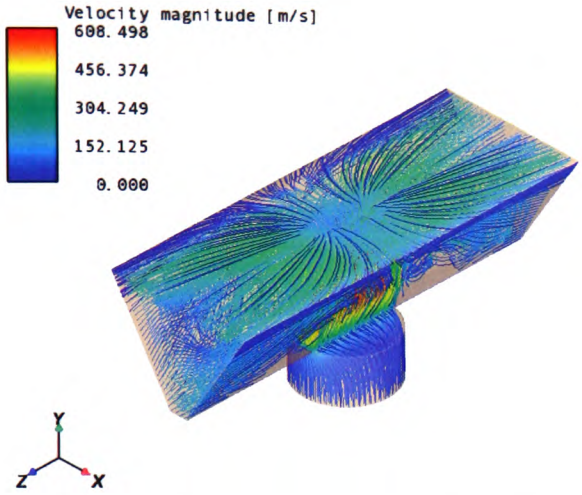

Figure 15 – Commercially available splicing chamber simulation

Throughout these simulations a common characteristic airflow was revealed. All splicing chambers produce a pair of equal but opposite vortices either side of the blast hole, separating the yarn bundles for intermingling. This common airflow creates a distinctive formation of the splice. This splice structure is described in greater detail in a later paper.

The function of all the splicing chambers is therefore broadly the same. The work seems to confirm the earlier deduction that the principal difference between all these chambers is simply their splicing efficiency.

Effect of mass flow rate on splicing

One of the outputs from the CFD simulations is that of the rate of mass flow of fluid through the chamber blast hole. There are many references in the literature to choked flow (Schmidtchen, 2004; Bar-Kohany *et al.*, 2007). The laws of aerodynamics dictate that in circumstances, which involve fluid at high pressure passing through small orifices, there is a maximum velocity for the fluid on the high-pressure side of the orifice. After this critical point, as pressure rises on the inlet side, the velocity remains constant, but the fluid density rises. Although the volume flow through the orifice is then constant, the rising density results in an increasing mass flow. This is the condition known as choked flow as shown in Figure 16.

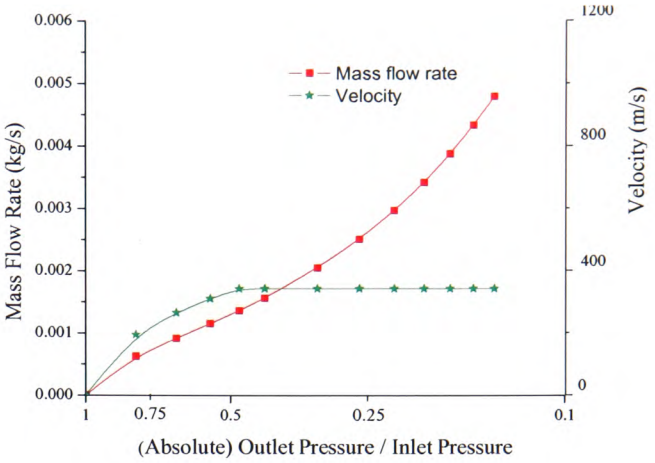

Figure 16 - Mass flow rate for the 4483 straight chamber

The CFD work, in yielding mass flow information, showed that under certain circumstances, splicing chambers are operating under choked flow conditions. Limited to the peak value of velocity under high pressure, until it passes through the inlet orifice, the fluid is then able to expand and accelerate, as the flow channel diverges.

It is clear that, under choked flow conditions, the original convention of using air pressure as a principal splicing parameter is far from appropriate. Indeed, air pressure is an indirect measure at best, for example, it reveals nothing about differences between splicing chambers, and nothing about differences between filament counts. As a basis for formulating a physical model of splicing, pressure is too far removed from the actual process.

Close examination of the results obtained from the simulations suggested that the 'mass flow rate' at the orifice between blast hole and chamber profile should be a more pertinent measure. Mass flow rate has the merit of being a direct measure of how the fluid is behaving, and it is easy to relate mass flow, in terms of Newtonian mechanics, to how the air may interact with the yarn filaments in the splicing chamber.

CFD results demonstrated that, for a given incoming air pressure, the mass flow rate changes markedly from chamber to chamber, because of variations of orifice diameters and chamber volumes. The CFD work therefore resulted in a subtle change in our approach to splicing parameters.

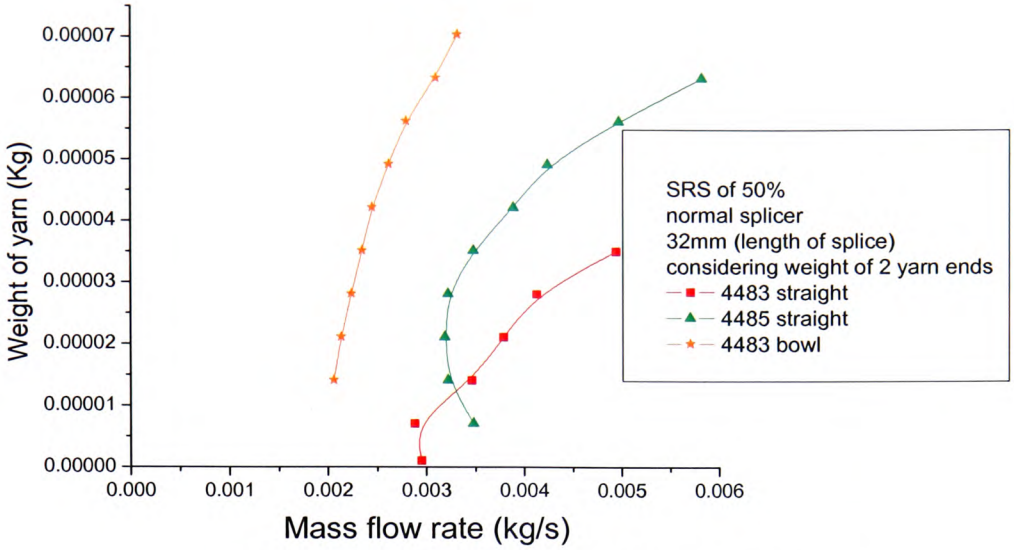

Figure 17 – mass flow rate representation of each chamber

Instead of following the established convention of using input air pressure as the principal variable, the previous research work by Webb *et al.* (2007) was now reinterpreted in terms of mass flow rate.

Interesting conclusions emerged quickly from this work:

- The air velocity in a 4485 straight chamber is similar to that of the 4483 straight chamber. However, the 4485 straight has a greater mass flow rate, associated with its larger diverging volume and its larger area orifice. The greater mass flow rate produces stronger rotational forces along the walls of the chamber. These observations may explain why the 4485 straight chamber can handle a wider range of yarn counts than the 4483 straight, but why it also produced splices of worse appearance.
- Despite having a modest mass flow, similar to the 4483 straight, the 4483 bowl performance closely matched the 4485. This is probably related to the presence of the bowl; the chamber has a larger diverging volume than either of the other chambers, creating greater rotational forces, and producing acceptable splices at lower upstream pressures.

The adoption of mass flow rate as the primary process parameter yielded a much better understanding of the splicing process, allowing easy comparison between different splicing chambers at different yarn counts. By combining the CFD simulation results with previous research work by Webb *et al.* (2007), it was possible to produce a characteristic performance curve for each chamber as shown in Figure 17.

From the original splice strength experiments, results for each splicing chamber were analysed to yield the original process parameters, which had produced a splice strength of 50 per cent, in the yarn count ranges of 1100dtex to 9900dtex. Combining these past results with the results emerging from the CFD work, it became possible to create a characteristic curve for each of the three chambers, to identify the mass (per second) of air required to splice a given mass (per unit length) of yarn.

Analysis of these curves (Figure 17):

The principal conclusion is that splicer geometry has a marked effect on splicing performance. Provided that yarn counts are within the chambers' performance envelopes, successful splices will result. But different mass flows, and hence different energy consumptions, will be needed.

Along the main sections of each curve, there is a roughly linear relationship between the required mass flow rate and the yarn count. The three principal (linear) gradients are markedly different. The 4483 bowl is steepest, the 4485 straight is next, and the 4483 straight is flattest. These gradients represent the concept of splicing efficiency, the steepest curve demonstrating that

the bowl chamber can cope with higher counts with a modest increase of mass flow, while the 4483 straight chamber struggles as count rises.

The curves have strange shapes, but the three principal (linear) gradients seem to be converging approximately to mass flow figures of between 0.0020 Kg/sec and 0.0025 Kg/sec. This probably corresponds to the observation when pressure was being used as the measure of performance that there was a minimum pressure for each chamber, below which the splicer would not perform.

As the curves approach the upper limits of measured count, there is some evidence of a reduction of the gradient of each curve. The response of the 4483 straight stops early, because it could not handle larger yarn counts. The suggestion of a fall-off of gradient is probably related to the fact that chambers eventually fail when yarns simply become too bulky for that given chamber profile.

The curves behave most oddly as they approach the *x*-axis, with two of the curves reversing sharply, and the third indicating that it might also go into reverse, were it to splice a much smaller yarn. The inference is that, when yarns become sufficiently small, there is something about the relationship between yarn geometry and chamber geometry, which means that the interaction between airflow and yarn begins to fail.

It should be noted that, while these curves have been derived from data accumulated on yarns whose overall count varies from 1100dtex upward, the individual filament count has remained constant throughout. It is reasonable to conjecture about the consequence of changing the filament count. There is no reason to suppose that the general principles of what has been observed in this work will change as say, filament count is increased. However, a small volume of work, conducted outside the main experiment, suggests very strongly that the curves will change in detail; as filament count increases, the gradient will become less steep, and the curves will shift slightly to the right along the x-axis. These results are the inevitable consequence of a greater mass flow being needed to distort the stiffer filaments.

CONCLUSION

In this paper, two main visualisation and simulation techniques were used to model the splicing process:

- A large scaled model for real-time representation of fluid flow and real splicing.
- The application of computational fluid dynamics simulation software to model 3D airflows within given chamber profiles.

The results of the CFD simulations revealed a common airflow characteristic between all chambers in industry, which leads to the conclusion that all chambers have the same general splicing process but with varying levels of efficiency.

In general, in all splicing chambers, a blast of high velocity compressed air is produced within microseconds. This blast, interacting with the chamber surfaces, takes on the form of strong contra rotating vortices, which continue outward to the end of the chamber, fading in intensity as they move away from the centre. Yarns are swept up into these vortices, and by a complex process involving false twist, swiftly become intermingled.

A new parameter of mass flow rate was introduced, to assess the efficiency of a splicing chamber. The mass flow rate clearly varies with applied air pressure, but not uniquely with pressure, it also varies according to the detailed profile of the splicing chamber design.

A reliable prediction method has emerged, which uses the objective measure of mass flow in a given chamber geometry, to indicate how any splicing chamber design would perform on a given yarn count, with the yarn count size deciding the chamber dimensions.

Finally, it has been possible, from these new insights, to develop a completely new physical model of the splicing process, which explains many phenomena, which have been observed, but never understood. This research is continued in a later paper, which is the final paper of a series.

REFERENCES

Bar-Kohany, T., Sher, I. and Sher, E., 2007. *Choked Flow of a Bubbly Mixture Through an Effervescent and Flash-Boiling Atomizer: A Theoretical Approach*, Journal of the International Institutes for Liquid Atomization and Spray Systems, 17(5), 431-449.

Cheng, K.P.S. and Lam, H.L.I., 2003. *Evaluation and Comparing the Physical Properties of Spliced Yarns by Regression and Neural Network Techniques*, Textile Research Journal, 70(3), 161-164.

Cheng, S. and Fung, W.Y., 2004. *Joining yarn ends together by pneumatic splicing*, ATA Journal, 15(3), 40-45.

Daws, L.F., Penwarden, A.D. and Waters, G.T., 1965. *A Visualization Technique for the Study of Air Movement in Rooms*, Journal of the Institution of Heating and Ventilating Engineers, 33, 24-28.

Fluent Inc., 2005a. *Fluent 6.2 User's Guide*, 155-223.

Fluent Inc., 2005b. *Fluent 6.2 User's Guide*, 719-806.

Haber, R.B., 1990. *Visualization techniques for engineering mechanics*, Computing Systems in Education, 1(1), 37-50.

Lamar, J.E., 2001. *Flow-Visualization Techniques Used at High Speed by Configuration Aerodynamics Wind-Tunnel-Test Team*, Technical Report: NASA/TM-2001-210848.

Lewandowski, S. and Drobina, R., 2004. *Strength and geometric sizes of pneumatic spliced combed wool ring spun yarns*, Fibres & textiles in Eastern Europe, 12, 2(46), 31-37.

Mingjie, x., Peijie, H., Shihua, S., Bingchang, Q. and Tao, L., 1999. *Study on pneumatic splice*, Journal of China Textile University, 16(2), 109-112.

Oxenham, W. and Basu, A., 1993. *Effect of Jet design on the properties of air-jet spun yarns*, Textile research journal, 63(11), 674-678.

Schmidtchen, U., 1994. *Choked flow of helium II through phase separators*, Journal of Low Temperature Physics, 97(5-6), 365-392.

Webb, C.J., Waters G.T., Thomas, A.J., Liu, G.P. and Thomas C., 2007. *The use of the Taguchi Design of Experiment method in optimising splicing conditions for a Nylon 66 yarn*, Journal of the Textile Institute, 98(4), 327-336.

Webb, C.J., Waters G.T., Thomas, A.J., Liu, G.P. and Thomas C., *Optimising splicing parameters for splice aesthetics for a continuous filament synthetic yarn*, Journal of the Textile Institute, accepted 2007.

Zhou J. and Qin, P., 2005. *Air Flow in a Pneumatic Splicer by CFD*, Textile Research Journal, 75(2), 106-110.

APPENDIX 1

The realizable $\kappa-\varepsilon$ turbulence model

The turbulent kinetic energy κ and its rate of dissipation ε can be obtained from the following transport equations (Fluent Inc., 2005b):

$$\frac{\partial}{\partial t}(\rho\kappa)+\frac{\partial}{\partial x_j}(\rho\kappa u_j)=\frac{\partial}{\partial x_j}\left[\left(\mu+\frac{\mu_t}{\sigma_\kappa}\right)\frac{\partial\kappa}{\partial x_j}\right]+G_\kappa+G_b-\rho\varepsilon-Y_M$$

$$\frac{\partial}{\partial t}(\rho\varepsilon)+\frac{\partial}{\partial x_j}(\rho\varepsilon u_j)=\frac{\partial}{\partial x_j}\left[\left(\mu+\frac{\mu_t}{\sigma_\varepsilon}\right)\frac{\partial\varepsilon}{\partial x_j}\right]+\rho C_1 S_\varepsilon-\rho C_2\frac{\varepsilon^2}{\kappa+\sqrt{\nu\varepsilon}}+C_{1\varepsilon}\frac{\varepsilon}{\kappa}C_{3\varepsilon}G_b$$

Where

$$C_1=\max\left[0.43,\frac{\eta}{\eta+5}\right]$$

$$\eta=S\frac{\kappa}{\varepsilon}$$

$$S=\sqrt{2S_{ij}S_{ij}}$$

μ_t = turbulent viscosity

G_κ = generation of turbulence kinetic energy due to mean velocity gradients

G_b = generation of turbulence kinetic energy due to buoyancy

Y_M = contribution of the fluctuating dilatation in compressible turbulence to the overall dissipation rate

C_2 and $C_{1\varepsilon}$ are constants

σ_κ and σ_ε are the turbulent Prandtl numbers for κ and ε, respectively

The turbulent viscosity is computed from:

$$\mu_t = \rho C_\mu \frac{\kappa^2}{\varepsilon}$$

Where

$$C_\mu = \frac{1}{A_0 + A_s \frac{\kappa U^*}{\varepsilon}}$$

The model constants A_0 and A_s are given by

$$A_0 = 4.04,\ A_s = \sqrt{6}\cos\phi$$

It can be seen that C_μ is a function of the mean strain and rotation rates, the angular velocity of the system rotation, and the turbulence fields (κ – ε).

The turbulent production, G_κ, is modeled identically for all 3 κ – ε models. From the exact equation for the transport of κ, G_κ is evaluated in a manner consistent with the Boussinesq hypothesis as

$$G_\kappa = \mu_t S^2$$

Where S is the modulus of the mean rate-of-strain tensor, defined as:

$$S \equiv \sqrt{2 S_{ij} S_{ij}}$$

with

$$S_{ij} = \frac{1}{2}\left(\frac{\partial u_j}{\partial x_i} + \frac{\partial u_i}{\partial x_j}\right)$$

The effects of buoyancy on turbulence in this model occurs when a non-zero gravity field and temperature gradient are present simultaneously. The generation of turbulence due to buoyancy is given by:

$$G_b = \beta g_i \frac{\mu_t}{\mathrm{Pr}_t}\frac{\partial T}{\partial x_i}$$

where Pr_t is the turbulent Prandtl number for energy and g_i is the component of the gravitational vector in the i_{th} direction. For the realizable κ – ε model, the default value of Pr_t is 0.85. For ideal gasses, the coefficient of thermal expansion, β, is defined as

$$\beta = -\frac{1}{\rho}\left(\frac{\partial \rho}{\partial T}\right)_P$$

The degree to which ε is affected by the buoyancy is determined by the constant $C_{3\varepsilon}$ and is defined as:

$$C_{3\varepsilon} = \tanh\left|\frac{v}{u}\right|$$

where v is the component of the flow velocity parallel to the gravitational vector and u is the component of the flow velocity perpendicular to the gravitational vector. In this way, $C_{3\varepsilon}$ will become 1 for buoyant shear layers for which the main flow direction is aligned with the direction of gravity. For buoyant shear layers that are perpendicular to the gravitational vector, $C_{3\varepsilon}$ will become zero.

For high Mach number flows, compressibility affects turbulence through so called 'dilatation dissipation', which is normally neglected in the modeling of incompressible flows. To account for this effect, the dilatation dissipation term, Y_M, is included in the turbulent kinetic energy κ transport equation and is defined as:

$$Y_M = 2\rho\varepsilon M_t^2 \left(= 2\rho\varepsilon \frac{\kappa}{a^2}\right)$$

Where $a\left(\equiv\sqrt{\gamma RT}\right)$ is the speed of sound and M_t is the turbulent Mach number, defined as

$$M_t \equiv \sqrt{\frac{\kappa}{a^2}}$$

The turbulent heat transport is modeled using the concept of Reynolds' analogy to turbulent momentum transfer. The 'modeled' energy equation is thus given by the following:

$$\frac{\partial}{\partial t}(\rho E)+\frac{\partial}{\partial x_i}\left[u_i(\rho E+p)\right]=\frac{\partial}{\partial x_j}\left(\kappa_{eff}\frac{\partial T}{\partial x_j}+u_i\left(\tau_{ij}\right)_{eff}\right)+S_h$$

where E is the total energy, k_{eff} is the effective thermal conductivity, and $\left(\tau_{ij}\right)_{eff}$ is the deviatoric stress tensor, defined as

$$\left(\tau_{ij}\right)_{eff}=\mu_{eff}\left(\frac{\partial u_j}{\partial x_i}+\frac{\partial u_i}{\partial x_j}\right)-\frac{2}{3}\mu_{eff}\frac{\partial u_i}{\partial x_i}\delta_{ij}$$

For the realizable $\kappa-\varepsilon$ model, the effective thermal conductivity is given by

$$\kappa_{eff}=\kappa+\frac{c_p\mu_t}{\mathrm{Pr}_t}$$

where κ, in this case, is the thermal conductivity.

The model constants $C_{1\varepsilon}$, C_2, σ_κ and σ_ε have been extensively validated for a wide range of flows, including rotating homogeneous shear flows, free flows including jets and mixing layers, channel and boundary layer flows, and separated flows to ensure that the model performs well. For all these cases, the performance of the model has been found to be substantially better than that of the standard $\kappa-\varepsilon$ model. The model constants are:

$C_{1\varepsilon}=1.44$, $C_2=1.9$, $\sigma_\kappa=1.0$, $\sigma_\varepsilon=1.2$